



MDOT RC-1563



High Skew Link Slab Bridge System with Deck Sliding over Backwall or Backwall Sliding over Abutments

FINAL REPORT – SEPTEMBER 2011

Part II



Western Michigan University
Department of Civil & Construction Engineering
College of Engineering and Applied Sciences

RESEARCH

Intentionally left blank

Technical Report Documentation Page

1. Report No. Research Report RC-1563	2. Government Accession No.	3. MDOT Project Manager Steve Kahl, P.E.	
4. Title and Subtitle High skew link slab bridge system with deck sliding over backwall or backwall sliding over abutments		5. Report Date September 30, 2011	
7. Author(s) Dr. Haluk Aktan, P.E., and Dr. Upul Attanayake, P.E.		6. Performing Organization Code WMU	
9. Performing Organization Name and Address Department of Civil and Construction Engineering College of Engineering and Applied Sciences Western Michigan University 1903 W. Michigan Ave, Kalamazoo, MI 49008		8. Performing Org Report No.	
12. Sponsoring Agency Name and Address Michigan Department of Transportation Construction and Technology Division PO Box 30049, Lansing MI 48909		Work Unit No.	
		11. Contract Number : 2006-0415	
		11(a). Authorization Number: 3	
15. Supplementary Notes		13. Type of Report and Period Covered Final Report, 2008-2011	
		14. Sponsoring Agency Code	
16. Abstract <p>A new bridge design and construction trend to help improve durability and rideability is to remove expansion joints over piers and abutments. One approach to achieve this is to make the deck continuous over the piers by means of a link slab while the girders remain simply supported. The need to implement link slabs is indicated by AASHTO LRFD section 2.5.2.4 which requires using a minimum number of expansion joints to improve rideability. Further, due to durability concerns associated with bridge deck joints, it is preferred to have a least number of joints or develop jointless decks. The expansion joints over the abutments can be removed by one of three methods: deck sliding over back wall, semi-integral abutments, and integral abutments. This results in expansion joints at either or both ends of the approaches. The design concerns other than link slab include backwall and wing-wall design and bearing movement. The behavior of a jointless bridge brings about many challenges to bridge designers. The complexity is augmented when skew is involved.</p> <p>This report complements an earlier report based on previous research on <i>Combining Link Slab, Deck Sliding Over Backwall and Revising Bearings</i> (Aktan et al., 2008) where the behavior of straight and moderately skew (skew < 20⁰) link slab bridges were investigated and design recommendations were developed. This report describes the behavior and performance of high skew (skew > 20⁰) jointless bridges with link slabs and two abutment configurations. These abutment configurations are deck sliding over backwall and backwall sliding over abutments (i.e. semi-integral abutments).</p> <p>Four tasks were performed in this project. The first task was to review and synthesize information related to the behavior, performance, design, and analysis of skew bridges. The second task was field assessment of skew bridge behavior under static truck loads and thermal loads. The third task was analytical and numerical analysis of skew link slabs. The final task was analytical and numerical analysis of skew sliding deck over backwall systems and semi-integral abutments.</p> <p>Design recommendations are developed based on literature, field assessment data analysis, finite element modeling, and subsequent simulations of the numerous models developed in this project. One recommendation deals with the skew link slab design and the remaining recommendations are for bearing selection and selection and design of a transverse restraint system at abutments of skew link slab bridges.</p>			
17. Key Words: Abutment, Concrete, Finite Element, Jointless Bridge, Link Slab, and skew.		18. Distribution Statement No restrictions. This document is available to the public through the Michigan Department of Transportation.	
19. Security Classification (report) Unclassified	20. Security Classification (Page) Unclassified	21. No of Pages 249	22. Price

Intentionally left blank

High Skew Link Slab Bridge System with Deck Sliding over Backwall or Backwall Sliding over Abutments

Project Manager: Mr. Steve Kahl, P.E.

Submitted to:



Submitted by

Dr. Haluk Aktan, P.E.
Professor & Chair
(269) – 276 – 3206
haluk.aktan@wmich.edu

Dr. Upul Attanayake, P.E.
Assistant Professor
(269) – 276 – 3217
upul.attanayake@wmich.edu



Western Michigan University
Department of Civil & Construction Engineering
College of Engineering and Applied Sciences
Kalamazoo, MI 49008
Fax: (269) – 276 – 3211

Intentionally left blank

DISCLAIMER

The content of this report reflects the views of the authors, who are responsible for the facts and accuracy of the information presented herein. This document is disseminated under the sponsorship of the Michigan Department of Transportation in the interest of information exchange. The Michigan Department of Transportation assumes no liability for the content of this report or its use thereof.

Intentionally left blank

ACKNOWLEDGEMENTS

This project is funded by the Michigan Department of Transportation. The authors would like to acknowledge the support and effort of Mr. Steve Kahl for initiating this research. The authors also wish to acknowledge the continuing assistance of the Research Advisory Panel (RAP) members in contributing to the advancement of this study. Contribution of graduate students Abdul Mohammed, Alp Servi, Duy Nguyen, Michael Romkema, and Mohamed Rusthi for the successful completion of this study is highly appreciated.

Intentionally left blank

3 MODELING AND FIELD TESTING OF A HIGH SKEW BRIDGE

3.1 OBJECTIVE AND APPROACH

The objective of this chapter is to document high skew bridge load response to truck and thermal loads. Reactions and deformations of the bridge are also obtained by finite element (FE) analysis and compared with the measured deflections and translations. Field measurements were made using a non-contact *Laser Tracker*. This chapter details the bridge configuration, instrumentation and measurement process, and FE bridge model development and analysis. The chapter also includes measurements and comparisons to the FE analysis results.

3.2 BRIDGE DESCRIPTION

The bridge (S12 of 03035) is located in Allegan, Michigan, and carries I-196 over Ottogan Street (one mile east of Holland city limits (Figure 3-1 and Figure 3-2)). The 120 ft long, 44 ft wide, single span simply supported bridge has a 42⁰ skew and carries two lanes of traffic (Figure 3-3). The bridge superstructure consists of seven steel built-up I-girders with cast-in-place concrete deck. The elevation and cross-section of the bridge is shown in Figure 3-4. The girders are connected transversely via “intermediate diaphragms” within the span and “end diaphragms” at both ends of the bridge. The diaphragm labels, locations, and cross-sections are shown in Figure 3-5 and Figure 3-6. The girders back into concrete backwalls at both ends as shown in Figure 3-7. The bridge is supported on the north abutment by a fixed bearing and on the south abutment by an expansion bearing (Figure 3-9), respectively. The expansion bearings are orientated along the bridge axis.

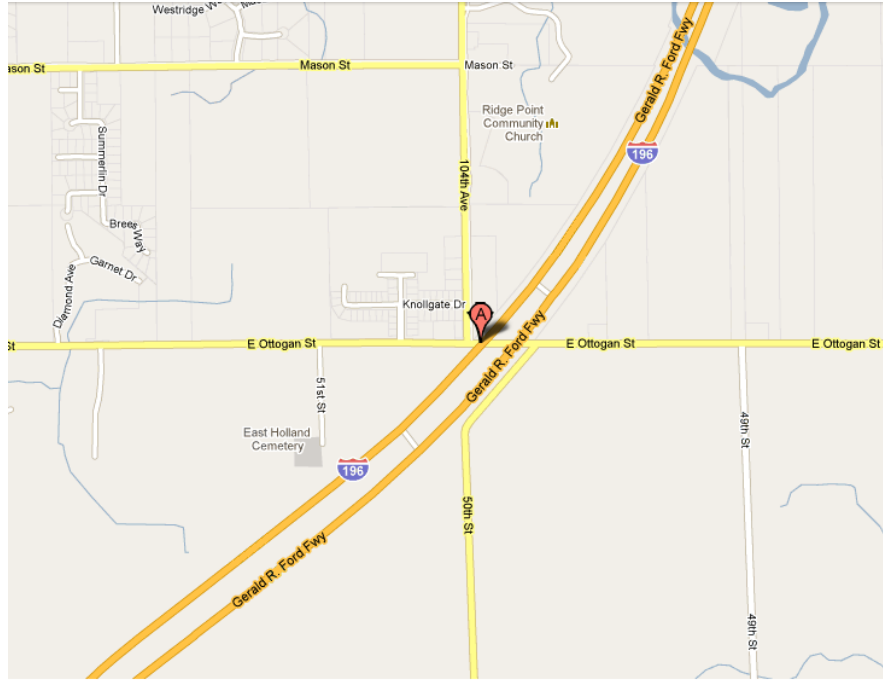


Figure 3-1. Bridge location (Source: Google map)



Figure 3-2. Aerial view of the bridge (Source: Google map)

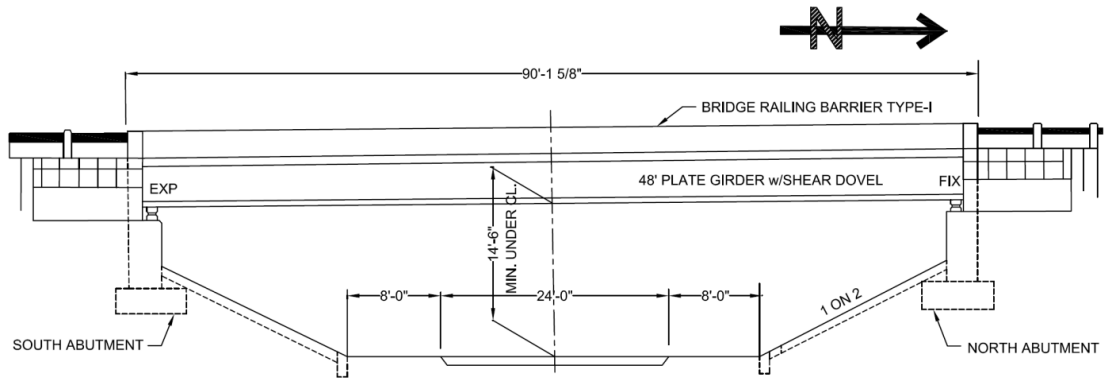


Figure 3-3. Isometric and elevation views of the bridge

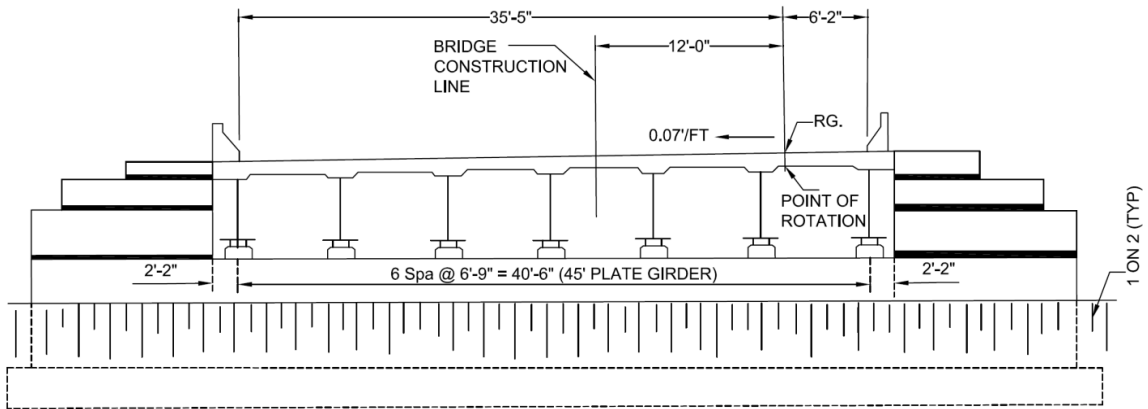


Figure 3-4. Schematic view of bridge cross section

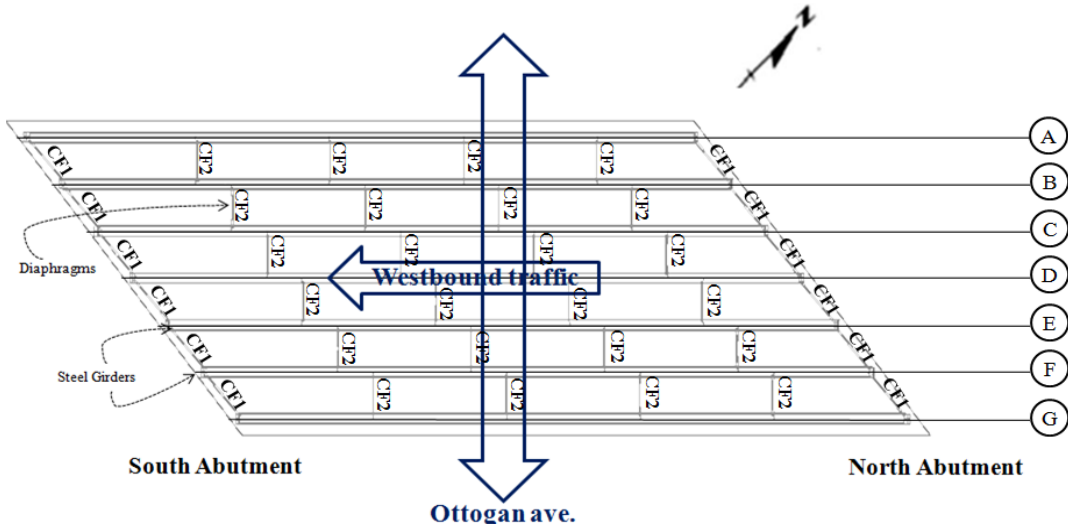


Figure 3-5. Schematic view of diaphragms and girders with labels

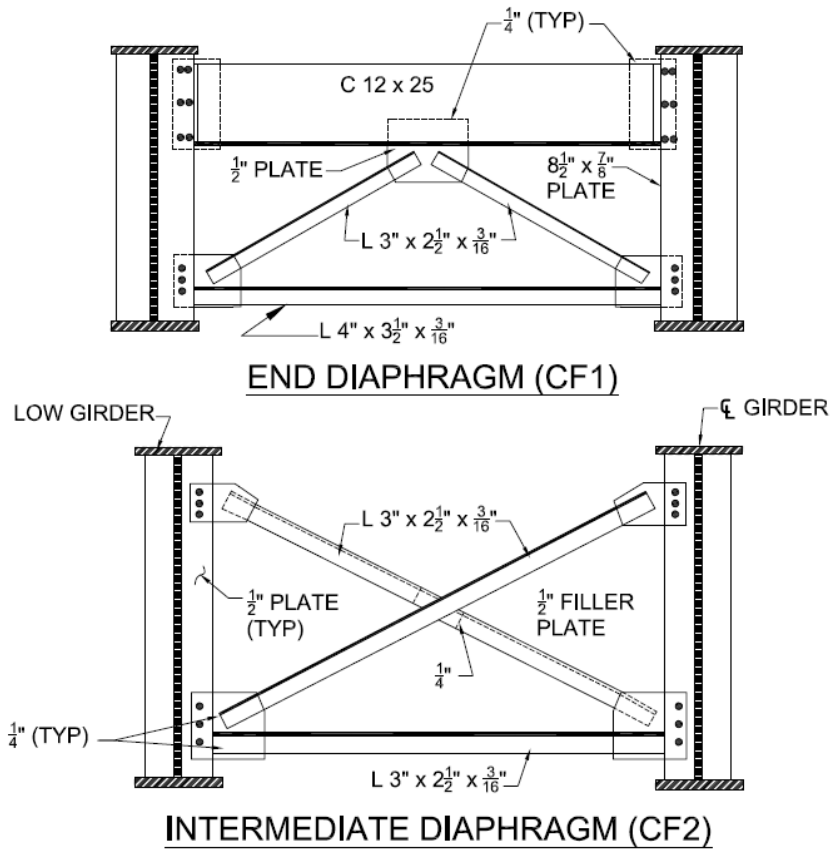


Figure 3-6. Schematic view of end and intermediate diaphragms (cross frames)

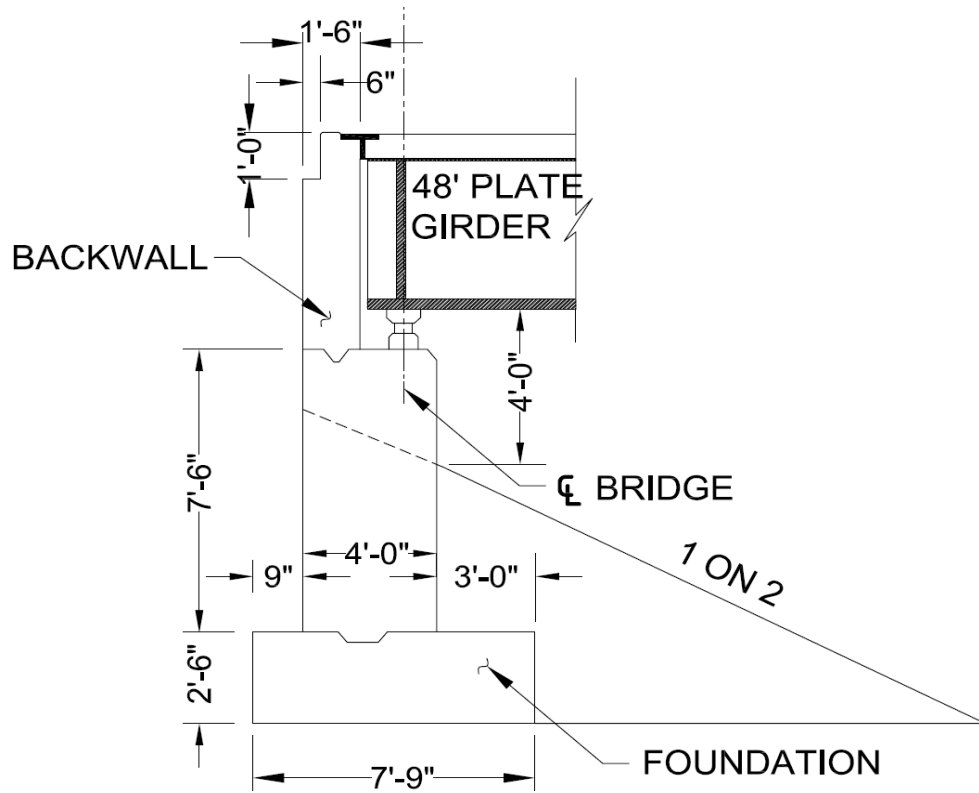


Figure 3-7. Schematic view of abutment section with backwall, girder and foundation

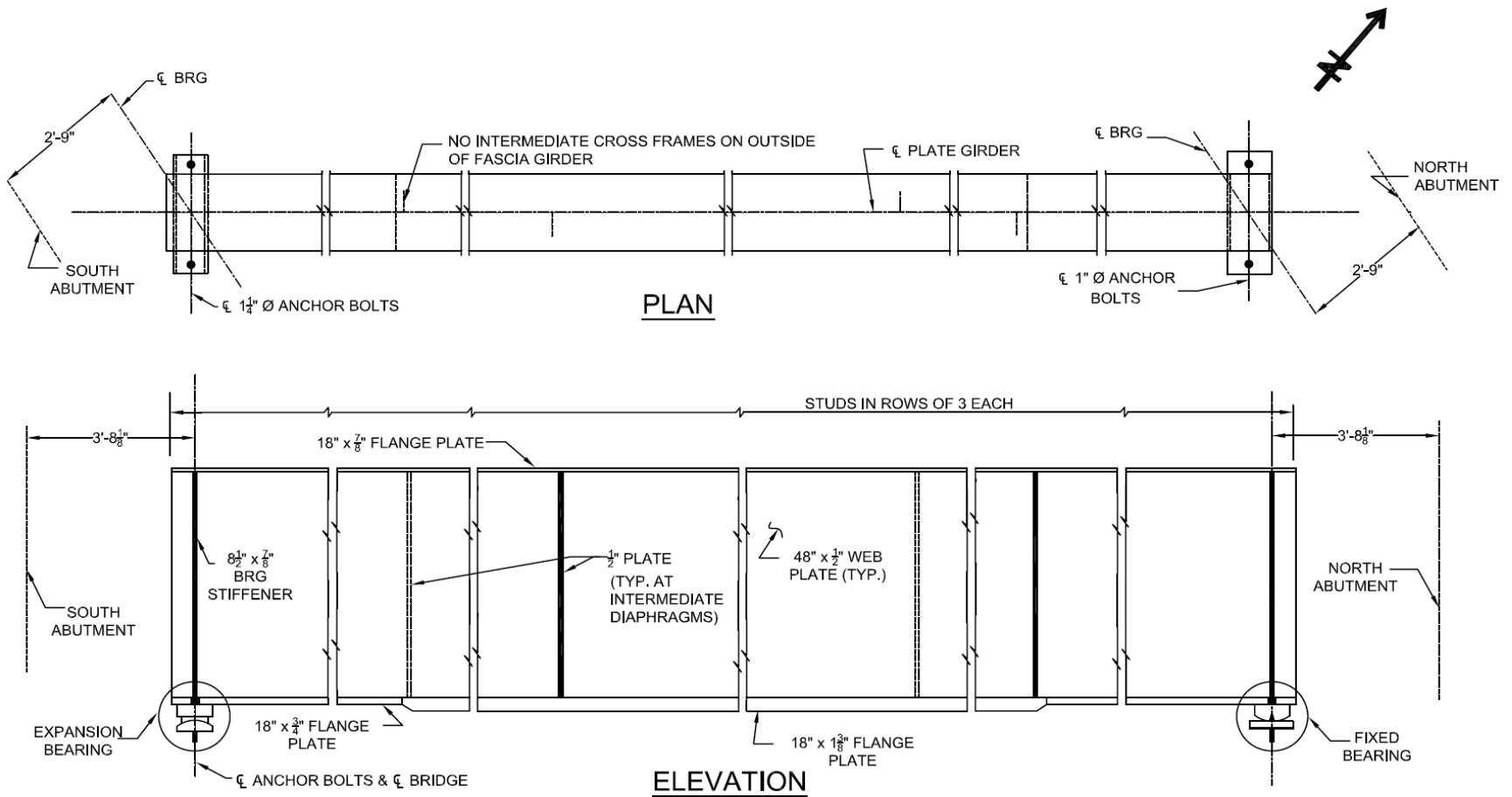
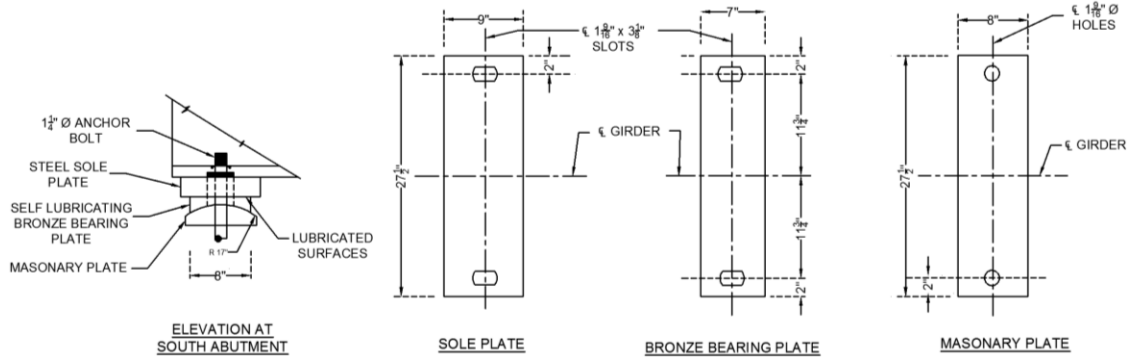
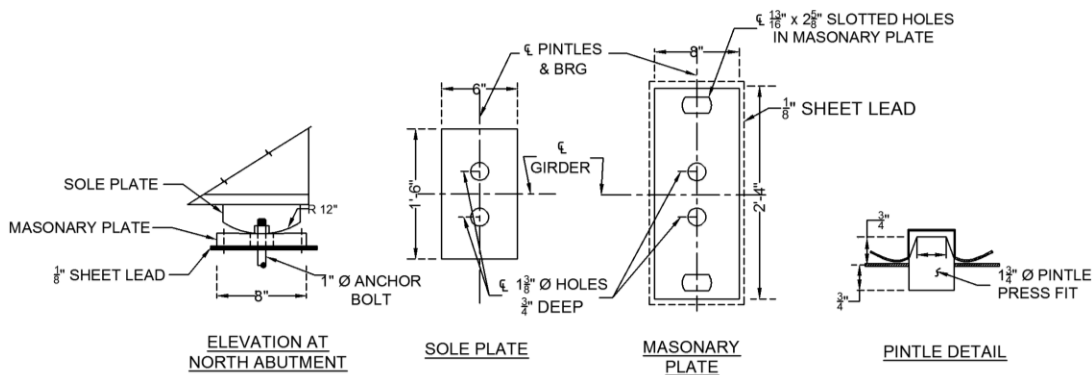


Figure 3-8. Schematic view of girder plan and elevation



(a) Expansion bearing details at south abutment



(b) Fixed bearing details at north abutment

Figure 3-9. Schematic view of respective bearing details

3.3 ABUTMENT, BEARING, AND DECK CONDITION

3.3.1 Abutment Condition

Abutments are in good condition with only a few vertical cracks.

3.3.2 Bearing Condition

Expansion and fixed bearings are used at south and north abutments, respectively (Figure 3-3 and Figure 3-8). Except for the bearings at fascia girders over north abutment, the bearings are in good condition (Figure 3-10). Steel on bronze plate bearings are used at the south abutment (Figure 3-3 and Figure 3-9a). Anchor bolt diameter of the expansion bearing is 1.25 in. The length of the sole plate slot is 3.125 in. Hence, 1.875 in. space is provided at the bearing to accommodate bridge movement due to thermal expansion and contraction. However, the majority of anchor bolts provided with expansion bearings are inclined indicating they have reached the slip limit (Figure 3-11 and Figure 3-12).



(a) Support bearing condition at interior girders (b) Support bearing condition at exterior girders

Figure 3-10. Interior and exterior bearing condition at north abutment



Figure 3-11. Expansion bearing and joint condition at south abutment

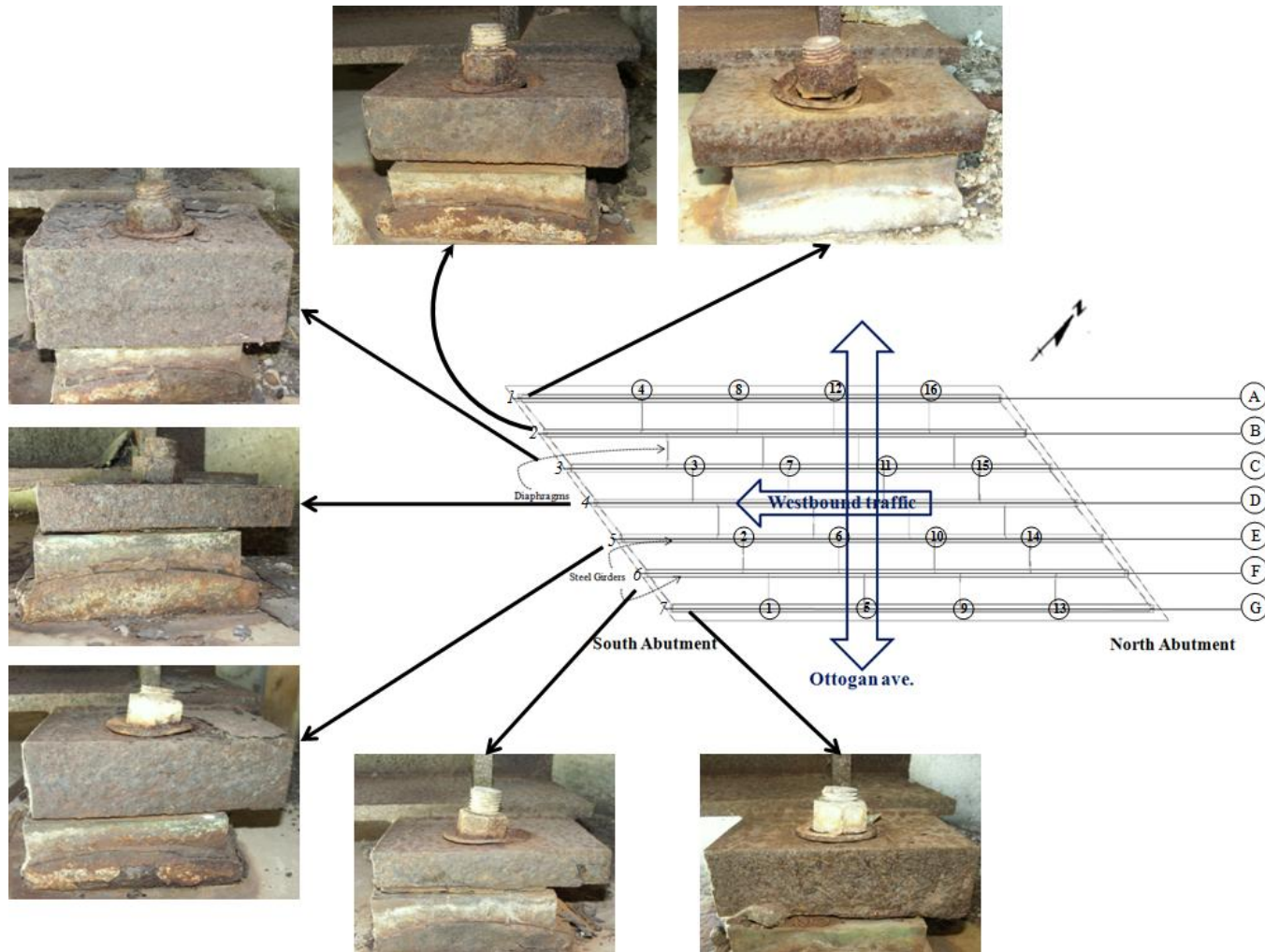


Figure 3-12. Expansion bearing condition at south abutment

3.3.3 Deck Condition

The deck is in good condition with minor areas of scaling and cracking. Repair history shows that expansion joints were replaced in 2004. During inspection, joint gaps were filled with fine debris. Minor cracking was observed adjacent to the joints (Figure 3-13).



(a) Joint over south abutment



(b) Joint over north abutment



(c) Deck cracking close to the obtuse corner of the deck over south abutment

Figure 3-13. Expansion joint and deck condition

3.4 FE MODELING AND PRELIMINARY ANALYSIS FOR LOAD TESTING

The objective of the preliminary analysis is to calculate the anticipated displacement of the girders and maximum girder and deck stresses during load testing.

3.4.1 Bridge FE Modeling

A detailed finite element model is developed with multiple element types (Figure 3-14). The element types used for the modeling of specific bridge components is included in Table 3-1.

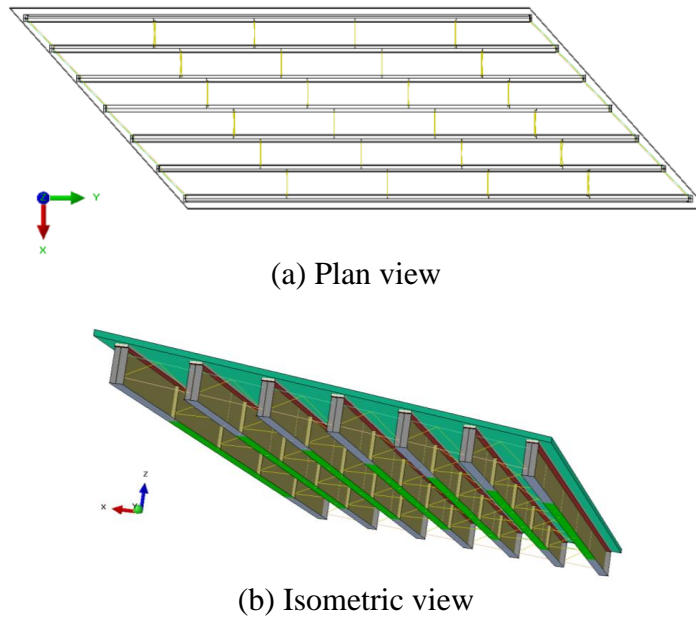


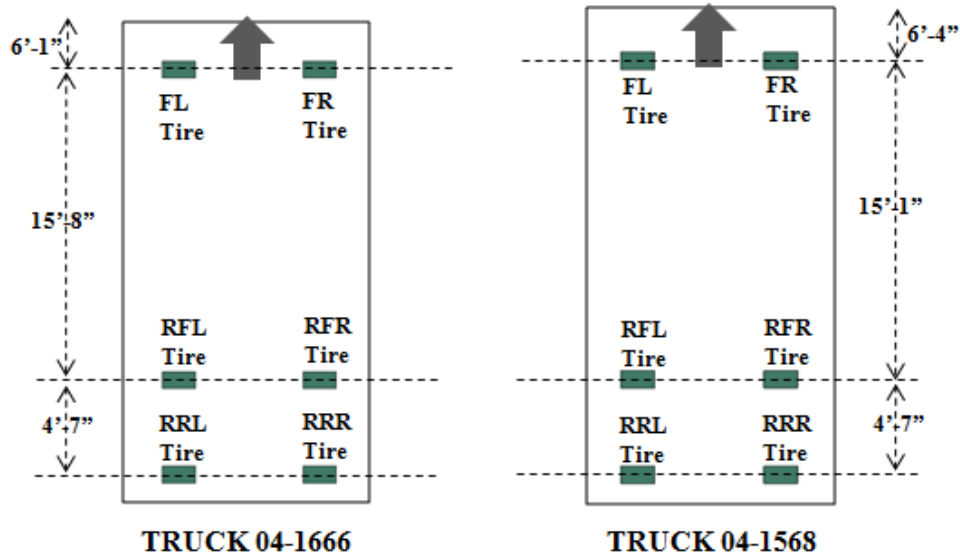
Figure 3-14. FE model configuration

Table 3-1. Bridge Components, Dimensions, and Element Types used in the Model

Component		Component Dimension (in.)	Element Types
Girder	Web	0.5	S4R (4-node general-purpose shell with reduced integration element)
	Intermediate stiffeners		
	Bearing stiffeners	0.875	
	Bottom flange	1.375	
		0.75	
Top flange	0.875		
Haunch		1.5	C3D8R (8-node linear brick with reduced integration) C3D6 (6-node linear triangular prism)
Deck		8	
Intermediate diaphragms		L 2.5 x 3.0 x 5/16	B31 (2-node linear beam element)
End diaphragms		C 12 x 25	
		L 3.5 x 4.0 x 5/16	

3.4.2 Truck Placement and Loading Configurations

The bridge is to be loaded using two trucks (Truck 04-1666 and Truck 04-1568 with axle dimensions and wheel loads shown in Figure 3-15) in four configurations as depicted in Figure 3-16 and Figure 3-17.



(a) Truck configuration

Truck Tire Position	Truck 04-1666 (GVW per Tire)	Truck 04-1568 (GVW per Tire)
Front Left (FL)	9000 lbs	9000 lbs
Front Right (FR)	9000 lbs	9000 lbs
Rear Front Left (RFL)	11500 lbs	11500 lbs
Rear Front Right (RFR)	11500 lbs	11500 lbs
Rear Rear Left (RRL)	11500 lbs	11500 lbs
Rear Rear Right (RRR)	11500 lbs	11500 lbs

(b) Wheel loads (GVW: Gross Vehicle Weight)

Figure 3-15. Truck configuration and wheel loads

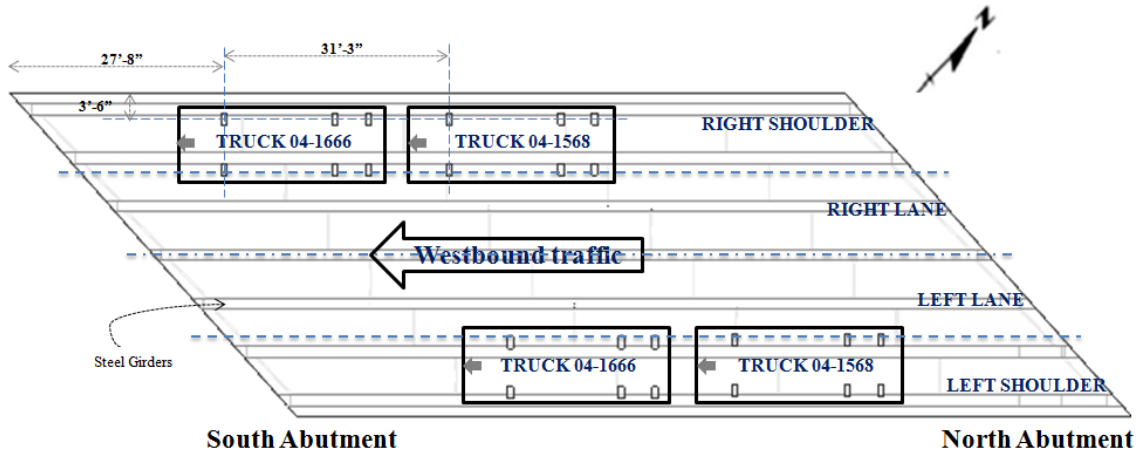


Figure 3-16. Truck positions and bridge configuration

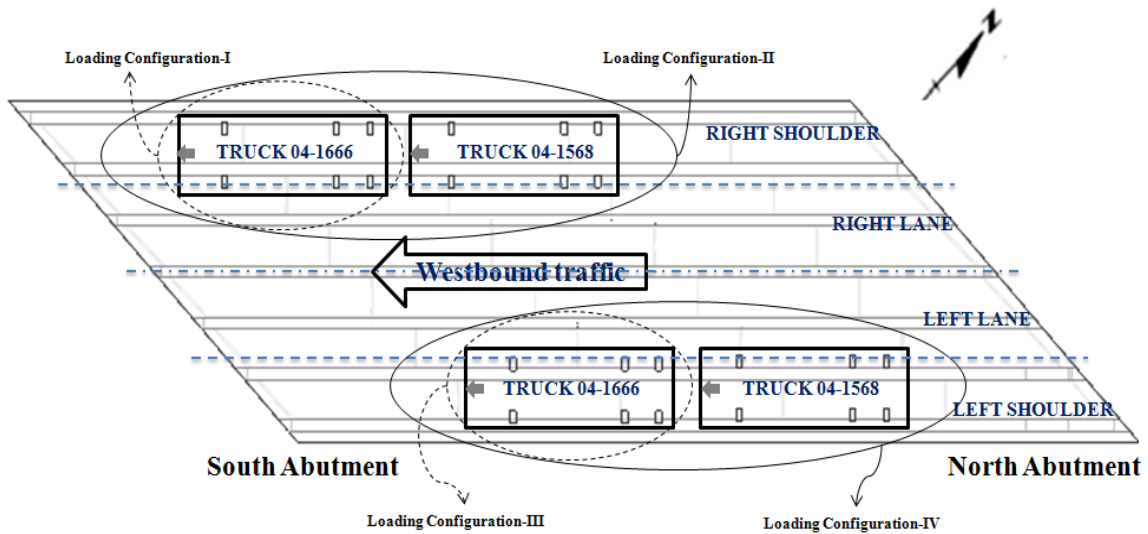


Figure 3-17. Mutually exclusive bridge loading configurations

3.4.3 Calculated Bridge Deflections and Translations

Girder ends over the south abutment are supported on expansion bearings while fixed bearings are used at the north abutment. Girder deflections and translations are calculated at girder ends and some intermediate diaphragm locations shown in Figure 3-18 . The bridge deflection profile was calculated for each loading configuration, as shown in Figure 3-19, Figure 3-20, Figure 3-21, and Figure 3-22. The figures show the girder bottom flange out of plane deformations and the color contours represent the value of vertical deflection under each loading configuration.

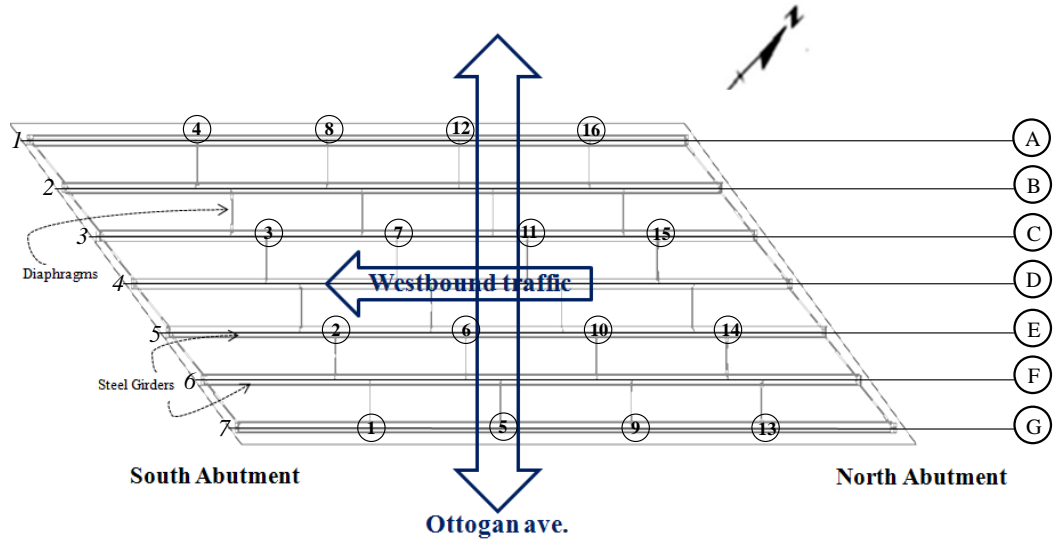


Figure 3-18. Girder labels and 16 displacement measurement points

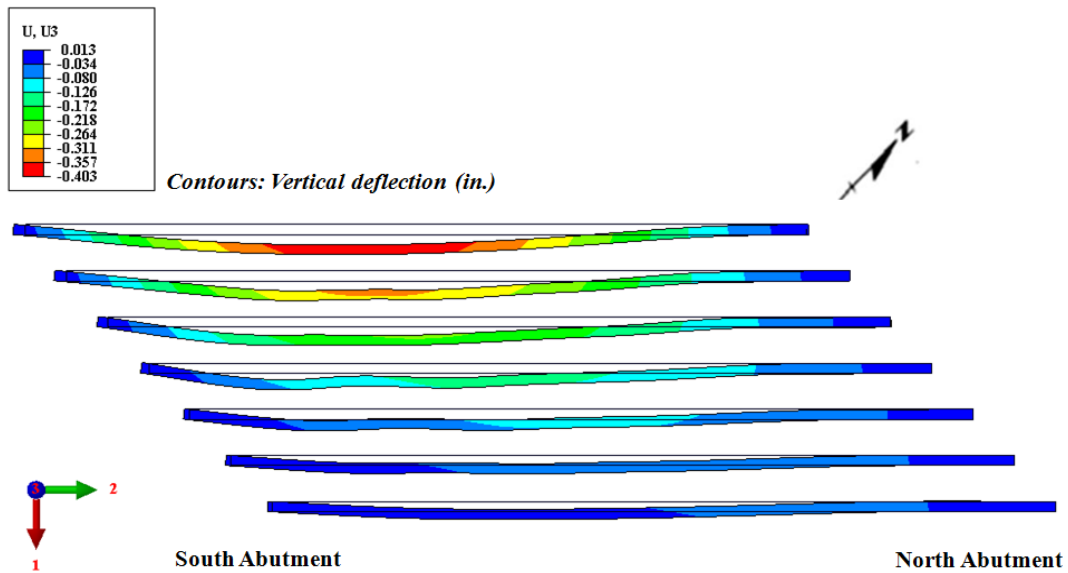


Figure 3-19. Girder bottom flange out of plane deformation, girder end translations, and vertical deflection contours under loading configuration-I

(Note: Color contours represent vertical deflection. Deformed shape depicts the girder bottom flange movement in 1-2 plane.)

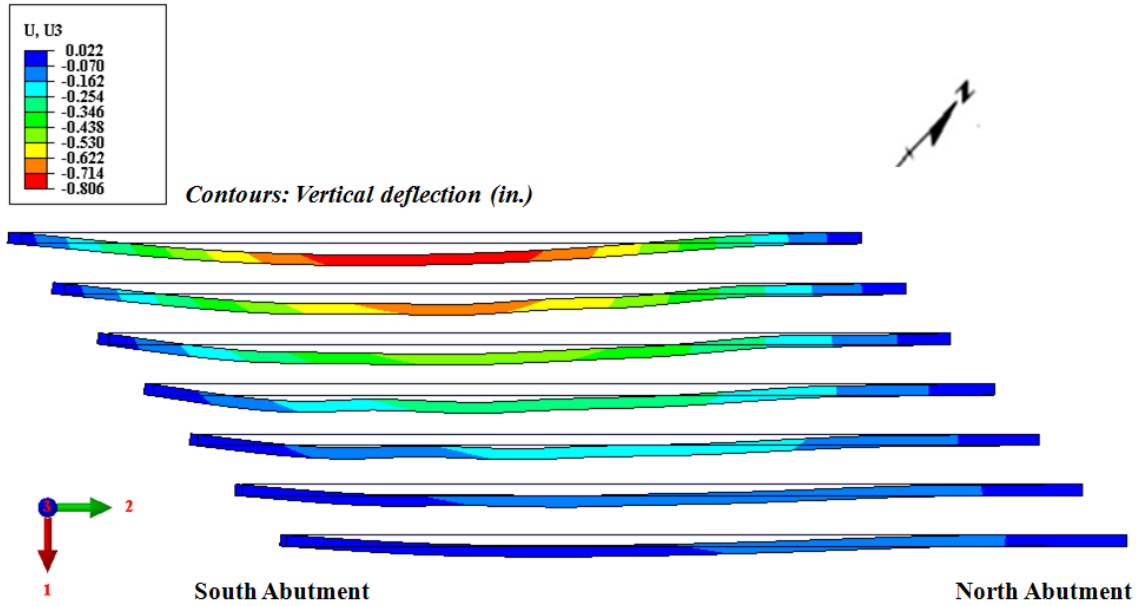


Figure 3-20. Girder bottom flange out of plane deformation, girder end translations, and vertical deflection contours under loading configuration-II

(Note: Color contours represent vertical deflection. Deformed shape depicts the girder bottom flange movement in 1-2 plane.)

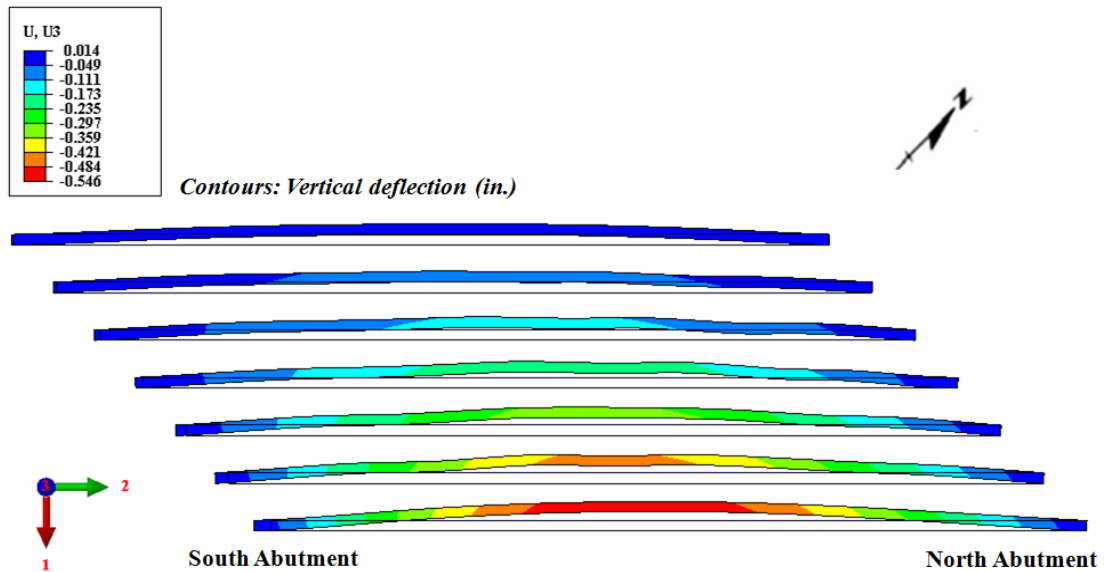


Figure 3-21. Girder bottom flange out of plane deformation, girder end translations, and vertical deflection contours under loading configuration-III

(Note: Color contours represent vertical deflection. Deformed shape depicts the girder bottom flange movement in 1-2 plane.)

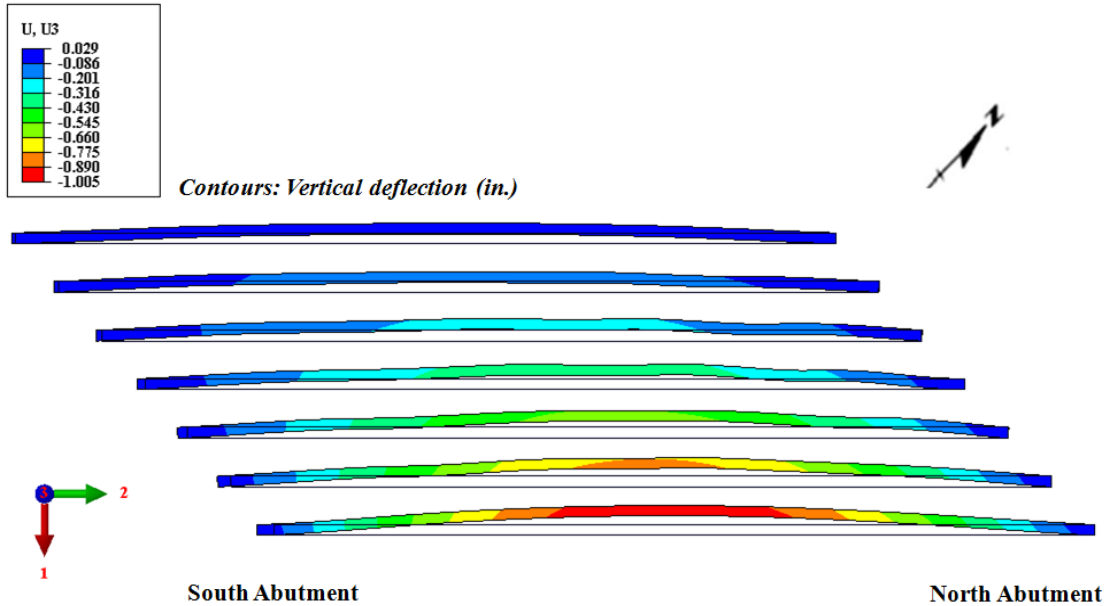


Figure 3-22. Girder bottom flange out of plane deformation, girder end translations, and vertical deflection contours under loading configuration-IV

(Note: Color contours represent vertical deflection. Deformed shape depicts the girder bottom flange movement in 1-2 plane.)

Girder stress representations are shown as the maximum von Mises stress under each load configuration. The maximum von Mises stress is 4.1 ksi calculated for loading configuration-I, 9.3 ksi for loading configuration-II, 3.7 ksi for loading configuration-III and 5.9 ksi for loading configuration IV.

3.5 MEASURED BRIDGE DEFLECTIONS AND TRANSLATIONS

3.5.1 Field Measurement Equipment and Procedures

3.5.1.1 Laser Tracker, Reflectors, and Meteorological Station

Displacement measurements are made using a laser-based device called Laser Tracker shown in Figure 3-23. For measuring the displacement of a point, first a target is placed at the point of interest. The displacement is measured by the tracker by generating a laser beam and computing the time of flight for the beam to be received by the tracker after reflecting back from a target. The measurement resolution is about 0.00003 in. Two types of targets (reflectors), shown in Figure 3-24a and Figure 3-24b, are used with the Laser Tracker. The first one is a 0.5 in. diameter glass prism reflector (Figure 3-24a) made of non-magnetic

anodized aluminum and can be attached to any surface using hot-glue. This reflector may have built in errors; hence, it is recommended to label and replace them accordingly when repeated measurements are made at different times. The 0.5 in. reflector has an acceptance angle of $\leq \pm 50^\circ$. The second type is a 1.5 in. diameter red-ring-reflector (RRR) (Figure 3-24b) made of surface-hardened magnetic stainless steel. This target is costly due to high precision manufacturing. The 1.5 in. reflector has an acceptance angle of $\leq \pm 30^\circ$. Having at least one of these red-ring reflectors is required with the equipment.

Field measurements require having at least one 1.5 in. reflector to guide the laser beam to help the tracker locate the 0.5 in. reflectors. A meteorological station (Figure 3-25) with temperature, humidity and pressure sensors is attached to the tracker for measuring ambient conditions as well as the structure temperature. The ambient weather data is used to make necessary compensations to the laser beam to improve measurement accuracy. A Laptop with Graphical user interface (GUI) is used to control the tracker (Figure 3-26).



Figure 3-23. Laser Tracker



(a) 0.5 in. glass prism reflector (b) 1.5 in. red-ring reflector (RRR)

Figure 3-24. Reflectors (targets) used with the Laser Tracker



Figure 3-25. AT MetroStation

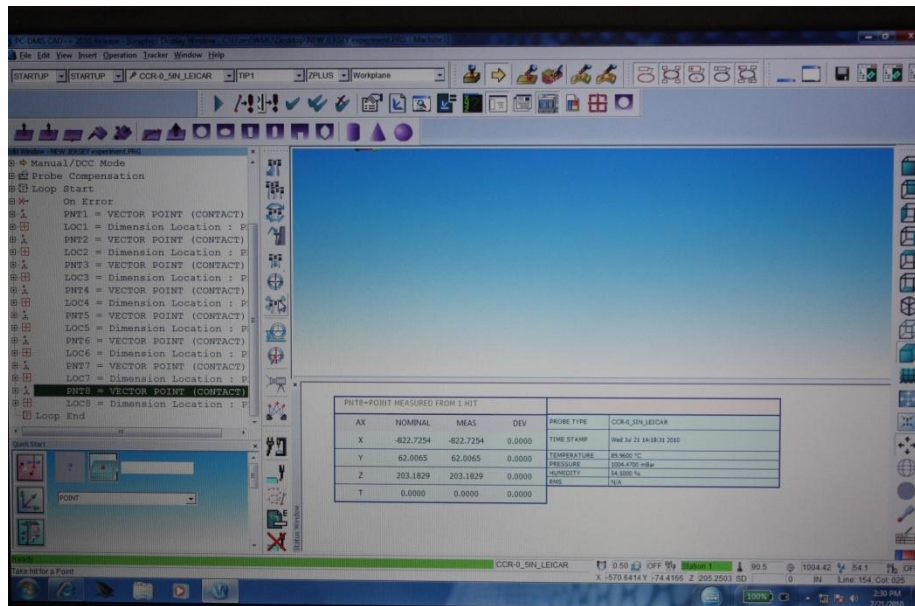


Figure 3-26. Graphical user interface (GUI) window

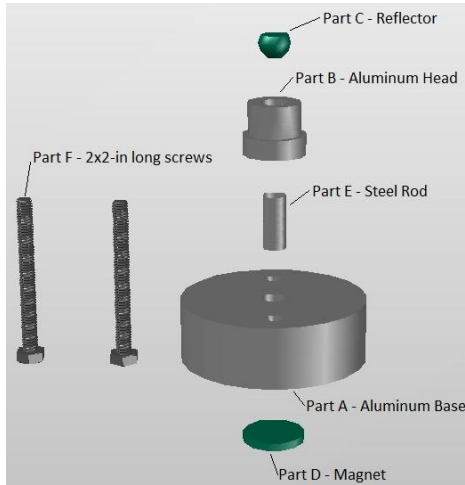
3.5.1.2 Target Locations and Placement

Monitoring the simple span bridge translation, under thermal load, relative to the abutments, requires mounting targets at girder ends as well as on abutments. Measurement of bridge translation under seasonal temperature changes requires mounting, removal, and remounting of targets as needed and aligning the laser tracker with respect to several fixed references (bench marks) every time the equipment is taken back to the field for making measurements. Targets on the abutments are used as benchmarks. A coordinate system is defined using the benchmarks so that the reference coordinate system is fixed for each measurement. Position coordinates of girder end targets are measured with respect to the reference coordinate system. Baseline measurements are taken after installing the targets. The other measurements are taken after several weeks or months (as needed) with respect to the reference coordinate system. The thermal deformations are calculated by subtracting the subsequent measurements on girder ends from the baseline measurements. The assumption in this measurement process is that the benchmark positions remain static during seasonal temperature changes.

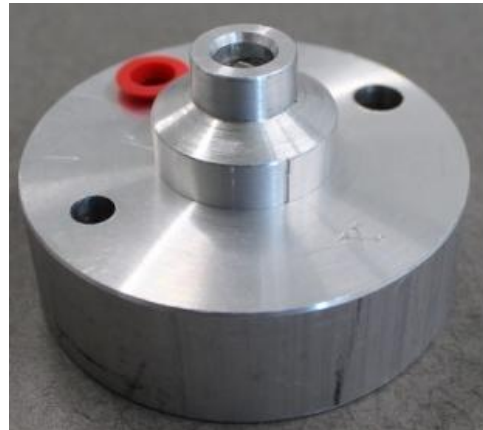
For mounting the targets, an aluminum base (part A) with a removable aluminum head (part B) was fabricated (Figure 3-27a). Reflector (part C) is placed in the removable aluminum head. The assembly is put together using a steel rod (part E) and a magnet (part D) attached to the back of the aluminum base. The target holder base is permanently attached to the abutments using 2-in. long cement screws (part F). At the girder end, they are mounted using high strength epoxy glue upon grinding and cleaning the girder surface.

Target holders on this particular bridge were mounted on December 16, 2011, and the ambient temperature was about 32 °F (Table 3-2). Cold weather conditions necessitate heating girder ends to promote curing of epoxy. However, use of regular heat guns to heat girder ends was not successful. Fortunately, having a magnet in the aluminum base helped hold the base against steel girders without using any clamping device until epoxy cured. The target is attached to the removable aluminum head using hot glue. All the removable aluminum heads are labeled to make sure the same target is connected to the aluminum base during the remounting process to control systemic errors. Following measurements part B is

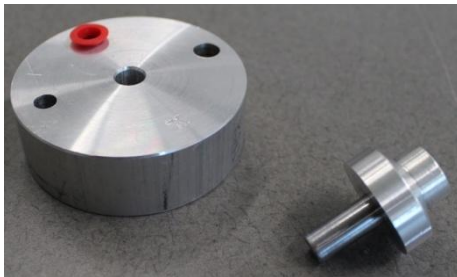
removed, and a plastic cap is placed over the hole in the aluminum base (part A) to keep it clean between measurements. Note that the plastic cap is mounted in an additional hole drilled in the aluminum base to avoid losing it during the reflector mounting/remounting process (Figure 3-27).



(a) Assembly



(b) Isometric view



(c) Top view



(d) Rear view

Figure 3-27. Accessories used for mounting girder end and abutment targets

Following the target installation, the Laser Tracker can be placed at a convenient location that is within the view of all targets (Figure 3-28).



Figure 3-28. Laser Tracker, server, and computer

The targets were mounted, and baseline measurements were taken on December 16, 2010. During that day four targets were mounted on each abutment (Figure 3-29 and Figure 3-30) as benchmarks. Also, eight more targets were mounted: four at each end of exterior girders and at the 3rd and 5th girders (Figure 3-29, Figure 3-30 and Figure 3-31). Fourteen more targets (3 @ the 1st diaphragm line, 4 @ the 2nd diaphragm line, 4 @ the 3rd diaphragm line, and 3 @ the 4th diaphragm line) were mounted to measure bridge deformations under static truckloads during load testing of the bridge (Figure 3-31). As seen from the figures, all the targets on the abutments and girder ends were labeled alphabetically while targets within the span used numerals. Target G, one of the benchmarks, was chosen as the origin of the coordinate system. The X-axis was defined along the exterior girder (on line A) while the Z-axis was defined in vertical direction (Figure 3-32). X-Y defined a horizontal plane. The position coordinates of the targets were measured on Dec. 16, 2010 with respect to the defined coordinate system. These coordinates serve as the baseline measurements to calculate bridge translations.

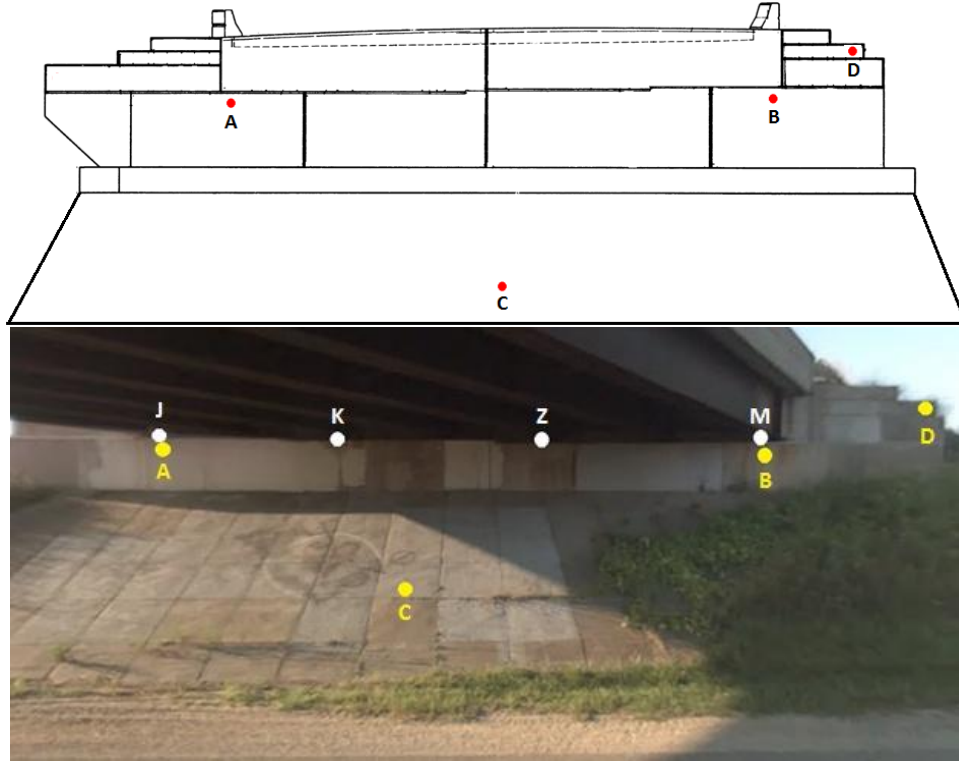


Figure 3-29. South abutment of the westbound bridge (targets on abutment and girder ends)

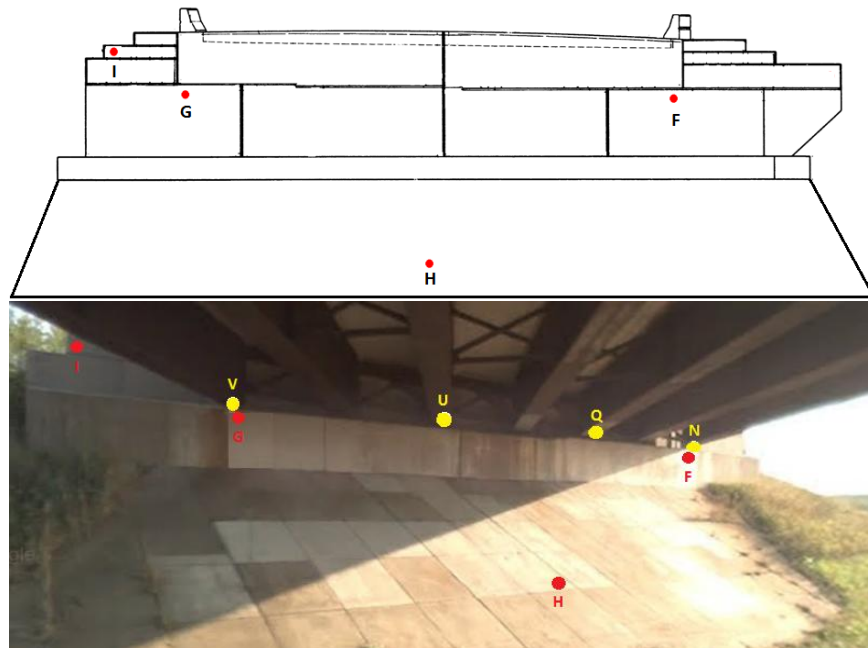


Figure 3-30. North abutment of the westbound bridge (targets on abutment and girder ends)

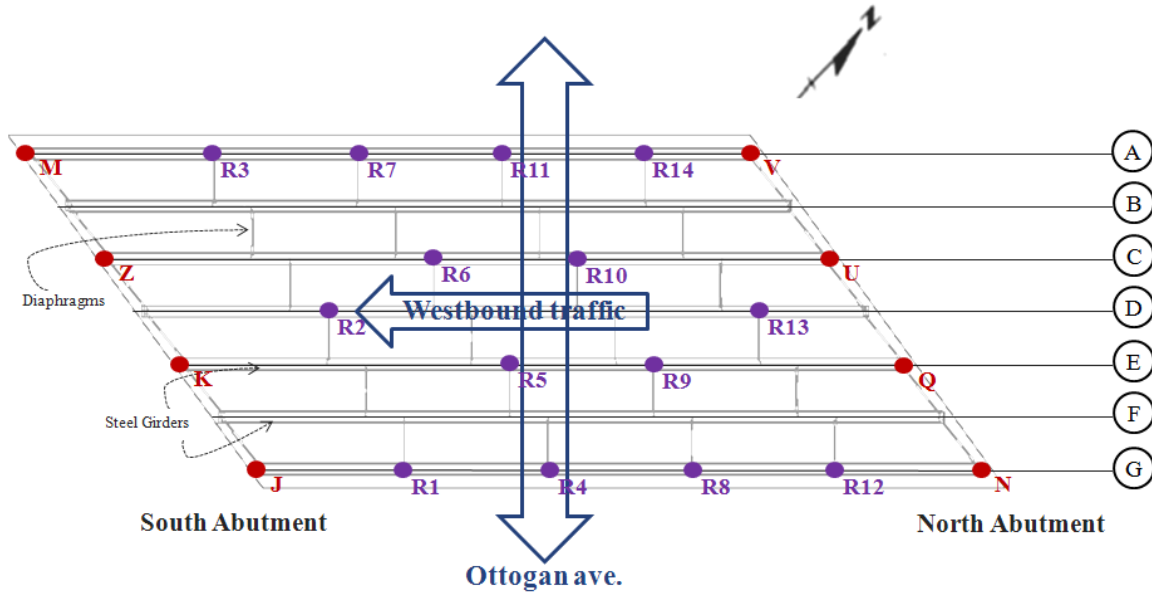


Figure 3-31. Target positions on girders

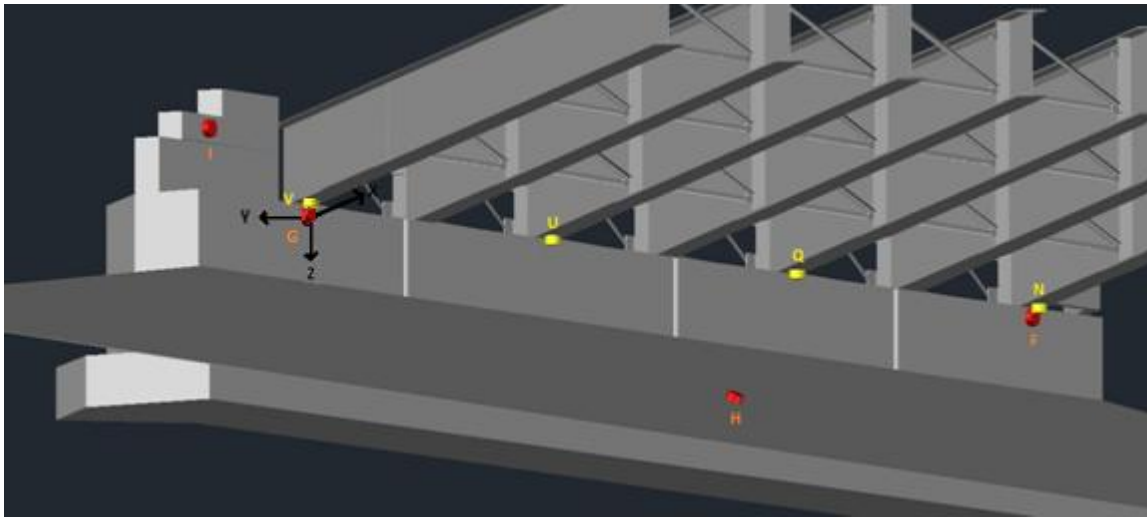


Figure 3-32. Coordinate system for Tracker measurements and target positions on north abutment and girder ends

Table 3-2. Ambient Conditions at 2:30pm on December 16 2010

Temperature (⁰ F)	32
Pressure (mmHg)	1181.91
Humidity (%)	51.7

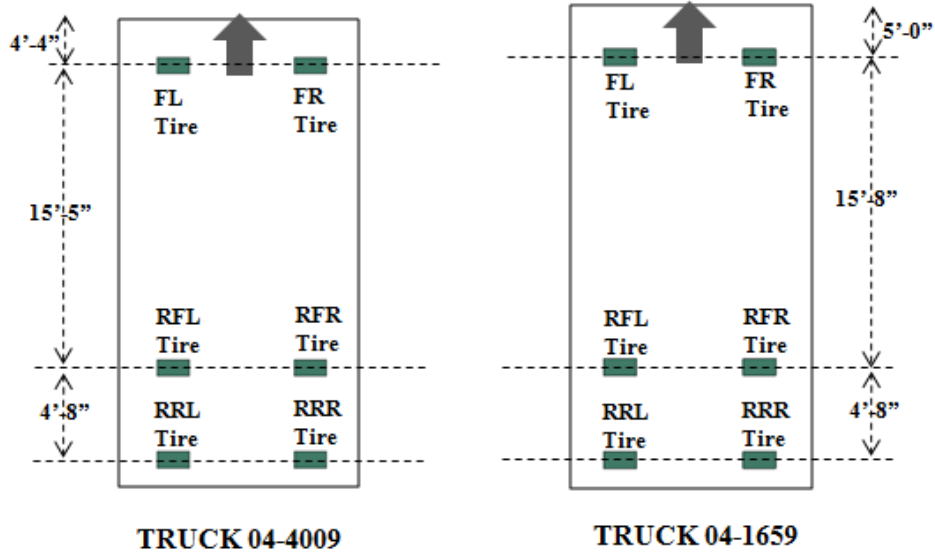
Table 3-3. Target Position Coordinates – Baseline Measurements (Dec. 16, 2010)

Reflector	Coordinates (in.)		
	X	Y	Z
A	892.5477	-472.3196	9.5949
B	1315.7579	4.0789	25.6603
C	965.7680	-166.5963	137.1540
D	1458.3465	119.4952	-18.3121
F	-434.1164	-488.0187	-11.3823
G	0	0	0
H	-78.4595	-313.7452	121.6880
I	42.8870	92.3908	-47.2806
J	884.1517	-486.8722	0.3646
K	1029.7024	-324.7426	5.3189
M	1310.6744	0.0678	16.0533
N	-432.4237	-482.4572	-23.9580
Q	-289.8550	-323.1314	-19.5721
U	-148.4056	-161.3447	-14.2191
V	-2.2858	2.6509	-9.2133
Z	1169.3041	-163.7294	10.6191

3.5.2 Bridge Deflection

3.5.2.1 Truck Configurations and Loading

The trucks, which were used for preliminary analysis, were not available on the day of load testing; hence, two similar trucks, shown in Figure 3-33 (Truck 04-4009 and Truck 04-1659), were used to serve the purpose. Four loading configurations similar to the preliminary analysis were used to load the bridge (Figure 3-34 and Figure 3-35).



(a) Truck configuration

Truck Tire Position	Truck 04-4009 (GVW per Tire)	Truck 04-1659 (GVW per Tire)
Front Left (FL)	8700 lbs	7650 lbs
Front Right (FR)	8900 lbs	7850 lbs
Rear Front Left (RFL)	10,650 lbs	10,150 lbs
Rear Front Right (RFR)	10,100 lbs	11,400 lbs
Rear Rear Left (RRL)	10,650 lbs	10,000 lbs
Rear Rear Right (RRR)	10,200 lbs	11,200 lbs

(b) Wheel loads (GVW: Gross Vehicle Weight)

Figure 3-33. Truck configurations and wheel loads

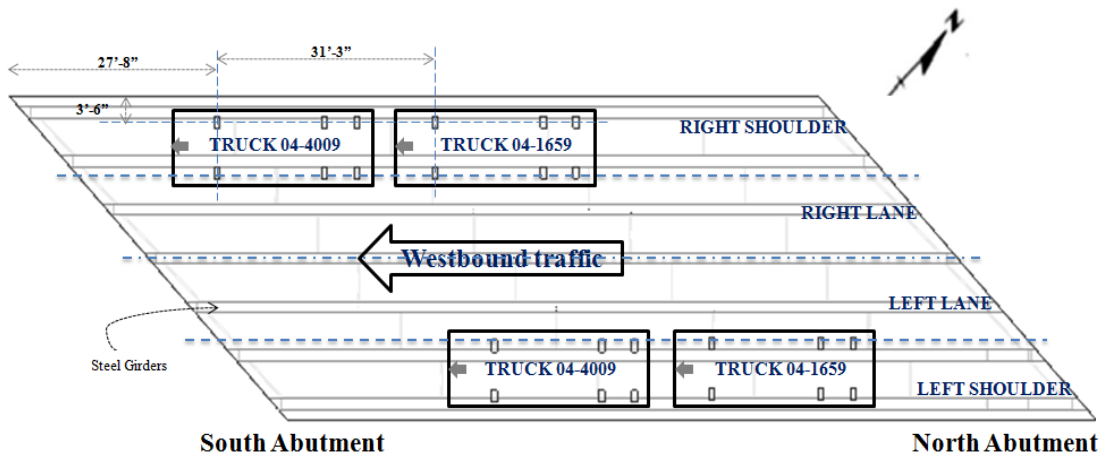


Figure 3-34. Truck positions and bridge configuration

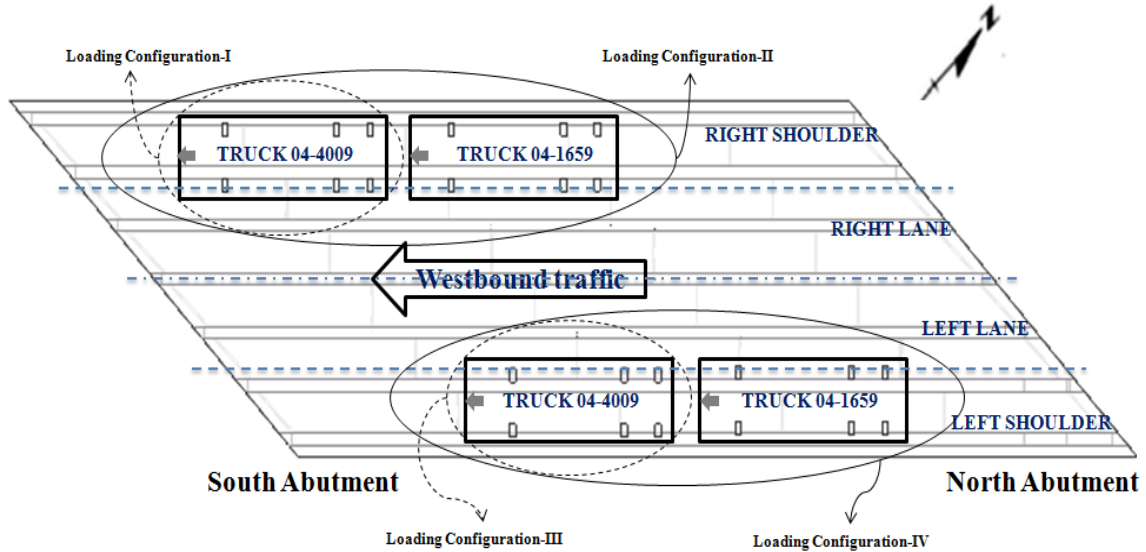


Figure 3-35. Mutually exclusive bridge loading configurations

3.5.2.2 Bridge Deflection

Deflections calculated from the FE model with ideal support conditions (i.e., girder ends over the north abutment are on fixed bearings and girder ends over the south abutment are on expansion bearings) are more than the measured values. The deflection calculated from the calibrated FE model, with support conditions incorporating frozen bearings, is more comparable to the measured displacements. The decision to include frozen bearing conditions in the FE model was based on visual inspection results detailed in section 3.3.2. Girder deflection comparisons from both FE analyses with field measurements are shown Figure 3-36 and Figure 3-37. All the raw data is presented in Appendix B. As seen from the figures, the forces developed at the girder ends due to static truck loads are not large enough to overcome the friction at the bearings; hence, bridge behavior under static truck loads resembles frozen bearing conditions.

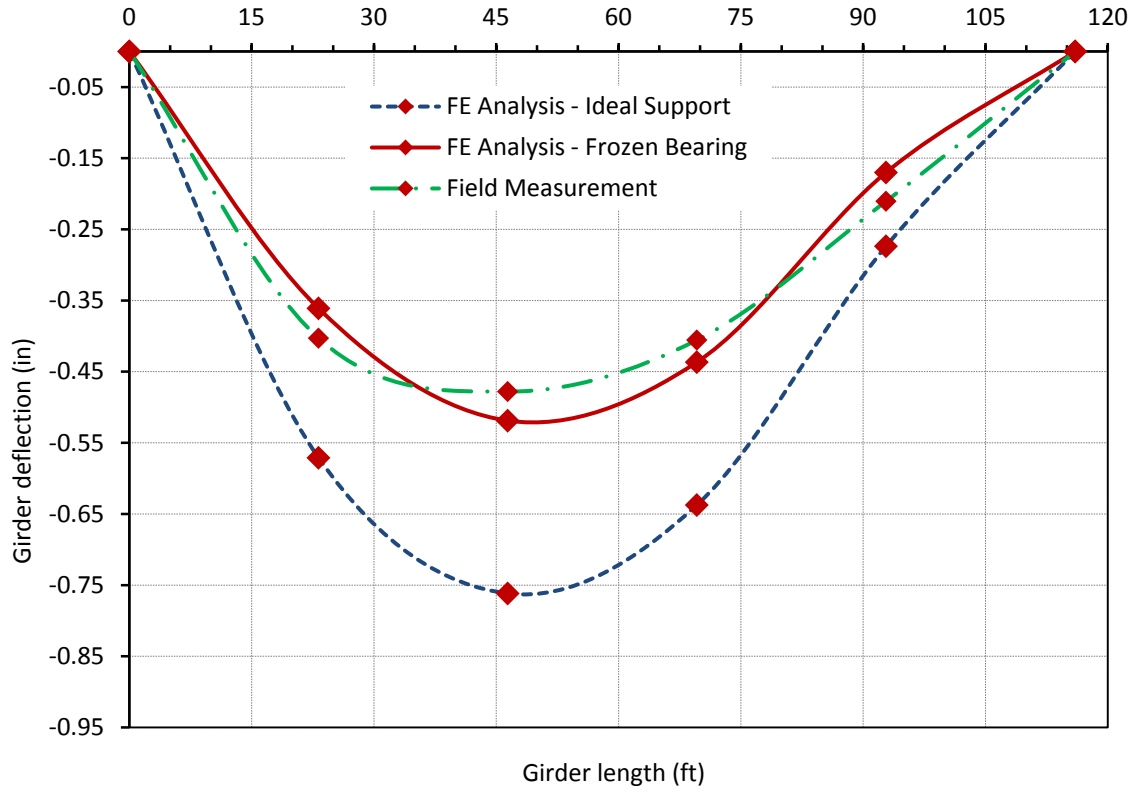


Figure 3-36. Girder A deflection under loading configuration II

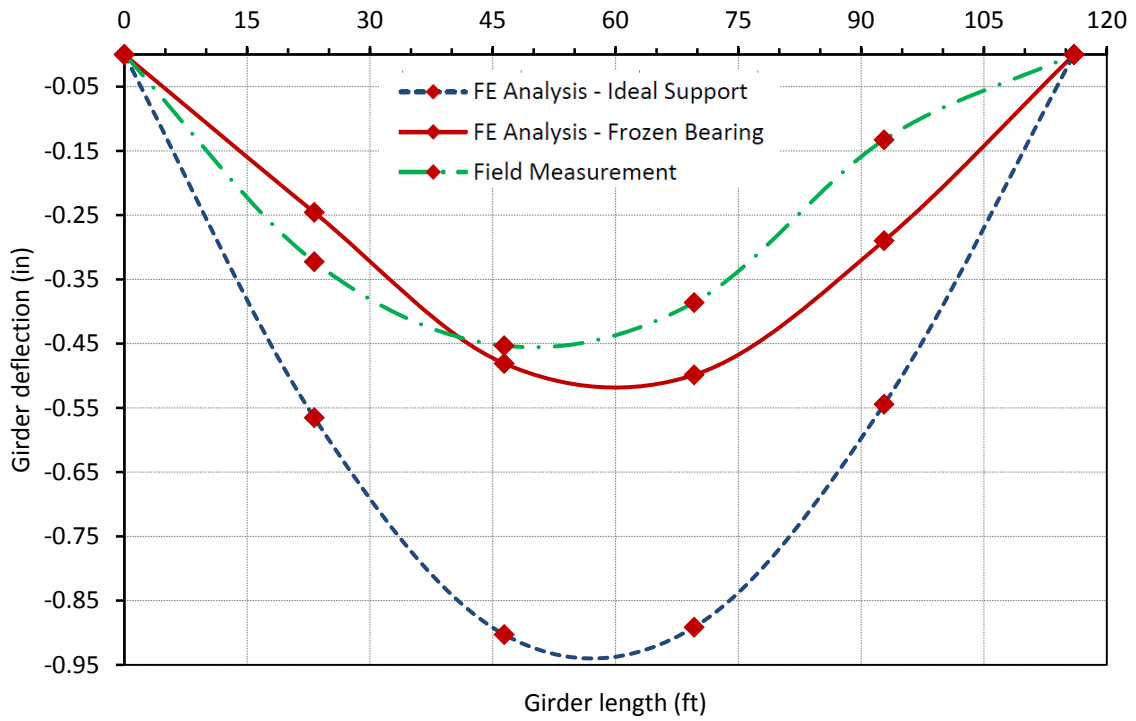


Figure 3-37. Girder G deflection under loading configuration IV

3.5.3 Bearing Translation

3.5.3.1 Bearing Translation under Truck Loads

Bearing movement over the south abutment is calculated using the FE model with ideal boundary conditions representing fixed and expansion bearings under each loading configuration and is depicted in Figure 3-38. Bearings move away from the bridge under truckloads because the neutral axis of the section is too close to the deck and pushes the girder bottom flange towards the abutment during bending as depicted in Figure 3-39. Under ideal boundary conditions (fixed and expansion), maximum bearing movement is less than 0.16 in., which is much smaller than the design movement.

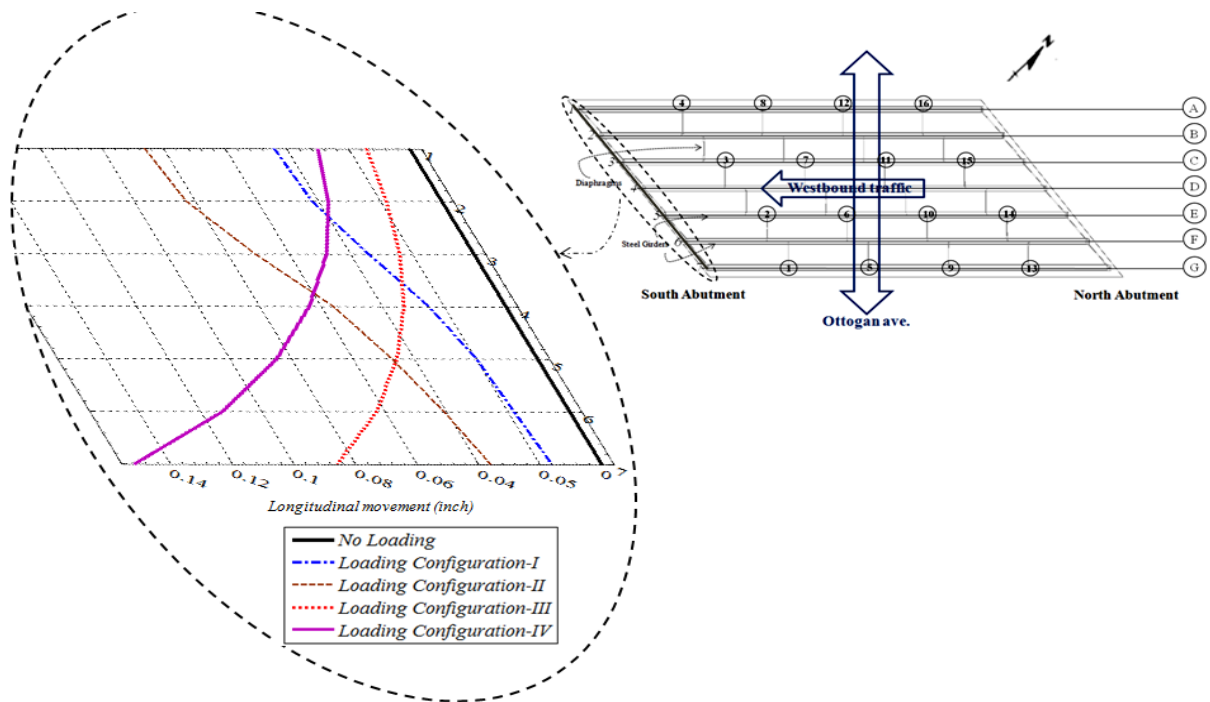
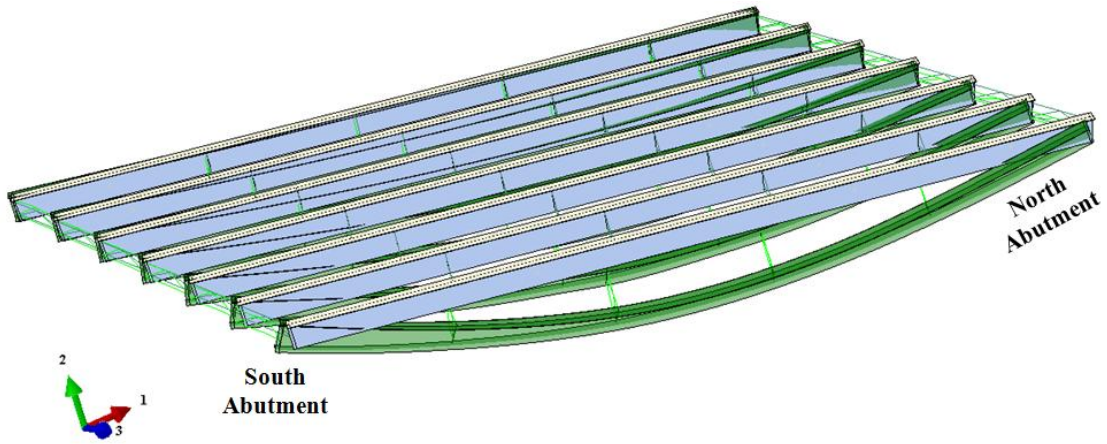
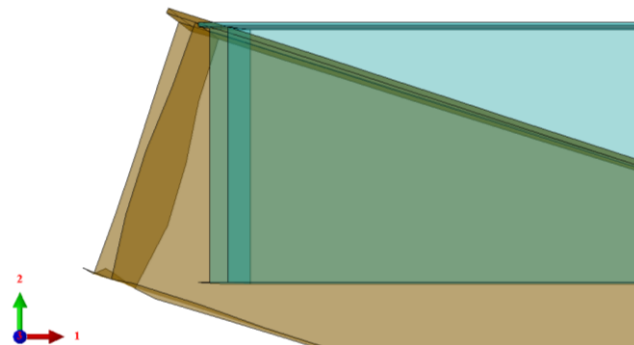


Figure 3-38. Bearing movement under truck loads (FE analysis)



(a) Isometric view of deformed and undeformed bridge



(b) Close-up of girder end movement

Figure 3-39. 3-D view of bearing movement (towards south abutment) under loading configuration IV

As measured bearing movements are depicted in Figure 3-40. The bearing movement measured for loading configurations I and II is in agreement predicted by FE analysis. It is worth stating that the maximum bearing movements under all loading configurations are very small. Tracker measurements show a similar trend in bearing movements as calculated from the FE model under loading configurations III and IV; but greater movements are measured at the acute corner (i.e., at target locations M and Z) than calculated from the FE model. Measured data, also shows that bearings do not slide back to their original positions at once upon the removal of live loads (Figure 3-41). The differences in measurements and FE analysis can be attributed to the bearing friction. These observations support the observations made during deflection calculation under static truckloads and calibration of the FE model using frozen bearing conditions.

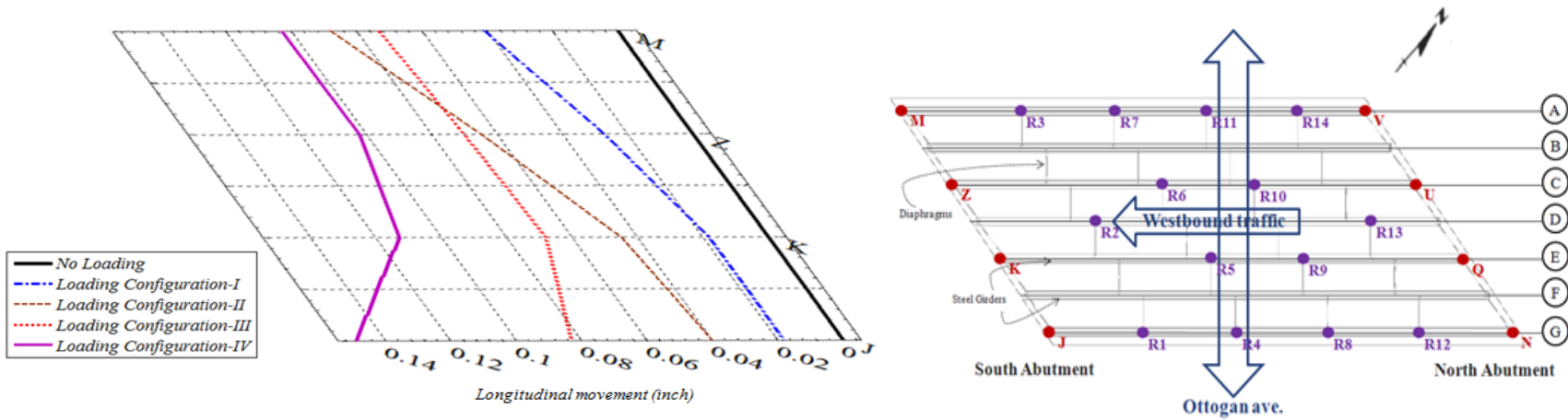


Figure 3-40. Bearing movement under truck loads (Tracker measurements)

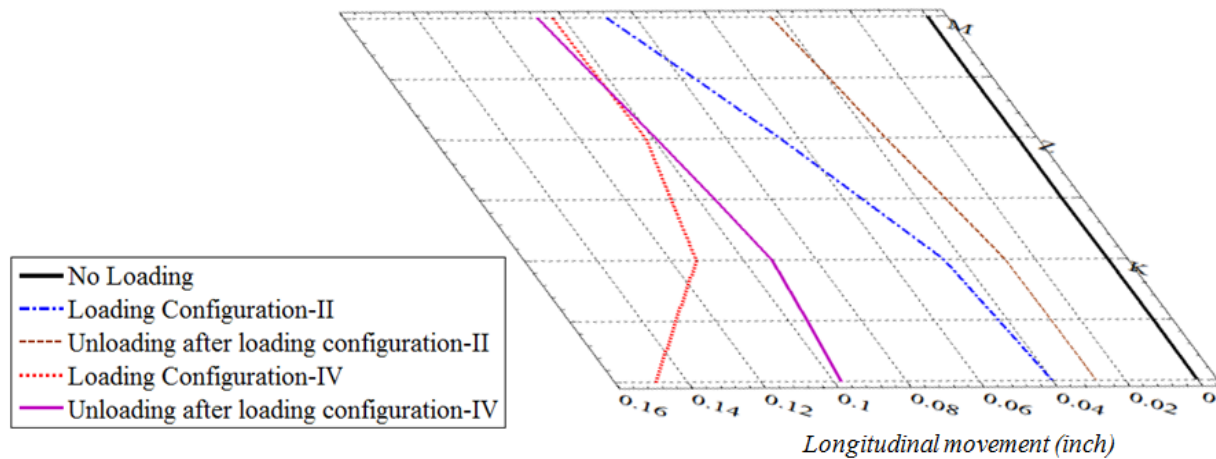


Figure 3-41. Bearing positions after loading and unloading following load configuration II and IV

3.5.3.2 Bearing Translation under Thermal Loads

Calculated bearing translations with the FE model under uniform thermal expansion and contraction as per AASHTO LRFD (2010) procedure B are given in Table 3-4 and shown in Figure 3-42. Calculated maximum bearing translation due to expansion ($\Delta T = 45^{\circ}\text{F}$) and contraction ($\Delta T = 70^{\circ}\text{F}$) occurs at the end of girder A. The bearing should allow 0.5 in. expansion and 0.77 in. contraction movement under girder A, which gives a total movement of 1.27 in. Though this movement is less than 1.875 in., shown in the bridge plans, the position of the dowel bar may not have been near the center. Also, dowel bar damage indicates lack of sufficient travel allowed for the bearing.

Tracker measurements were made to establish bearing travel over the south abutment under thermal changes. The initial measurements were made on December 16, 2010 and repeated on May 10, 2011 and again on July 13, 2011 (Figure 3-45). Ambient temperatures at the time of measurements on December 16, May 10, and July 13 are 32°F , 82.6°F , and 67.3°F . Bridge expansion is not due to daily temperature changes; it is due to the average temperature variation during a specific time period. Hence, maximum, minimum, and average temperature variation at the site from December to August are obtained from a nearby weather station, as shown in Figure 3-43 and Figure 3-44. According to Figure 3-44, average temperatures at the site on December 16, May 10, and July 13, are 27.5°F , 55°F , and 75°F , respectively. Hence, temperature difference from December 16 to May 10 and December 16 to July 13 are 25.7°F and 47.5°F , respectively. Calculated expansions at bearing from December 16 to May 10 and from December 16 to July 13 are 0.3 in. and 0.52 in. According to the calculations, the bearing at location M, shown in Figure 3-45, is expected to move 0.22 in. from May 10 to July 13. As shown in Figure 3-45, there was hardly any movement at bearing M (< 0.01 in.). However, there is 0.05 in. movement at bearing J, an indication that there is some rotation of the bridge deck about its normal axis. The observations indicate that there is significant restraint for movement.

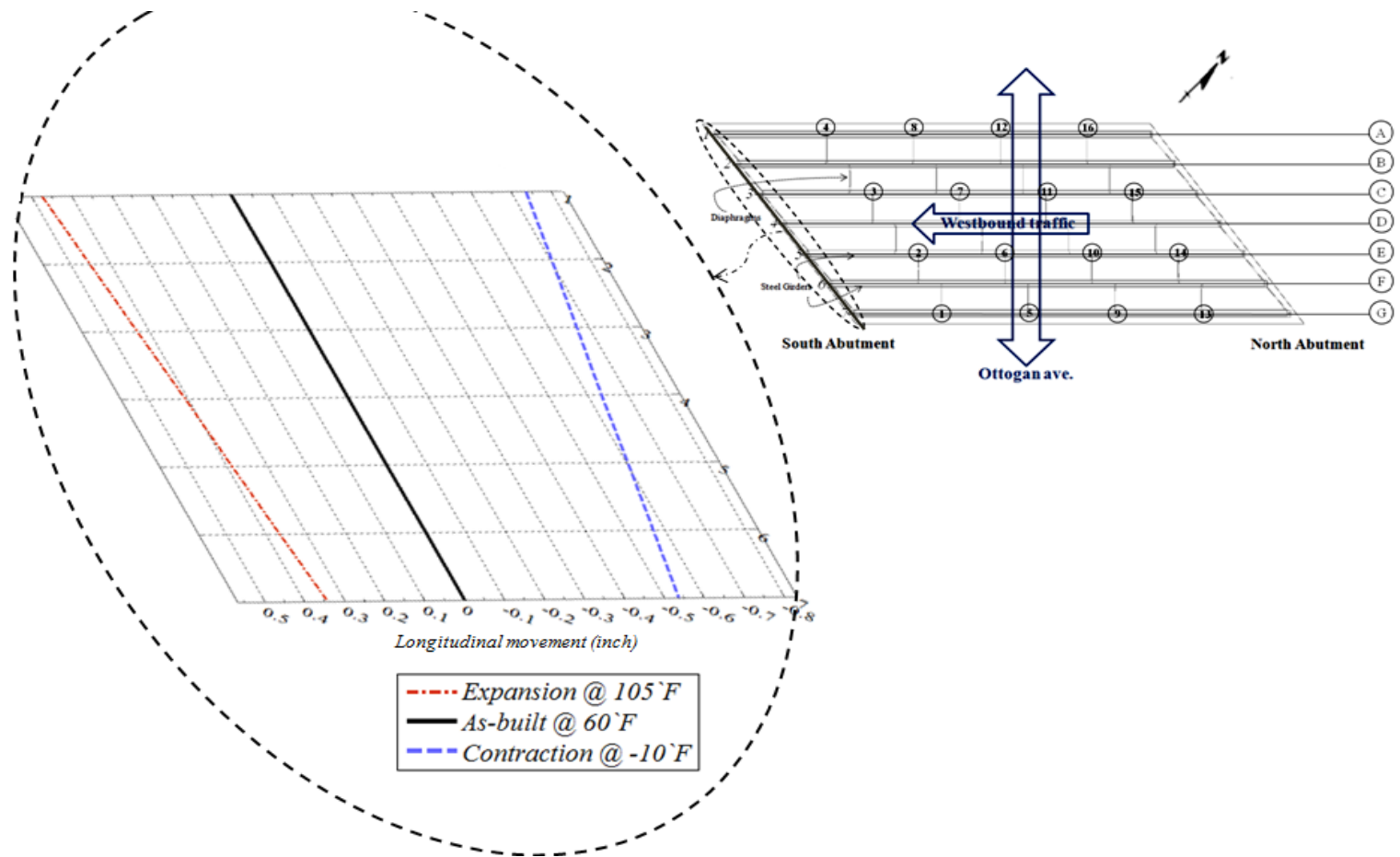


Figure 3-42. Bearing translation under uniform thermal loads (FE analysis)

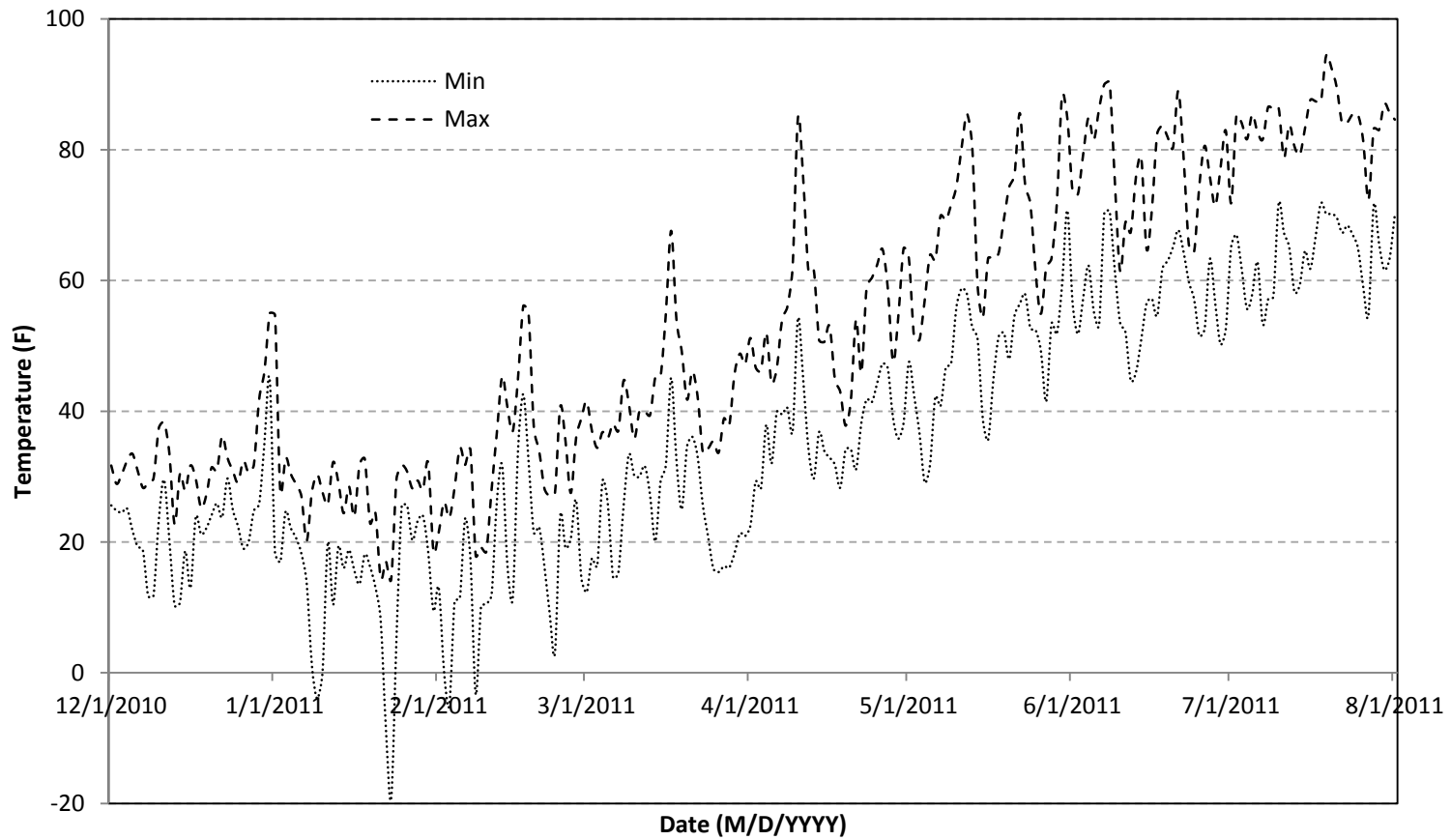


Figure 3-43. Maximum and minimum daily temperature variation at the site

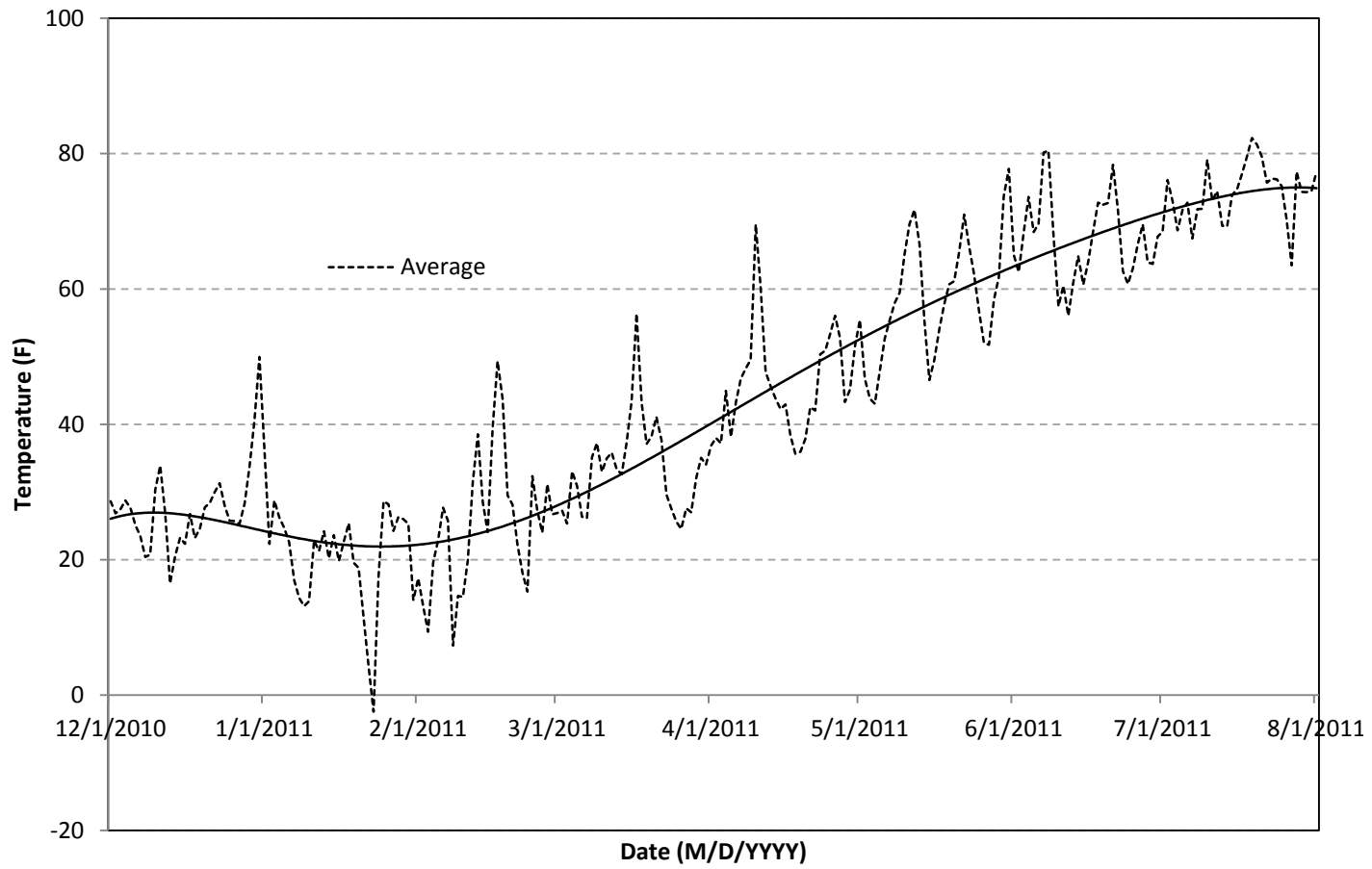
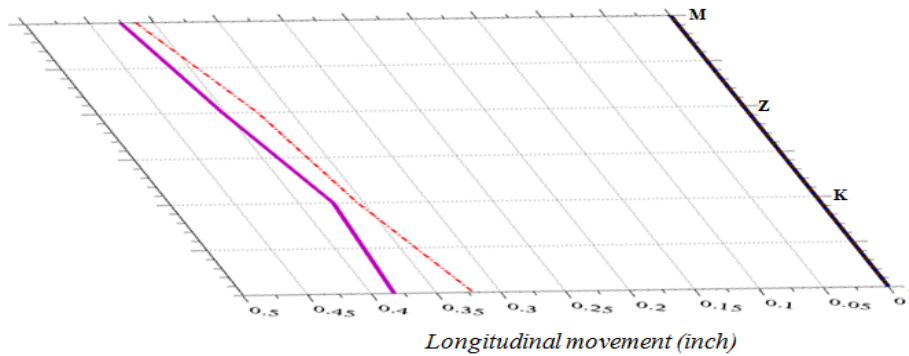


Figure 3-44. Average temperature variation at the site

Table 3-4. Girder-End Translations over South Abutment under Uniform Temperature Loading

Girder Label	FE Analysis (in.) ⁺	
	Expansion (in.) at 105 ^o F ($\Delta T = 45^{\circ}\text{F}$)	Contraction (in.) at -10 ^o F ($\Delta T = -70^{\circ}\text{F}$)
A	-0.474	0.737
B	-0.452	0.703
C	-0.430	0.669
D	-0.408	0.635
E	-0.387	0.602
F	-0.366	0.569
G	-0.344	0.535

+ Temperature at the time of construction is 60^oF



--- Expansion on May 10, 2011 (82.6 F)
 — Expansion on July 13, 2011 (67.3 F)

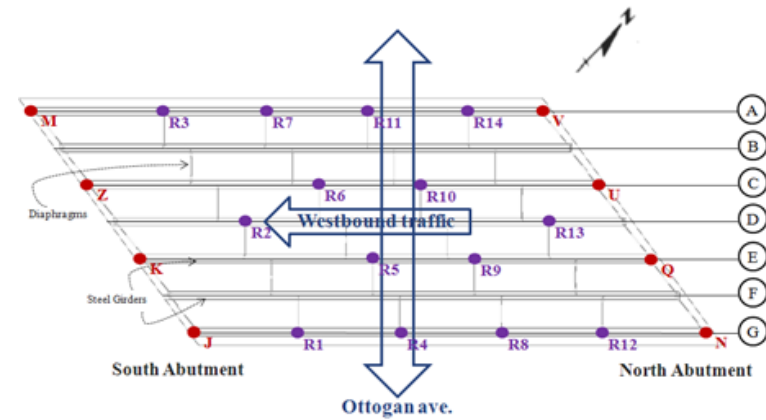


Figure 3-45. Bearing translation from Dec. 2010 to May 2011 and July 2011 (Tracker measurements)

3.6 SUMMARY

Bridge deflections and bearing translations were measured under static truck as well as thermal loads. Measured girder deflections showed that girder end movements were restrained due to friction. It is worth mentioning here that the bearing movements under static truck loads were very small compared to allowance made at the design for thermal expansion and contraction. The measured bearing movement under thermal expansion loads from May to July indicates that the bearings are frozen and the in-plane twist of the deck occurs due to bearing movement that is not expected at the design stage. Though there was no damage to the superstructure and substructure of this 120 ft long single span bridge, this behavior is critical when link slabs are implemented and the deck over the abutments is made continuous. The observations highlight the importance of using durable bearings that are capable of accommodating large deformation and a certain degree of rotation demands.

4 LINK SLAB ANALYSIS AND DESIGN GUIDELINES

4.1 OVERVIEW AND OBJECTIVES

The objective of this chapter is to present a detailed analysis of skew link slabs and moment and force demand envelopes with respect to the skew angle at the link slab section directly over the pier centerline. The analysis is performed for a specific bridge configuration (i.e., span length, width, and girder type), at various skew angles from 0° to 45° . The finite element (FE) models, for selected skew configurations, up to 45° , are analyzed under loads and configurations specified in AASHTO (2010). Further, the influence of different bearing configurations on the link slab moment and force resultants are also investigated. Finally, the design recommendations are developed for the utilization of links slabs in high skew bridges. The design recommendations are developed based on literature review, analysis results, and AASHTO (2010) requirements on strength and service load combinations.

4.2 CONTACT SIMULATION

The full-bridge FE models are developed using a detailed model of the link slab, deck, and girders. Unfortunately when doing so, differences in the mesh densities prevent nodes on different components from coinciding, thus preventing a way to “tie” the components together. Fortunately, the contact surface options available in Abaqus/Standard version 6.10.1 are available to overcome this challenge (Abaqus 2010). Table 4-1 summarizes contact surface option syntax used. For further information on the functions and use of each option can be found in Romkema et al. (2010).

Table 4-1. ABAQUS Syntax for Various Contact Options

Row	Contact Definitions	ABAQUS Syntax
a	General contact (automatic option)	*CONTACT *CONTACT INCLUSIONS, ALL EXTERIOR
b	General contact (user defined option)	*CONTACT *CONTACT INCLUSIONS surface_1, surface_2
c	Contact pair with separation	*CONTACT PAIR, INTERACTION=interaction1, ADJUST=nodes_to_adjust_to slave_surface, master_surface *SURFACE INTERACTION, NAME=interaction1
d	Contact pair with tied option	*CONTACT PAIR, INTERACTION=interaction1, TIED, ADJUST=nodes_to_adjust_to slave_surface, master_surface *SURFACE INTERACTION, NAME=interaction1 *SURFACE BEHAVIOR, NO SEPARATION
e	Contact pair with friction	*CONTACT PAIR, INTERACTION=interaction1 slave_surface, master_surface *SURFACE INTERACTION, NAME = interaction1 *FRICTION 1.0, 0.0, 0.0, 0.0

4.3 MODELING AND ANALYSIS OF A LINK SLAB BRIDGE

4.3.1 Overview and Objectives

The objective is to design and analyze high-skew bridges that meet current design standards. A prototype bridge is identified and modified so that it complies with current standards. Next, the bridge is modeled with contact surface options so that the link slab debonding from the girders is accurately represented. Boundary conditions are prescribed, and the AASHTO LRFD specified loads and combinations are applied. Lastly, the results are extracted, post-processed, and presented in graphical/tabular format.

4.3.2 Prototype Bridge

An in-service bridge, S12-7 of 25042, is identified for finite element (FE) modeling (Figure 4-1). The bridge carries eastbound I-69 over I-75 in Flint, Michigan. The bridge consists of two 69 ft 6 in. spans with a 1 in. gap between girders at the center pier for a total length of 139 ft 1 in. The bridge features a 9 in. thick concrete deck with five PCI Type III girders spaced at 66 in. The bridge was designed in 1966 to handle two lanes of traffic and does not meet current design standards; specifically the shoulder width is narrow. As a result, additional girders are added to make the bridge comply with the current standards.

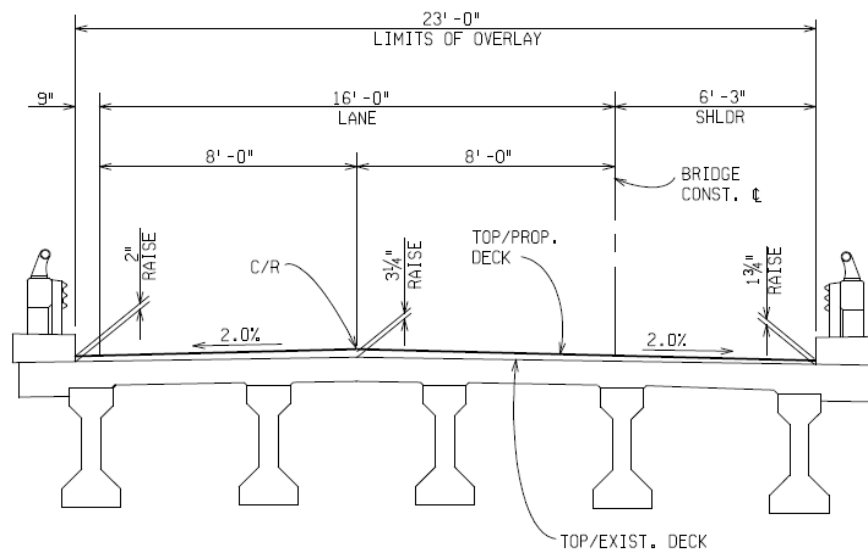


Figure 4-1. Cross section of Bridge S12-7 of 25042

4.3.3 Material Properties

The girder and deck concrete properties are assumed the same. Bridge deck concrete strength specified in MDOT design (f'_c) is 4500 psi (MDOT 2009). The modulus of concrete is calculated using Eq. 4-1 as per AASHTO Section 5.4.2.4 (AASHTO 2010). The unit weight of concrete (w_c) is assumed to be 0.15 kcf. The Poisson's ratio of 0.2 is used per AASHTO Section 5.4.2.5. Thermal expansion coefficient of $6.00 \times 10^{-6} / ^\circ\text{F}$ is used (AASHTO 2010, section 5.4.2.2).

$$E_c = 33,000 \times w_c^{1.5} \times \sqrt{f'_c} \quad (4-1)$$

4.3.4 Bridge Model Geometry

The current MDOT bridge design guide requires different shoulder widths depending on the number of traffic lanes. The existing bridge has two lanes of traffic. Each traffic lane width is 12 ft, as required for highways. A median shoulder of 8 ft and an outside shoulder of 8 ft plus 2 ft, or 10 ft, are required for an average daily traffic volume of 2000 vehicles per day or above (Figure 4-2) (MDOT 2011).

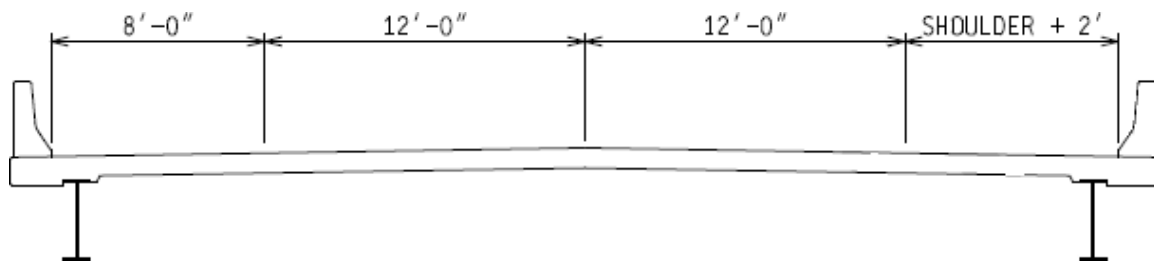


Figure 4-2. Current MDOT requirements for two-lane highway bridges

Bridge barriers are assumed to be MDOT New Jersey Type 4 (Figure 4-3) (MDOT 2011). In addition, the deck is to extend 1.5 in. beyond the barrier per drawings but is modeled as 2.25 in. to be compatible with the smallest FE mesh increment.

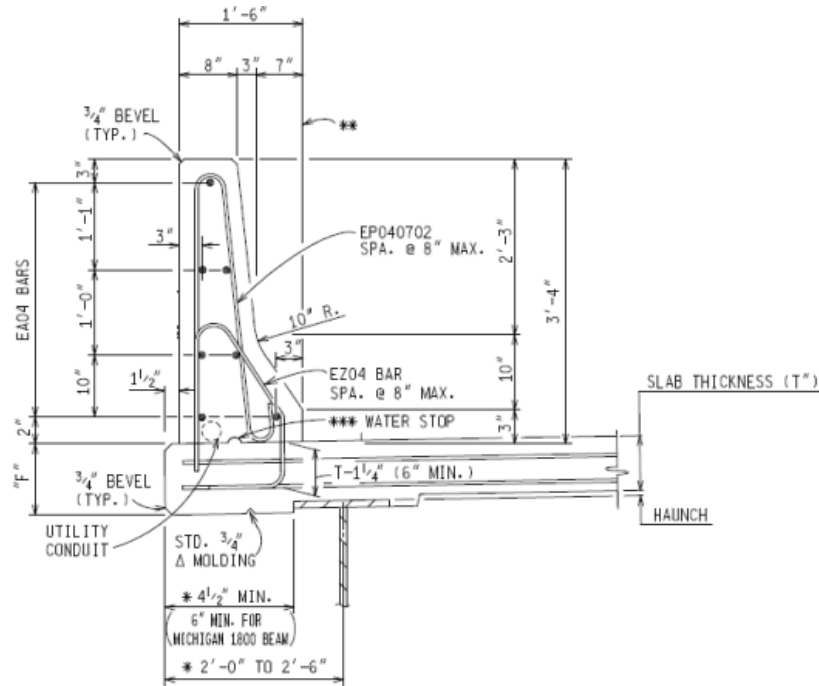


Figure 4-3. MDOT New Jersey Type 4 barriers

The deck thickness is kept at 9 in., and the crown is neglected. With girders spacing at 66 in., the final bridge cross section is shown in Figure 4-4. The FE model does not include barriers except as dead load as they are assumed not to contribute to structural capacity. The FE bridge model length is 139 ft 1 in. The model consists of two 69 ft 6 in. spans and a 1 in. gap between girder ends at the center pier (Figure 4-5).

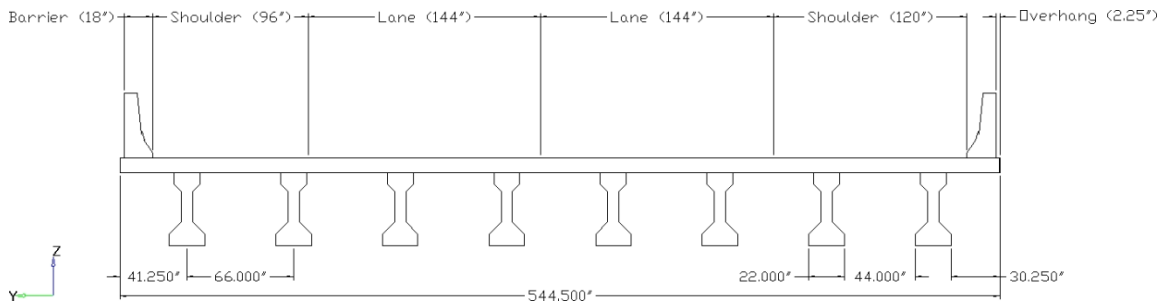


Figure 4-4. Cross section of bridge

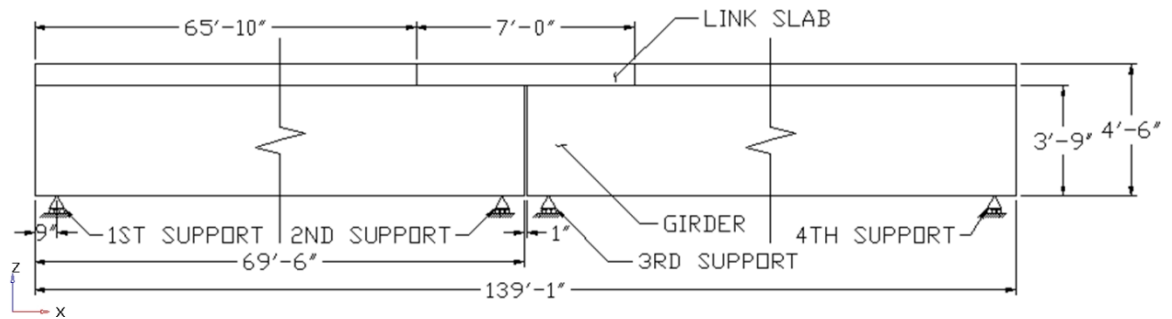


Figure 4-5. Elevation view of FE bridge

4.3.5 Bridge Model Orientation

The longitudinal axis of the bridge, along the direction of traffic, is defined as the X-axis. The transverse direction of the bridge is along the Y-axis, and gravity loads act along the negative Z-axis. A labeling system is also devised. The bridge orientation is assumed to run from south to north where the “South” end of the bridge lies at the origin along the X-axis. The span closer to the south end of the bridge is named “Span A,” and the remaining span as “Span B.” Girders are then numbered 1 to 8 with increasing index from east to west. Axis layout and the bridge labeling system are shown in Figure 4-6.

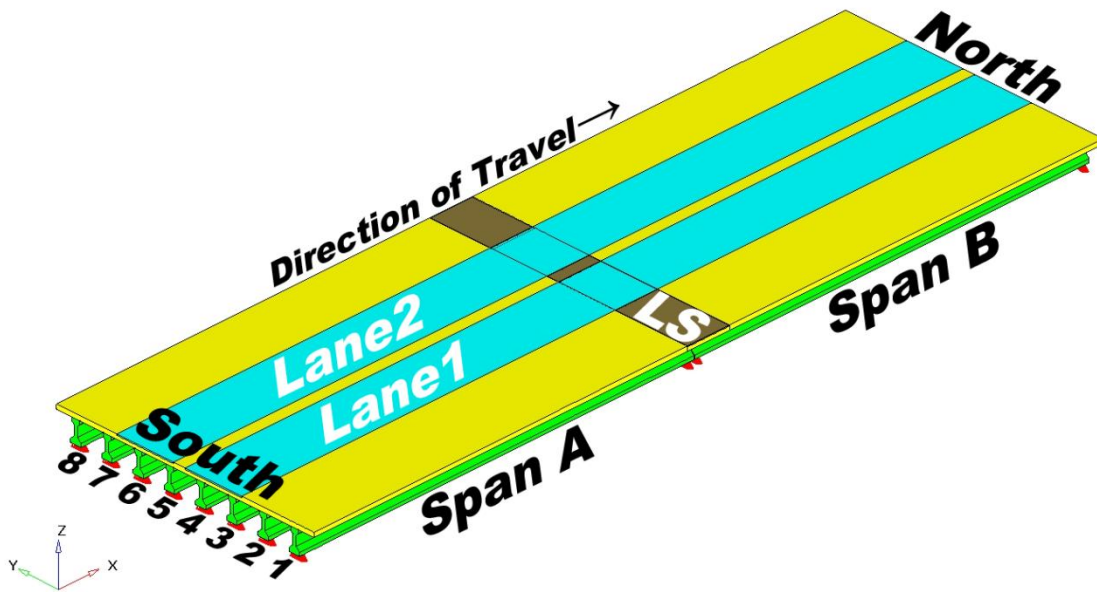


Figure 4-6. Bridge model orientation and labeling system

4.3.6 Link Slab Length

Ulku et al. (2009) recommends a link slab length of 5% of the span length. The link slab length would then be 5% of 69 ft 6 in. multiplied by 2 spans plus 1 in. for the gap between girders (i.e., 84.4 in.). The link slab length of 84 in. is used in the model for compatibility with the FE mesh.

4.3.7 FE Discretization of the Bridge Model

4.3.7.1 Discretization of the Link Slab

Element width (along the y-axis) of 4.125 in. is selected for the deck and link slab. Mesh needed to be refined at the link slab region for improved accuracy of the stresses. An element height (along the z-axis) of 1.5 in. is used to allow for a node line along the mid-height of the link slab. The length (along the x-axis) of the link slab elements must be determined in such a way that a node line lies along the middle of the gap between the girder ends. This is to allow calculation of the forces and moments along that middle section. Hence, an element length of 2 in. is selected for the link slab region. Finally, the element length adjacent to the deck is increased to 2.5 in. to satisfy the link slab length requirement. The resulting FE mesh is shown in Figure 4-7 and Figure 4-8.

4.3.7.2 Discretization of the Deck

Uniform element width of 4.125 in. is chosen for the deck. Since stresses in the deck are not of focus in this research, a coarser mesh with an element length of 10 in. is used for the remainder of the deck outside the link slab region. A deck element thickness of 2.25 in is used.

4.3.7.3 Discretization of the Girders

A coarser mesh with 10 in. long elements is chosen for the girders since accurate girder stresses are not required. Mesh length near the bearings is reduced to 4.5 in. for accurate placement of support restraints.

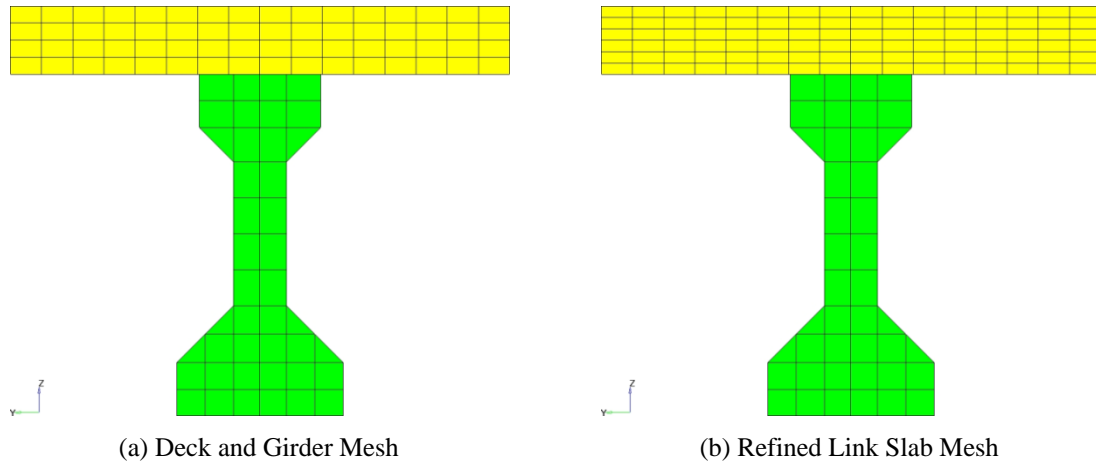


Figure 4-7. Cross section view of single girder and deck

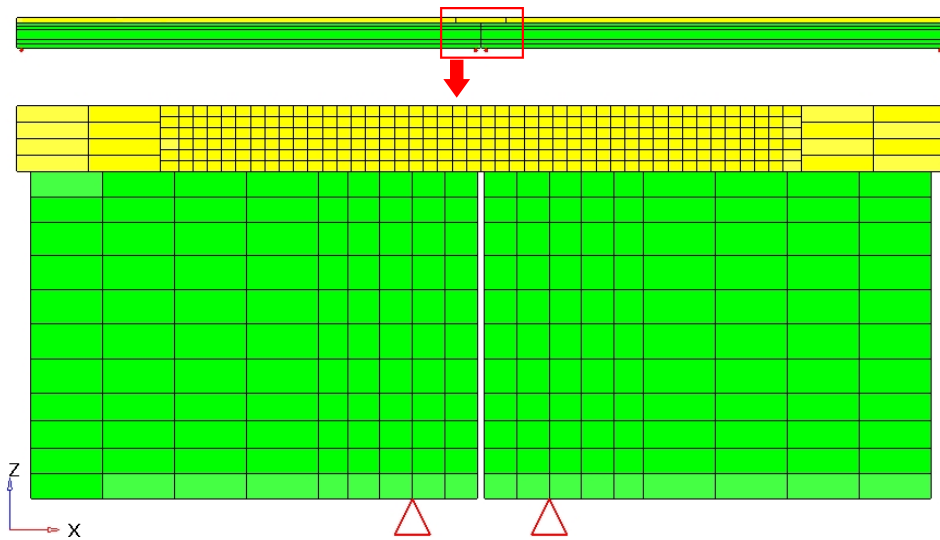


Figure 4-8. Elevation view of mesh at link slab region

4.3.8 Skew Mesh

The FE mesh is first developed for a straight bridge. The mesh is altered to generate bridge models with the same structure and with skew angles of 20°, 30°, and 45°. Link slab and deck element skew match bridge skew so that a surface parallel to the skew angle directly over the pier centerline is generated to calculate the link-slab force resultants. The MDOT Bridge Design Manual (2009) requires the concrete I-beam ends to be square for all angles of skew. As a result, girder elements are not skewed, but rather the entire girder is offset so that the center of the girder end is along the angle of skew. The FE models for all skews are shown in Figure 4-9, and mesh details are shown in Figure 4-10.

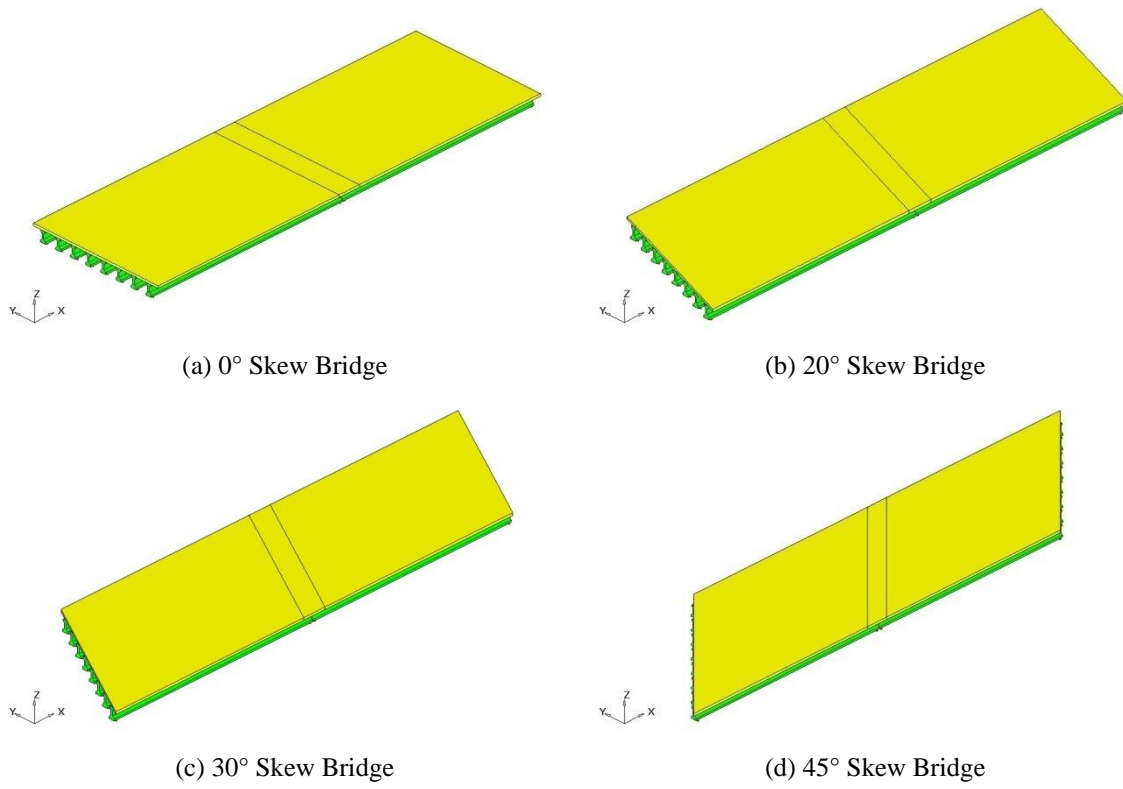


Figure 4-9. Isometric view of bridge models

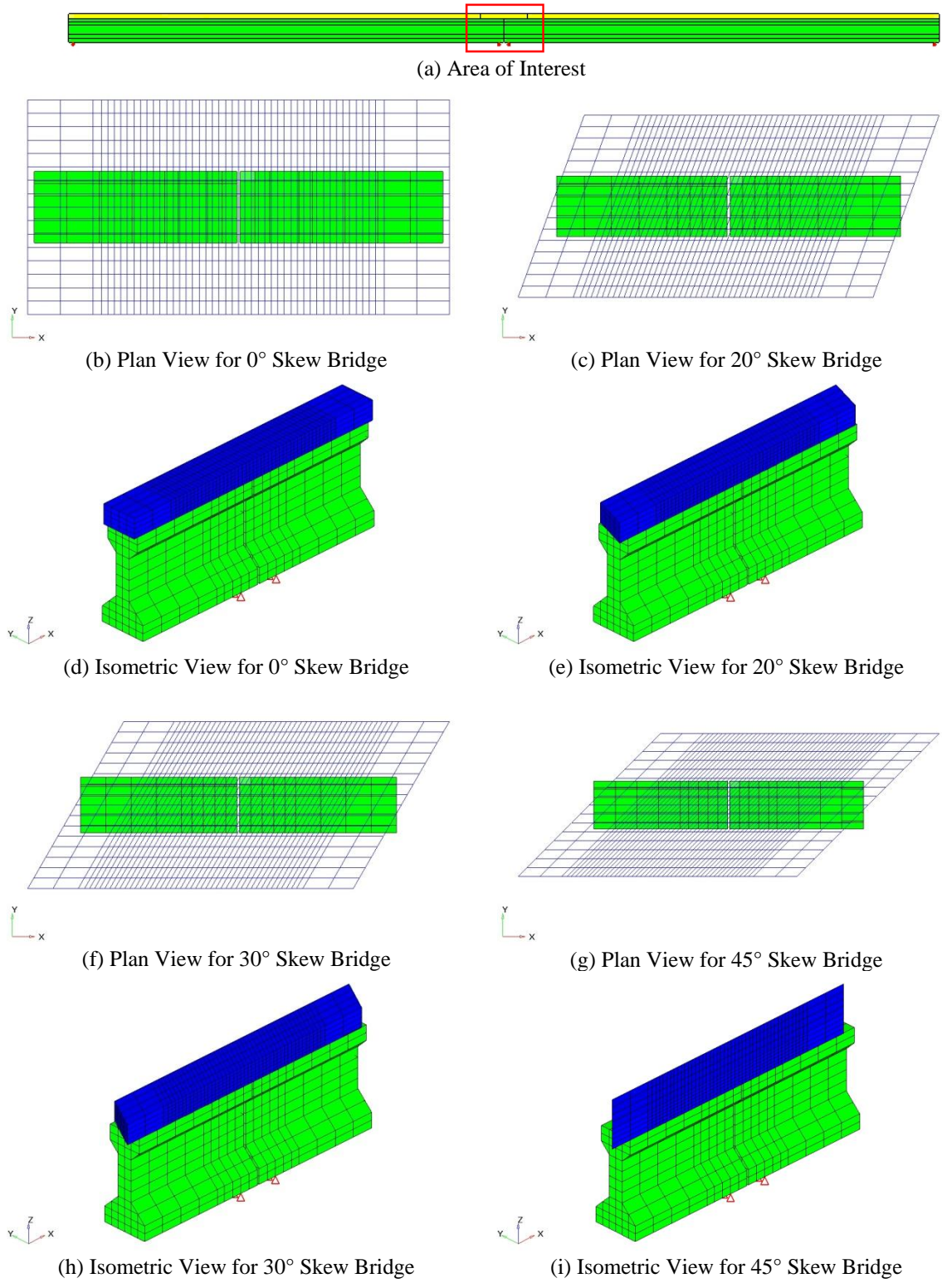


Figure 4-10. Skew link slab mesh

4.3.9 Contact Surfaces in the FE Model

Contact surfaces are created at the interfaces between each section: link slab and deck, link slab and girders, and deck and girders. The surface-to-surface option is used for optimized stress accuracy on the surface. The top surface of the girder is defined as the master surface and the link slab and deck as slave surfaces. Between the deck and the link slab interface, the deck is defined as the master surface. The surfaces are shown in Figure 4-11. The ‘NO SEPARATION’ with ‘TIED’ option is used for the contact between the deck and girders as well as the deck and the link slab. The contact between the link slab and the girders is established without the ‘TIED’ option in order to allow separation of the link slab from the girders. Contact surface definitions are given in Figure 4-12.

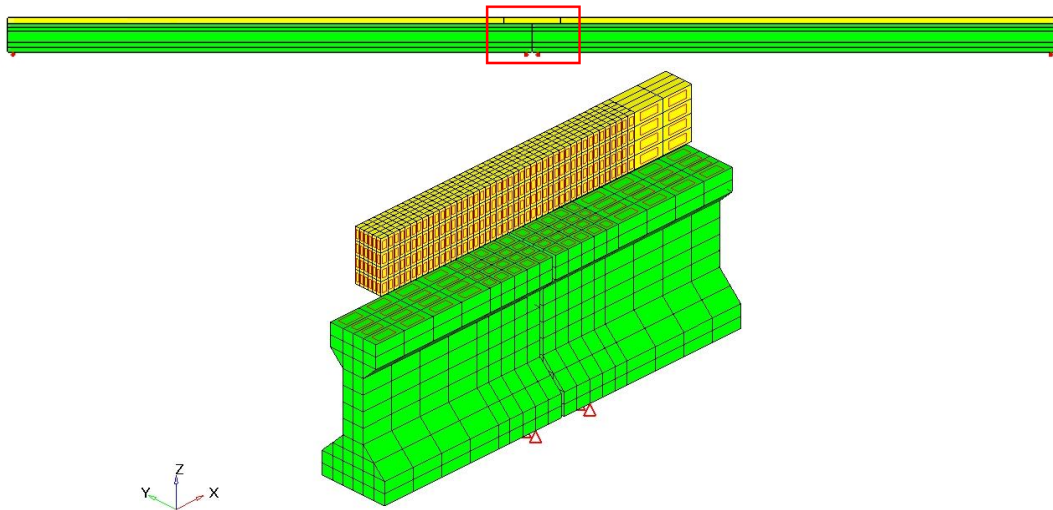


Figure 4-11. Contact surfaces in the FE models

```
*SURFACE INTERACTION, NAME = int_sep
*SURFACE INTERACTION, NAME = int_nosep
*SURFACE BEHAVIOR, NO SEPARATION
**
*CONTACT PAIR, INTERACTION=int_sep, TYPE=SURFACE TO SURFACE
surf-ls_bot, surf-girder_top
*CONTACT PAIR, INTERACTION=int_nosep, ADJUST=nset-girder_adj, TIED,
TYPE=SURFACE TO SURFACE
surf-deck_bot, surf-girder_top
*CONTACT PAIR, INTERACTION=int_nosep, ADJUST=nset-girder_adj, TIED,
TYPE=SURFACE TO SURFACE
surf-ls_south, surf-spana_north
*CONTACT PAIR, INTERACTION=int_nosep, ADJUST=nset-girder_adj, TIED,
TYPE=SURFACE TO SURFACE
surf-ls_north, surf-spanb_south
```

Figure 4-12. Abaqus syntax used in FE bridge model

4.3.10 Boundary Conditions

Elastomeric bearing pads supporting girder ends allow movement and rotation of the girder ends while providing limited restraint. Research conducted by Ulku et al. (2009) identified that the difference between the restraining effects of the bearing pads and the ideal support conditions on the link slab stresses are negligible. Accordingly, the ideal boundary conditions are specified in the models.

Three different bearing configurations are investigated: hinge-roller-roller-roller (HRRR), roller-hinge-hinge-roller (RHHR), and roller-roller-hinge-roller or roller-hinge-roller-roller (RRHR or RHRR). The first support (roller or hinge) is the boundary condition over the first abutment, the second support is the boundary condition over the pier, and so forth. This can be visually seen in Figure 4-13 and Table 4-2.

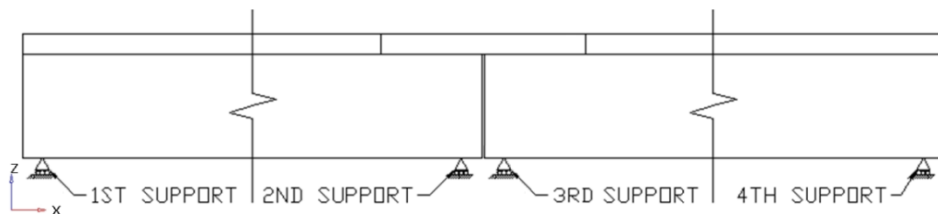


Figure 4-13. Bearing configuration layout

Table 4-2. Bearing Configurations and Corresponding Support Conditions

Bearing Configuration	1 st Support (Abutment)	2 nd Support (Pier)	3 rd Support (Pier)	4 th Support (Abutment)
HRRR	H	R	R	R
RHHR	R	H	H	R
RRHR (RHRR)	R (R)	R (H)	H (R)	R (R)

R = roller, H = hinge

4.3.11 Loads

The purpose here is to establish the design moment and axial force envelopes in the link slab under various skew conditions. Five load cases are defined for this purpose. The first four cases are truck and lane loads (i.e., AASHTO HL-93), and the last two cases are thermal gradient loads. Deck and girder self weight effects on the link slab are often eliminated when link slab placement is the last activity. In addition, barrier load effects are eliminated when link slabs are implemented as part of a repair activity.

4.3.11.1 Live Loads

The AASHTO HL-93 live load, consisting of a truck load and a lane load, is used. Loading patterns are shown in Figure 4-14 with detailed dimensions in Figure 4-15. Wheel loads, shown in Figure 4-15, include the dynamic amplification factor of 1.33. In addition, a 640 pound per linear foot lane load is applied. The load is represented as a pressure load over a 10 ft wide lane. However, due to mesh resolution, the lane width load is applied over 9 ft 11.625 in.

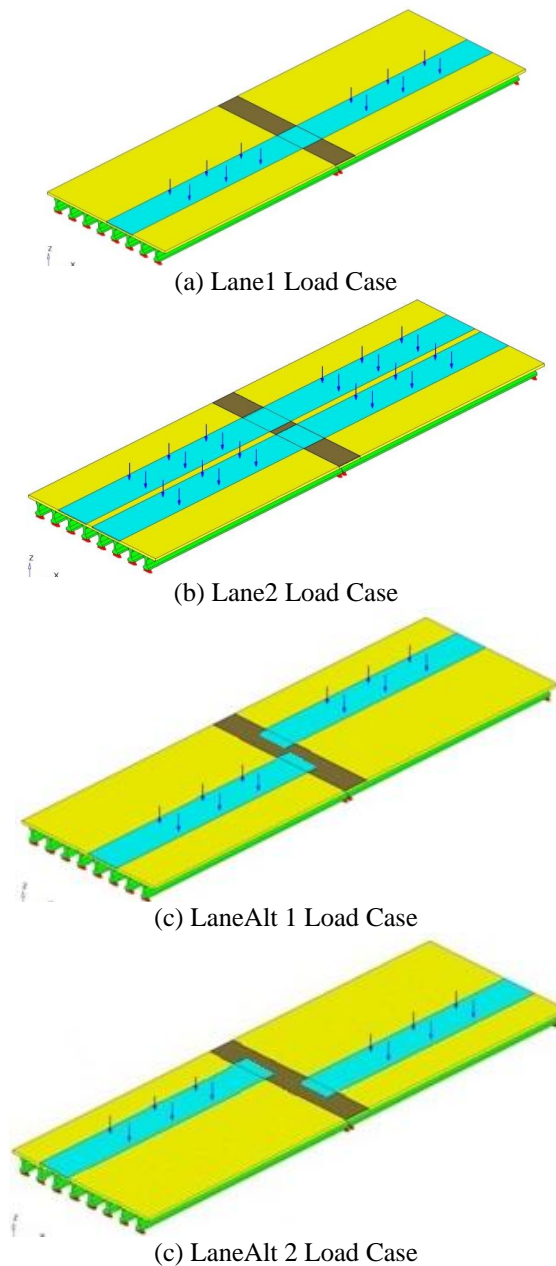


Figure 4-14. Live load cases

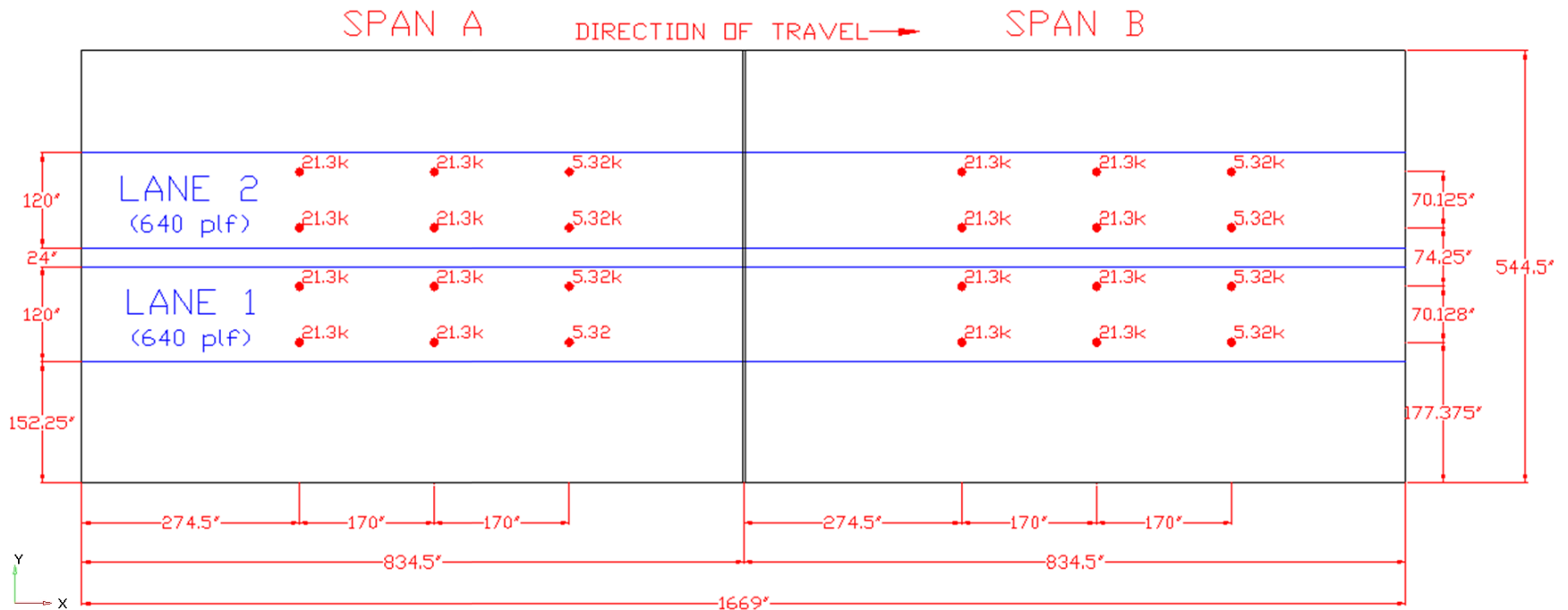


Figure 4-15. Truck and lane load locations

4.3.11.2 Temperature Gradient

The AASHTO (2010) Specification divides the United States into four zones based on solar radiation. Each zone is assigned a temperature for the top of the deck and a temperature 4 in. below the top of the deck. For Michigan, these are 41°F and 11°F for the positive temperature gradient (PTG). The resulting temperature gradient is shown in Figure 4-16a. The negative temperature gradient (NTG) values are obtained by multiplying the PTG values by -0.30 for plain concrete and -0.20 for a deck with asphalt overlay. The value of -0.30 is selected and the resultant temperature gradient profile is shown in Figure 4-16b.

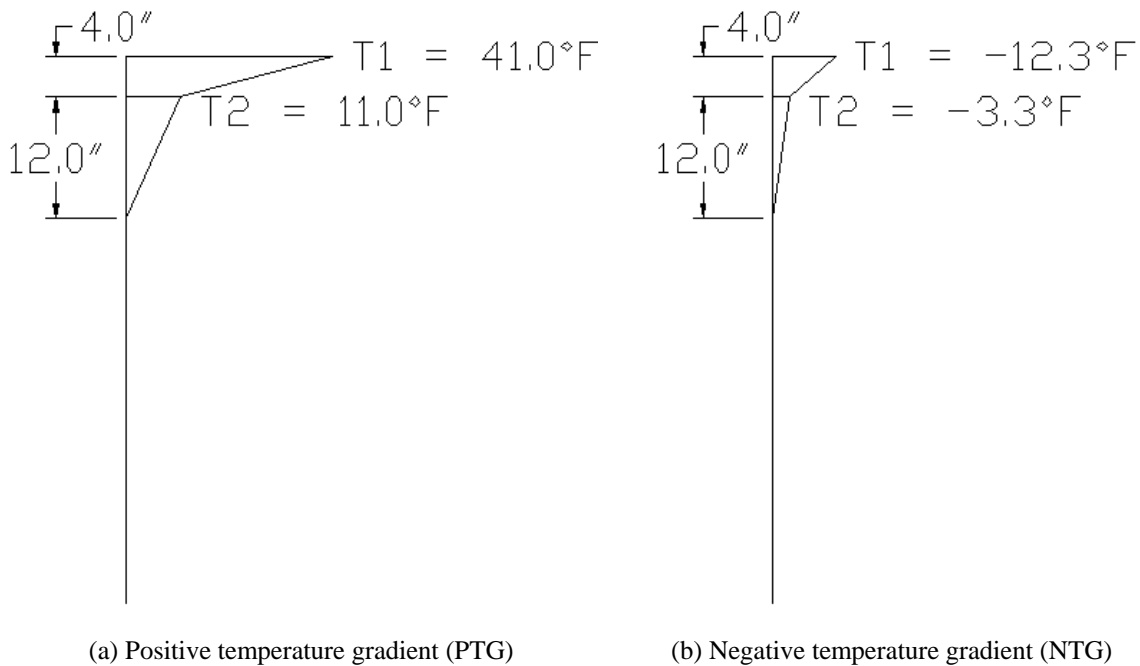


Figure 4-16. Temperature gradient

4.4 SIGN CONVENTION, MODEL VERIFICATION, AND RESULTS

4.4.1 Overview

The objective of analysis is to develop design recommendations for link slabs; hence, stresses in the link slab are required. Envelopes of moments and forces that are needed for link slab design are calculated from the link slab stresses. Abaqus allows for stresses to be averaged at nodes so that they may be interpreted by the user. In addition, Abaqus has an option to calculate forces and moments about a user-defined section. This option is utilized at the center of the link slab where such a section is defined. The section provides the total force and moment at the user-defined section along the center of the link slab. Finally, the reaction forces are checked to assure FE model equilibrium.

4.4.2 Sign Convention

A sign convention is defined as shown in Figure 4-17. The longitudinal axis of the bridge lies along X-axis. Link slab force in the X-direction is the axial force (F_x). Moment about the X-axis is the torsion (M_{xx}). The transverse axis of the bridge is along the global Y-axis. Force in the link slab in this direction is the transverse shear (F_y), and moment about this axis is the bending moment (M_{yy}). The vertical axis of this bridge is along the global Z-direction, the opposite direction gravity acts. Force in this direction is the vertical shear (F_z), and moment about this axis is the in-plane twist (M_{zz}). Force in tension has a negative sign. A negative bending moment generates tension at the link slab top fiber.

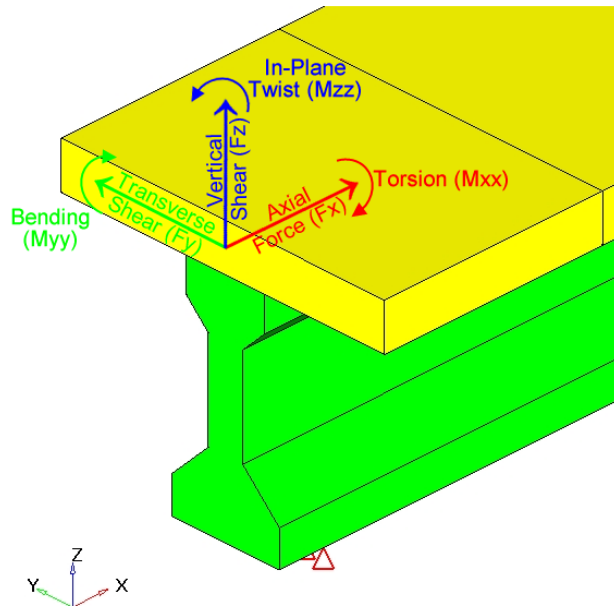


Figure 4-17. Sign convention

4.4.3 FE Model Verification

Equilibrium checks are performed to verify the model accuracy. Loads are applied only in the vertical direction so the net longitudinal and transverse reactions must be zero. The reaction forces in the vertical direction are the sum of the lane load plus truck load (HL-93). Models with thermal loads develop a null net vertical reaction. For each load case under gravity loads, the vertical reaction forces are calculated using Eq. 4-2 through Eq. 4-4.

$$R.F._{lane1} = (1 \text{ lane})(0.640 \text{ k/ft/lane})(139.083 \text{ ft}) + (2 \text{ trucks})(1.33(72\text{k/truck})) \quad (4-2)$$

$$R.F._{lane1} = 250.533\text{k}$$

$$R.F._{lane2} = (2 \text{ lanes})(0.640 \text{ k/ft/lane})(139.083 \text{ ft}) + (4 \text{ trucks})(1.33(72\text{k/truck})) \quad (4-3)$$

$$R.F._{lane2} = 561.067\text{k}$$

$$R.F._{lanealt} = (2 \text{ lanes})(0.640 \text{ k/ft/lane})(69.5 \text{ ft}) + (2 \text{ trucks})(1.33(72\text{k/truck})) \quad (4-4)$$

$$R.F._{lanealt} = 280.48\text{k}$$

The reaction forces calculated from analytical and FE models are compared. The forces at the center of the link slab are verified by the state of equilibrium at the section along the center of the link slab.

4.4.4 Results

Resultant forces and moments are calculated at a section defined as a surface. This feature is utilized to calculate total force and moment acting at the user-defined surface along the midspan of the link slab. Forces at a section are useful to draw general conclusions about the effect of the angle of skew. In designing the section, a designer requires the effective force and moment for a unit width. Both results are calculated and discussed below.

4.4.4.1 Cross Sectional Moments and Forces

Moments and forces are generated by the FE software about the local coordinate system of the surface along the center of the link slab. Each angle of skew has a different orientation, thus a local coordinate system of this surface. To have comparable forces for all skew cases, the moments and forces about the local coordinate system are transformed into the global coordinate system. The transpose of the transformation matrix between the local and global systems is multiplied by vector of displacements, forces, moments, etc. in the local coordinate system to obtain the values in relationship to the global coordinate system (Nelson and McCormac2003). This relationship is given in Eq. 4-5.

$$\{f\} = [T]^T \{f'\} \quad (4-5)$$

where

$$\begin{aligned} \{f\} &= \text{Vector of forces in global coordinates} \\ [T] &= \text{Transformation matrix} \\ \{f'\} &= \text{Vector of force in local coordinates} \end{aligned}$$

As an example, a straight bridge with an HRRR boundary condition and *Lane1* load case is selected. Eq.4-6 shows the link slab moments in the local coordinate system. The first term in the force vector shown in Eq.4-6 is the moment about the local x-axis (torsion), the second is about the local y-axis (bending moment), and the third is about the local z-axis (in-plane twist). The transformation matrix is shown in Eq. 4-7. The first row of the transformation matrix is the direction cosines of local x-axis with respect to the global coordinates. Similarly, row 2 and row 3 represent direction cosines of local axes y and z.

From here, the transformation matrix is transposed and multiplied by the moments about the local coordinate system as shown in Eq. 4-8. Lastly, the moments about the global coordinate system are shown in Eq. 4-9. This process is performed for all the models so that the results allow direct comparison of forces and moments in all cases of changing skew.

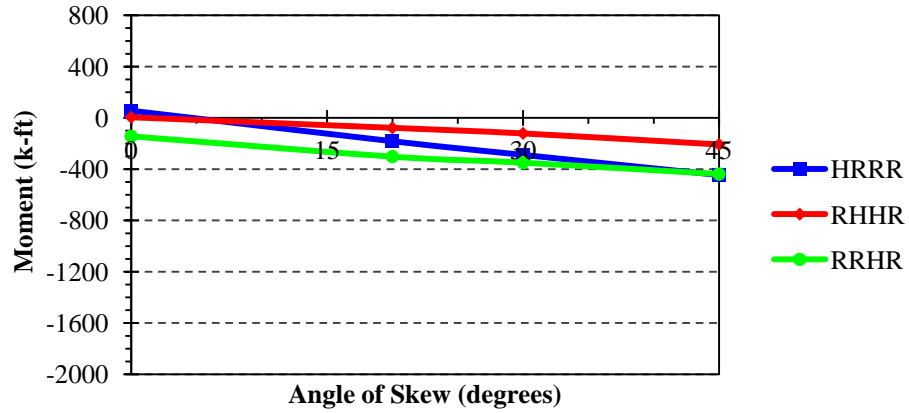
$$\{f\}' = \{47 \quad -501 \quad 190\} \text{ kip} - ft \quad (4-6)$$

$$[T] = \begin{bmatrix} 1 & 0 & 0 \\ 0 & 0 & 1 \\ 0 & -1 & 0 \end{bmatrix} \quad (4-7)$$

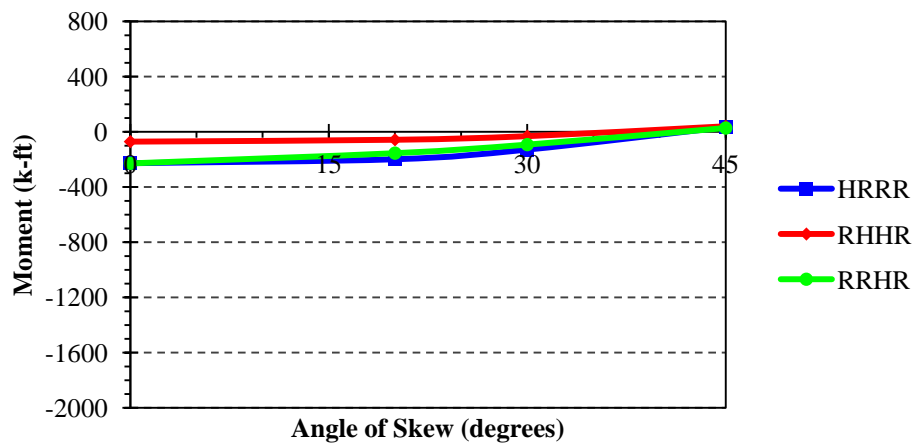
$$[T]^T = \begin{bmatrix} 1 & 0 & 0 \\ 0 & 0 & 1 \\ 0 & -1 & 0 \end{bmatrix}^T \{47 \quad -501 \quad 190\} \quad (4-8)$$

$$\{f\} = \begin{pmatrix} 47 \\ -190 \\ -501 \end{pmatrix} \text{ kip} - ft \quad (4-9)$$

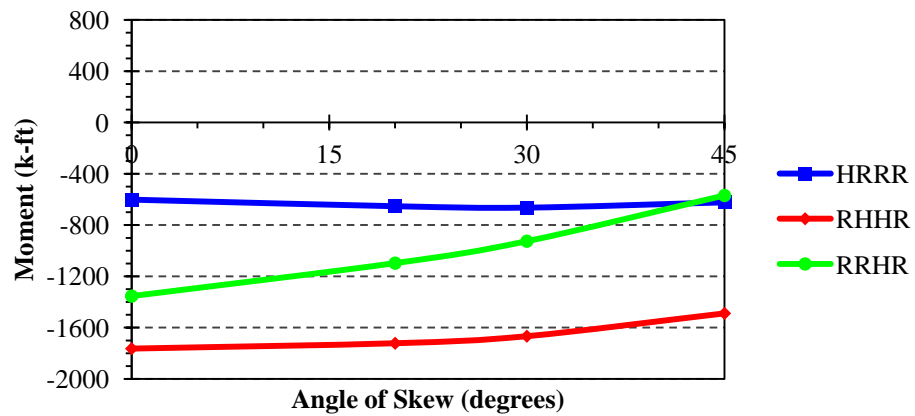
The total sectional moments and forces, with respect to the global coordinate system, are shown graphically in Figure 4-18 through Figure 4-29 with respect to each load case.



(a) Link slab torsion (M_{xx})

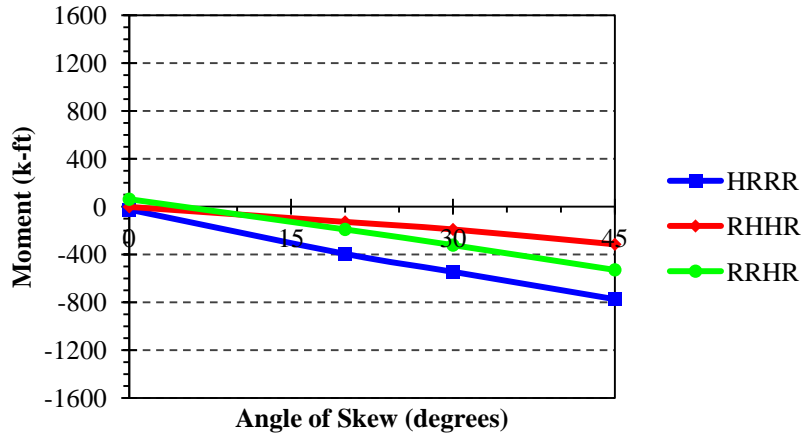


(b) Link slab bending moment (M_{yy})

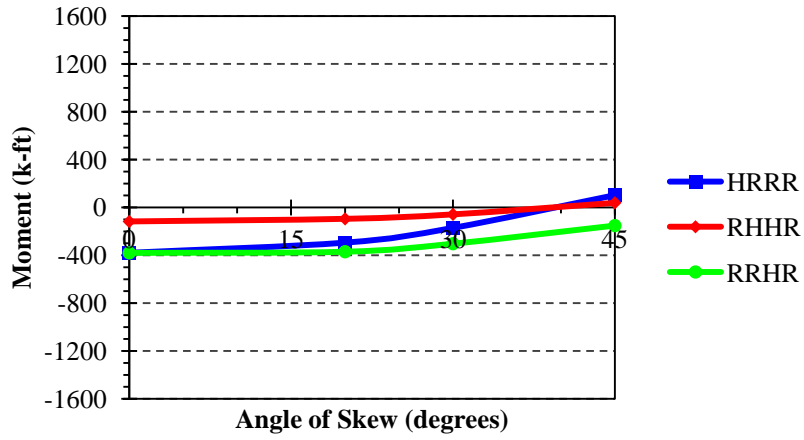


(c) Link slab in-plane twist (M_{zz})

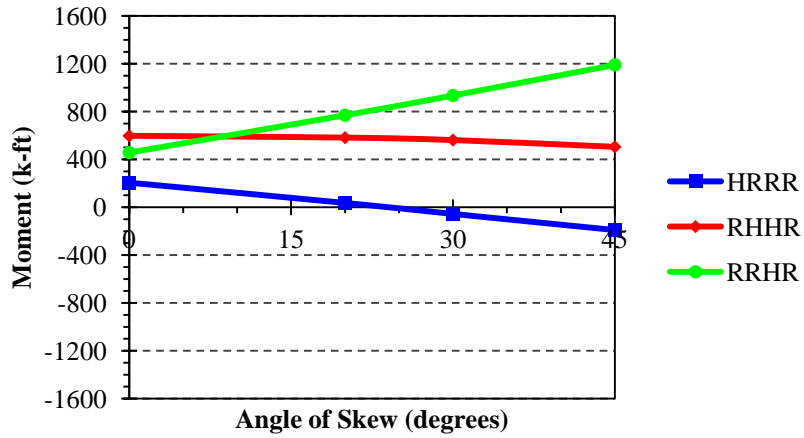
Figure 4-18. Total sectional moment - Lane1 load case



(a) Link slab torsion (M_{xx})

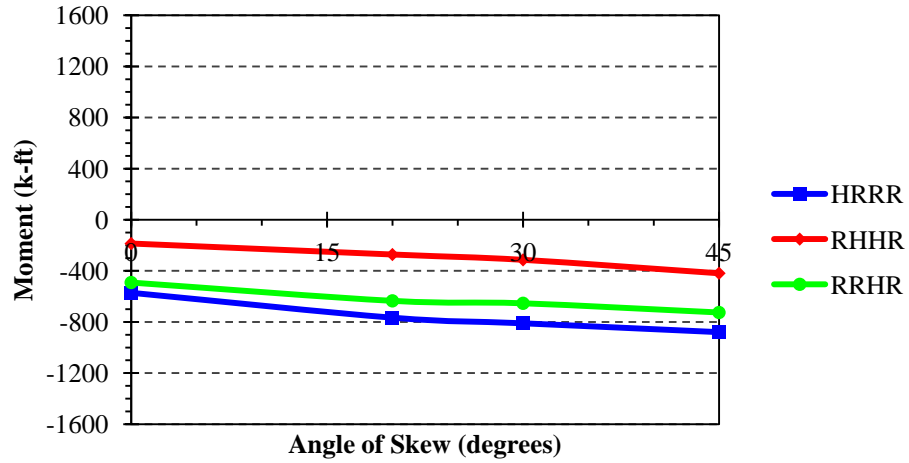


(b) Link slab bending moment (M_{yy})

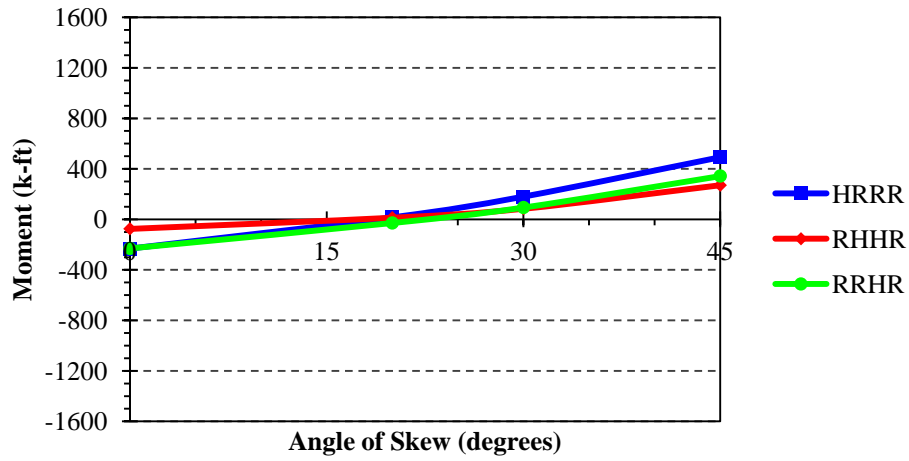


(c) Link slab in-plane twist (M_{zz})

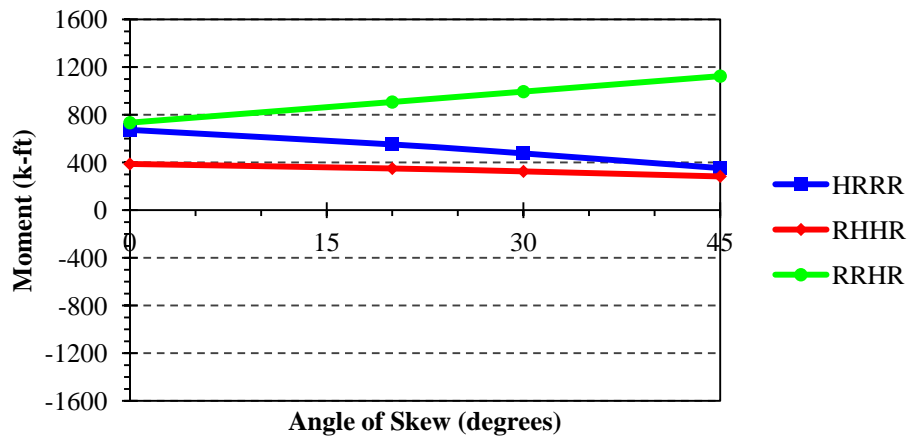
Figure 4-19. Total sectional moment - Lane2 load case



(a) Link slab torsion (M_{xx})

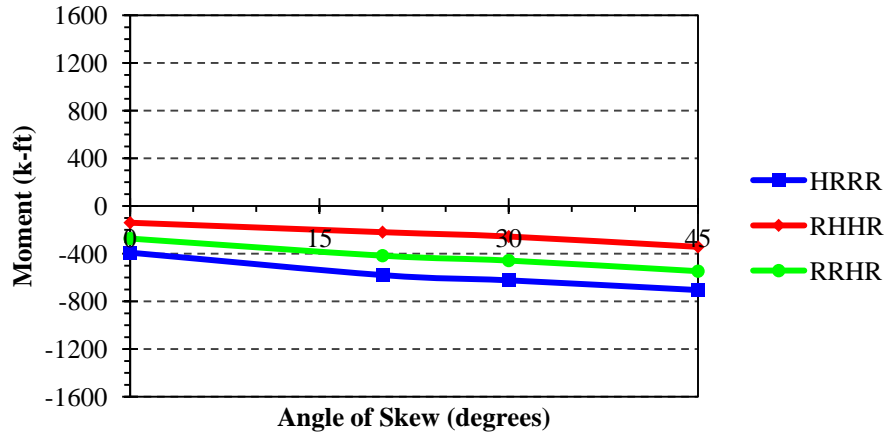


(b) Link slab bending moment (M_{yy})

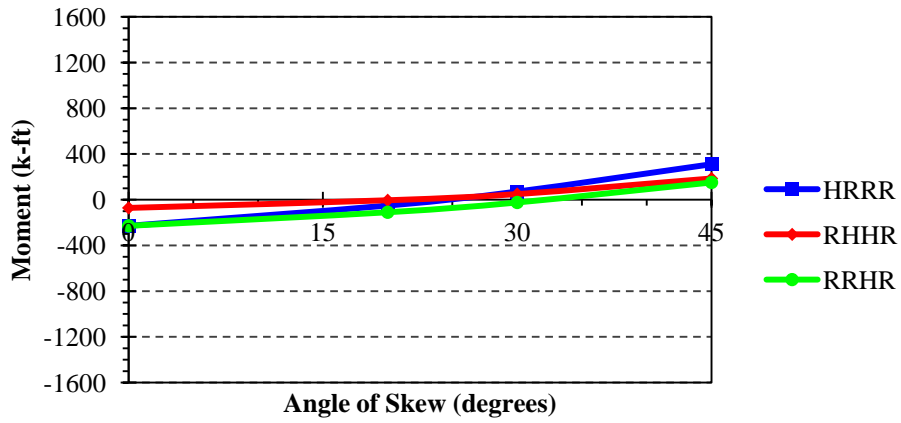


(c) Link slab in-plane twist (M_{zz})

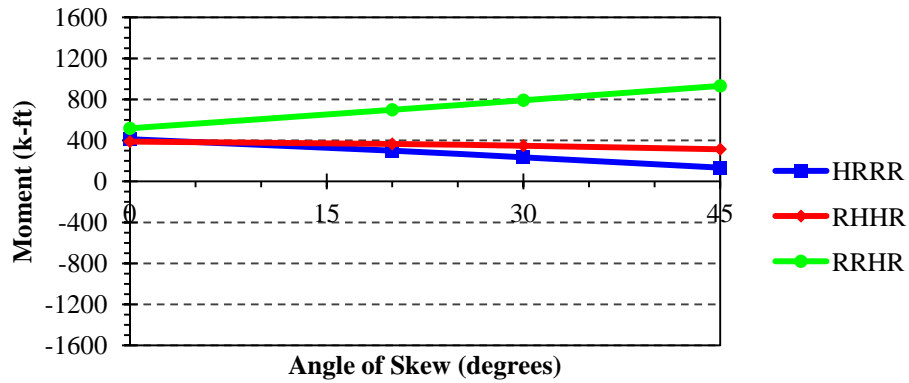
Figure 4-20. Total sectional moment – LaneAlt1 load case



(a) Link slab torsion (M_{xx})

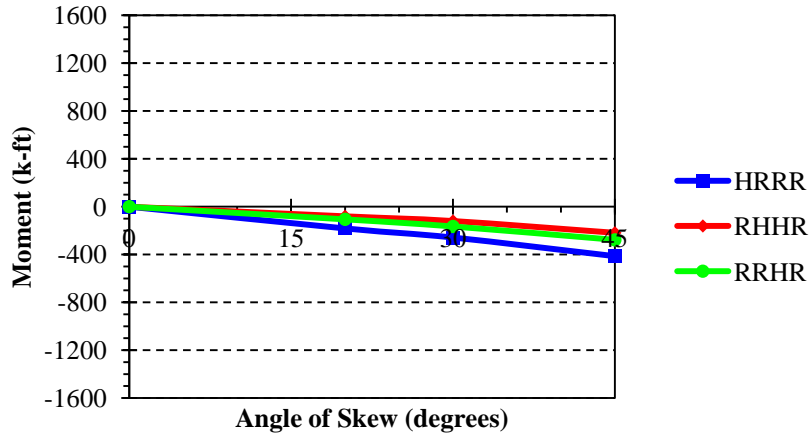


(b) Link slab bending moment (M_{yy})

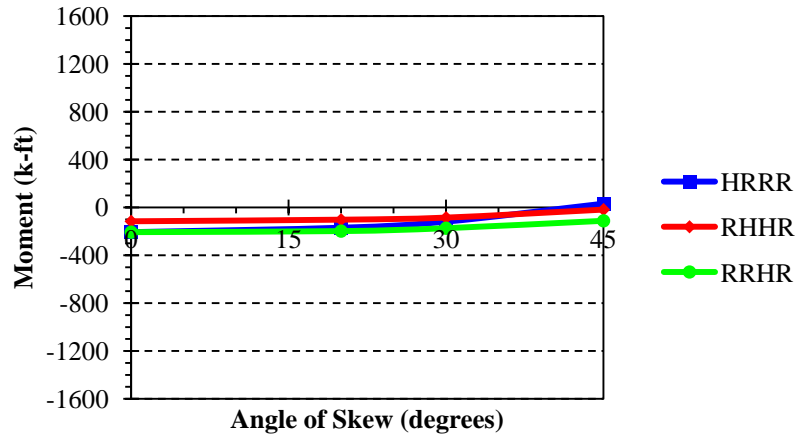


(c) Link slab in-plane twist (M_{zz})

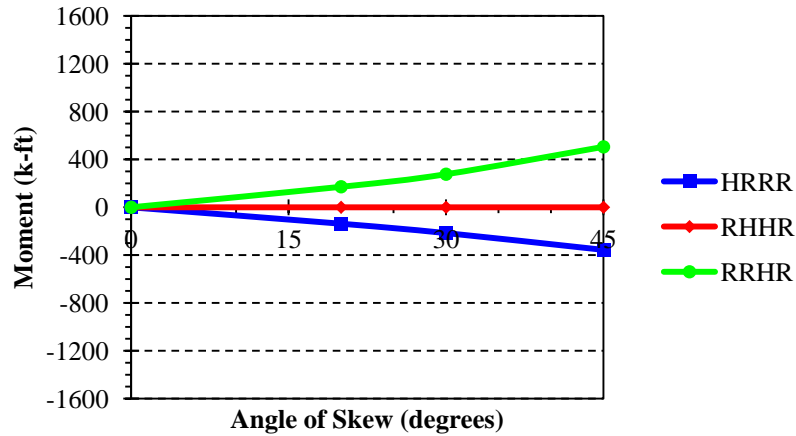
Figure 4-21. Total sectional moment – LaneAlt2 load case



(a) Link slab torsion (M_{xx})

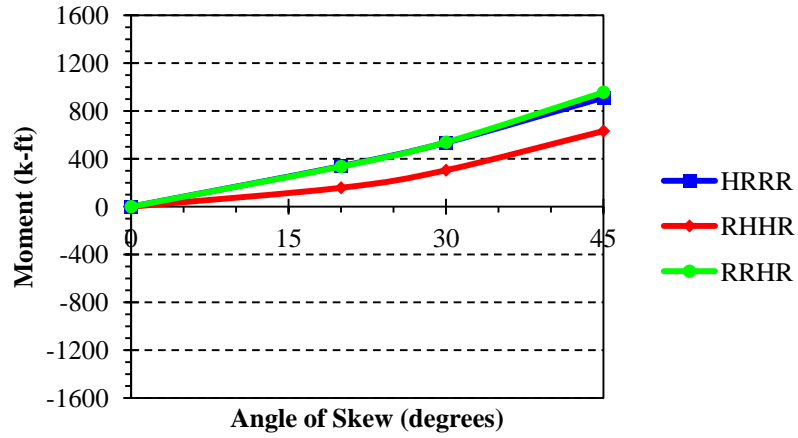


(b) Link slab bending moment (M_{yy})

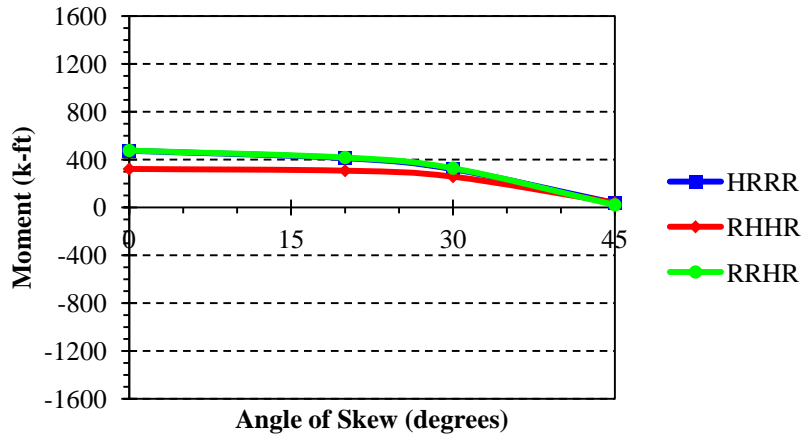


(c) Link slab in-plane twist (M_{zz})

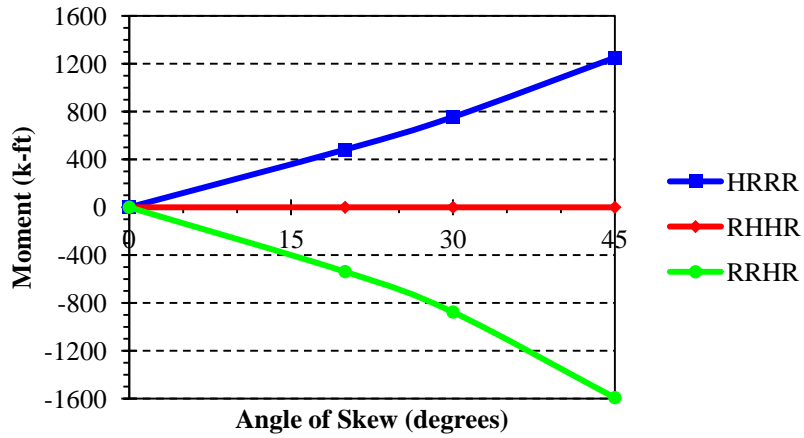
Figure 4-22. Total sectional moment - NTG load case



(a) Link slab torsion (M_{xx})

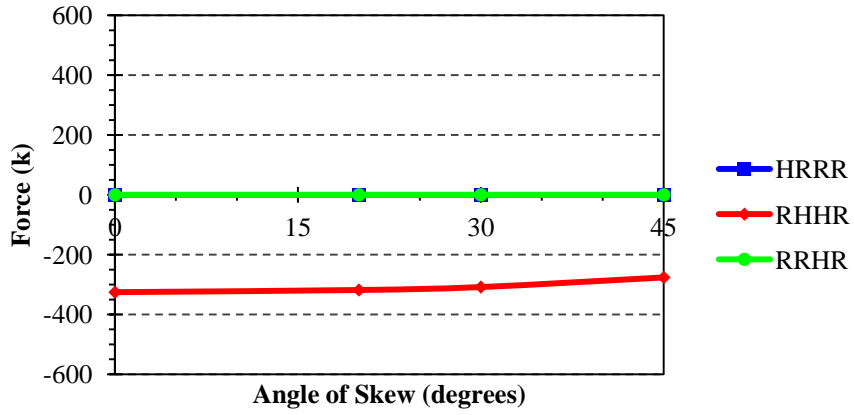


(b) Link slab bending moment (M_{yy})

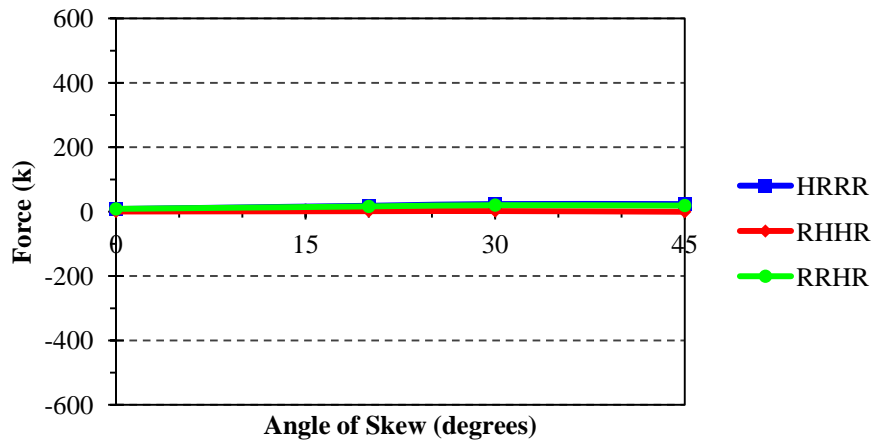


(c) Link slab in-plane twist (M_{zz})

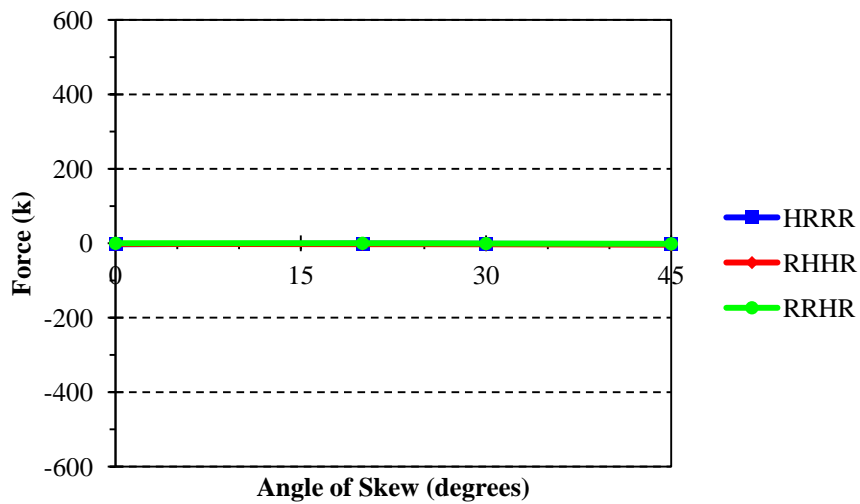
Figure 4-23. Total sectional moment - PTG load case



(a) Link slab axial force (F_x)

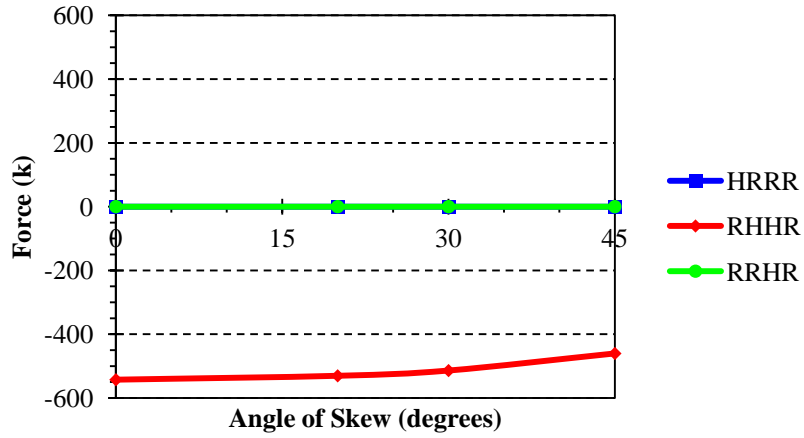


(b) Link slab transverse shear (F_y)

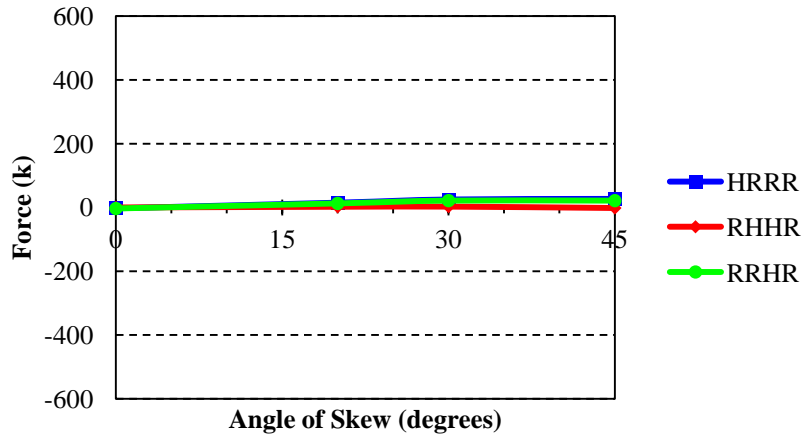


(c) Link slab vertical shear (F_z)

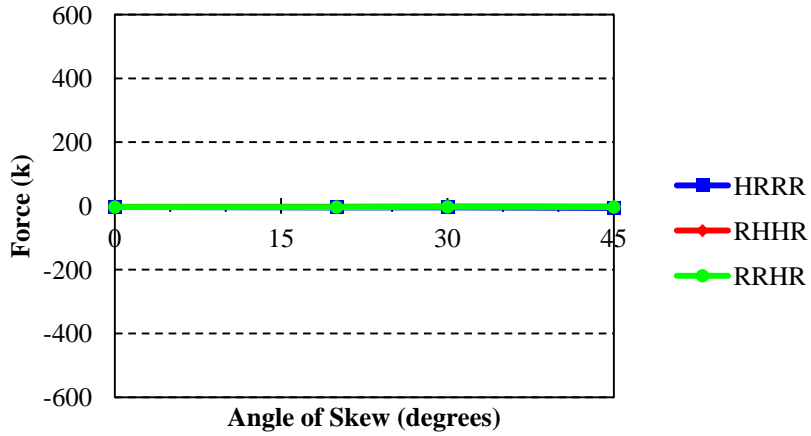
Figure 4-24. Total sectional force - Lane1 load case



(a) Link slab axial force (F_x)

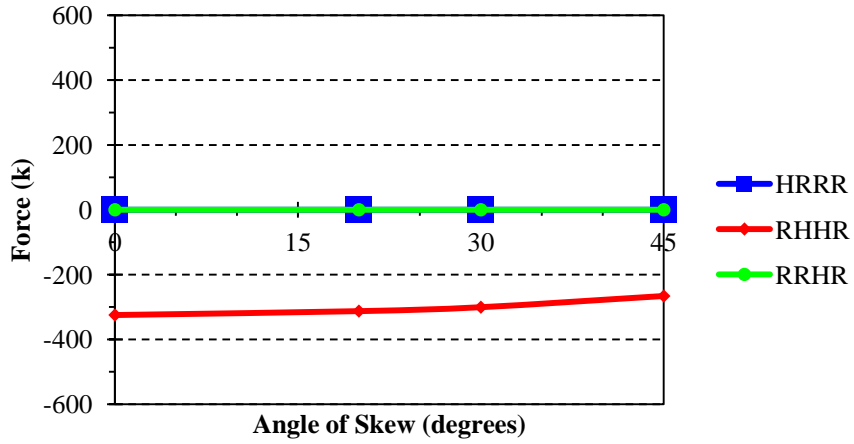


(b) Link slab transverse shear (F_y)

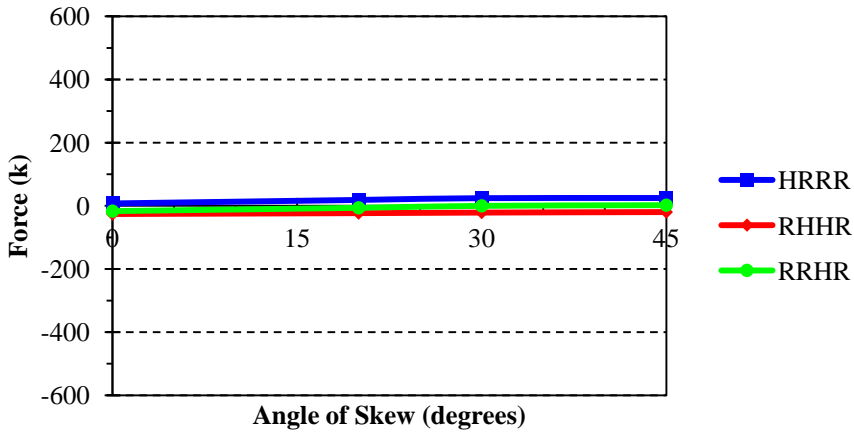


(c) Link slab vertical shear (F_z)

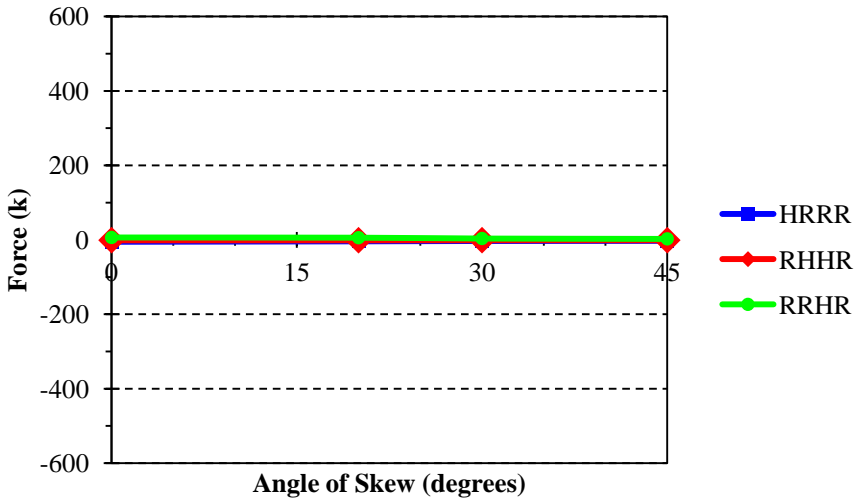
Figure 4-25. Total sectional force - Lane2 load case



(a) Link slab axial force (F_x)

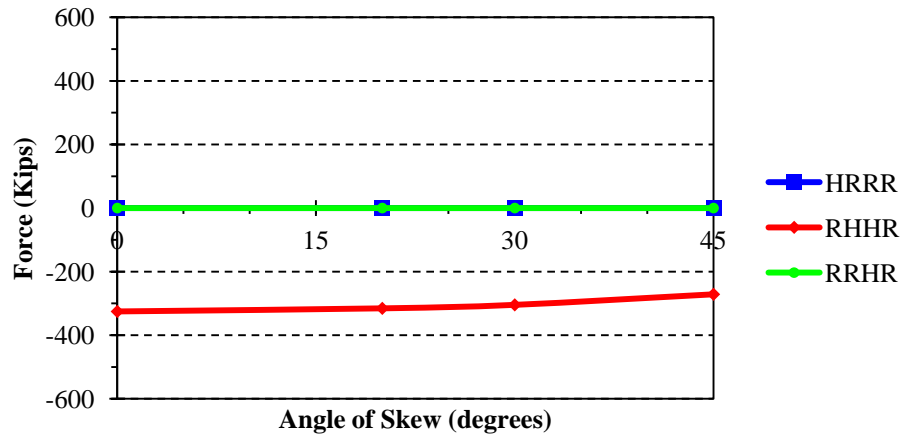


(b) Link slab transverse shear (F_y)

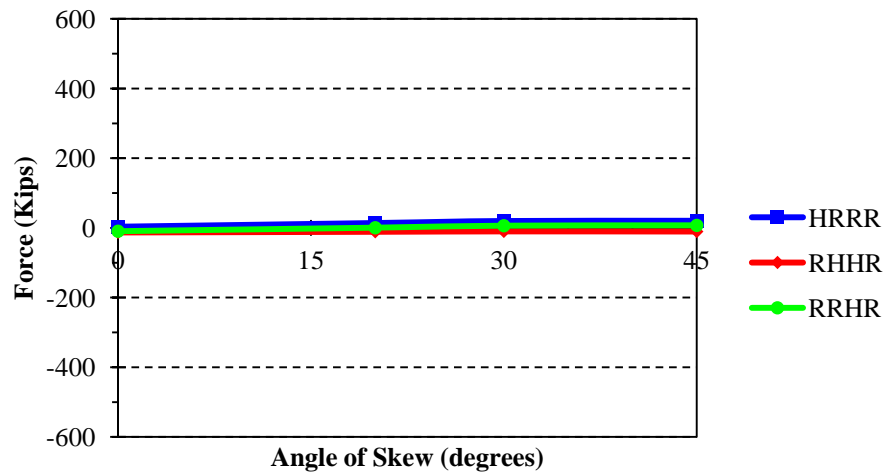


(c) Link slab vertical shear (F_z)

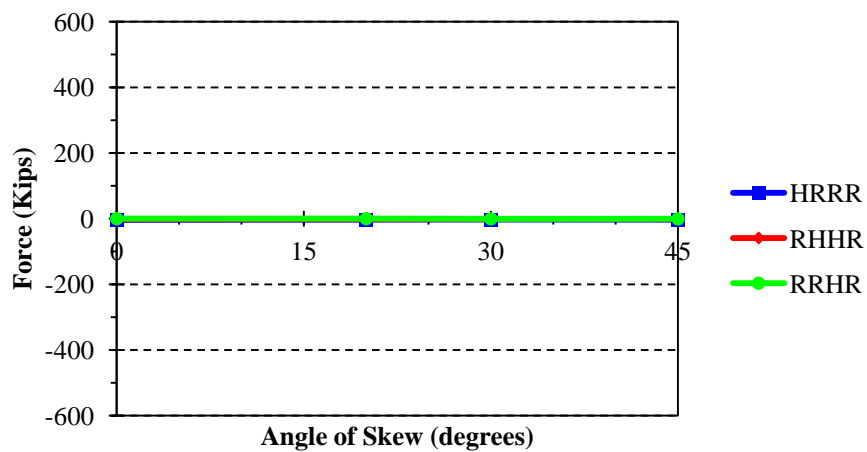
Figure 4-26. Total sectional force – LaneAlt1 load case



(a) Link slab axial force (F_x)

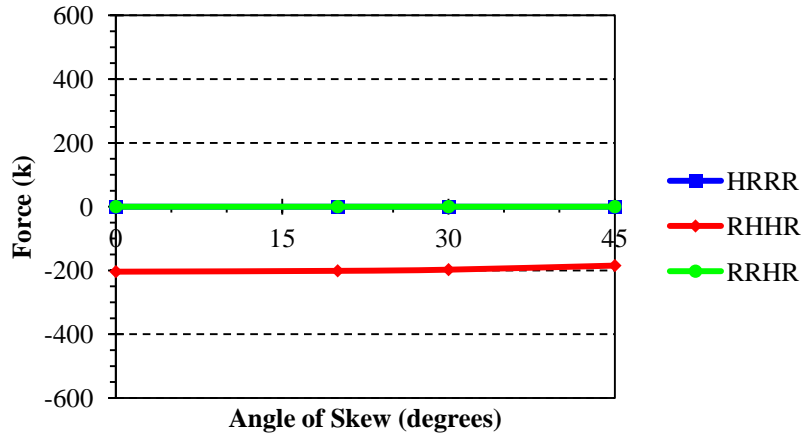


(b) Link slab transverse shear (F_y)

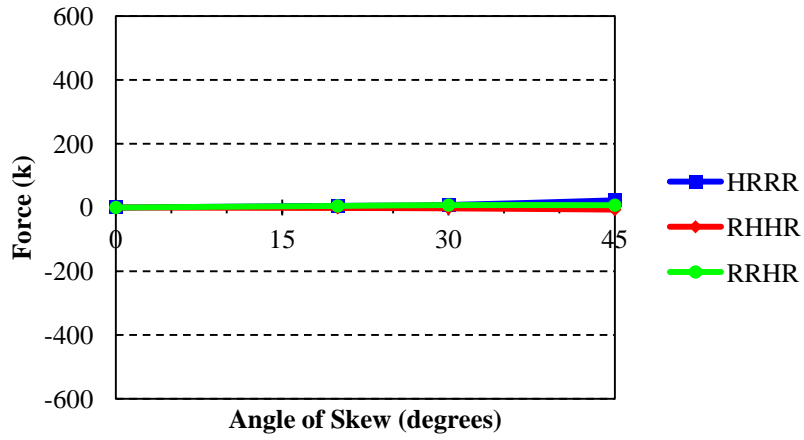


(c) Link slab vertical shear (F_z)

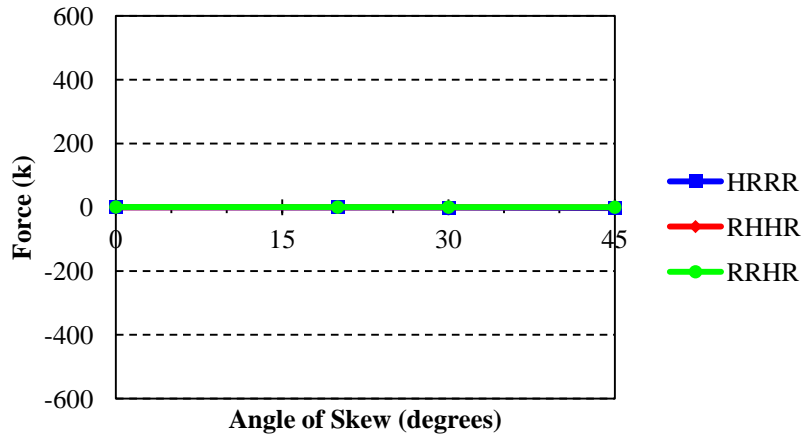
Figure 4-27. Total sectional force – LaneAlt2 load case



(a) Link slab axial force (F_x)

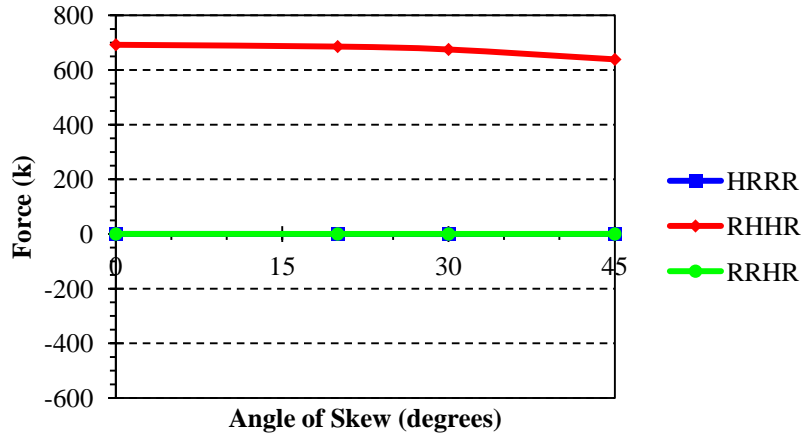


(b) Link slab transverse shear (F_y)

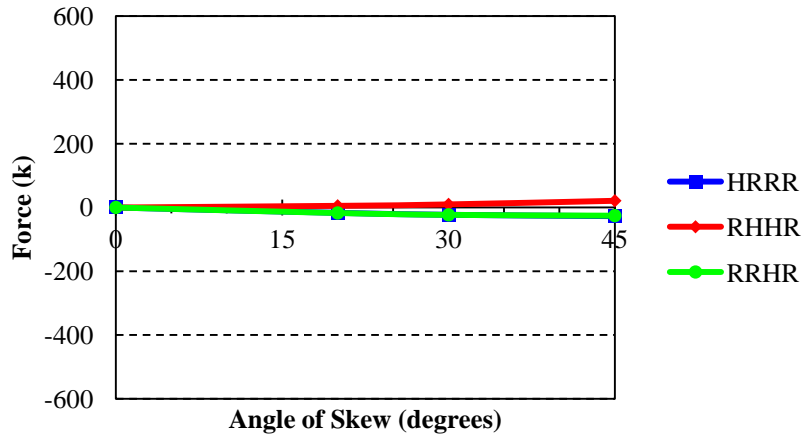


(c) Link slab vertical shear (F_z)

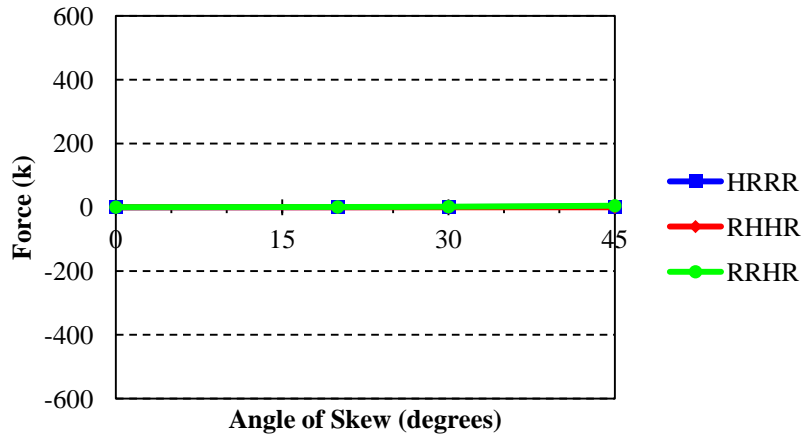
Figure 4-28. Total sectional force - NTG load case



(a) Link slab axial force (F_x)



(b) Link slab transverse shear (F_y)



(c) Link slab vertical shear (F_z)

Figure 4-29. Total sectional force - PTG load case

Table 4-3 presents a summary of the total sectional moments and forces shown in Figure 4-18 through Figure 4-29. From Table 4-3, the following general conclusions are derived.

- 1) The torsion (M_{xx}) magnitude in the link slab increases as the angle of skew increases for all load cases and boundary conditions. The RHHR boundary condition generates the lowest torsion.
- 2) The bending moment, under the *LaneAlt 1 and 2* load cases, reverses from negative to positive. The bending moment magnitude decreases as the angle of skew increases in load cases *Lane1* and *Lane2* as well as both positive temperature gradient (PTG) and negative temperature gradient (NTG). The lowest bending moment magnitude is developed with RHHR boundary condition while magnitudes are the same for HRRR and RRHR boundary conditions.
- 3) The link slab with an RHHR support configuration does not develop in-plane twist (M_{zz}) under PTG or NTG, irrespective of bridge skew. Twist remains constant under live loads with RHHR support configuration. Under PTG or NTG, significant twist is developed with HRRR and RRHR support configurations. Link slab twist shows mixed behavior under live loads with HRRR or RRHR support configurations.
- 4) Axial force in the link slab slightly decreases under all load cases with increasing skew and with RHHR boundary conditions. The largest axial force is developed under the PTG.
- 5) Axial force is zero under HRRR and RRHR boundary conditions. Vertical or transverse shear forces developed in the link slab are insignificant irrespective of loads, support configurations, or skew.

The above conclusions are based on the moments and forces developed at the entire cross-section of the link slab. These moments and forces are helpful in understanding the link slab behavior with changing skew. Design forces and moments will be calculated combining forces and moments within an effective width of a link slab. Hence, such forces and moments are calculated and presented in the following section.

Table 4-3. Total Sectional Moment and Force Variation Trend with Increased Skew under Various Load and Support Configurations

Load	Support Configuration	Moment (kip-ft)			Force (kip)		
		M _{xx}	M _{yy}	M _{zz}	F _x	F _y	F _z
Lane 1	HRRR	↑ (0 - -400)	↓ (-200-0)	~ (-600)	~ 0	~ 0	~ 0
	RRHR	↑ (-100 - -400)	↓ (-200-0)	↓ (-1400--600)	~ 0	~ 0	~ 0
	RHHR	↑ (0 - -100)	↓ (-100-0)	↓ (-1800--1500)	↓ (-300--250)	~ 0	~ 0
Lane 2	HRRR	↑ (0 - -800)	↓↑ (-400-100)	↑↓ (200--200)	~ 0	~ 0	~ 0
	RRHR	↑ (0 - -500)	↓ (-400--200)	↑ (400 - 1200)	~ 0	~ 0	~ 0
	RHHR	↑ (0 - -300)	↓ (-100-0)	↓ (600-500)	↓ (-550--450)	~ 0	~ 0
LaneAlt 1	HRRR	↑ (-600 - -900)	↓↑ (-200-500)	↓ (700-400)	~ 0	~ 0	~ 0
	RRHR	↑ (-500 - -700)	↓↑ (-200-400)	↑ (700 - 1100)	~ 0	~ 0	~ 0
	RHHR	↑ (-200 - -400)	↓↑ (-100-200)	↓ (400-300)	↓ (-300--250)	~ 0	~ 0
LaneAlt 2	HRRR	↑ (-400 - -700)	↓↑ (-200-300)	↓ (400-100)	~ 0	~ 0	~ 0
	RRHR	↑ (-300 - -600)	↓↑ (-200-100)	↑ (500 - 900)	~ 0	~ 0	~ 0
	RHHR	↑ (-200 - -400)	↓↑ (-100-100)	↓ (400-300)	↓ (-300--250)	~ 0	~ 0
NTG	HRRR	↑ (0 - -400)	↓ (-200-0)	↑ (0 - -400)	~ 0	~ 0	~ 0
	RRHR	↑ (0 - -300)	↓ (-200--100)	↑ (0 - 500)	~ 0	~ 0	~ 0
	RHHR	↑ (0 - -300)	↓ (-100-0)	~ 0	~ -200	~ 0	~ 0
PTG	HRRR	↑ (0 - 900)	↓ (500-0)	↑ (0 - 1200)	~ 0	~ 0	~ 0
	RRHR	↑ (0 - 900)	↓ (500-0)	↑ (0 - -1600)	~ 0	~ 0	~ 0
	RHHR	↑ (0 - 600)	↓ (300-0)	~ 0	↓ (700-650)	~ 0	~ 0

Note: ↑ - Increase; ↓ - Decrease; ↓↑ - Change from (-) to (+); ↑↓ - Change from (+) to (-); ~ - No significant change

4.4.4.2 Effective Section Axial Force and Bending Moment

In order to calculate the forces and moments within an effective width of a link slab, the full bridge cross-section is divided into eight segments as shown in Figure 4-30. The force and moment within an effective width of a link slab are referred to as the effective force and effective moment.

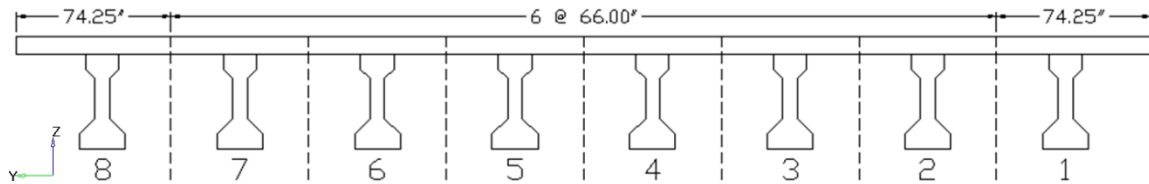
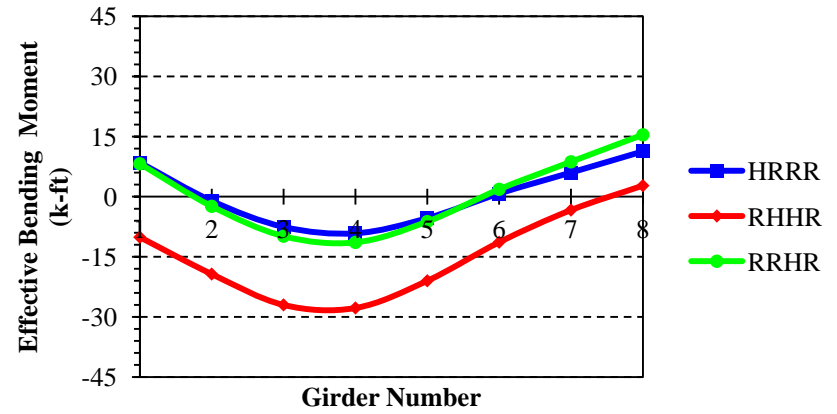


Figure 4-30. Effective width segments

The effective axial force for each segment is calculated from summation of average nodal axial stress multiplied by the projected area of each node. The effective bending moment for each segment is computed by summation of nodal axial forces multiplied by the vertical distance from the neutral axis of the link slab to the node. Effective moments versus skew, under different load configurations are presented in Figure 4-31 through Figure 4-42, and effective forces are presented in Figure 4-37 through Figure 4-42. In these figures, segments are defined by the associated girder index.



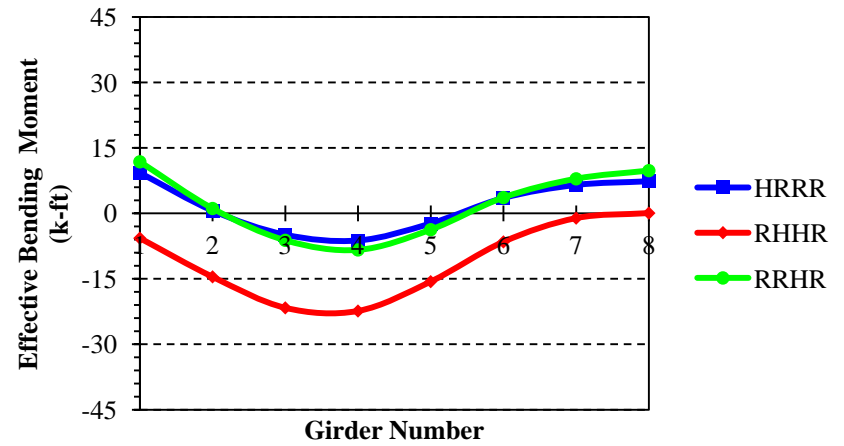
(a) Skew angle of 0°



(b) Skew angle of 20°

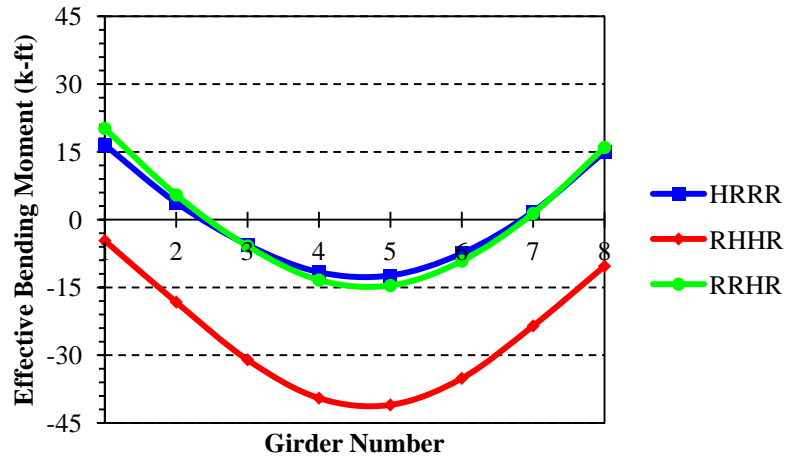


(c) Skew angle of 30°

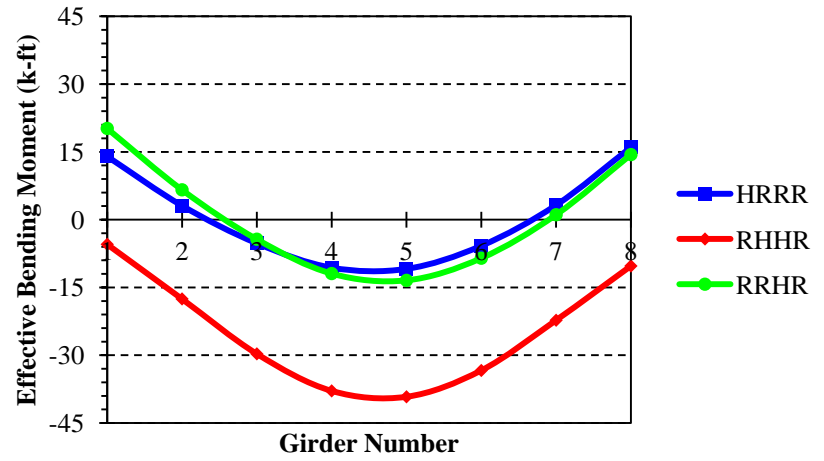


(d) Skew angle of 45°

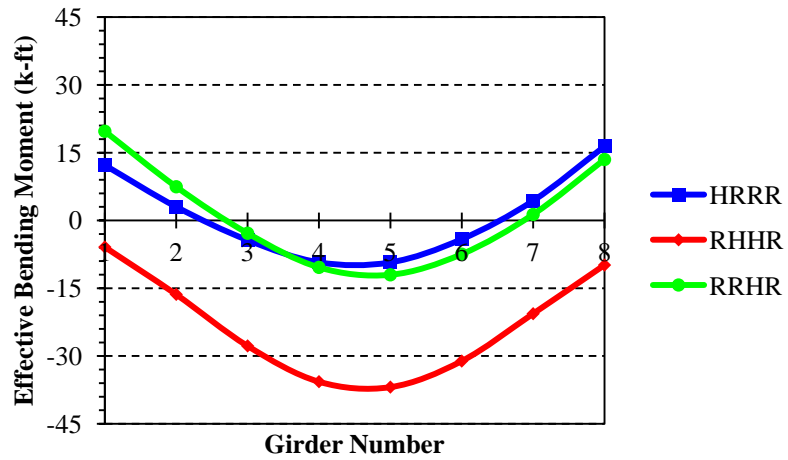
Figure 4-31. Effective moment - Lane1 load case



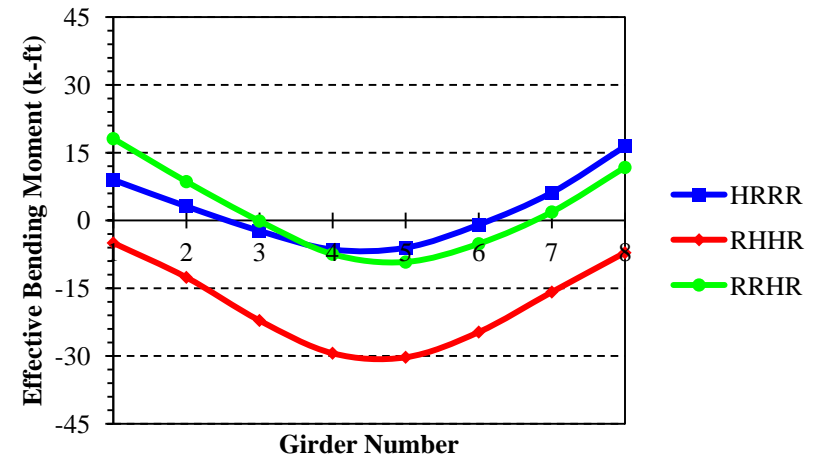
(a) Skew angle of 0°



(b) Skew angle of 20°

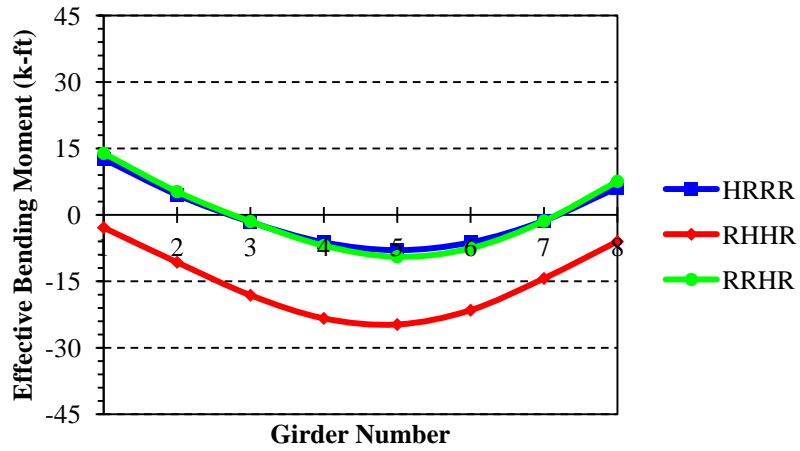


(c) Skew angle of 30°

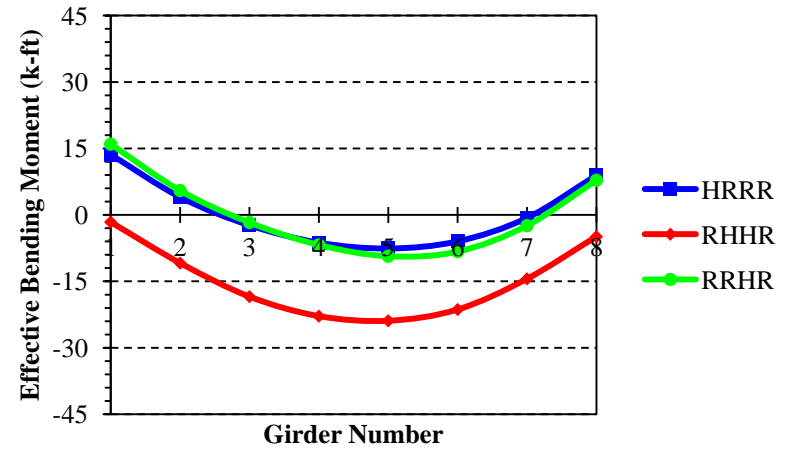


(d) Skew angle of 45°

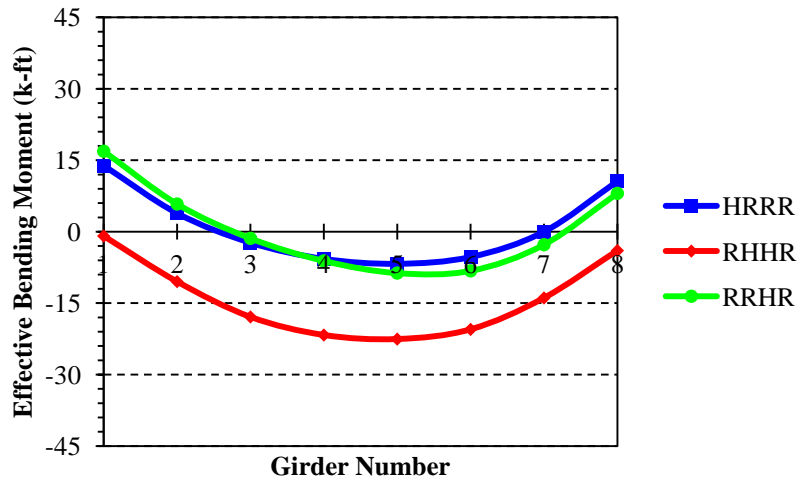
Figure 4-32. Effective moment - Lane2 load case



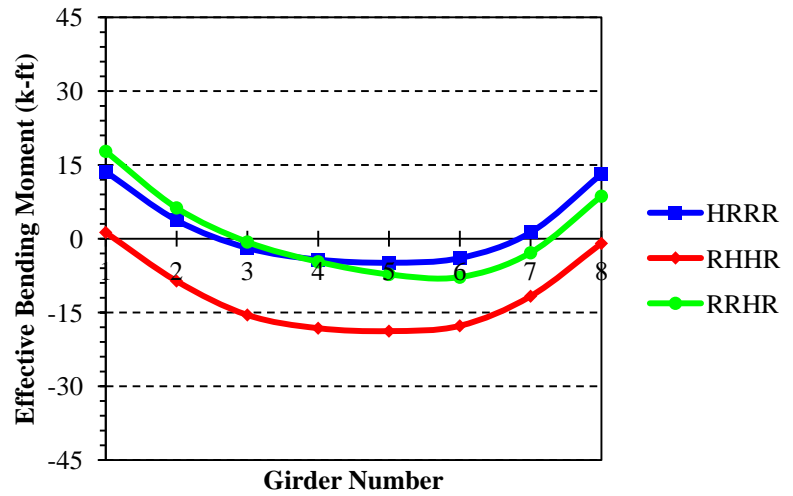
(a) Skew angle of 0°



(b) Skew angle of 20°

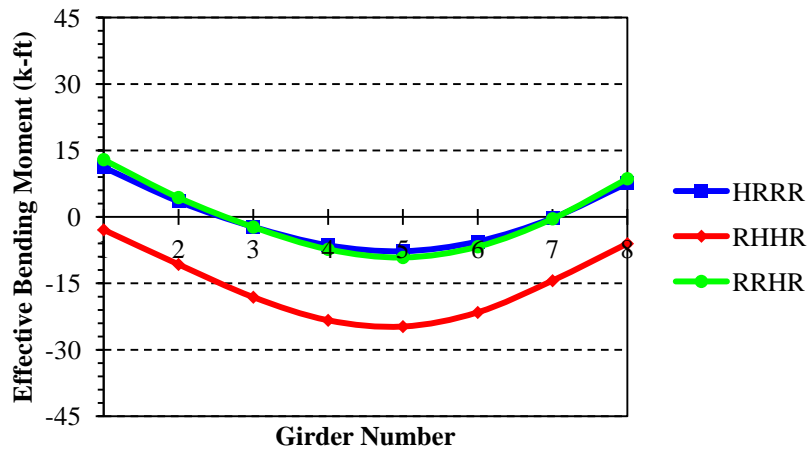


(c) Skew angle of 30°

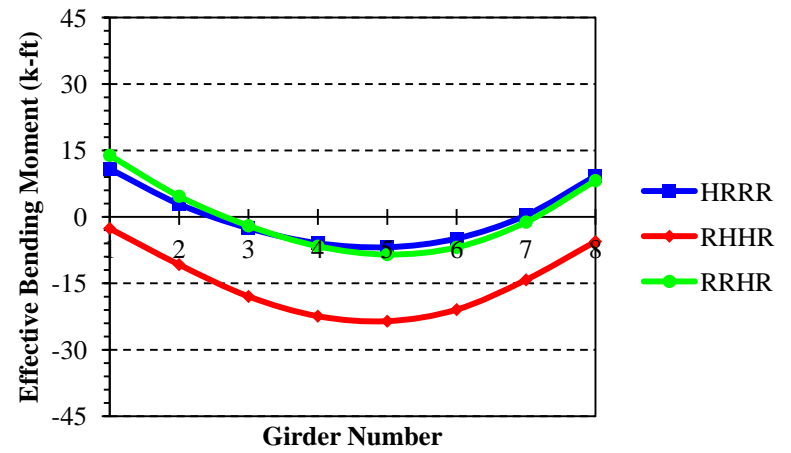


(d) Skew angle of 45°

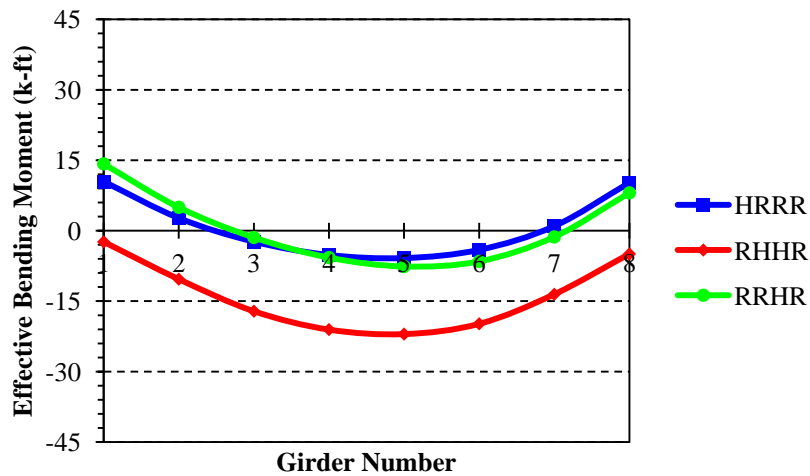
Figure 4-33. Effective moment – LaneAlt1 load case



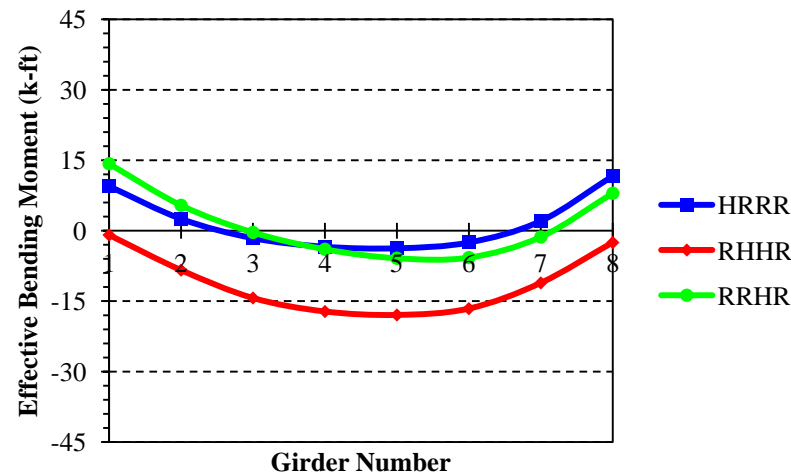
(a) Skew angle of 0°



(b) Skew angle of 20°

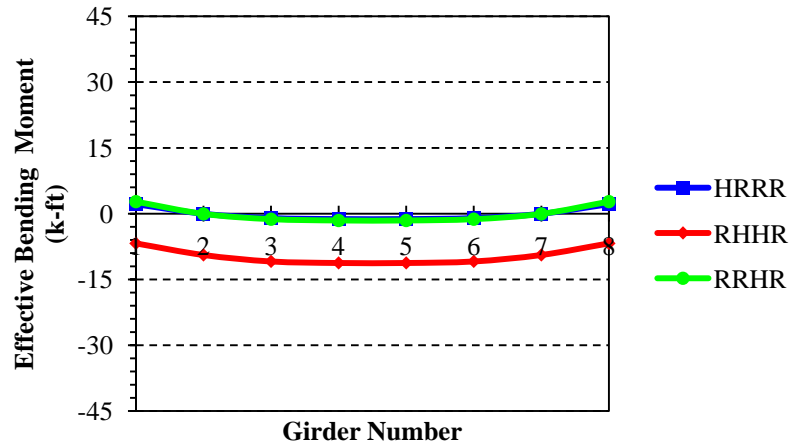


(c) Skew angle of 30°

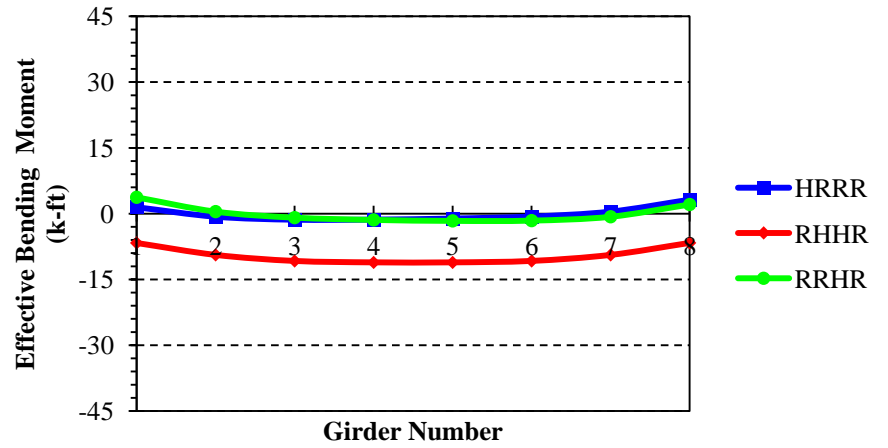


(d) Skew angle of 45°

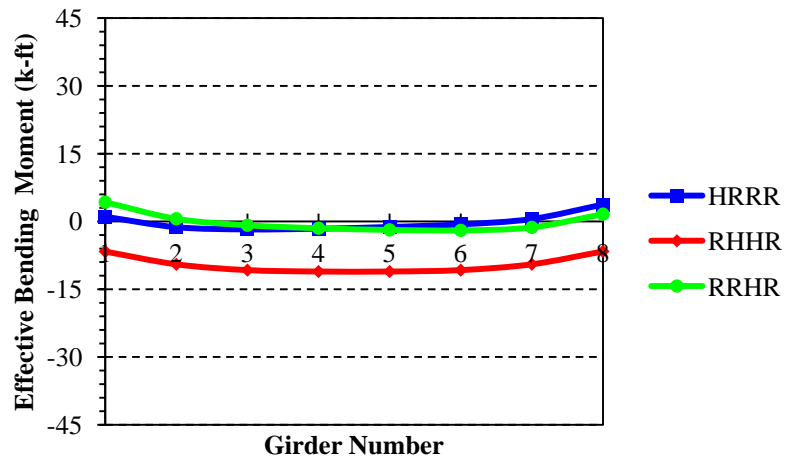
Figure 4-34. Effective moment – LaneAlt2 load case



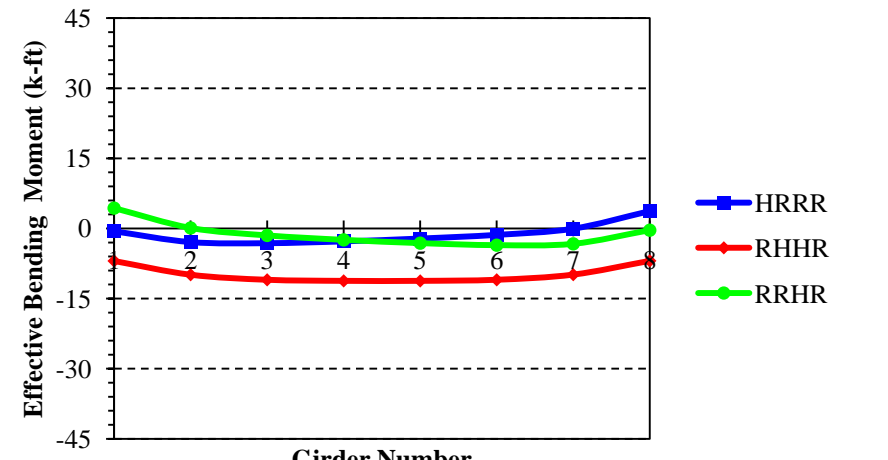
(a) Skew angle of 0°



(b) Skew angle of 20°



(c) Skew angle of 30°



(d) Skew angle of 45°

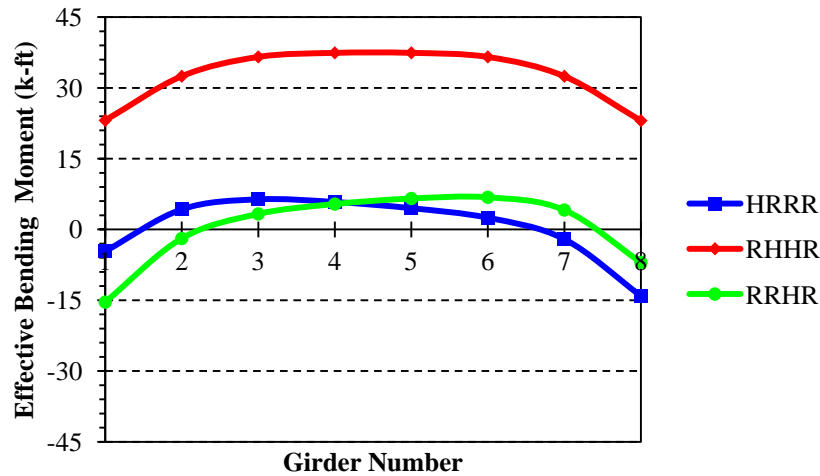
Figure 4-35. Effective moment - NTG load case



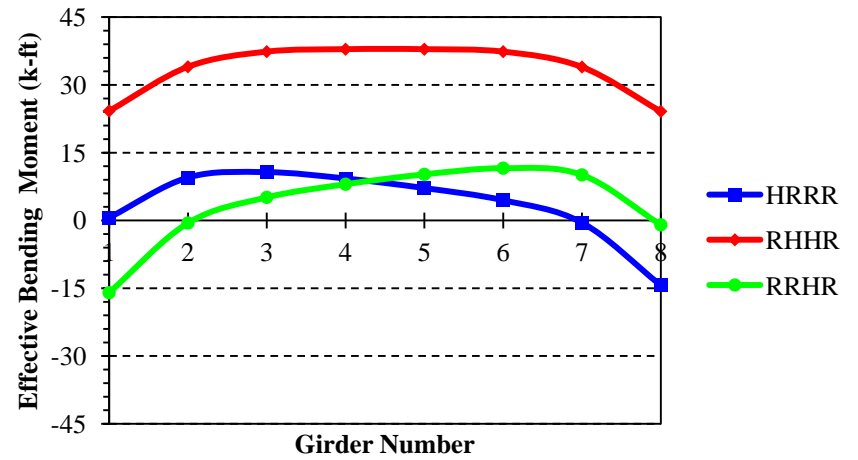
(a) Skew angle of 0°



(b) Skew angle of 20°

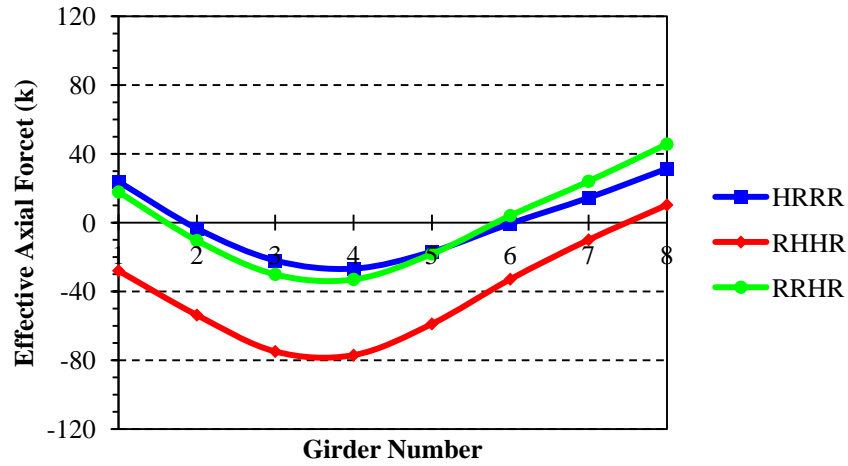


(c) Skew angle of 30°

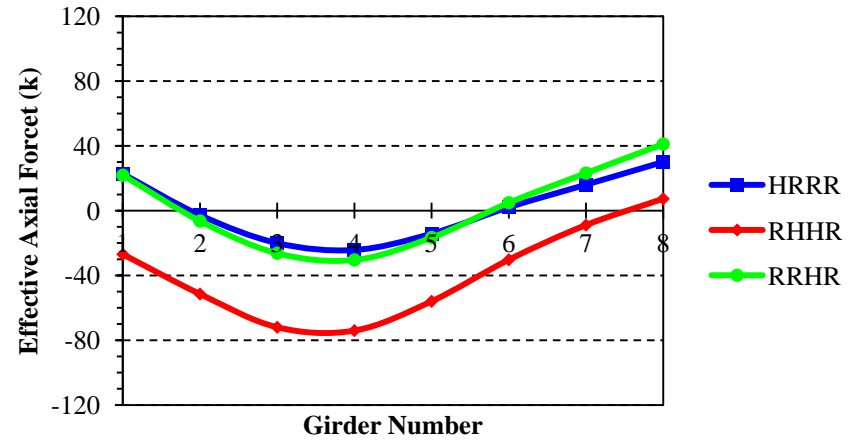


(d) Skew angle of 45°

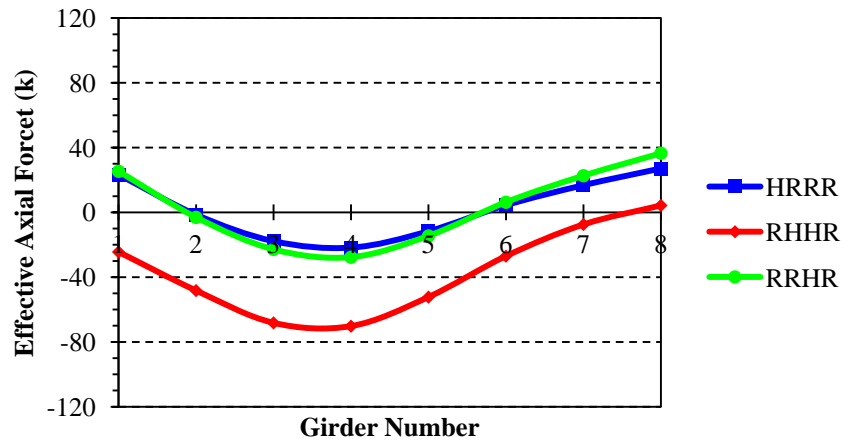
Figure 4-36. Effective moment - PTG load case



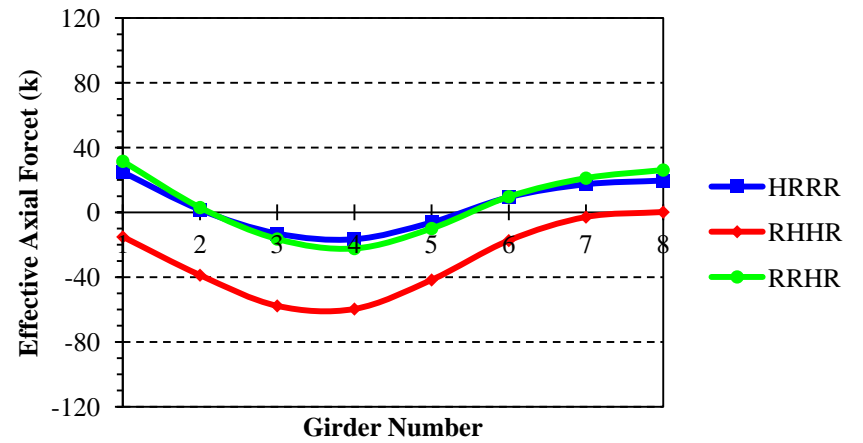
(a) Skew angle of 0°



(b) Skew angle of 20°

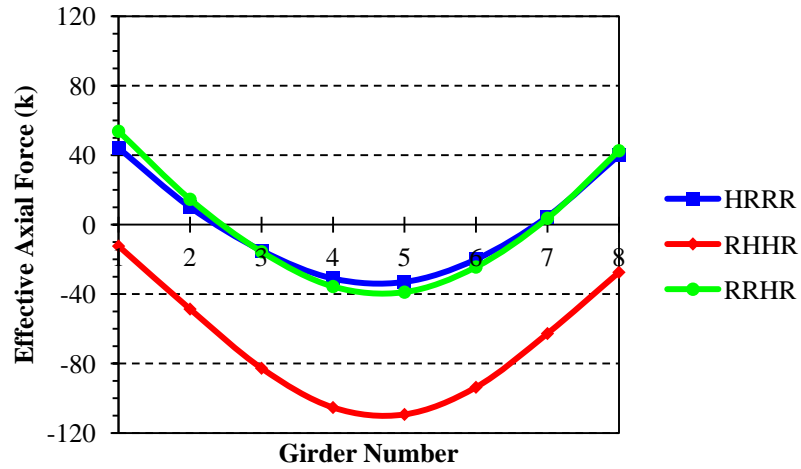


(c) Skew angle of 30°

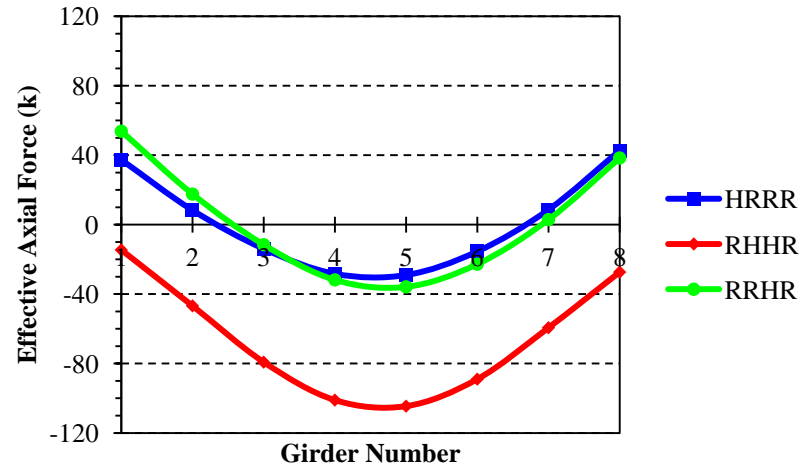


(d) Skew angle of 45°

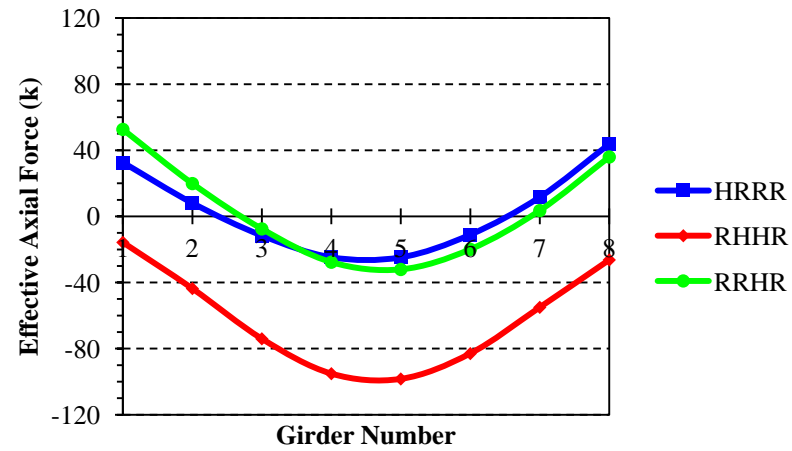
Figure 4-37. Effective force - Lane1 load case



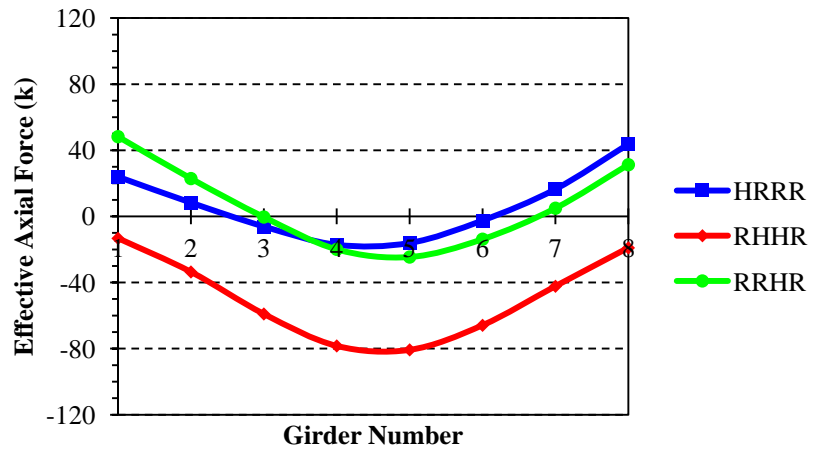
(a) Skew angle of 0°



(b) Skew angle of 20°

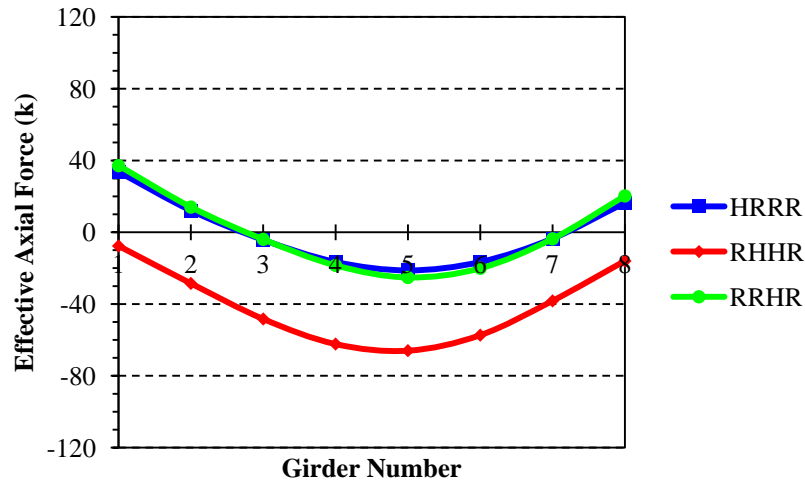


(c) Skew angle of 30°

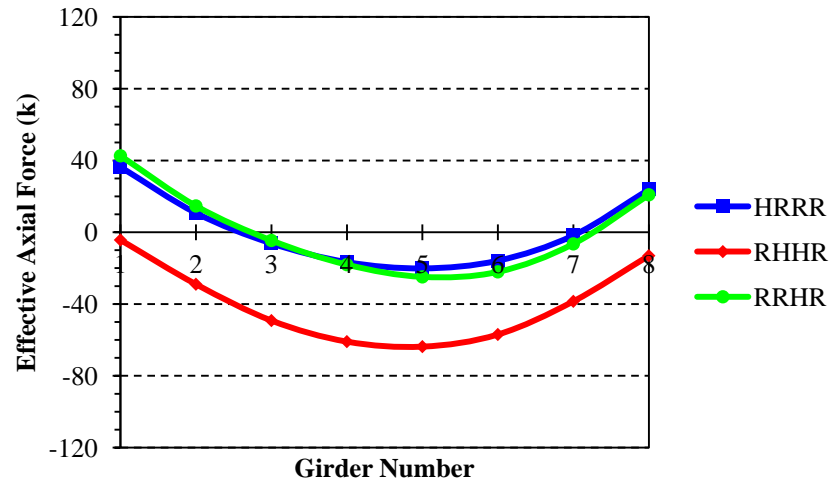


(d) Skew angle of 45°

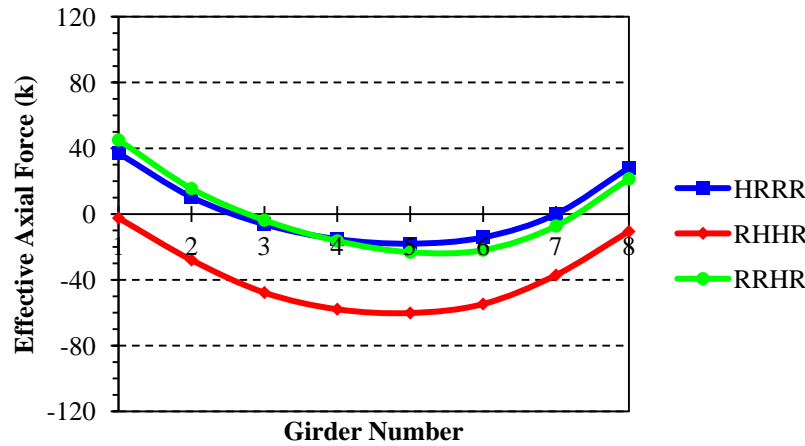
Figure 4-38. Effective force - Lane2 load case



(a) Skew angle of 0°



(b) Skew angle of 20°

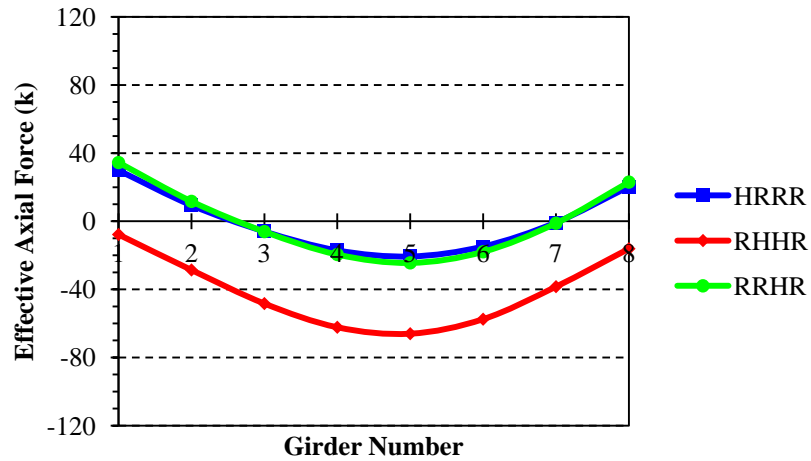


(c) Skew angle of 30°

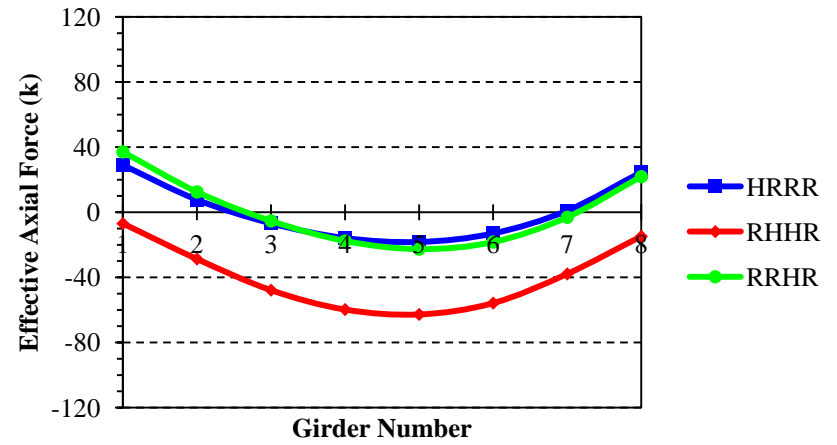


(d) Skew angle of 45°

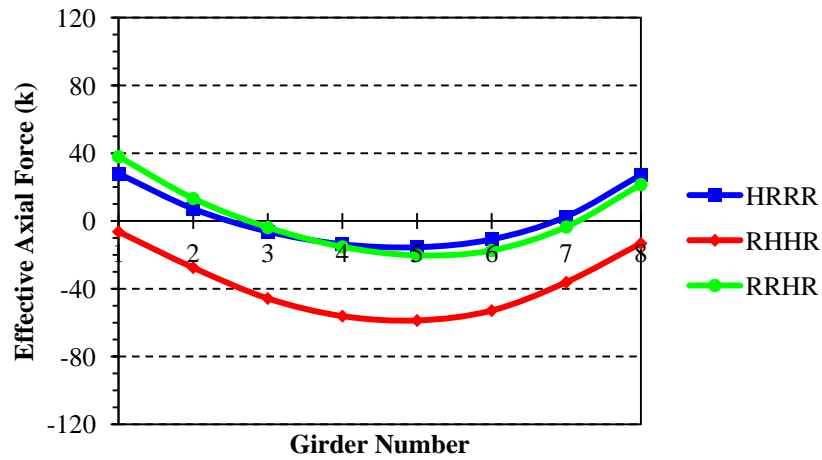
Figure 4-39. Effective Force – LaneAlt1 load case



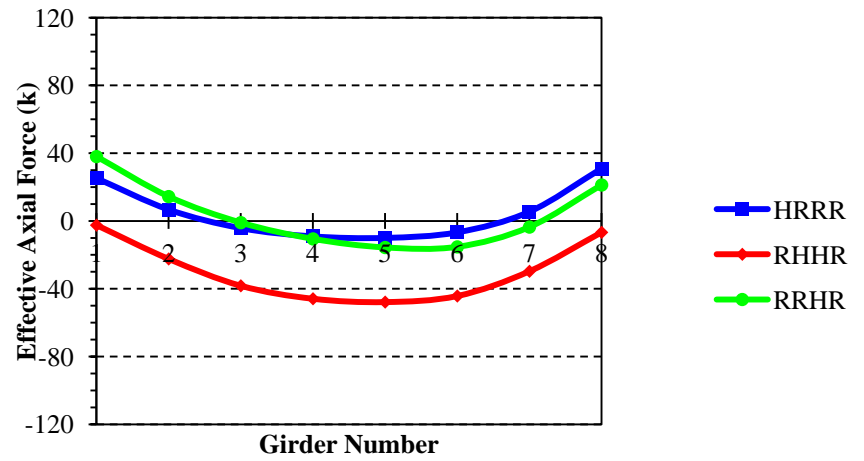
(a) Skew angle of 0°



(b) Skew angle of 20°



(c) Skew angle of 30°

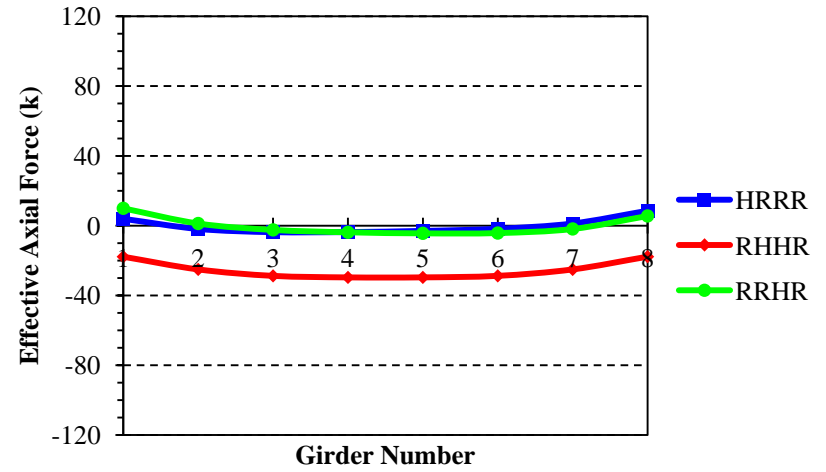


(d) Skew angle of 45°

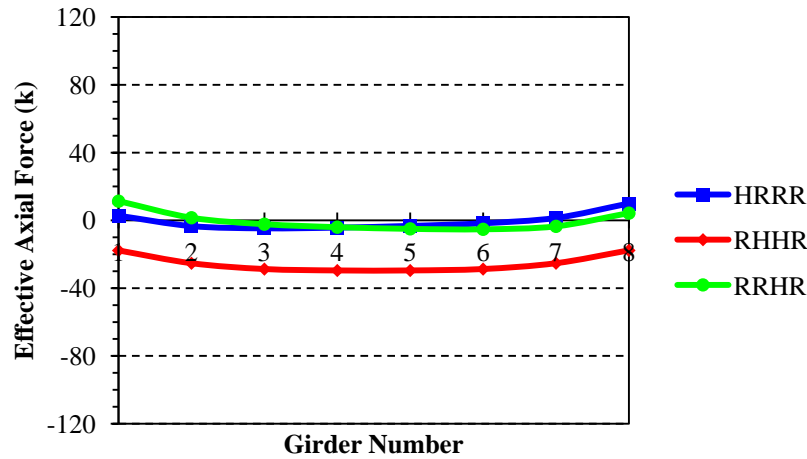
Figure 4-40. Effective Force – LaneAlt2 load case



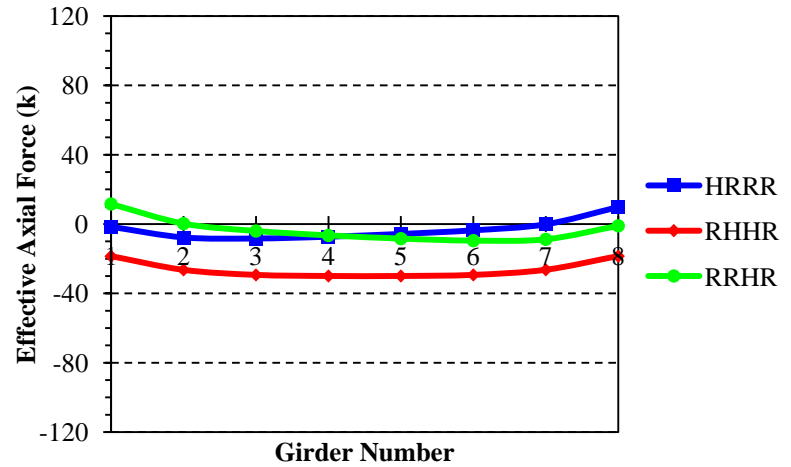
(a) Skew angle of 0°



(b) Skew angle of 20°

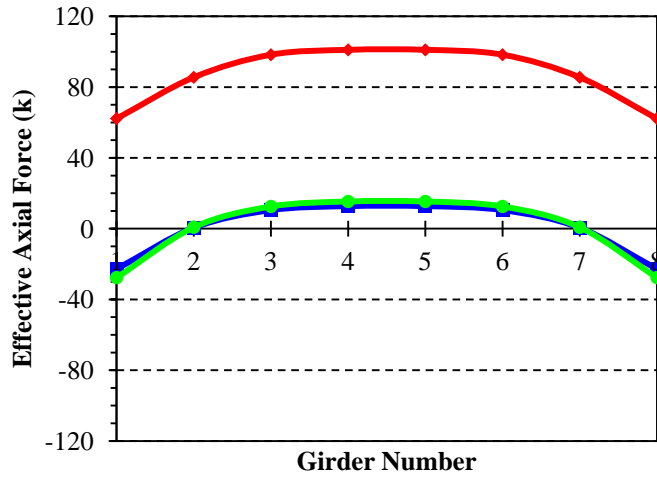


(c) Skew angle of 30°

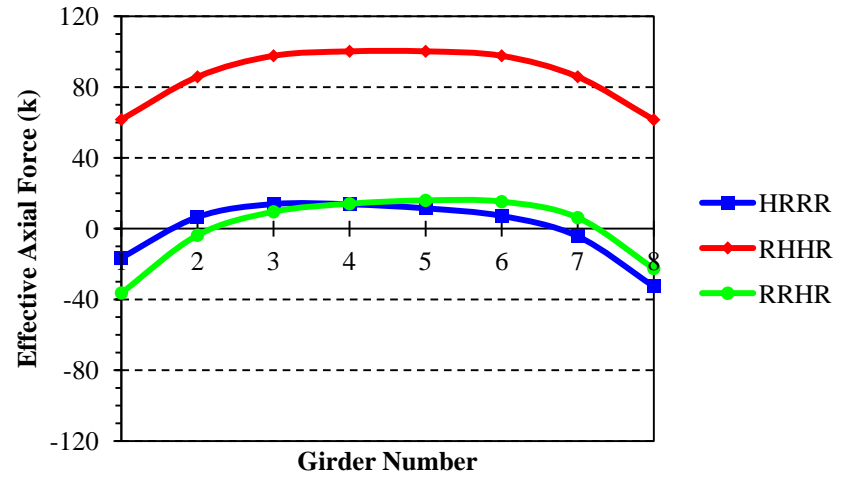


(d) Skew angle of 45°

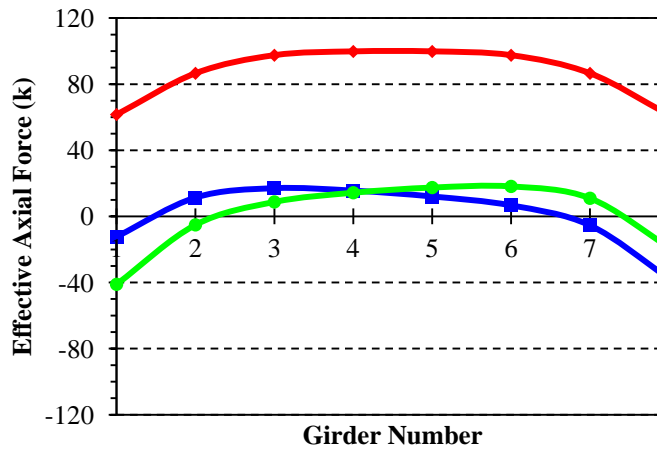
Figure 4-41. Effective force - NTG load case



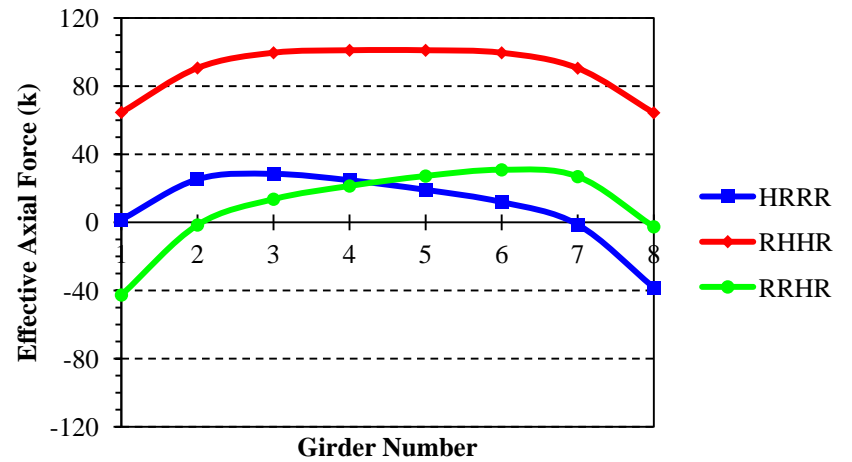
(a) Skew angle of 0°



(b) Skew angle of 20°



(c) Skew angle of 30°



(d) Skew angle of 45°

Figure 4-42. Effective force - PTG load case

The following are the key findings of the effective moment and force results:

- 1) Effective bending moments and axial forces decrease as the angle of skew increases.
- 2) Live load on both lanes (*Lane2*) is the critical load case for a two-lane bridge, effective link-slab negative moment and axial force.
- 3) Under NTG, with HRRR and RRHR boundary conditions, link-slab axial force is negligible
- 4) PTG with RHHR boundary condition is the critical load case for effective positive moments and effective forces.
- 5) The RHHR support configuration generates negative moments under live and NTG loads developing tensile stresses at the top fiber of the link slab.
- 6) Under live and NTG loads, with HRRR or RHHR support configurations, the effective link slab sections closest to the deck edges develop positive moment which increases with skew angle while the rest of the sections develop negative moments. Conversely, under PTG, negative moments develop at link slab sections close to the deck edges and increase with skew angle while the rest of the sections develop positive moments.
- 7) The effective axial force for each segment is calculated from summation of average nodal axial stress multiplied by the projected area of each node. The effective bending moment for each segment is computed by summation of nodal axial forces multiplied by the vertical distance from the neutral axis of the link slab to the node. Hence, variation of effective axial force with respect to loads, boundary conditions, and skew resembles the variation of the effective moment.
- 8) As per the results presented in Figure 4-31 through Figure 4-42, live and NTG load develop the critical load combination for negative moment whereas PTG load is critical for positive moment design.

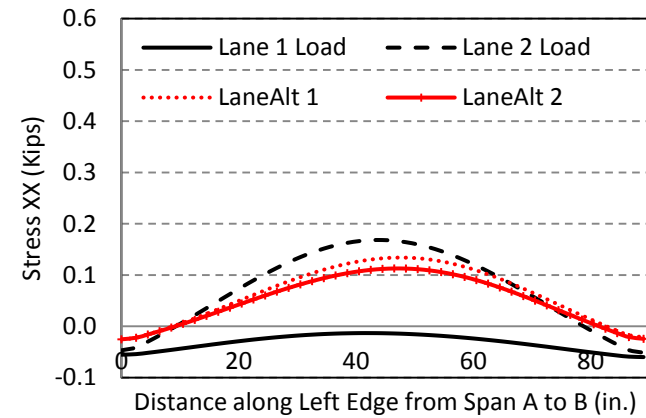
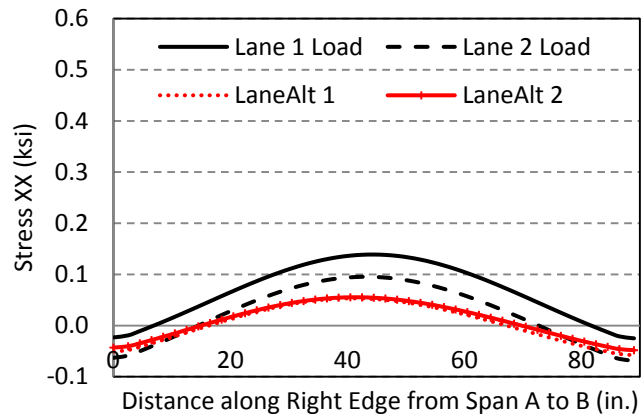
- 9) Effective moments and axial forces calculated from 3D analyses show that moment-axial force interaction should be included in the link slab design for RHHR support configuration.
- 10) In addition to axial force and moment effects, the design of high skew link slabs may need to consider additional effects of link slab torsion and in-plane twist.

4.4.4.3 Link Slab Edge Stresses under In-plane Twist

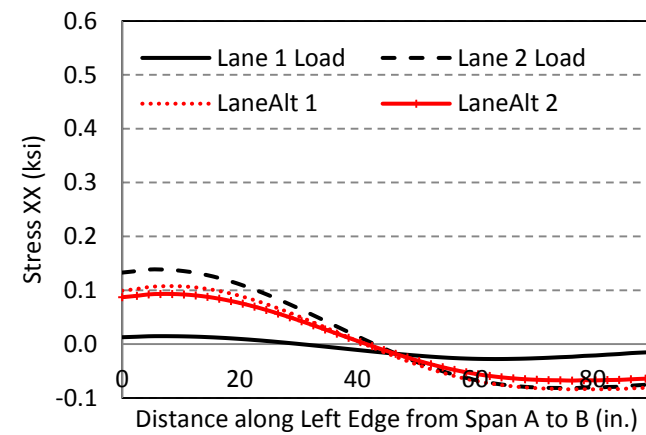
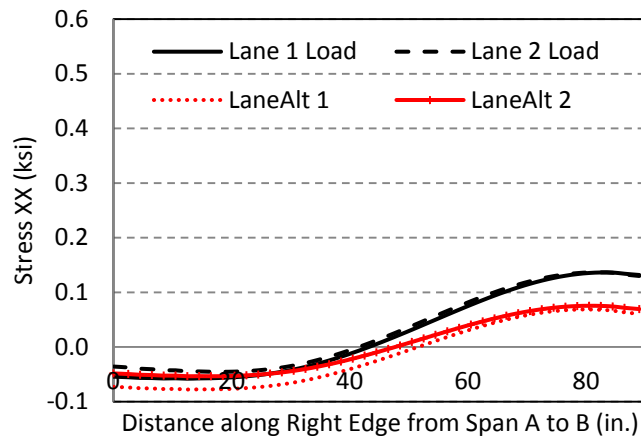
HRRR and RRHR support conditions under PTG load develop the critical in-plane twist (M_{zz}) in the link slab with increasing skew. The link slab develops axial loads under M_{zz} linearly increasing towards the outside edges of the slab. Link slab edge stresses due to twist are calculated along the right and left edges (note: right and left edges are defined based on the vehicle traveling direction, i.e., from span A to span B, shown in Figure 4-6). Live loads and NTG develop the largest tensile stresses at the edge top fiber while PTG develops the largest stresses at the link slab bottom fiber. Top fiber stresses are calculated for live loads and NTG loads are shown in Figure 4-43 and Figure 4-44. Bottom fiber stresses are calculated for PTG and shown in Figure 4-45.

The debonded length of the link slab is measured from span A to span B as defined in Figure 4-6. In skew bridges, the maximum longitudinal stresses are developed near link slab ends (i.e., at the point of debonding). The stresses developed under PTG are greater than the stresses developed under live loads and NTG. In this particular bridge with HRRR support conditions, stress developed under PTG is about 600 psi and exceeds tensile strength of grade D concrete used in bridge decks (i.e., $0.24\sqrt{f'_c}$). Deck concrete compressive strength is 4500 psi.

In order to accommodate high stresses developed along the link slab edges along the debonded zone, a joint near the link slab end is provided allowing rebars to resist the entire load. The joint needs to be saw cut and sealed for durability. Link slab reinforcement designed for moment should be checked for twist developed at the edge segments. Additional longitudinal reinforcement should be provided along the link slab edges if found inadequate.

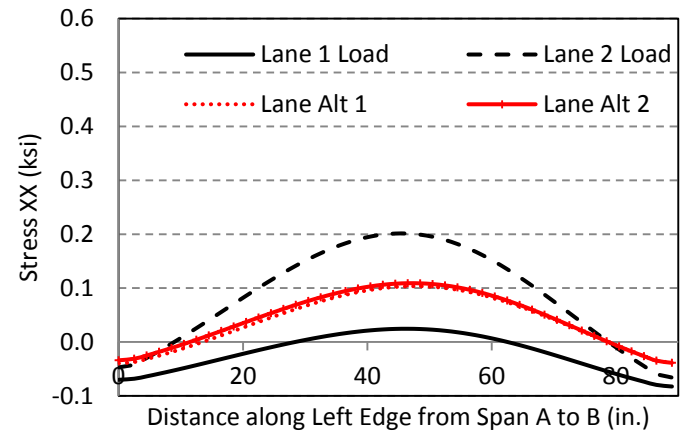
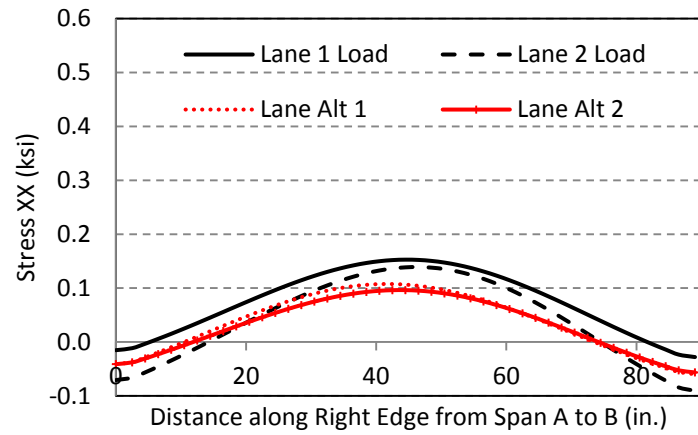


(a) Straight bridge

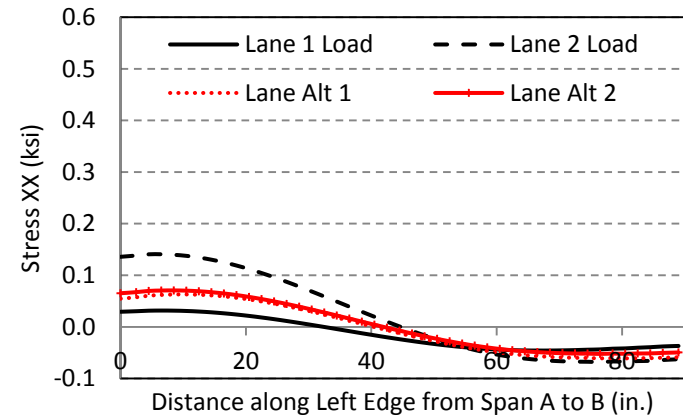
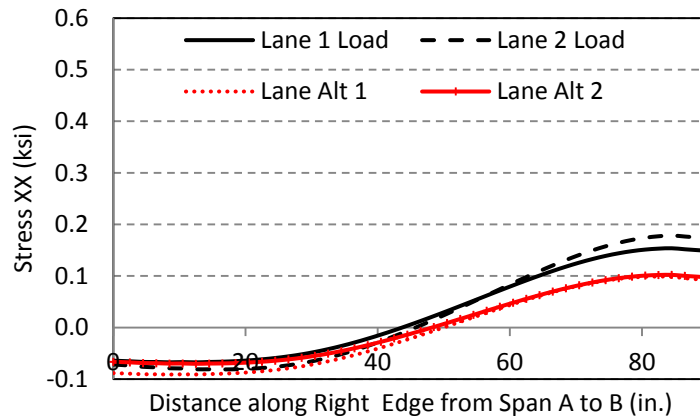


(b) 45° skew bridge

Figure 4-43. Edge stresses of link slab with HRRR support conditions under live loads



(a) Straight bridge



(b) 45° skew bridge

Figure 4-44. Edge stresses of link slab with RRHR support conditions under live loads

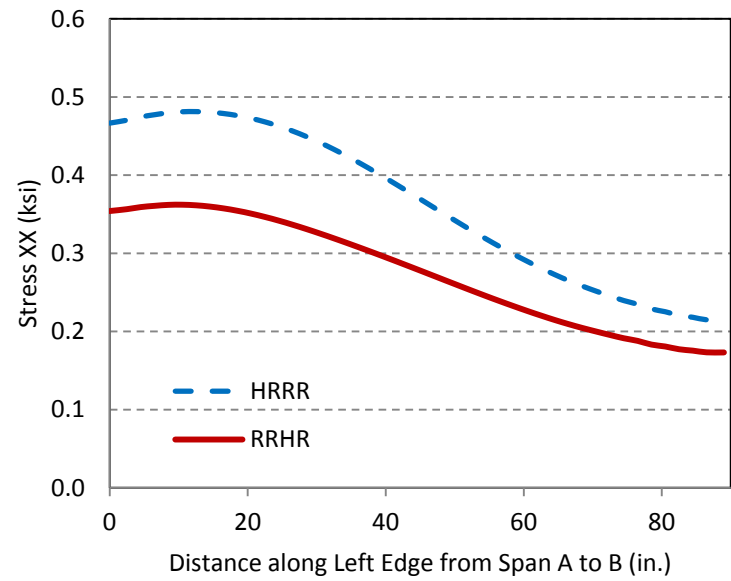
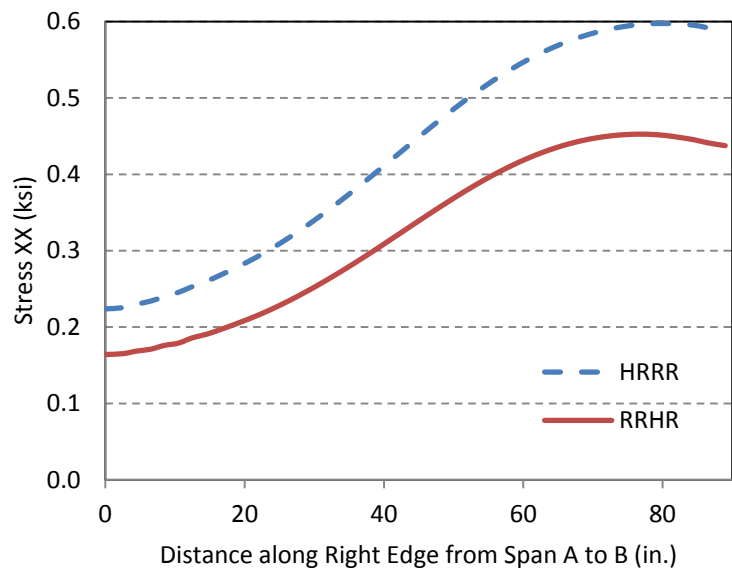
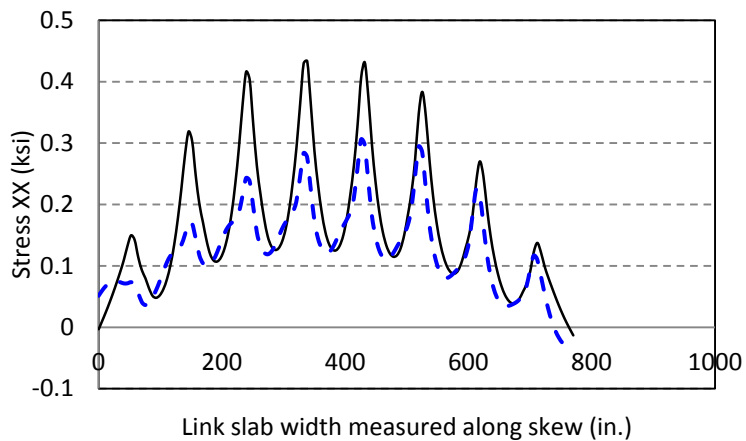


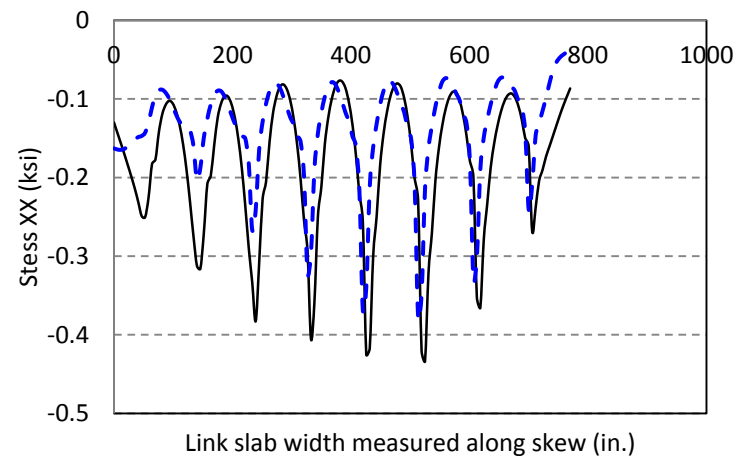
Figure 4-45. Edge stresses of a 45° skew link slab under PTG

4.4.4.4 *Link-Slab Torsion with Skew*

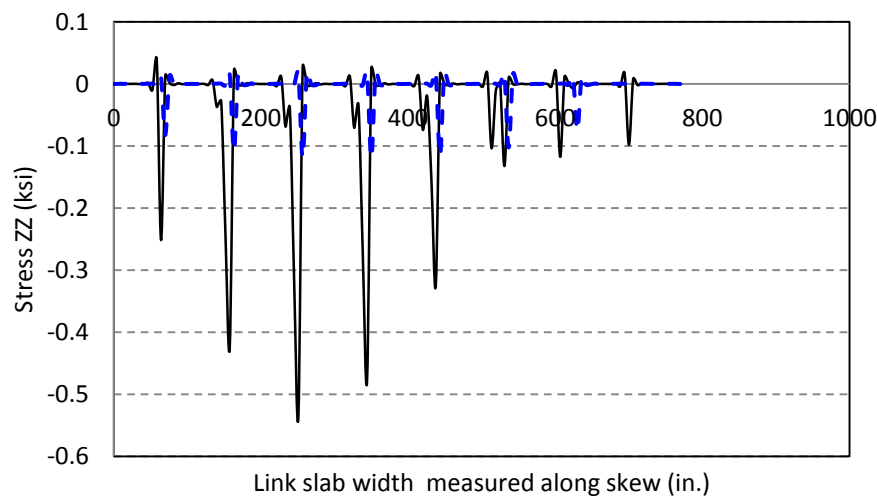
As skew increases, link slab torsion (M_{xx}) is developed under the LaneAlt1 load case (Figure 4-20). One way to deal with the torsion would be by providing cushioning between the girder ends and the link slab. For this purpose, use of a *soft* material like neoprene or Styrofoam over the girder ends underneath the link slab is investigated. The most critical case of a 45° skew link slab is analyzed under the LaneAlt1 load case, and the results are presented below. As shown in Figure 4-46, longitudinal tensile stresses and contact stresses developed underneath the link slab-girder contact points are reduced from the case without cushioning. Further, resultant gross-section moments are reduced when cushioning materials are introduced in between girder ends and the link slab (Figure 4-47).



(a) Longitudinal stress at top fiber



(b) Longitudinal stress at bottom fiber

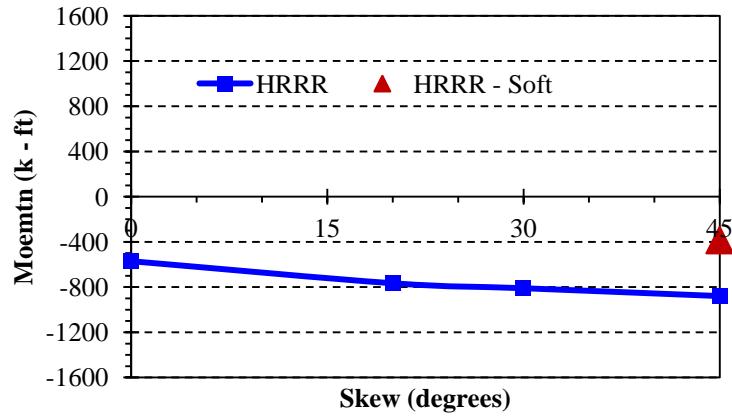


(c) Vertical stress along bottom fiber

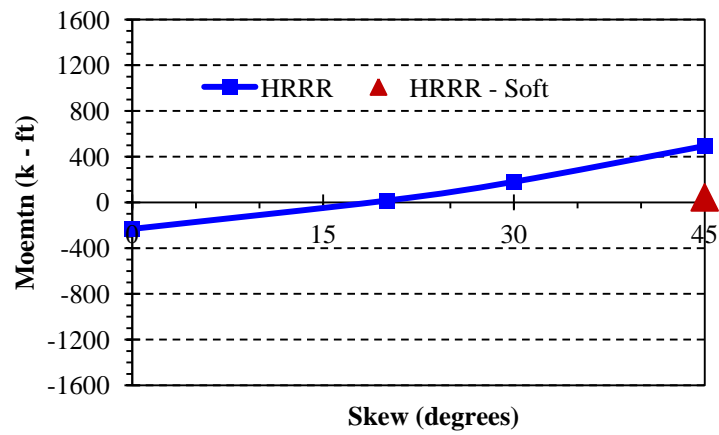
Note: The *soft* material emulates the properties similar to neoprene

Legend:
 — Without *Soft* material
 - - - - With *Soft* material

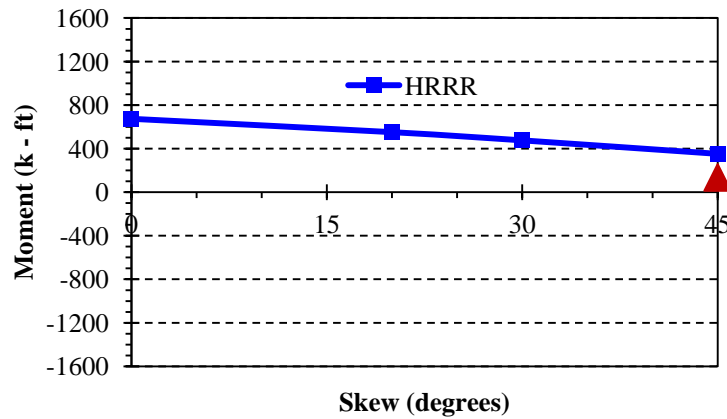
Figure 4-46. Stresses developed in 45° skew link slab with HRRR support conditions under LaneAlt1 load case



(a) Link slab torsion (M_{xx})



(b) Link slab bending moment (M_{yy})



(c) Link slab in-plane twist (M_{zz})

Note: The *soft* material emulates the properties similar to neoprene.

Figure 4-47. Gross section moment with and without soft material – LaneAlt1 load case

Placing cushioning material between girder ends and the link slab reduces torsion and resultant moments. However, there is no significant reduction in longitudinal stresses developed along the link slab edge near the transition zone at the start of the debonded region. There is a benefit in reducing contact stresses (stress zz in Figure 4-46) by using cushioning material. Also, providing construction joints between the link slab and the deck near the deck edges and additional reinforcement along the link slab's outside edges needs to be incorporated for link slabs with HRRR and RRHR support configurations. Additional reinforcement is not required for a link slab with RHHR support configuration because there is no in-plane twist (M_{zz}) under PTG (Figure 4-36).

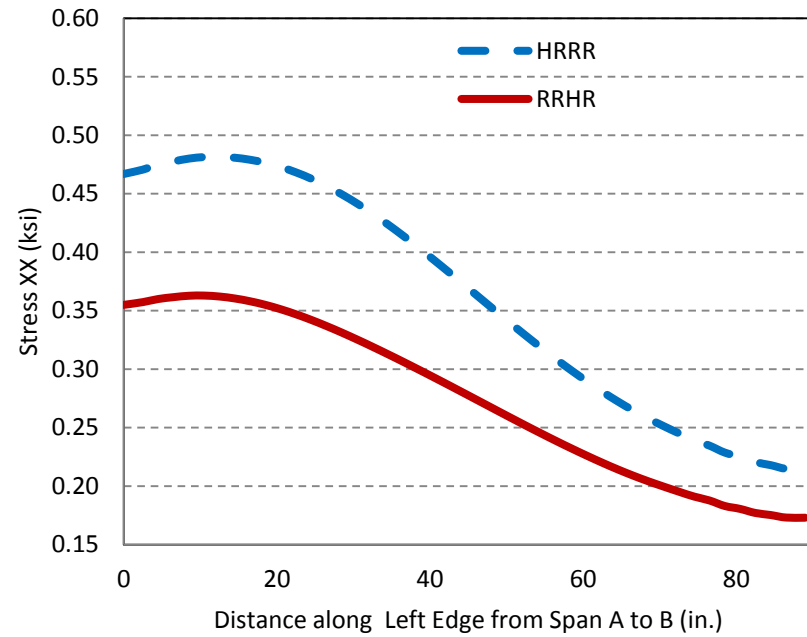
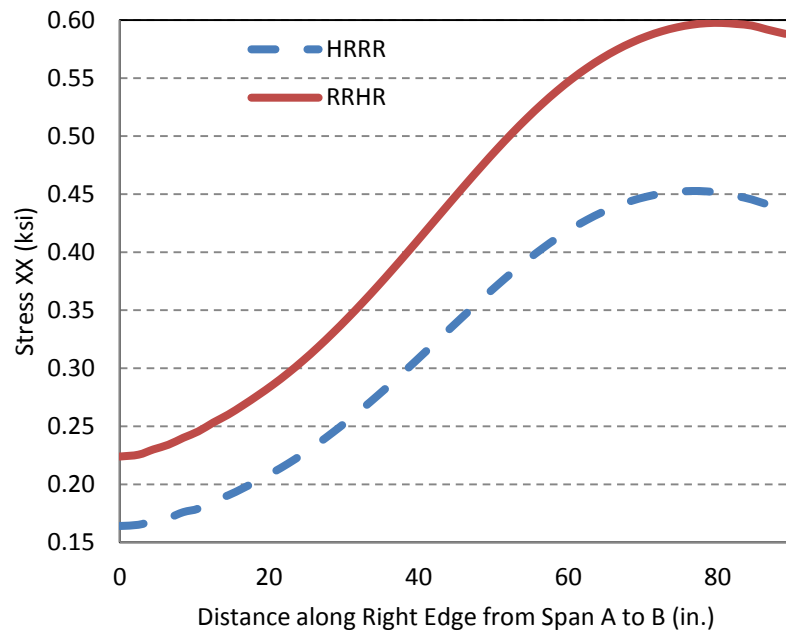


Figure 4-48. Edge stresses developed under PTG - 45° skew link slab with soft material over girder ends

4.4.4.5 Link Slab Stresses at the Transition Zone

Positive temperature gradient (PTG), with HRRR and RRHR support configurations, generate large tensile stresses at the link slab bottom fibers near the end of the link slab debonded region. Stress magnitude significantly increases directly over the girders (Figure 4-49). Longitudinal stress along the link slab bottom fiber at the end of the link slab debonded region is shown in Figure 4-50 and Figure 4-51. As seen in the figures, the stresses are greater than the tensile strength of concrete. Potential cracking can be dealt with by introducing construction joints at the boundary of debonded and fully bonded regions. Also, additional reinforcement may be required to resist the axial force.

Axial force developed within the tension region over the girders is calculated from the stresses. Elements with tensile stresses are identified and shown in Figure 4-52. The resultant tensile forces are the summation of incremental forces calculated by the stress multiplied by the associated area. The maximum tensile forces calculated for HRRR and RRHR support configurations are 33.3 kips/ft and 36.3 kips/ft. Adequacy of provided reinforcement to resist such forces should be checked. See the link slab design example provided in Appendix C for the methodology of checking the adequacy of link slab reinforcement to resist the axial load developed in the link slab.

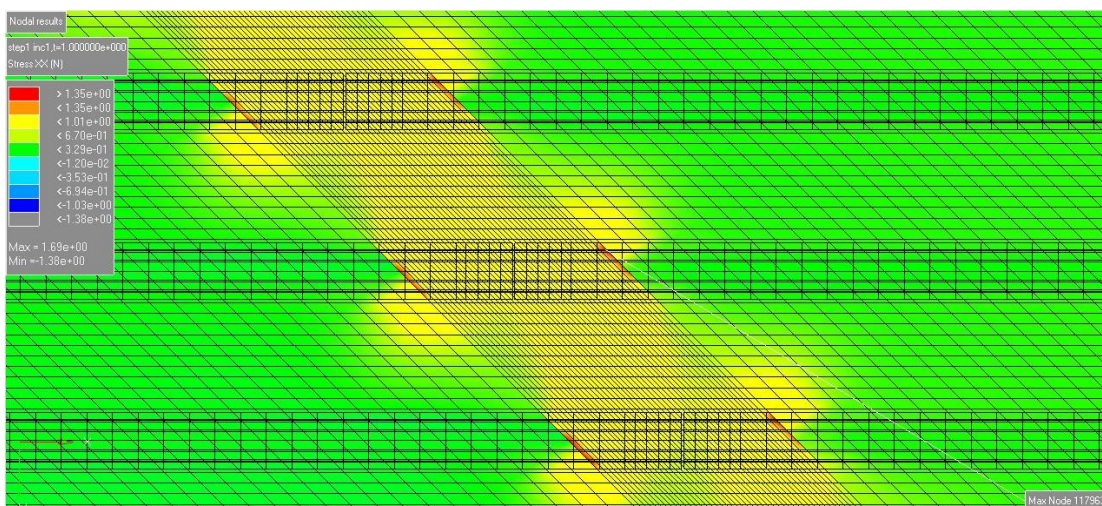


Figure 4-49. Link slab bottom fiber stresses under PTG load

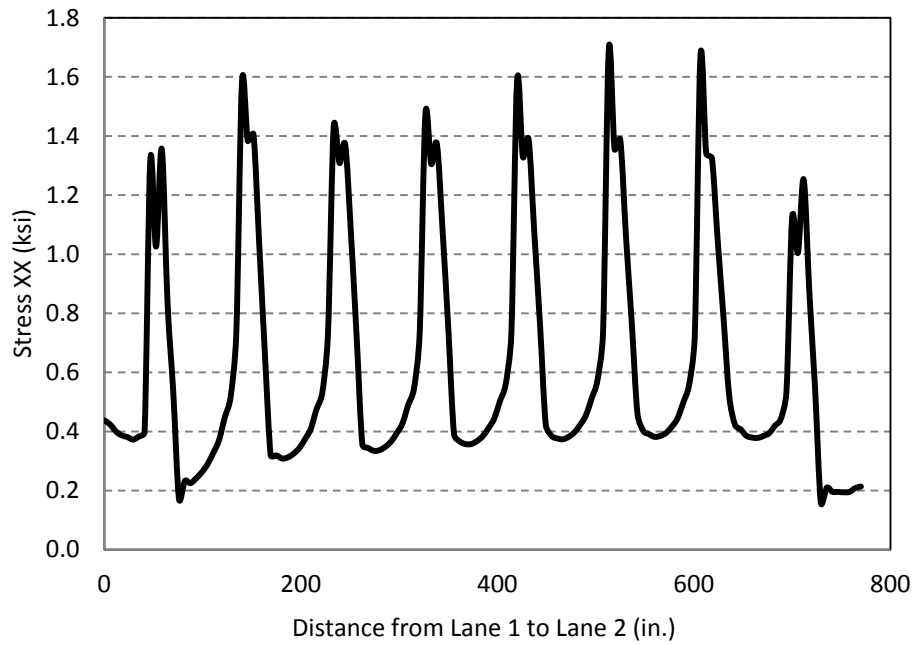


Figure 4-50. Longitudinal stress distribution across north end of the 45° skew link slab bottom fiber under PTG with HRRR support configuration

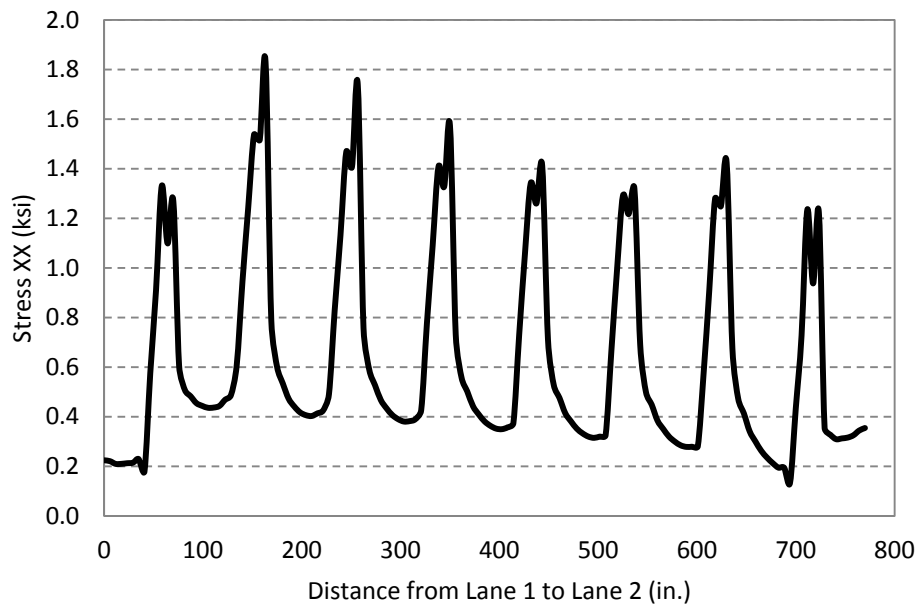


Figure 4-51. Longitudinal stress distribution across south end of the 45° skew link slab bottom fiber under PTG with RRHR support configuration

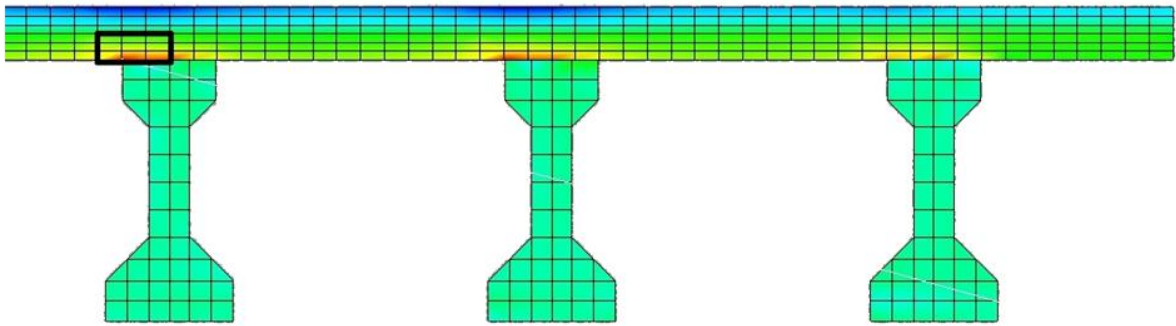


Figure 4-52. Stresses in link slab with HRRR under PTG

4.4.4.6 *Moment Reduction Factors based on Skew*

The moment demand on skew link slabs is calculated as follows. First, the maximum positive and negative moments per unit length of link slab are calculated by extracting maximum effective moments from respective figures (Figure 4-31 - Figure 4-36) and dividing them by the effective width of 66 in. (Figure 4-30). Second, the unit moment ratios with respect to the moment of link slab with zero skew (skew reduction factors) are calculated. The moment ratios for each load case are presented for all support conditions in Table 4-4, Table 4-5, and Table 4-6.

Similarly, this calculation process is duplicated for the axial force demands. Since, moments are calculated by multiplying forces by the moment arm, the axial force ratios will be the same of unit moment ratios. Thus, the ratio tables describing the skew effects will be valid for bending moments as well as axial forces.

The following conclusions are additional observations from the analysis results:

1. In general, moment demand on the link slab due to live load decreases as skew increases, irrespective of the support configuration (columns a, b, and c of Table 4-4, Table 4-5, and Table 4-6)
2. Moment demands under negative temperature gradient (NTG) and positive temperature gradient (PTG) on the link slab with RHHR (roller-hinge-hinge-roller) support configuration remains constant independent of skew (column e and f of Table 4-6).

3. The maximum effective negative and positive moment envelope patterns across the link slab under live (*Lane 2*) and NTG loads are similar (Figure 4-31 - Figure 4-36). Both load effects should be combined.
4. The link slab maximum effective positive and negative moment locations under PTG are different from NTG (Figure 4-31 - Figure 4-36). PTG should be considered independent from live loads and NTG.
5. *Lane 2* is the governing live load case for this specific bridge configuration, for all support configurations (column b of Table 4-4, Table 4-5, and Table 4-6).
6. The link slab moment with HRRR and RRHR support configuration is much less than the cracking moment capacity; additional reinforcement may be required to resist large tensile stresses developed along link slab bottom fibers within the end of the link slab debonded region (Figure 4-45 and Figure 4-48 - Figure 4-52).

Table 4-4. Skew Reduction Factors for HRRR

HRRR						
Load Case						
	Lane 1 (a)	Lane 2 (b)	Lane Alt 1 (c)	Lane Alt 2 (d)	NTG (e)	PTG (f)
Maximum Effective Positive Moment of Zero Skew Link Slab (kip – ft)/ft	2.1	3.0	1.9	2.0	0.4	0.9

Skew (Degree)	Ratio of Maximum Positive Link-Slab Effective Moment (Skew/Zero Skew) (Skew Reduction Factors)					
0	1.00	1.00	1.00	1.00	1.00	1.00
20	0.76	0.88	0.95	0.74	1.11	1.43
30	0.68	0.75	0.85	0.63	1.40	1.65
45	0.52	0.52	0.61	0.40	2.51	1.68

HRRR						
Load Case						
	Lane 1	Lane 2	Lane Alt 1	Lane Alt 2	NTG	PTG
Maximum Effective Negative Moment of Zero Skew Link Slab (kip - ft)/ft	-1.8	-2.2	-1.2	-1.4	-0.2	-1.6

Skew (Degree)	Ratio of Maximum Negative Link-Slab Effective Moment (Skew/Zero Skew) (Skew Reduction Factors)					
0	1.00	1.00	1.00	1.00	1.00	1.00
20	0.79	≈1.00	1.08	0.81	1.47	1.09
30	0.72	≈1.00	1.10	0.78	1.73	1.33
45	0.66	≈1.00	1.08	0.87	1.71	2.23

Table 4-5. Skew Reduction Factors for RRHR

	RRHR					
	Load Case					
	Lane 1 (a)	Lane 2 (b)	Lane Alt 1 (c)	Lane Alt 2 (d)	NTG (e)	PTG (f)
Maximum Effective Positive Moment of Zero Skew Link Slab (kip - ft)/ft	2.6	3.7	2.1	2.0	0.5	1.0

Skew (Degree)	Ratio of Maximum Positive Link-Slab Effective Moment (Skew/Zero Skew) (Skew Reduction Factors)					
0	1.00	1.00	1.00	1.00	1.00	1.00
20	0.92	0.92	0.99	0.93	1.05	1.32
30	0.84	0.83	0.92	0.83	1.25	1.49
45	0.68	0.63	0.83	0.64	2.29	1.54

	RRHR					
	Load Case					
	Lane 1	Lane 2	Lane Alt 1	Lane Alt 2	NTG	PTG
Maximum Effective Negative Moment of Zero Skew Link Slab (kip - ft)/ft	-1.9	-2.7	-1.4	-1.4	-0.3	-1.9

Skew (Degree)	Ratio of Maximum Negative Link-Slab Effective Moment (Skew/Zero Skew) (Skew Reduction Factors)					
0	1.00	1.00	1.00	1.00	1.00	1.00
20	0.90	1.00	1.15	1.08	1.36	1.04
30	0.80	0.98	1.21	1.10	1.56	1.18
45	0.69	0.90	1.28	1.10	1.59	2.01

Table 4-6. Skew Reduction Factors for RHHR

	RHHR					
	Load Case					
	Lane 1 (a)	Lane 2 (b)	Lane Alt 1 (c)	Lane Alt 2 (d)	NTG (e)	PTG (f)
Maximum Effective Zero Skew Link Slab Moment (kip - ft)/ft	-4.4	-7.5	-3.7	-3.7	-2.0	4.2
Skew (Degree)	Ratio of Maximum Link-Slab Effective Moment (Skew/Zero Skew) (Skew Reduction Factors)					
0	1.00	1.00	1.00	1.00	1.00	1.00
20	0.96	0.96	0.97	0.95	≈ 1.00	≈ 1.00
30	0.91	0.90	0.91	0.89	≈ 1.00	≈ 1.00
45	0.77	0.74	0.76	0.72	≈ 1.00	≈ 1.00

4.4.4.7 Skew Reduction Factors based on Girder-End Rotations

Girder-end rotations are calculated from nodal displacements at the North end of each girder in Span A. These results are shown in Table 4-7 through Table 4-12, columns a-c. The ratios of the maximum girder-end rotation to the maximum girder-end rotation from the model with no skew, much like what was done for the effective bending moment, are calculated and presented in Table 4-7 through Table 4-12, columns d-f.

For the live load cases, rotations decrease for the HRRR and RRHR boundary conditions and for angles of skew greater than 30°. The RHHR boundary condition has no appreciable difference in the girder-end rotations under live loads even with an angle of skew of 45°. Lane2 load case is the controlling load configuration for a two lane bridge as demonstrated by the girder-end rotations under live loads shown in Table 4-7 through Table 4-12. The HRRR and RRHR boundary conditions show a decrease in girder-end rotations of 24% and 25%, respectively for the 45° skew bridge with the Lane2 load case. When the Lane2 load case and RHHR boundary conditions are considered, there is only 3% reduction in the girder rotations in the 45° skew bridge compared to that of the straight bridge.

In the design process girder-end rotations are calculated from simple beam analysis considering the girder-end displacement in the global X-direction; hence they fail to represent resultant girder-end rotation calculated from a 3D model. For this reason, the use of skew reduction factors calculated using the moment ratio is recommended (Table 4-4, Table 4-5, and Table 4-6).

Table 4-7. Girder-End Rotations and Skew Reduction Factors - Lane1 Load Case

Angle of Skew	Girder-End Rotation (radians)			Skew Reduction Factors		
	HRRR (a)	RRHR (b)	RHHR (c)	HRRR (d)	RRHR (e)	RHHR (f)
0	0.000562	0.00601	0.000196	1.0000	1.0000	1.0000
20	0.000562	0.000593	0.000200	0.9995	0.9870	1.0173
30	0.000548	0.000574	0.000201	0.9744	0.9549	1.0221
45	0.000481	0.000494	0.000194	0.8554	0.8230	0.9884

Table 4-8. Girder-End Rotations and Skew Reduction Factors - Lane2 Load Case

Angle of Skew	Girder-End Rotation (radians)			Skew Reduction Factors		
	HRRR (a)	RRHR (b)	RHHR (c)	HRRR (d)	RRHR (e)	RHHR (f)
0	0.000926	0.000984	0.000263	1.000	1.000	1.000
20	0.000873	0.000926	0.000259	0.943	0.942	0.985
30	0.000834	0.000881	0.000261	0.900	0.896	0.993
45	0.000699	0.000732	0.000254	0.755	0.745	0.967

Table 4-9. Girder-End Rotations and Skew Reduction Factors – LaneAlt1 Load Case

Angle of Skew	Girder-End Rotation (radians)			Skew Reduction Factors		
	HRRR (a)	RRHR (b)	RHHR (c)	HRRR (d)	RRHR (e)	RHHR (f)
0	0.000562	0.00601	0.000196	1.000	1.000	1.000
20	0.000562	0.000593	0.000200	0.9995	0.9870	1.0173
30	0.000548	0.000574	0.000201	0.9744	0.9549	1.0221
45	0.000481	0.000494	0.000194	0.8554	0.8230	0.9884

Table 4-10. Girder-End Rotations and Skew Reduction Factors – LaneAlt2 Load Case

Angle of Skew	Girder-End Rotation (radians)			Skew Reduction Factors		
	HRRR (a)	RRHR (b)	RHHR (c)	HRRR (d)	RRHR (e)	RHHR (f)
0	0.000492	0.000148	0.000526	1.000	1.000	1.000
20	0.000468	0.000148	0.000497	0.9501	0.9955	0.9442
30	0.000454	0.000151	0.000472	0.9219	1.0149	0.8971
45	0.000397	0.000150	0.000407	0.8068	1.0084	0.7735

Table 4-11. Girder-End Rotations and Skew Reduction Factors - NTG Load Case

Angle of Skew	Girder-End Rotation (radians)			Skew Reduction Factors		
	HRRR (a)	RRHR (b)	RHHR (c)	HRRR (d)	RRHR (e)	RHHR (f)
0	0.000264	0.000273	0.000064	1.000	1.000	1.000
20	0.000257	0.000261	0.000079	0.975	0.958	1.225
30	0.000255	0.000249	0.000086	0.966	0.912	1.341
45	0.000234	0.000223	0.000095	0.886	0.818	1.483

Table 4-12. Girder-End Rotations and Skew Reduction Factors - PTG Load Case

Angle of Skew	Girder-End Rotation (radians)			Skew Reduction Factors		
	HRRR (a)	RRHR (b)	RHHR (c)	HRRR (d)	RRHR (e)	RHHR (f)
0	-0.000989	-0.001019	-0.000220	1.000	1.000	1.000
20	-0.000982	-0.000994	-0.000271	0.993	0.975	1.230
30	-0.000978	-0.000963	-0.000298	0.989	0.946	1.351
45	-0.000930	-0.000901	-0.000335	0.940	0.885	1.523

4.4.5 Skew Link Slab Design Procedure

4.4.5.1 Overview

The skew link slab design is based on the bending moment and axial force calculated from analysis that incorporates the effects of skew under specific load combinations. The simplified analysis procedure for bridges with no skew was presented in Ulku et al. (2009). The analysis procedure assumes that the link slab does not provide any continuity between spans. Therefore, the spans are analyzed as simply supported. The girder-end rotations are calculated from the design load combinations. Imposing compatibility, the link slab is subjected to a rotation equal to the girder-end rotation. The link slab moment is calculated from Eq. 4-10 by substituting the beam end rotation.

$$M = \frac{2E_c I_{LS} \theta}{L_{LS}} \quad (4-10)$$

where

M = Link slab bending moment (k-in)

E_c = Elastic modulus of concrete (ksi)

I_{LS} = Moment of inertia of the link slab (in⁴)

L_{LS} = Length of link slab (in)

θ = Girder-end rotation (radians)

The simplified link-slab design procedure by Caner and Zia (1998) was updated by Ulku et al. (2009) to incorporate the effects of bearing configurations and thermal gradient loads, also for bridges with zero skew. The procedure developed here is the modification of the procedure by Ulku et al. (2009) to incorporate the effects of link-slab skew.

The load demand calculation based on the modified procedure and link slab design is described below on a numerical example with the geometry of the specific bridge used in the FE analysis. Geometric and material property data used in this section as well as in the design example presented in Appendix C are given in Figure 4-53 and Table 4-13.

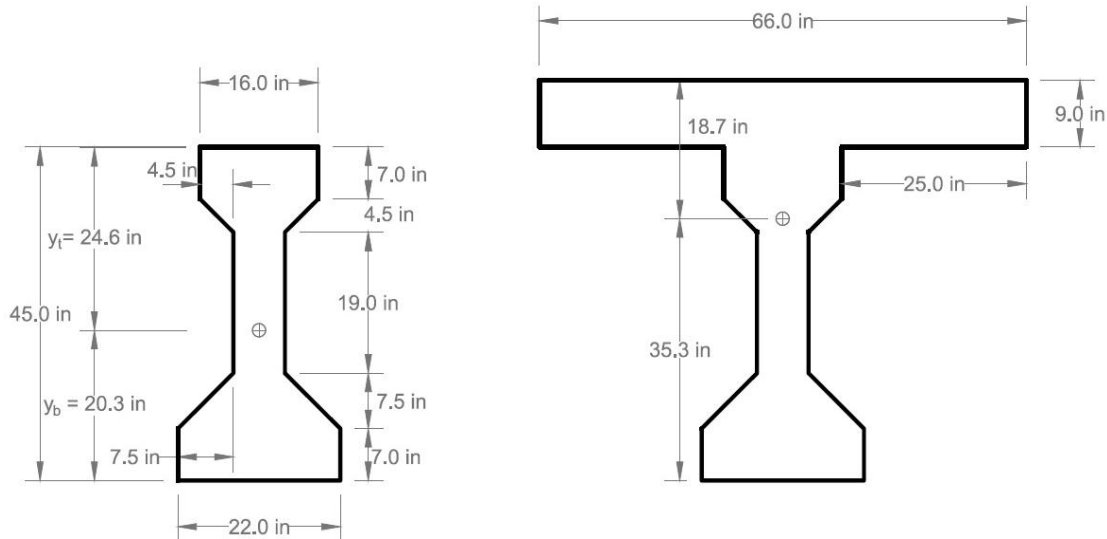


Figure 4-53. AASHTO Type III girder and composite section geometric properties

Table 4-13. Material and Geometric Properties used in Link Slab Design Example

Boundary condition	RHHR
Skew (θ)	45 deg.
Compressive strength of concrete (f_c')	4,500 psi
Unit weight of concrete (w_c)	0.15 kcf
Concrete modulus of elasticity (E_c) (AASHTO LRFD Section 5.4.2.4)	4,067 psi
Reinforcement yield strength (f_y)	60 ksi
Steel modulus of elasticity (E_s)	29,000 ksi
Link slab length (L_{LS})	84.4 in.
Effective deck width (B) ⁺	66 in.
Link slab thickness	9 in.
Moment of inertia of link slab (I_{LS})	4,009.5 in ⁴
Deck overhang (on either side of the beam)	25 in.
Moment of inertia of the girder (I_{girder})	125,390 in ⁴
Moment of inertia of the composite section ($I_{composite}$)	375,678 in ⁴

+ Link slab section perpendicular to bridge longitudinal axis is considered in the example because design moments are calculated perpendicular to bridge longitudinal axis (Figure 4-31 - Figure 4-42).

4.4.5.2 Live Load and Thermal Gradient Moments

In the analysis procedure for the skew link slab, girder-end rotation of 3.47×10^{-3} radians is calculated under HL-93 load on a 69.5 ft span of a zero-skew bridge as per AASHTO LRFD (2010). An impact factor of 1.33 is included with the truck load. The live load distribution factor for the zero-skew bridge is calculated as 0.508. The girder end rotation used in Eq. 4-10 (i.e., analytical design rotation) is calculated by multiplying 3.47×10^{-3} radians with 0.508 (Table 4-14).

Girder-end rotations for thermal gradient loads are calculated following the procedure presented by Ulku et al. (2009). (Design example in Appendix C is included for more details; a MathCAD calculation sheet is also included in Appendix D.) The analytical rotations and analytical design moments for all three loads are shown in Table 4-14. Thermal gradient load effects are not subjected to distribution factors; hence, the analytical-girder end rotations are directly used as design rotations. Lastly, analytical design moments under thermal gradient loads are calculated from Eq. 4-10 as shown in Table 4-14.

Table 4-14. Analytical Rotation and Analytical Design Moment Magnitudes

Load Case	Analytical Rotation (Radians)	Distribution Factor	Analytical Design Rotation	Analytical Design Moment (k-ft)/ft
Live	0.003470	0.508	0.001763	10.32
NTG	0.000484	N/A	0.000484	2.83
PTG	0.001613	N/A	0.001613	9.44

Note: NTG – negative temperature gradient; PTG – positive temperature gradient

4.4.5.3 Moment Reduction due to 3D Effect

The design moments calculated by this analytical procedure are significantly greater than the moments calculated from FE analysis. Design moments from FE analysis and the simplified analytical procedure are compared in Table 4-15 as the moment ratios obtained by the two procedures.

Table 4-15. Ratios of 3D FE to Analytical Design Moment for a Straight Bridge

Load Case	HRRR	RRHR	RHHR
Live	0.218	0.257	0.887
NTG	0.092	0.111	0.967
PTG	0.080	0.100	0.961

As observed in Table 4-15 , the maximum link slab live load moments calculated by FE analysis with RHHR support configuration is about 90% of the design moments calculated by the simplified analytical procedure. The maximum link slab live load moments calculated by FE analysis with HRRR and RRHR supports are approximately 22% and 26% of the design moments calculated by the simplified analytical procedure.

4.4.5.4 Span Effect on Link Slab Moment

Another parametric study was conducted to evaluate the span effect on link slab design moments. Spans ranging from 70 ft to 120 ft were identified by analyzing the Michigan bridge inventory. According to the data provided in Table 4-16, only moment due to live load increases with increasing span. The link slab moment due to temperature gradient load remain constant (Table 4-16 column y and z) because the curvature remains constant. According to Eq. C-9 and C-10, the length cancels and design moment due to temperature gradient is not a function of span.

Table 4-16. Analytical Rotation and Analytical Design Moment Magnitudes for Different Spans

Span (ft)	Analytical Rotation (rad)			DF*	Analytical Design Rotation (rad)			Analytical Design Moment (k-ft/ft)		
	LL	NTG	PTG		LL	LL	NTG	PTG	LL	NTG
	(a)	(b)	(c)	(d)	(a)*(d)= (e)	(b) = (f)	(c) = (g)	(x)	(y)	(z)
70	0.00347	0.00048	0.00161	0.51	0.00176	0.00048	0.00161	10.32	2.83	9.44
80	0.00475	0.00055	0.00185	0.49	0.00233	0.00055	0.00185	11.95	2.84	9.46
90	0.00627	0.00062	0.00208	0.48	0.00299	0.00062	0.00208	13.63	2.84	9.47
100	0.00803	0.00069	0.00231	0.46	0.00373	0.00069	0.00231	15.29	2.84	9.48
110	0.01005	0.00076	0.00254	0.45	0.00455	0.00076	0.00254	16.99	2.85	9.48
120	0.01236	0.00083	0.00277	0.44	0.00548	0.00083	0.00277	18.74	2.85	9.49

*No distribution factor (DF) used for NTG and PTG

The span effect on the ratio of 3D FE moment to analytical design moment for straight bridge was calculated and shown in Table 4-17. According Table 4-17, the ratios for both PTG and NTG remain approximately constant with span. Thus, the link slab moment due to temperature gradient is independent of span.

As observed from Table 4-17, live load (LL) moment ratio decreases with increasing span. However, from the simple calculation procedure, the LL moment increases with increasing

span (Table 4-16). This discrepancy is because the simple procedure uses girder end rotation to calculate the link slab moment. In doing so, the loads acting on the link slab are not considered. In 3D FE analysis, lane load is placed on both spans as per the AASHTO LRFD (2010) specifications is continuous over the link-slab. With increasing span the link slab length also increases; hence, the load on the link slab cantilevering from the beam reduces the link slab rotation. The link slab design moment with increasing span should be based on rotations calculated from the simple beam analysis. Increasing span results in increasing link-slab length. Consequently, increasing rotation will not increase the link slab-moment and providing minimum reinforcement will be adequate for bridges with span up to 110 ft.

Table 4-17. Ratio of 3D FE to Analytical Bending Moment for Straight Bridge with Different Spans

Span (ft)	LL			PTG			NTG		
	HRRR	RRHR	RHHR	HRRR	RRHR	RHHR	HRRR	RRHR	RHHR
70	0.218	0.257	0.887	0.092	0.111	0.967	0.080	0.100	0.961
80	0.171	0.215	0.798	0.082	0.106	1.015	0.066	0.093	1.006
90	0.141	0.178	0.791	0.093	0.117	1.032	0.075	0.103	1.022
100	0.113	0.144	0.768	0.099	0.123	1.042	0.080	0.107	1.031
110	0.093	0.120	0.768	0.101	0.125	1.048	0.081	0.109	1.037

4.4.5.5 Skew Effect on Link Slab Moment

Also of interest is skew effects on link slab moments. Skew reduction factors were calculated using moment ratios and were presented in Table 4-4, Table 4-5, and Table 4-6. Skew reduction factors presented in Table 4-4, Table 4-5, and Table 4-6 vary significantly with the live loads configurations, support configurations under the link slab, and whether the moment is negative or positive. For the specific bridge configuration used in the FE analysis, *Lane 2* is the governing live load configuration. Skew reduction factors show that load demand decreases with increasing skew.

A detailed link slab design example is included in Appendix C. The bridge in this example is with RHHR support configuration, which develops the largest link slab moments and axial forces under applied loads. Yet, the amount of required link slab reinforcement is governed by the minimum reinforcement amount requirements of AASHTO LRFD (2010).

4.4.5.6 *Summary of Link Slab Analysis Results*

The following are further key summary observations on analysis results:

1. The RHHR boundary condition develops significantly larger link-slab moments compared to other support conditions.
2. NTG can be excluded from design load combination with HRRR and RRHR support conditions.
3. NTG load case moments that develop in the link slab of bridges with zero skew and RHHR support configuration, should be directly used in design without any reduction for skew.
4. The negative moment design of a link slab with the RHHR support configuration is governed by the combined effect of live and NTG loads.
5. Positive moment design of a link slab with the RHHR support configuration is governed by a PTG load.
6. Moment developed in a link slab under thermal gradient loads (PTG and NTG) remains constant irrespective of span.
7. Providing the minimum reinforcement amount required in AASHTO LRFD Section 5.7.3.3.2 is adequate for the majority of skew link slabs with HRRR or RRHR support configuration for spans up to 110 feet. However, additional reinforcement at the bottom layer is needed to resist large tensile stresses developed near the boundaries of the debonded region. A top layer of #6 bars at 4 in. spacing and bottom layer of #6 bars at 4 in. spacing are adequate for high skew link slabs. Proposed detail in standard MDOT Bridge Design Guide format is presented in Appendix E.
8. Simplified analysis models are not able to represent three dimensional effects such as positive moments under live load or negative moments under PTG. New analysis models and procedures are required.

5 SKEW ABUTMENT ANALYSIS AND DESIGN GUIDELINES

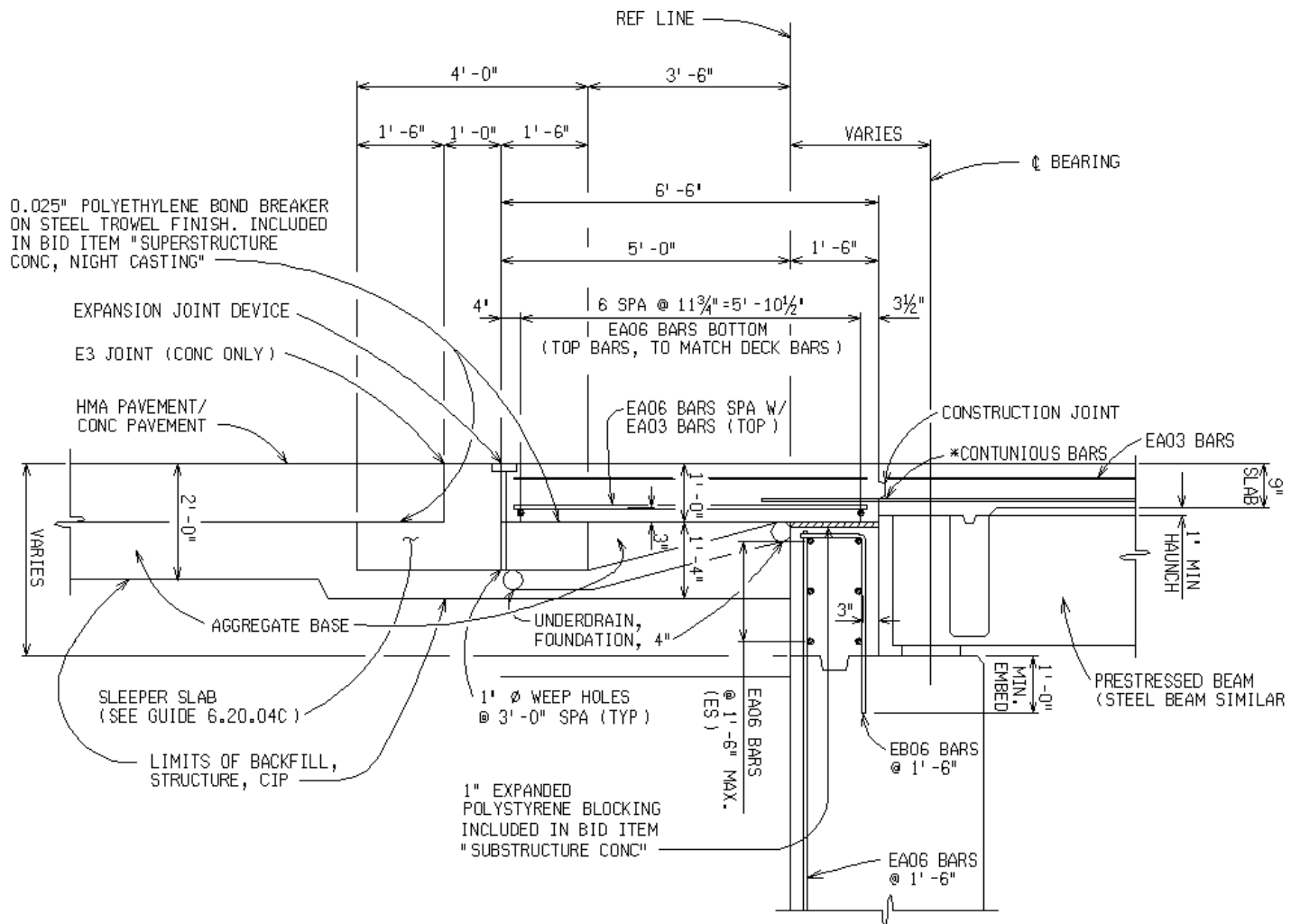
5.1 OVERVIEW AND OBJECTIVES

This chapter presents the detailed analysis of (1) two skew abutment configurations namely deck sliding over backwall and semi-integral systems, (2) deformation and rotation demands at bearings with respect to the skew angle, and (3) forces at girder ends and other components with respect to skew angle. The analysis was performed for a specific bridge (i.e., span length, width, and girder type) modeled for two different abutment configurations, and with various angles of skew from 0° to 45° . The finite element (FE) models, for selected skew configurations, were analyzed under loads and configurations as specified in AASHTO (2010) and the Michigan Bridge Design Manual (MDOT 2005). Design recommendations and design details were developed based on literature review, analysis results, and AASHTO (2010), AASHTO (2008), and MDOT (2005) requirements on strength and service load combinations.

5.2 ABUTMENT CONFIGURATIONS AND ANALYSIS MODELS

Deck sliding over backwall and semi-integral abutment details presented in Aktan et al. (2008) were considered in this analysis. Figure 5-1 shows the details of the deck sliding over backwall abutment configuration. Wingwalls were not included in the model.

The semi-integral abutment detail with backwall placed directly over the abutment is shown in Figure 5-2. This configuration was analyzed with and without wingwalls. Additional configuration considered in the analysis was the backwall offset from the abutment wall as depicted in Figure 5-3. Strictly speaking, the analysis models of the configurations shown in Figure 5-2 and Figure 5-3 are practically the same when adequate space is provided between the abutment and backwall, and the vertical load transfer from backwall to abutment is prevented.



* CONTINUE BOTTOM BARS 24" PAST CONSTRUCTION JOINT INTO THE APPROACH SLAB

Figure 5-1. Deck sliding over backwall details

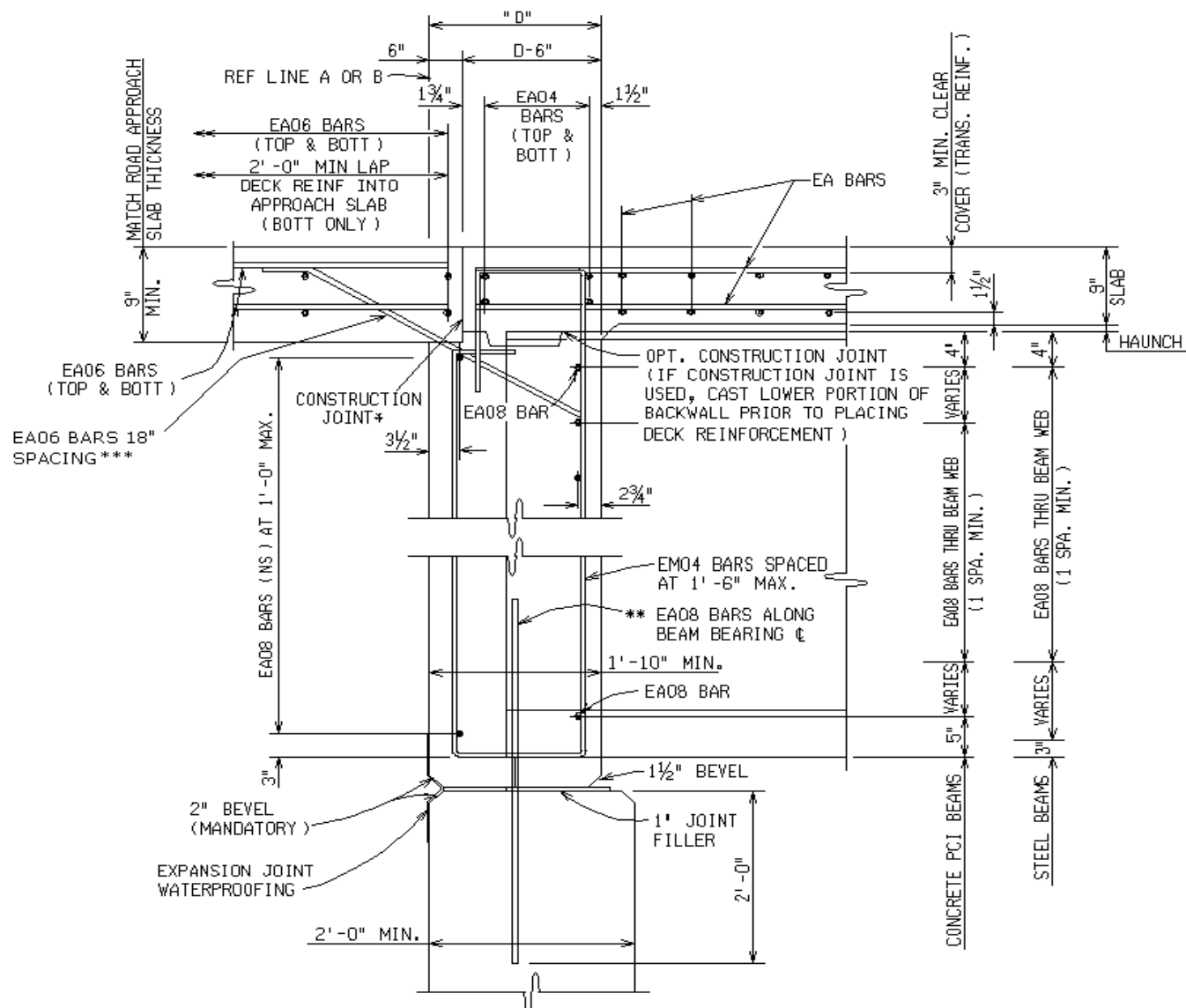


Figure 5-2. Semi-integral abutment details

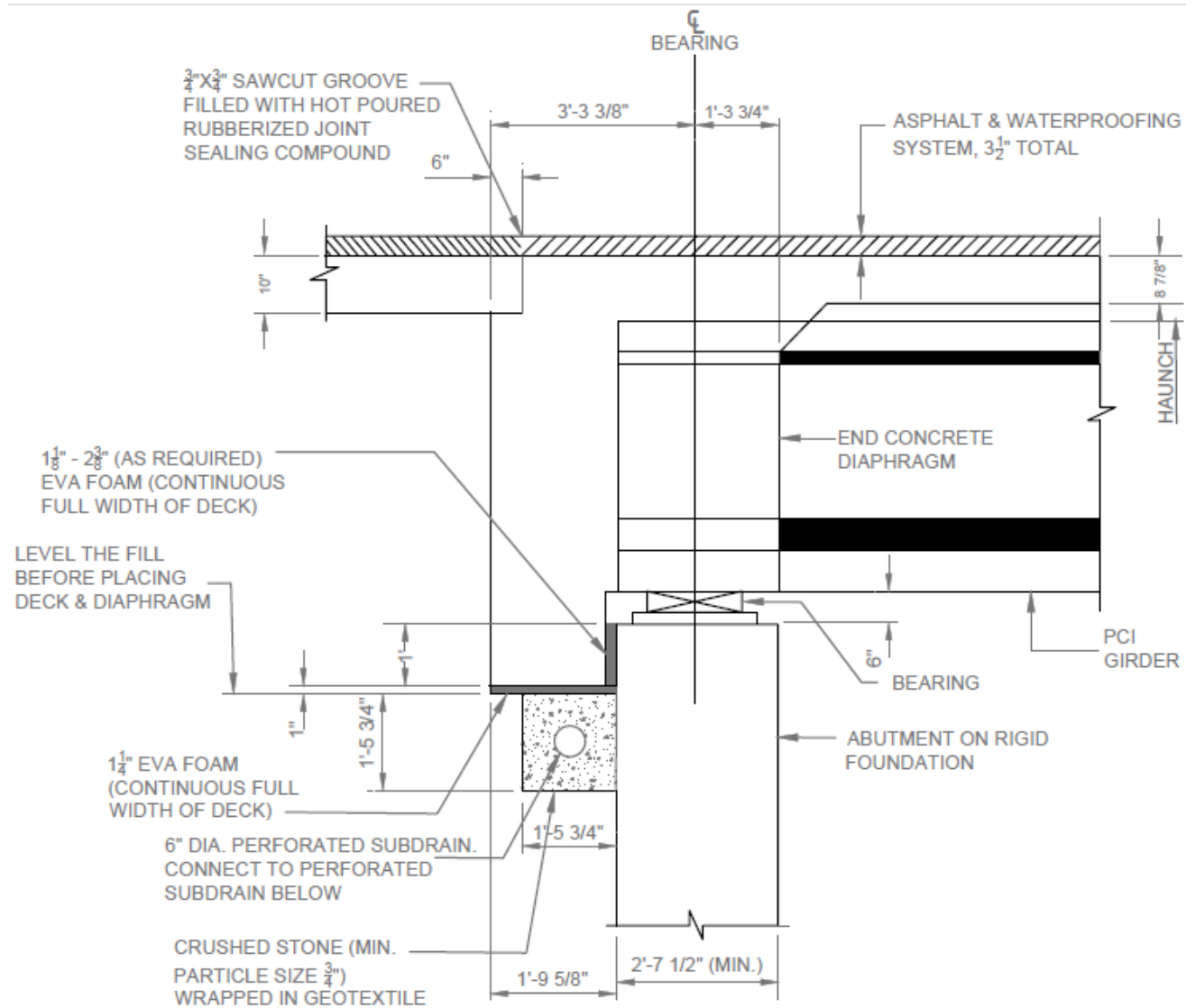


Figure 5-3. Semi-integral abutment detail used in Ontario and several other states

5.3 LATERAL RESTRAINT SYSTEMS IN SKEW BRIDGES

Various restraint systems are utilized for controlling transverse movement of skew bridge superstructures. A few examples are:

1. Sliding surfaces between the backwall and wingwall (rub plates) (Figure 5-4)
2. Sliding surfaces between the deck and wingwall (rub plates) (Figure 5-5)
3. Single angle bearing retainers against the steel plate of the bearing (Figure 5-6a)
4. Two-single angle bearing retainers against the steel plate of the bearing (Figure 5-6b)
5. Dowels in a slotted hole (Figure 5-7)
6. Concrete key system with rub plates (Figure 5-8)

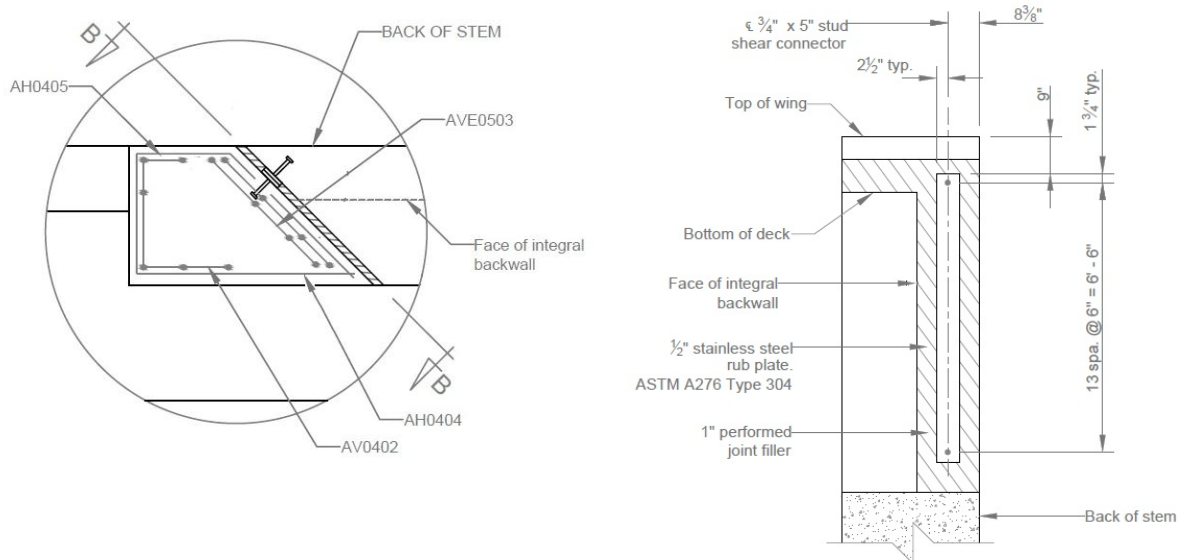


Figure 5-4. Rub plates at backwall - wingwall interface (Source: VDOT 2010)

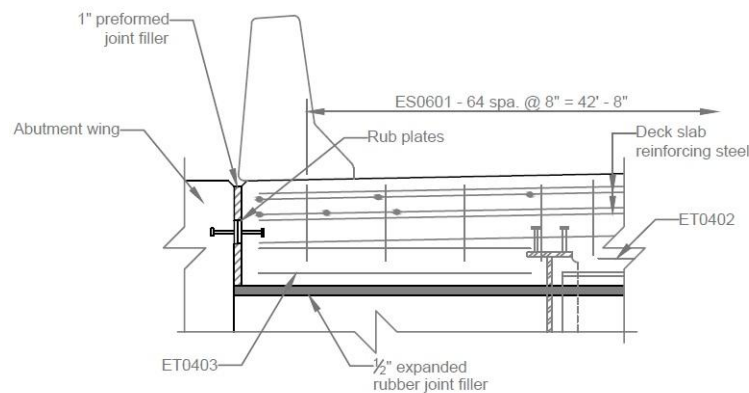


Figure 5-5. Rub plates at deck-wingwall interface (Source: VDOT 2010)

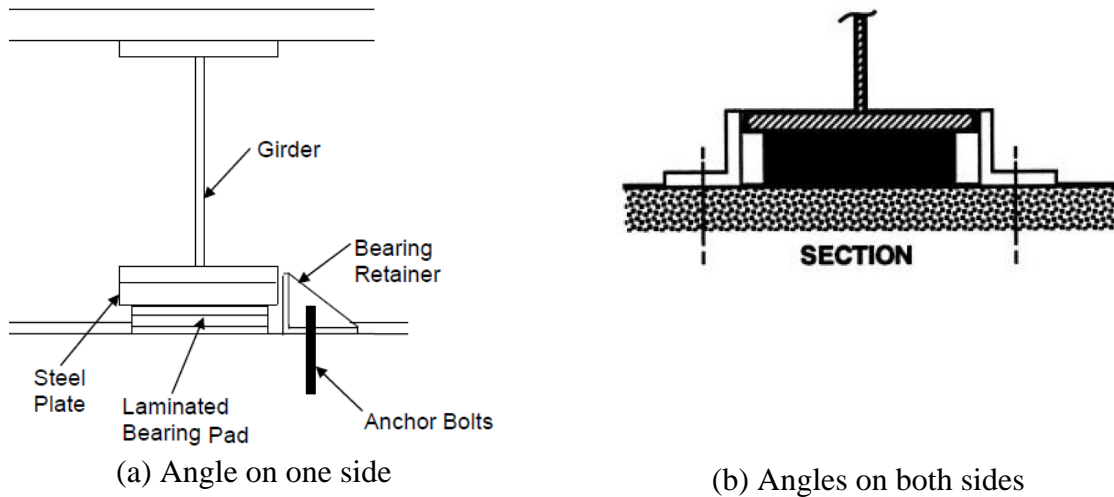


Figure 5-6. Bearing retainer detail (Source: Steinberg and Sargand 2010; Roeder and Stanton 1996)

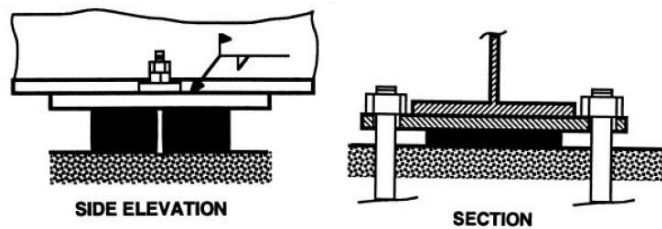


Figure 5-7. Dowel bar details for resisting lateral loads on shallow bearing (Source: Roeder and Stanton 1996).

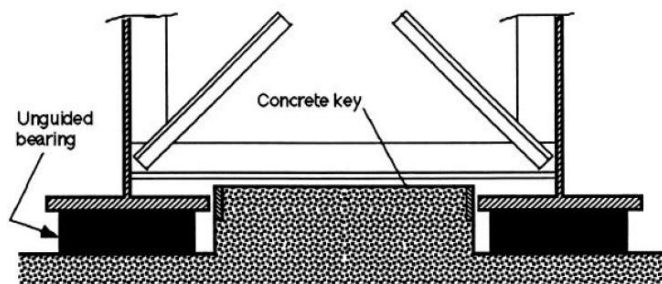


Figure 5-8. Concrete key system for resisting lateral forces (Source: Roeder and Stanton 1996).

Most viable configurations among these are those shown in Figure 5-4, Figure 5-5, and Figure 5-8. Still, utilizing these restraint systems in deck sliding over backwall and semi-integral systems with link slabs presents specific challenges.

5.3.1 Restraint Systems at the Abutment

5.3.1.1 Deck Sliding over Backwall System

Placing rub plates between the wingwall and deck at the acute corner of the deck poses several challenges. Rub plates should be placed on the span side of the deck with respect to the construction joint, if transverse movement is to be a restraint at the deck level. Also, the corner of the deck should be adequately detailed to accommodate the forces generated due to restraint. For deck sliding over backwall system, the most promising later load restraint system is the use of concrete key system shown in Figure 5-8.

5.3.1.2 Semi-Integral Backwall System

Semi-integral abutment details given in Figure 5-2 provide several advantages if adequate measures are taken to prevent backfill ingress through the abutment-backwall interface and load transfer between the backwall and abutment. A lateral movement restraint system can be developed by using the details shown in Figure 5-4. Forces on wingwalls can be minimized by providing transverse movement restraints at girders and/or providing EPS as a backfill material. Similar details can be developed to restrain transverse movement of the configuration given in Figure 5-3 by providing restraint against the diaphragm rather than the backwall.

5.3.2 Restraint System over the Pier

Deck level restraints cannot be implemented over the pier with the link slab. In addition, the restraint system that extends from the pier cap to the deck level has to accommodate a large moment. Considering these, an option to restrain transverse movement of the bridge superstructure is to provide concrete keys with a configuration similar to that shown in Figure 5-8 .

5.4 ANALYSIS OF HIGH SKEW BRIDGE WITH DECK SLIDING OVER BACKWALL AND SEMI-INTEGRAL ABUTMENTS

The objective of the analysis is to investigate the behavior of high skew bridge spans with specific abutment details presented in Figure 5-1, Figure 5-2, and Figure 5-3. The analysis results will establish the design load calculation procedures.

5.4.1 Material Properties

The girder and deck concrete properties are assumed to be the same. The bridge deck concrete strength specified in MDOT design (f_c') is 4500 psi (MDOT 2009). The modulus of concrete is calculated using Eq. 4-1 as per AASHTO Section 5.4.2.4 (AASHTO 2010). Unit weight of concrete (w_c) is assumed to be 0.15 k/ft³. The Poisson's ratio of 0.2 is used per AASHTO Section 5.4.2.5. The thermal expansion coefficient of 6.00×10^{-6} /°F is used (AASHTO 2010 section 5.4.2.2).

An expanded polystyrene (EPS) layer is placed in between the sliding deck and backwall. The use of EPS behind the backwall in semi-integral abutments will reduce passive pressure acting on the backwall during bridge expansion. The modulus of elasticity and Poisson's ratio of EPS are 0.2 ksi and 0.09, respectively. The peak and residual friction coefficients between EPS and concrete are 2.3 and 1, respectively. The peak friction coefficient value is used in the deck sliding over backwall abutment configuration for generating the extreme bearing forces under expansion and contraction loads.

5.4.2 Loads

5.4.2.1 Live Load

HL-93 loading with an impact factor of 1.33 is used in conjunction with wheel load as per AASHTO (2010) Section 3.6.1.2.3 and 3.6.2. Section 3.6.1.2.5 of AASHTO (2010) requires distributing wheel load over an area of 10×20 in.

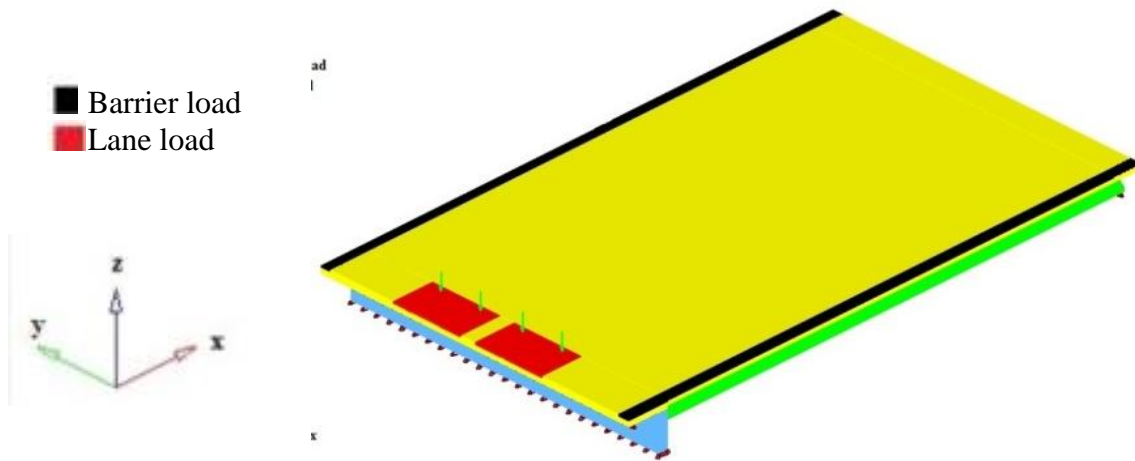
The MDOT Bridge Design Manual (2005) Section 7.03.01 specifies that abutment is designed for multiple load configurations. For the abutment models discussed in this report, the following load cases are considered:

CASE II: Bridge open to traffic with truck loading on the approach only.

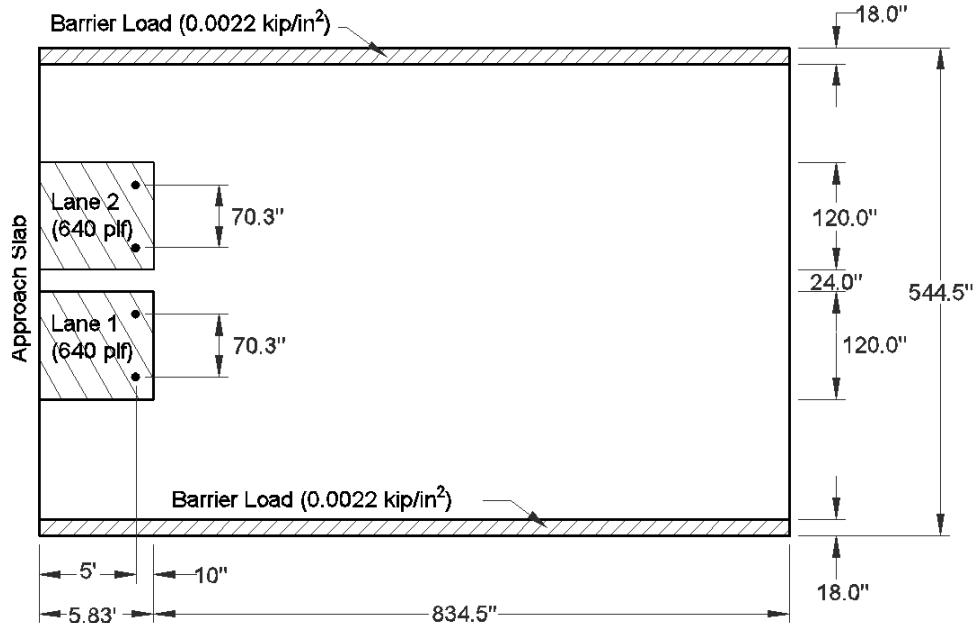
CASE III: Bridge with traffic on it and no load on approach.

CASE IV: Contraction – Case II loading plus the effects of uniform negative thermal in the deck transmitted to the abutment. Expansion – for integral abutments Case IV instead assumes the Case III loading plus the effect of uniform positive thermal transmitted from the deck.

Figure 5-9 shows the live load application for the *CASE IV Contraction* configuration; rear axles of the truck are placed on approach directly over the backwall and lane load is applied only on the approach. Figure 5-10 shows the live load application for the *CASE IV Expansion* configuration; two trucks are placed on the span such that the rear axle is over the bearings and the lane load is applied over the entire span. Wheel loads applied on the model include the dynamic impact factor of 33%.



(a) Isometric view



(b) Plan view

Figure 5-9. Live load configuration for *CASE IV Contraction*

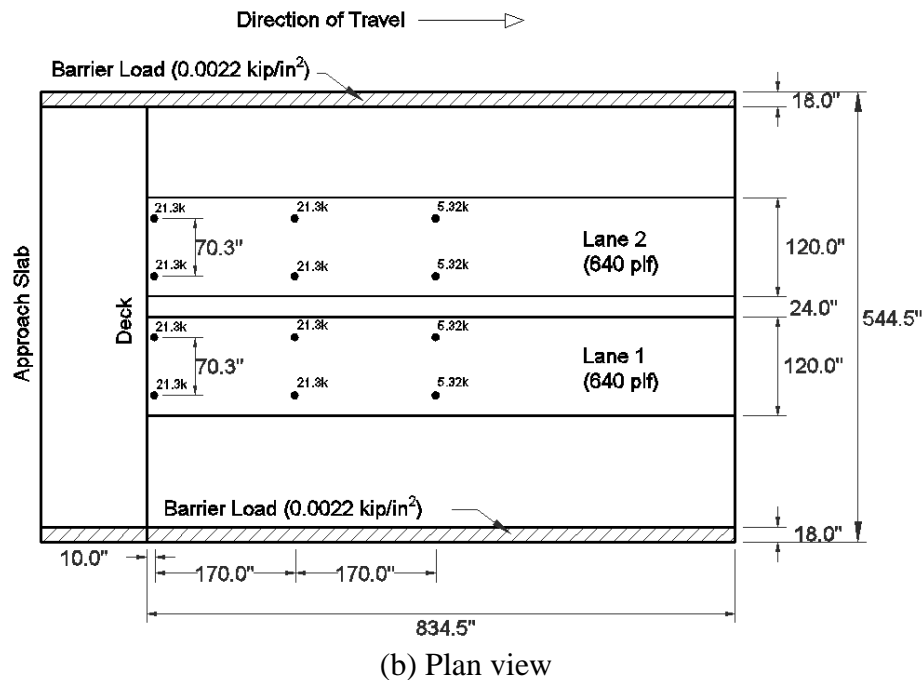
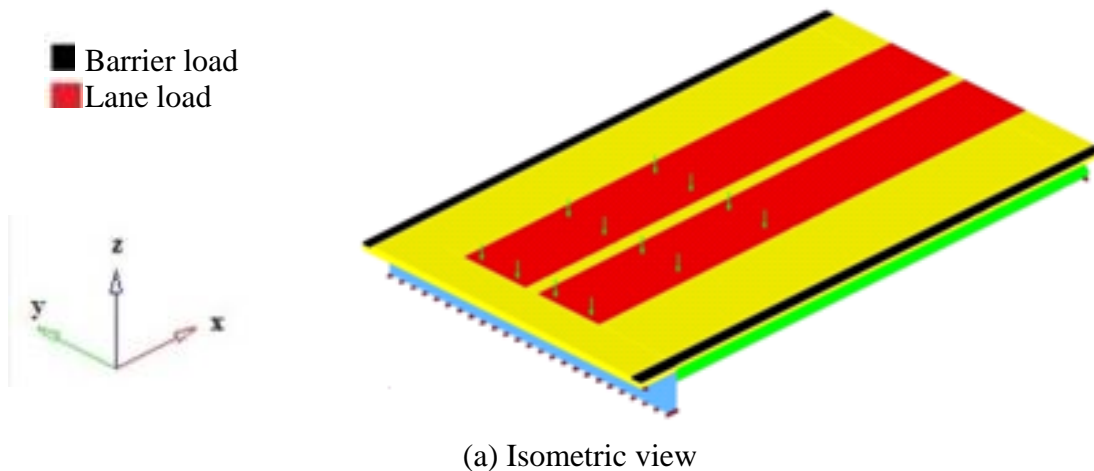


Figure 5-10. Live load configuration for CASE IV Expansion

Bearing type selection is controlled by the rotation, deformation, and load demands. Live load configurations specified were used to calculate bearing load and deformations. A parametric study was conducted to identify a live load position that generates maximum girder end rotation. As shown below, the trucks were placed at three different locations, and the girder end rotations were calculated. Two trucks were used and placed in each lane in opposite traffic direction. Trucks were placed on each lane such that one wheel line of each truck was directly above a girder. In this case, girder 8 and girder 1 were selected (Figure 5-11).

- Truck Position 1 –the trucks were placed as near as possible to the obtuse corner of the skew bridge (Figure 5-12). One of the rear wheels of the truck was placed approximately on the diagonal between the obtuse corners (load path).
- Truck Position 2 – the center of gravity of the trucks was placed at 1/3 of the span measured along the lane from the obtuse corners (Figure 5-13).
- Truck Position 3 – the center of gravity of the trucks was close to midspan of the girders (Figure 5-14). The trucks were positioned at locations that generate the maximum midspan moment of the girder.

Table 5-1 summarizes the girder 1 and 8 end rotations under above stated positions of the trucks. It is clear from the results that the girder end rotations increase as the trucks move towards the acute corner of the bridge. Hence, Truck Position 3 was used for further analysis in conjunction with dead and thermal gradient loads to calculate the girder end rotation. Additionally, girder end rotation values validate that the load path is along the diagonal between obtuse corners (i.e., the end rotation of girder 8 at the obtuse corner is larger than girder 1 for all the load cases).

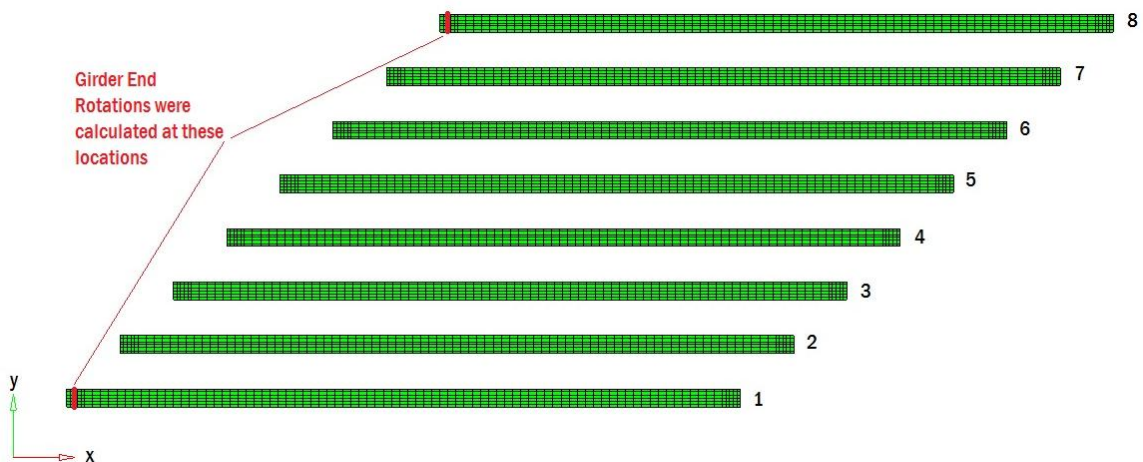


Figure 5-11. Location of girder 1 and 8 where girder end rotation was calculated

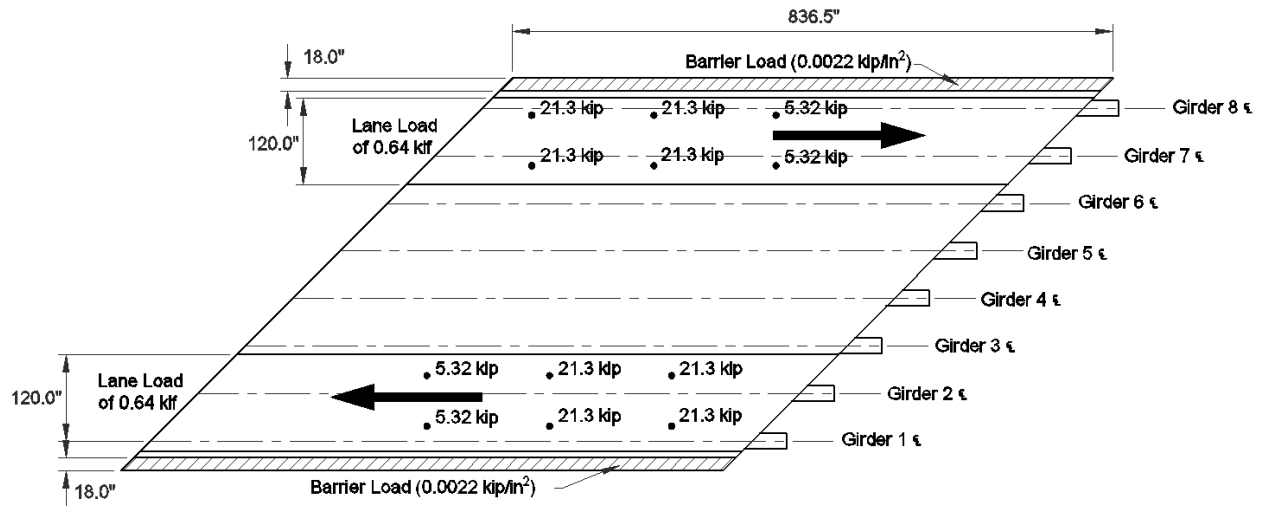


Figure 5-12. Truck position 1 for girder end rotation calculation

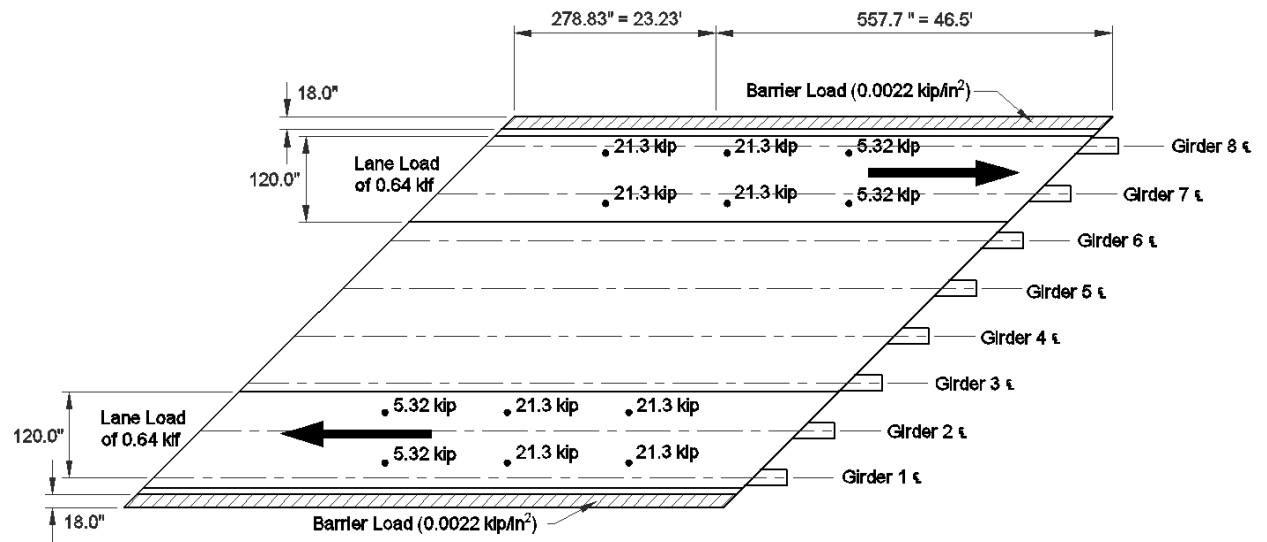


Figure 5-13. Truck position 2 for girder end rotation calculation

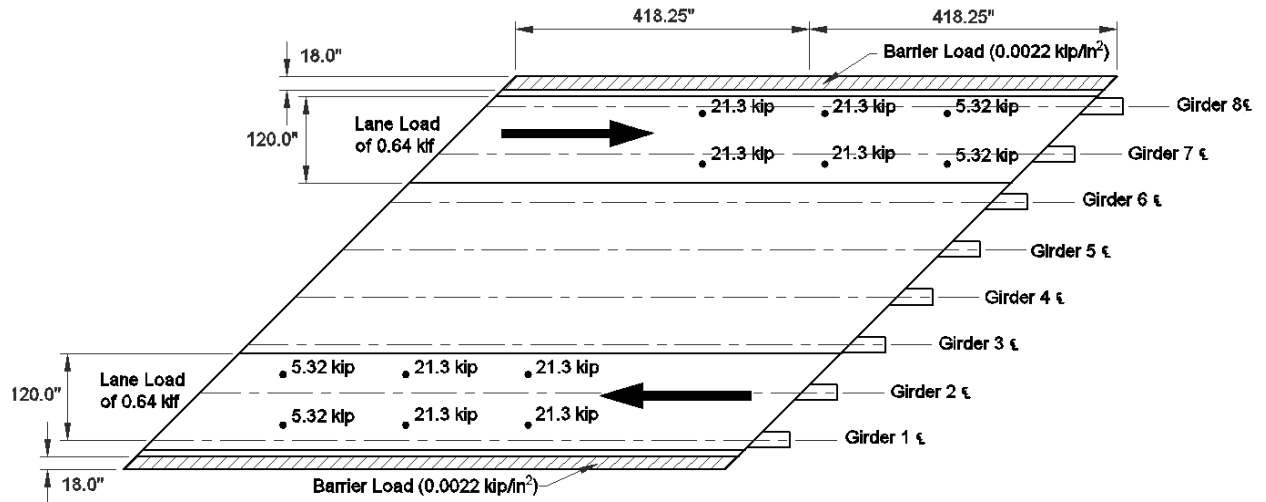


Figure 5-14. Truck position 3 for girder end rotation calculation

Table 5-1. Girder End Rotations against Different Truck Positions on Skew Bridge

	Girder1	Girder 8
Truck Position 1	0° 15' 56"	0° 19' 28"
Truck Position 2	0° 16' 38"	0° 20' 15"
Truck Position 3	0° 17' 10"	0° 20' 37"

5.4.2.2 Dead Load

The selfweight of the bridge components is included in the model. A New Jersey Type 4 barrier is selected. The selfweight of the barrier is 475 lb/ft. Instead of modeling the barrier, an area load of 2.2 lb/in² was applied within a 18 in. strip [i.e., 475 lb/ft / (18 in. x 12 in.) = 2.2 lb/in²] along the edge of the deck (Figure 5-9 and Figure 5-10).

5.4.2.3 Thermal Load

Uniform thermal loads that cause expansion and contraction of the bridge were calculated by Aktan et al. (2008) and used in this analysis. The values are summarized in Table 5-2. Negative and positive temperature gradient profiles and values are given in section 4.3.11.2 of the report.

Table 5-2. Thermal Load for Bridge Expansion and Contraction

Minimum Temperature (°F)	-10
Maximum Temperature (°F)	105
Base Temperature (°F)	62.7
Expansion (°F)	42.3
Contraction (°F)	-72.7

5.4.3 Load Combinations

Considering the construction sequence of a deck sliding over backwall, as a worst case scenario, only the approach slab and barrier loads will be acting on the backwall. The remaining loads are transferred through the bearings. In the case of semi-integral bridges, the entire superstructure loads including the approach are transferred through the bearings. Considering AASHTO (2010) strength and service limits, construction sequence of the bridge, and the load configurations suggested in the MDOT Bridge Analysis Guide, the following load combinations are used to calculate girder end rotations and translations and load demand on bearings and wingwalls.

Bridge Expansion (Deck sliding over backwall):

Strength 1-1: $1.25 DL_A + 1.75 LL_S + 1.2 UT_E$ Transverse forces at bearings
 Service 1-1: $1.0 DL_A + 1.0 LL_S + 1.2 UT_E$ Transverse forces at bearings

Bridge Contraction (Deck sliding over backwall):

Strength 1-1: $1.25 DL_A + 1.75 LL_A + 1.2 UT_C$ Transverse forces at bearings
 Service 1-1: $1.0 DL_A + 1.0 LL_A + 1.2 UT_C$ Transverse forces at bearings

Bearing Forces and Girder Rotation (Deck sliding over backwall):

Strength 1-1: $1.25 DL_{A+S} + 1.75 LL_S$ Vertical bearing forces
 Service 1-1: $1.0 DL_{A+S} + 1.0 LL_S$ Vertical bearing forces
 Service 1-2: $1.0 DL_{A+S} + 1.0 NTG + 1.0 LL_{S-mid}$ Girder rotation

Bridge Expansion (Semi-integral):

Strength 1-1: $1.25 DL_{A+S} + 1.75 LL_S + 1.2 UT_E + 1.0 EH$ Transverse forces at bearings and wingwall
 Service 1-1: $1.0 DL_{A+S} + 1.0 LL_S + 1.2 UT_E + 1.0 EH$ Transverse forces at bearings and wingwall

Bridge Contraction (Semi-integral):

Strength 1-1: $1.25DL_{A+S} + 1.75LL_A + 1.2 UT_C + 1.0EH$ Transverse forces at bearings and wingwall

Service 1-1: $1.0DL_{A+S} + 1.0 LL_A + 1.2 UT_C + 1.0EH$ Transverse forces at bearings and wingwall

Bearing Forces and Girder Rotation (Semi-integral):

Strength 1-1: $1.25DL_{A+S} + 1.75LL_S$ Vertical bearing forces

Service 1-1: $1.0DL_{A+S} + 1.0LL_S$ Vertical bearing forces

Service 1-2: $1.0DL_{A+S} + 1.0NTG + 1.0 LL_{S-mid}$ Girder rotation

Where DL_A – Dead load of approach

DL_{A+S} – Dead load of the entire superstructure including the approach

EH – Earth pressure

LL_A – Live load on approach (Figure 5-9)

LL_S – Live load on span (Figure 5-10)

LL_{S-mid} – Live load for maximum girder rotation

NTG – Negative temperature gradient

UT_C – Uniform temperature - contraction

UT_E – Uniform temperature - expansion

5.4.4 Boundary Conditions

An ideal boundary condition was used with all the abutment configurations. Ideal boundary condition generates maximum translations and rotations at the bearings. Bearing translations over the abutments are restricted to the bridge's longitudinal axis. Hence, reaction forces are developed in transverse and vertical directions and will be useful for bearing and girder end restraint design. In models with deck sliding over backwall configuration, friction between EPS and approach was included. Semi-integral models were analyzed with and without wingwalls to evaluate the forces at the bearings. As a worst case representation, transverse bearing restraint at the abutment is removed in order to calculate the maximum force on the wingwall. Further, forces at the wingwall are calculated with respect to the skew angle of the deck. The sliding surface between the deck and the wingwall is assumed friction free.

5.4.5 Deck Sliding over Backwall Abutment

The FE model of the deck sliding over backwall configuration shown in Figure 5-15 is based on the details provided in Figure 5-1. Models with different skew angles (i.e., 0, 20, 30 and 45 degrees) were developed and analyzed under strength and service loads to calculate the forces on the bearings. Interaction between approach and base and approach and sleeper slab were not incorporated into the models. Polyethylene sheets can be placed underneath the approach and at the interface between the approach and the sleeper slab of deck sliding over backwall system to minimize friction. Further, there is a potential for subgrade settlement and use of new material such as EPS as a backfill. Ideal boundary conditions were assigned at the end of the approach slab and girder ends. Friction at the deck and EPS interface over the backwall was included following literature recommendations though level of friction can be minimized by extending the polyethylene sheet that is placed underneath the approach over the EPS layer.

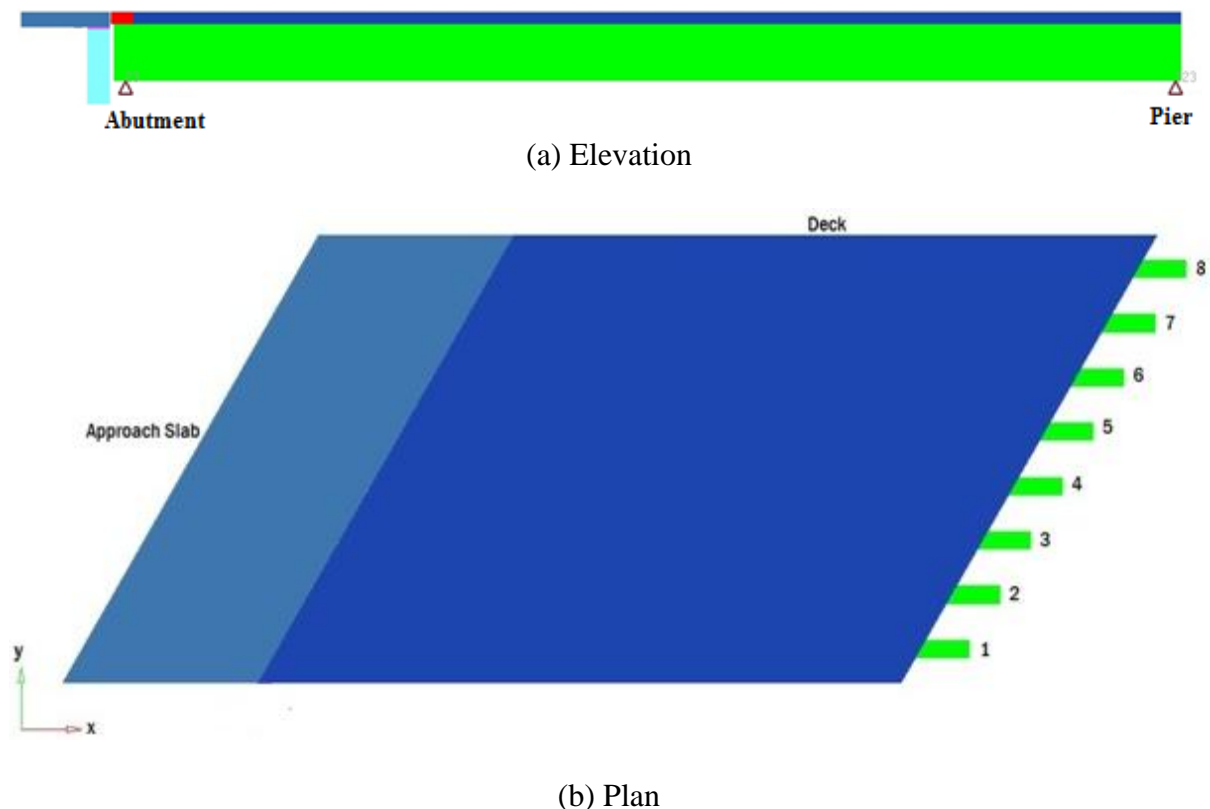


Figure 5-15. Deck sliding over backwall model description

5.4.5.1 Analysis Results – Girder End Rotations

Girder end rotations over the abutment of the deck sliding over backwall system were calculated under service loads. The maximum girder end rotations were calculated from the straight bridge model (Figure 5-17). As the skew increases, girder end rotation decreases.

The details provided in Figure 5-1 allow the span to act as simply supported. Hence, assuming the span is simply supported, the procedures given in Chapter 4 and Appendix C can be used to calculate girder end rotations under dead, live, and NTG loads. As discussed in step 2 of the Appendix C example, girder end rotation of a straight bridge under live load is calculated as 1.763×10^{-3} radians. The selfweight of an AASHTO Type II girder (0.583 k/ft) and self weight of an effective flange width of 66-in. deck (0.619 k/ft) generated a maximum dead load moment of 725.6 k-ft at the deck-girder composite section. Using this moment in conjunction with the section properties of the deck-girder composite section listed in Appendix C, girder end rotation was calculated as 2.4×10^{-3} radians. The girder end rotation, due to the negative temperature gradient load, was 4.84×10^{-4} radians (Table C-1). Hence the service rotation calculated at the girder end due to the combined effect of dead, live, and negative thermal gradient of a straight bridge is about 0.005 radians. This rotation is 60 percent greater than 0.003 radians calculated from the 3D FE model of a straight bridge.

AASHTO (2010) section 14.4.2.1 requires including 0.005 radians to the girder end rotation calculated from the service loads to account for uncertainties. The difference between the girder end rotation calculated from analytical methods described in Chapter 4 and Appendix C, and the FE models provide an adequate buffer for the uncertainties described in the AASHTO (2010). This is because the analysis procedure presented here accounts for all the possible loads except construction tolerances and intrinsic loads such as creep and shrinkage. Strong conclusions and recommendations can be derived for end rotation calculations after analyzing a large bridge population by incorporating various parameters such as span length and width, girder type, girder spacing, etc.

Following AASHTO recommendation, FE results plus 0.005 radians (i.e., 0.008 radians) is defined as the design rotation. The rotation of 0.008 radians is less than the maximum rotation limit of plain elastomeric pads given in Section 2.4.6 of Chapter 2 (i.e., 0.01 radians;

Table 2-3). Hence, plain elastomeric pads are recommended. The use of polytetrafluorethylene (PTFE) sliding bearing is not a viable option for bridges with such dimensions or longer. The use of sliding bearings in such bridges constraints girder end rotations and may result in girder end cracking, abutment D-cracking, and/or backwall cracking (Figure 5-16).



Figure 5-16. Abutment and girder end distress

Another option is the steel-reinforced elastomeric bearings. Use of plain elastomeric pads or steel-reinforced bearings should be carefully evaluated because vertical deformation of the bearings may result in reactions transferred through the backwall, instead of the bearings. Use of neoprene pads in between the approach and backwall is also an option to minimize the potential for the alternate load path. Another option for supporting the deck over the backwall is the use of EPS with a large elastic range as stated in Hoppe and Bagnall (2008). The special provisions presented in Hoppe and Bagnall (2008) require EPS with linear elastic stress-strain behavior up to 10 percent strain and linear proportional stress-strain behavior up to 30 percent strain.

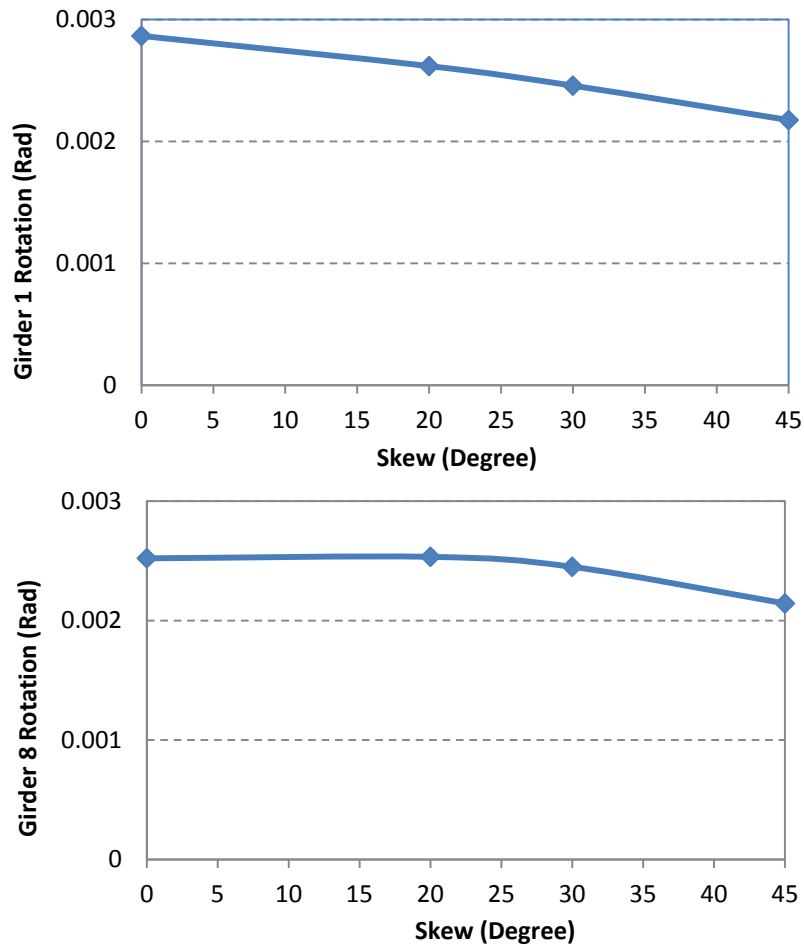


Figure 5-17. Girder 1 and 8 end rotation over abutment

5.4.5.2 Analysis Results – Bearing Translation

Uniform expansion and contraction temperatures are defined in Table 5-2. The length and width of the bridge deck are 834.5 in. and 544.5 in. Skew angle (θ), effective length of thermal movement (L_{th}), and angle between bridge longitudinal axis and L_{th} (β) are defined in Figure 5-18. The expansion or contraction is the greatest along the effective length of thermal movement, L_{th} (Hoppe and Bagnall 2008). For a 45° skew bridge with dimensions similar to what is defined above, the theoretical contraction and expansion in the longitudinal direction under the temperature values defined in Table 5-2 are calculated as 0.6 in. and 0.35 in.

The longitudinal bearing translation over the abutments was calculated from 3D FE models (Figure 5-19). Though FE results mirror the skew bridge behavior, the expansion and contraction values are reduced due to the model’s ability to represent the three-dimensional

(3D) behavior of the structure. The friction force at the sliding surface is small because the vertical load at the backwall is very small, and the majority of superstructure load in the model was transferred through the bearings. However, for these unremarkable bridges, calculation of longitudinal expansion and contraction by analytical methods is sufficient to determine the deformation demands at the bearings. As per the limitations given in Table 2-3, a plain elastomeric pad is not a viable option for the calculated maximum deformation of 0.6 in. Considering both rotation and translation demand, the steel-reinforced elastomeric bearing is the most suitable bearing type. The 45° skew bridge considered in the analysis is only 69.5 ft long and 45 ft wide, which resulted in an effective length of thermal movement (L_{th}) of 123 ft, of which the effective length for horizontal bearing translation ($L_{th} \times \cos\beta$) is 115 ft long. Bridges with effective length for horizontal bearing translation greater than 115 ft will require reinforced elastomeric bearings to accommodate rotation and deformation demands. Further, implementation of link slabs, depending on the bearing configuration, increases the effective length of longitudinal expansion.

The maximum longitudinal expansion of the deck sliding over backwall and semi-integral systems is limited by the effective movement rating of the bearings or the expansion joints provided at the sleeper slab. Published data on preliminary bearing selection shows that the maximum translation up to 5 in. can be accommodated with available bearing types. According to Roeder and Stanton (1996), the maximum translation that steel reinforced elastomeric bearings (SREB) can accommodate, based on the total compressive force and rotation demand, ranges from 2 in. to 4 in. Greater translations can be accommodated with flat PTFE or combined systems. However, the maintenance cost of PTFE is greater than that of SREB.

According to the Michigan Bridge Design Manual (MDOT 2005), modular expansion joint devices are required when the expansion joint opening, in the direction of traffic, is greater than 4 in. However, according to Purvis (2003), modular joints are complex and recommend avoiding whenever possible. Instead, he recommends using strip seal joints of which the effective movement rating is 4 in. In deck sliding over backwall and semi-integral systems expansion joints are placed at the sleeper slab. Hence, in addition to the bridge superstructure movement due to thermal loads, the expansion joints should accommodate fit-

in tolerances, approach slab expansion/contraction, deformation of substructure due to construction loads and sequence, and superstructure deformations due to creep and shrinkage in prestressed girders and selfweight. When strip seals are used, it is reasonable to assume available expansion range of 3 in. at the joint to accommodate thermal movement of a bridge superstructure.

According to published data, performance of expansion joints is well below expected (Purvis 2003). Further, expansion joint maintenance and replacement cost is much greater than that of bearings due to shorter service life of joints. Hence, expansion joint effective movement rating should be considered when bridge expansion length is specified. Bridge expansion length (i.e., L in Figure 5-18) is defined as the distance along the longitudinal axis measured from abutment to the nearest fixed bearing.

Bridge expansion length recommendations are developed considering width and skew ranges of single span steel and prestressed concrete bridges under the MDOT jurisdiction as shown in Figure 5-20 and Figure 5-21. Also assumed are a maximum strip seal joint width of 3 in., and an expansion and contraction thermal load of 115 °F. For example, from Figure 5-20, a straight concrete bridge superstructure expansion length should not exceed 300 ft. For a 45° skew concrete bridge of 100 ft wide superstructure expansion length should be limited to 200 ft. From Figure 5-21, when steel girder bridges are considered, expansion length should not exceed 275 ft for straight and 175 ft for a 100 ft wide 45° skew bridge (Figure 5-21).

On the other hand, transverse deformations of a bridge under uniform expansion and contraction thermal loads are only a function of the bridge width. Bridge width is measured perpendicular to the longitudinal axis of the bridge. The girder deformations and associated forces developed in a skew system due to transverse bearing restraint can be minimized by increasing bearing fit-in tolerances. As an example, when bearings are arranged in such a way that a bridge is allowed to expand in the transverse direction symmetrical to the longitudinal axis, a maximum of 0.5 in transverse movement can be expected under the exterior girder bearing of a 100 ft wide steel or concrete bridge that is exposed to a 115 °F expansion and contraction thermal range.

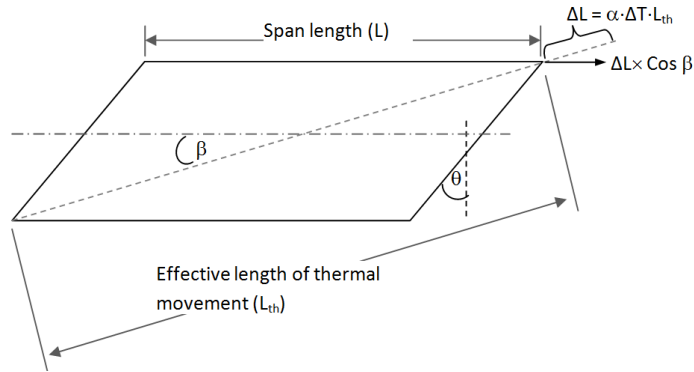
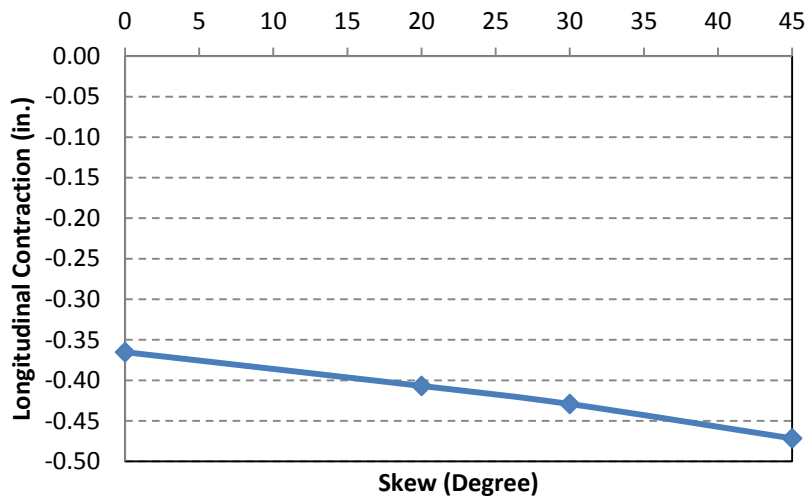
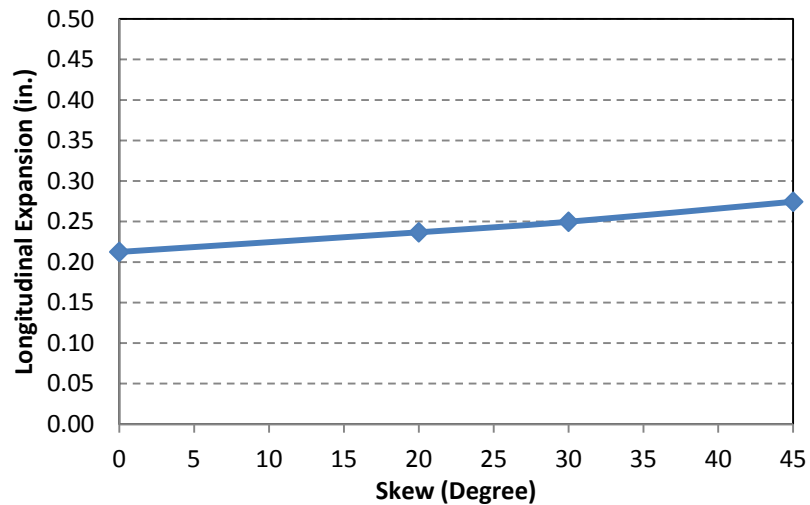


Figure 5-18. Thermal expansion of a skew bridge



(a) Maximum contraction in the longitudinal direction



(b) Maximum expansion in the longitudinal direction

Figure 5-19. Maximum longitudinal bridge contraction and expansion

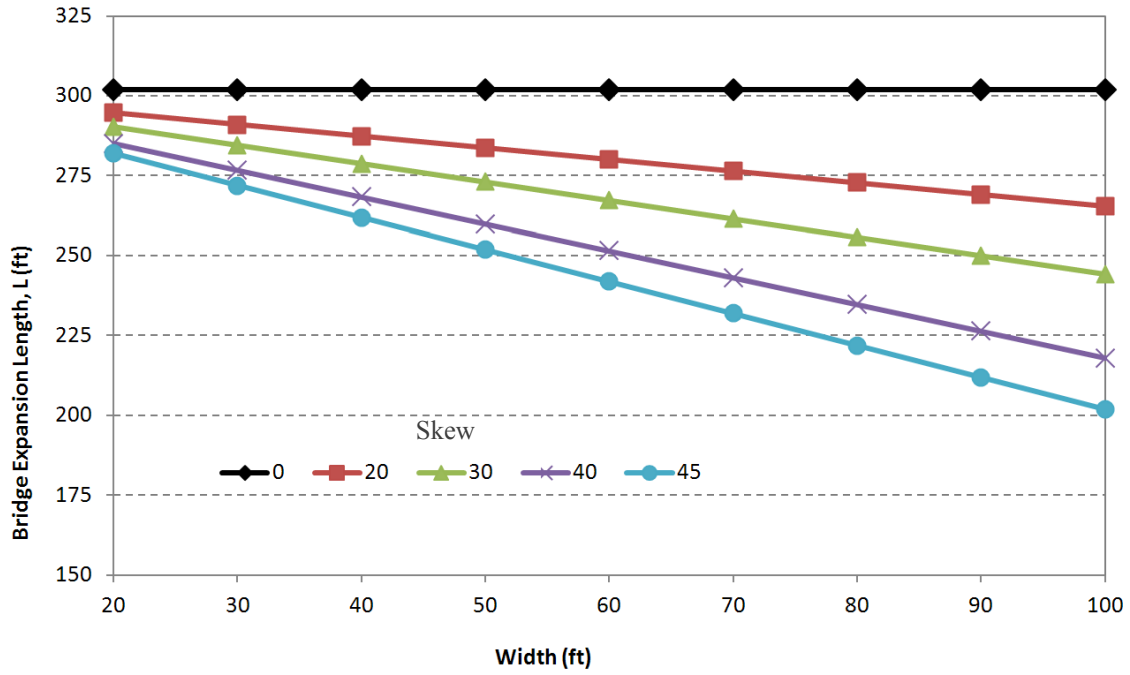


Figure 5-20. Variation of concrete bridge expansion length against width and skew when strip seal joint width of 3 in. available for thermal movement

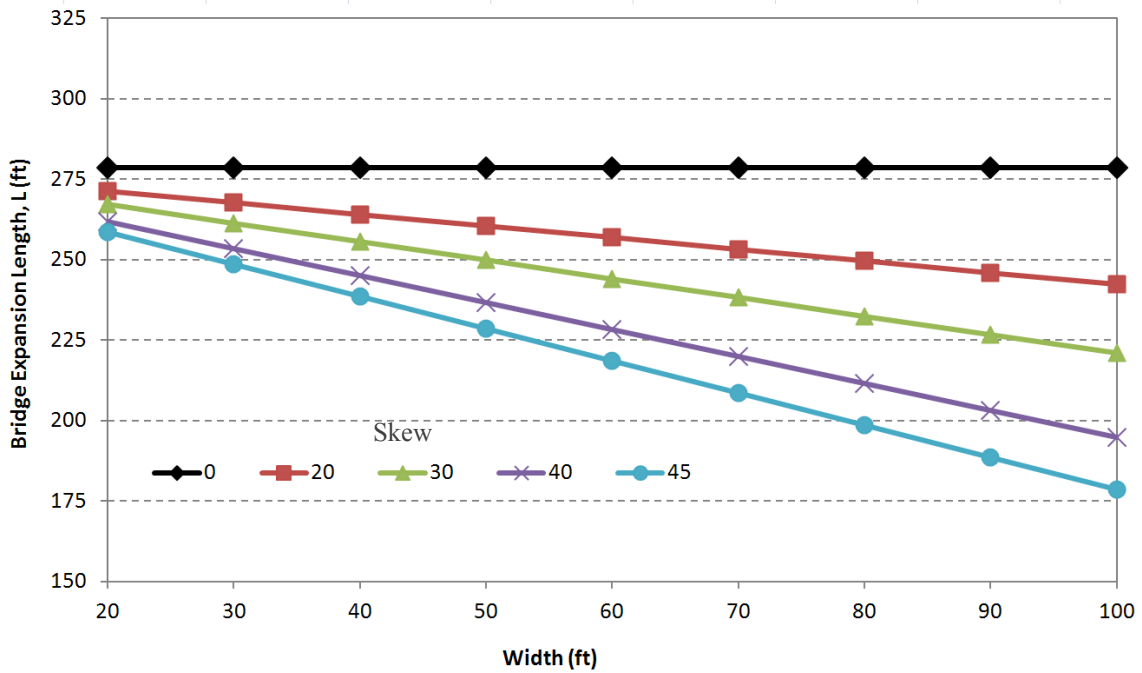
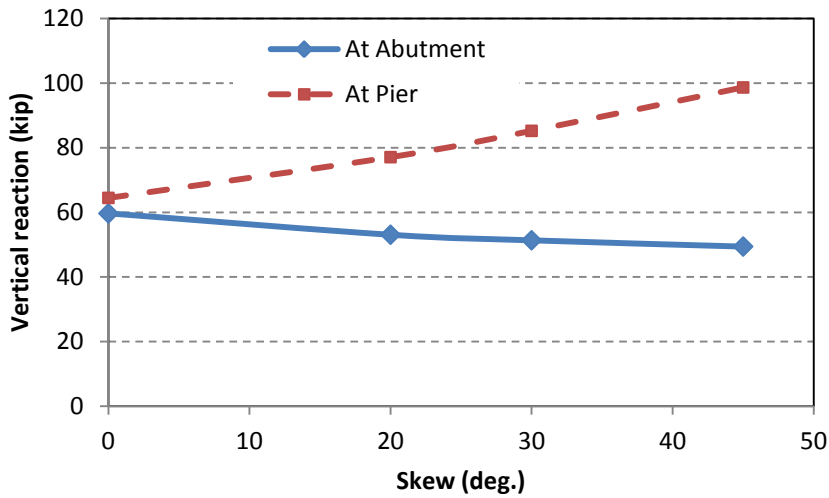


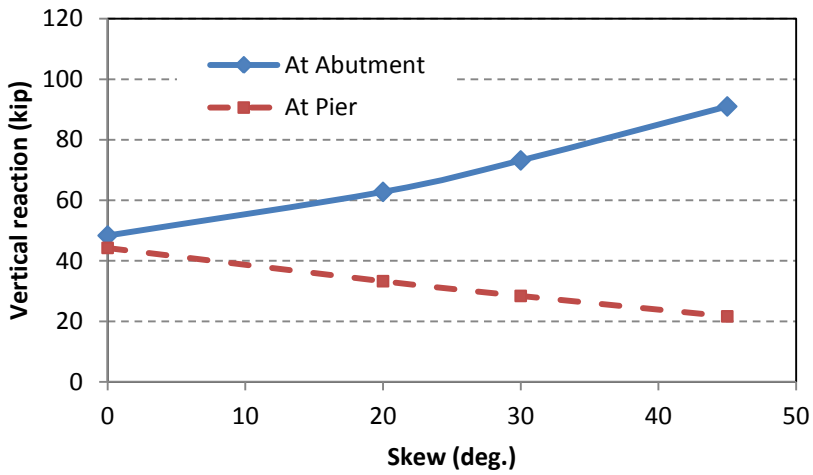
Figure 5-21. Variation of steel girder bridge expansion against width and skew when strip seal joint width of 3 in. available for thermal movement

5.4.5.3 Analysis Results – Vertical Bearing Forces

Bridge FE models were analyzed under the critical service load combination that generates the maximum vertical bearing forces. Results shown in Figure 5-22 show that the bridge response duplicates the skew behavior of a simple span, where girder end reactions reduce under the acute corner and increase under the obtuse corner with increasing skew. Vertical forces that develop on the bearing of this particular bridge are not a concern for any of the bearing types up to a 45° skew. This is because the maximum load recommended for a plain elastomeric pad, which is the lowest among other bearing types, is 100 kips. The two-lane bridge considered in the analysis is only 69.5 ft long. As the bridge length increases, the load demand on bearings will increase. Especially, the load demand on the bearings underneath the obtuse corner of wide high skew bridges will increase dramatically. Considering all these factors, reinforced elastomeric bearings are recommended for skew deck sliding over backwall configurations. This recommendation is supported by the translation and rotation demands presented in previous sections. Hence, the designer can use the simple span model to calculate the reactions and deformations of the bridge with deck sliding over backwall for the bearing design.



(a) Girder 1 vertical reaction variation over abutment and pier



(b) Girder 8 vertical reaction variation over abutment and pier

Figure 5-22. Girder 1 and 8 reaction variation over the abutment and pier

5.4.5.4 Analysis Results – Transverse Bearing Forces at Abutment

Transverse bearing forces were calculated at each bearing over the abutment under strength load combinations that include thermal contraction loads (Figure 5-23). Similarly, transverse bearing forces were calculated at each bearing over the abutment under strength load combinations that include thermal expansion loads (Figure 5-24). In both cases, no other transverse restraints were considered. As shown in the figures, in the transverse direction, thermal contraction generates the greatest forces on bearings. According to AASHTO LRFD (2010) section 14.7.9 *guides and restraints shall be designed using strength limit state load*

combinations for the larger of either (a) the factored horizontal design force or (b) 10 percent of the total factored vertical force acting on all the bearings at the bent divided by the number of guided bearings at the bent. Though the AASHTO recommendation is for the bearings over the bent, this can also be applied to the design of bearings over the abutment of the deck sliding over backwall configuration since there is no backfill pressure effect on the structure. The total vertical force on the abutment bearings that was calculated from strength load combinations is 1000 kips. According to AASHTO, if two girder ends are restrained in the transverse direction, the design load is 50 kips which is less than the 10% of the forces generated under thermal loads.

The bearing forces shown in Figure 5-23 and Figure 5-24 were calculated without any allowance for bearing movement in the transverse direction. Transverse bearing forces can be minimized or eliminated by increasing fit-in tolerances between position dowel and the sole plate. This is a practical solution for the deck sliding over backwall system once the friction at interfaces between approach-EPS, approach-base, and approach-sleeper slab is minimized by providing a polyethylene sheet. Bridge plans generally require a 0.125 in. fit-in tolerance between the position dowel bar and the slot in the sole plate (Figure 5-25). Further, AASHTO LRFD Bridge Construction Specification (2008) provides manufacturing and installation tolerances. With the tolerances achieved during manufacturing and installation, there is a great possibility of the total transverse force not being equally shared by all of the bearings. Providing adequate tolerance for transverse movement of the bearings and constraining a single or a two middle girder ends should be considered. The transverse expansion of a 40 ft wide concrete bridge under differential uniform thermal load of 80 °F is about 0.23 in. whereas the allowable tolerance specified in the specifications is 0.125 in. Most of the analysis and design examples in the literature have dealt with other structural systems such as semi-integral or integral abutments that are subjected to thermal expansion loads. This is because the passive earth pressure built up at the backwall tends to rotate the superstructure and increases the bearing forces than those developed under contraction thermal loads. In the case of deck sliding over backwall, for expansion thermal loads, only restrain force is from the interface friction which can be minimized as suggested above.

Implementation of some of the bearing configurations discussed in Chapter 2 section 2.3 can release girder end forces developed under thermal expansion and contraction loads. Because of the link slab over the pier, the only possible bearing configuration is the radial from center (Figure 2-17 c). The recommendation is to restrain the transverse movement of the middle girder end (if odd number of girders) or two middle girder ends (if even number of girders) using concrete keys with rub plates (shown in Figure 5-8) and to increase the tolerance of the slot in the sole plate and bearing to accommodate transverse movement of unrestrained girder ends. Once the middle girder(s) is restrained in the transverse direction, the transverse movement the bearing needs to accommodate is proportional to only half of the bridge width. For example, the required tolerance for a 40 ft wide bridge under differential uniform thermal load of 80 °F is about 0.12 in. This is less than the allowable tolerance of 0.125 in. recommended for the position dowels by the AASHTO LRFD Bridge Construction Specification (2008).

It is recommended the maximum bearing tolerance in the transverse direction is limited to 0.25 in. until further investigations are carried out investigating the impact of the increased fit tolerances on the girder position dowels on the rest of the bridge components. The maximum limit was established as the summation of fit-in tolerance provided with general bearing details (Figure 5-25) and the AASHTO Bridge Construction Specification tolerance of $|+0.125|$ or $|-0.125|$ in.

Further, friction at the approach-EPS, approach-base, and approach-sleeper slab has a great influence on link slab stresses. The analysis discussed in Chapter 4 used three different support configurations, HRRR, RRHR, and RHHR, where H and R represent hinge (i.e., fixed bearing) and roller (i.e., expansion bearing). In the case of HRRR, the bearings underneath the link slab are expansion bearings (R) while the bearings over the abutments are fixed (H) and expansion (R) types. If large frictional forces develop at the approach of the abutment with expansion bearings, large stresses will develop at the link slab. This is because the restrains that develop at the supports will result in an HRRR support system to approach HRRH. As discussed, this support configuration is not recommended for link slab bridges. In order to reduce the friction forces, providing a polyethylene sheet underneath the entire surface of the approach is recommended (MnDOT 2011). Reducing the friction force

at interfaces and providing adequate tolerances for girder end movement under thermal expansion and contraction releases the restraint forces developed at the supports.

Details of the bearings over the abutment and independent backwall abutment configuration were developed to accommodate the reduced restraint forces. Proposed detail in standard MDOT Bridge Design Guide format is presented in Appendix F. All the required mathematical relationships and variables are presented with the drawings. The rub plate design procedure was adopted from VDOT Bridge Design Manual section 20.04 (2010) with some modifications and presented in Appendix G.

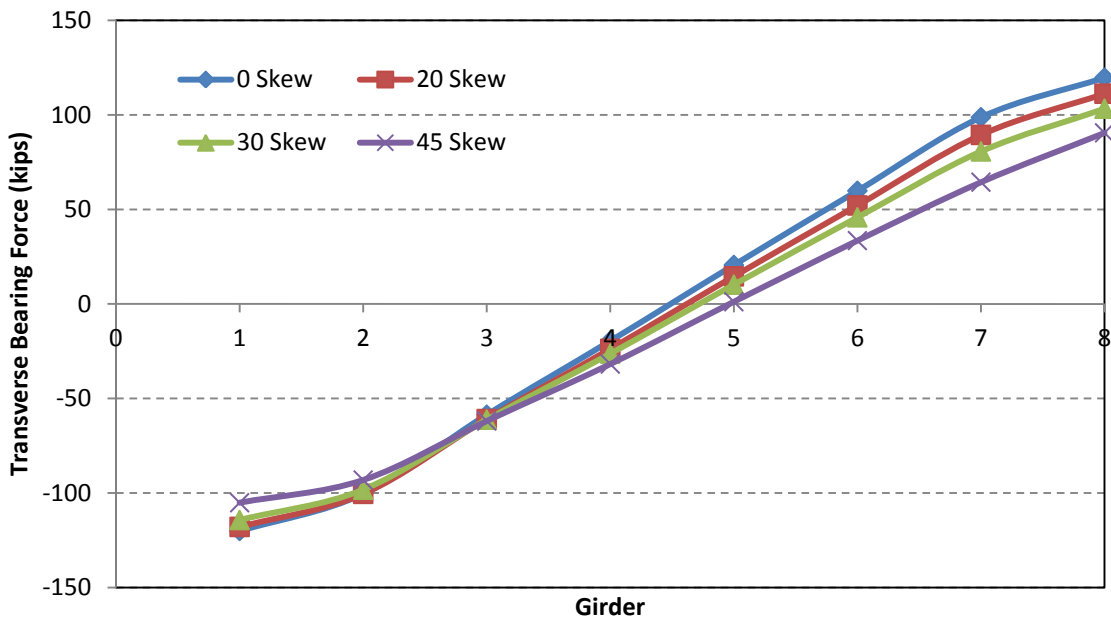


Figure 5-23. Transverse bearing force over abutment under thermal contraction strength load combination

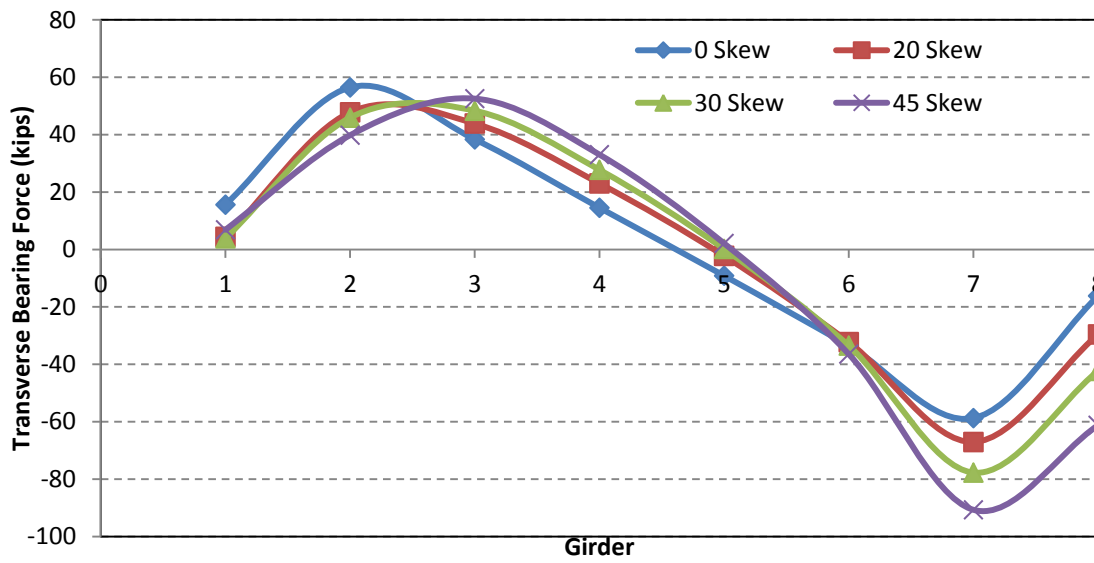


Figure 5-24. Transverse bearing force over abutment under thermal expansion strength load combination

5.4.6 Semi-Integral Abutment

Two different configurations shown in Figure 5-2 and Figure 5-3 were analyzed. Even though there is a difference in the position of backwalls in these two configurations, the same FE model is applicable for both configurations because the load transfer is only through the bearings. FE models were developed with and without wingwalls (Figure 5-26) and analyzed under the load combinations listed above to calculate translation, rotation, and force demand at the bearing as well as the forces that develop at the wingwalls. EPS was included as the backfill material.

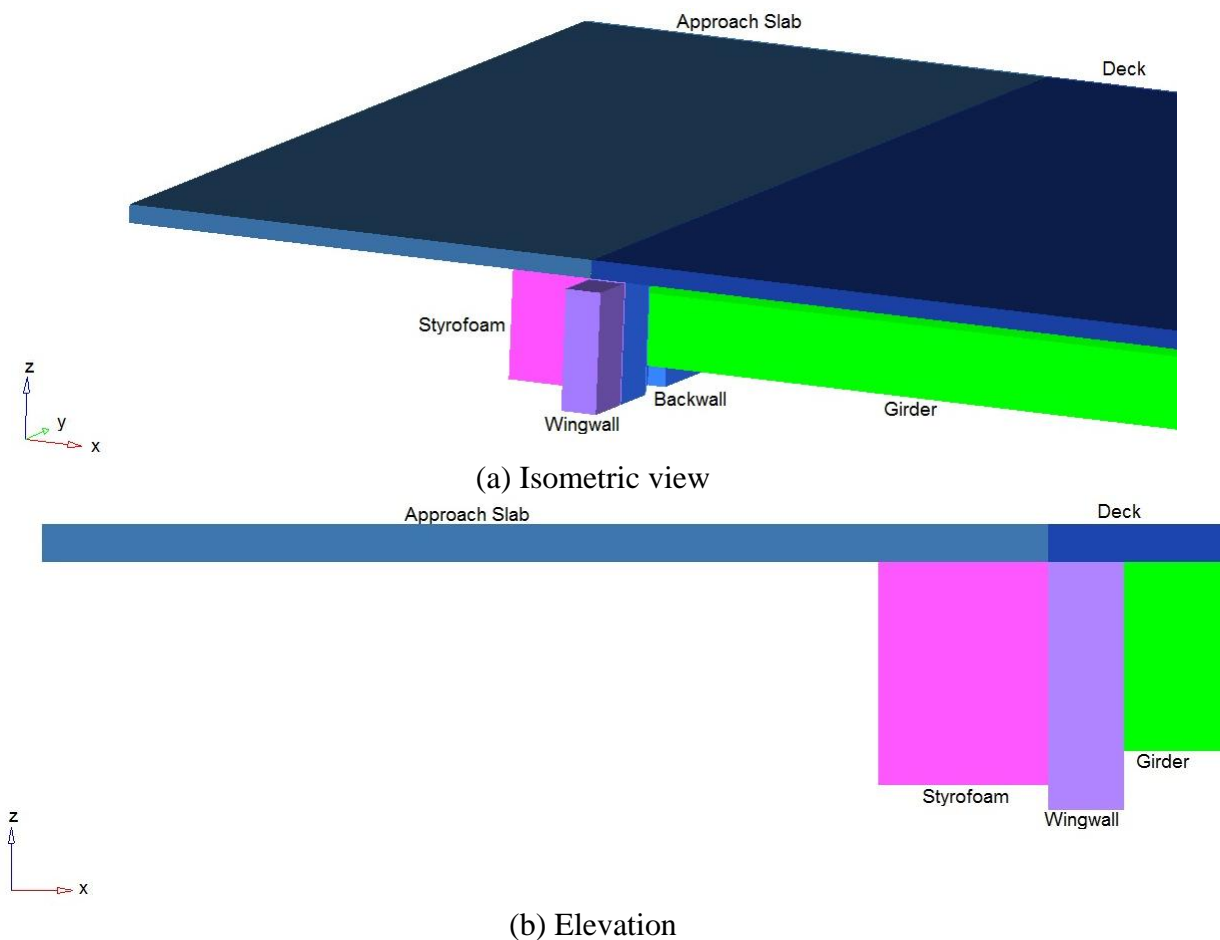


Figure 5-26. Semi-integral bridge model with wingwalls (not drawn to scale)

5.4.6.1 Analysis Results – Girder End Rotations

Girder end rotations were calculated over the abutment under the 1.0 DL_{A+S} + 1.0 NTG + 1.0 LL_{S-mid} load combination. Beyond a 25° skew, girder end rotations decrease as skew increases (Figure 5-27). Girder 1 rotation was calculated to be the largest. As shown in Figure 5-2, the approach slab is connected to the backwall by a diagonal reinforcement. This detail is assumed as a hinge, and the moment is not transferred across the connection. The bridge span can then be modeled conservatively as a simply supported system. The girder end rotations are similar to from the results of the deck sliding over backwall system. Subsequently, the analytical calculations and recommendations for the bearing selection provided in section 5.4.5.1 are also applicable for semi-integral system.

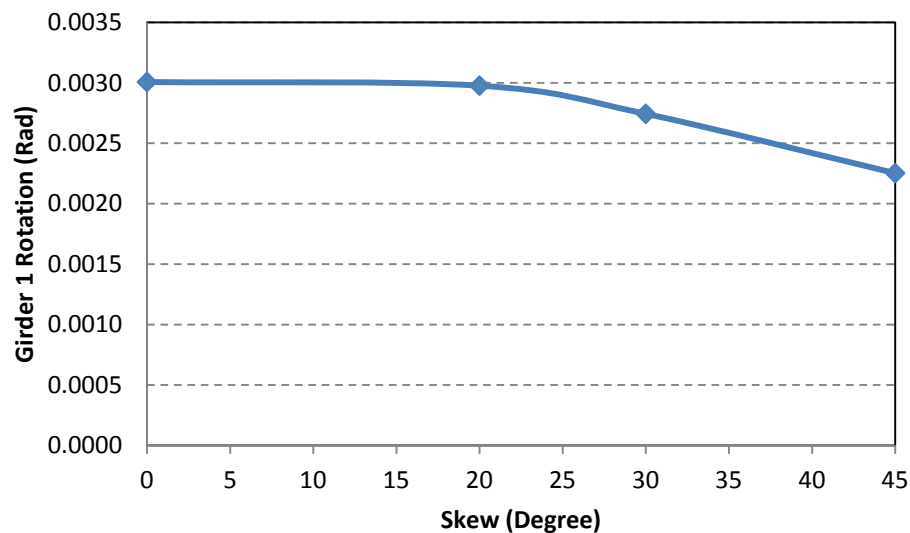


Figure 5-27. Girder 1 rotation of semi-integral bridge

5.4.6.2 Analysis Results - Bearing Translation

Theoretical bridge contraction and expansion in the longitudinal direction calculated in section 5.4.5.2 as 0.6 in. and 0.35 in. are applicable to the semi-integral configuration when backfill and bearings do not restrain the longitudinal movement. As discussed in section 5.4.5.2, bridge expansion length limitations due to expansion joint movement rating should be considered when link slabs are implemented in semi-integral bridges. Bridge expansion and contraction in the longitudinal direction at girder 1 over the abutment is shown in Table 5-3. The results are also similar to those calculated for the deck sliding over backwall

configuration. The idealized boundary conditions were assumed in order to calculate the maximum beam end translations. The FE model includes EPS backfill material but provides very limited constraint to the expansion of the structure due to its low stiffness ($K_p = \nu/(1 + \nu)$; $\nu = 0.09$; $K_p = 0.08$). The difference in analytical and 3D analysis is due to the 3 dimensional effects as discussed in section 5.4.5.2. The model without wingwalls slightly overestimates the deformations due to the uncontrolled movement of the deck.

Hoppe and Bagnall (2008) indicated that to minimize forces on the backwall and wingwalls, EPS with desired properties can be procured for placement at the backwall by incorporating special provisions to the project documentations. The Virginia DOT has developed special provisions for inclusion of EPS and geotextile. These special provisions are provided in Hoppe and Bagnall (2008).

Table 5-3. Expansion and Contraction of Girder 1 End over Semi-Integral Abutment

		FE Model	
		Without Wingwall	With Wingwall
	Skew	Δx (in.)	Δx (in.)
	Contraction	0	-0.36
20		-0.40	-0.40
30		-0.42	-0.42
45		-0.49	-0.45
Expansion	0	0.21	0.21
	20	0.23	0.25
	30	0.24	0.26
	45	0.26	0.27

5.4.6.3 Analysis Results – Transverse Bearing and Wingwall Forces at Abutment

Transverse bearing forces were calculated at each bearing over the abutment under strength load combinations that include thermal contraction loads (Figure 5-28). Similarly, transverse bearing forces were calculated at each bearing over the abutment under strength load combinations that include thermal expansion loads (Figure 5-29). In both cases, no other transverse restraints on the bridge deck were considered. As shown in the figures, thermal contraction generates the largest force on bearings in the transverse direction in the absence of backfill pressure under expansion loads. The forces are developed due to expansion or contraction in the transverse direction because of girder restraints in that direction. These

forces are generated when supports do not accommodate transverse movement. These forces are much greater than the ones developed in the deck sliding over backwall system with similar dimensions. This is mainly due to the expansion and contraction of the stiff concrete mass consisting of the backwall at the girder end.

As discussed earlier, according to AASHTO LRFD Bridge Construction Specifications (2008), construction and manufacturing tolerances are specified up to 0.125 in. Incorporating the tolerances, the forces developed at the girder ends, especially under thermal contraction loads, will be reduced. Transverse forces under thermal contraction can be reduced substantially by specifying an increased tolerance for transverse movement. However, thermal expansion also develops bearing forces due to backfill pressure. This backfill pressure effect can be minimized by using an EPS layer in between the backwall and the backfill. EPS is a very soft material, and the passive pressure coefficient can be as low as $K_p = 0.08$ (see section 5.4.6.2). After monitoring a 45° skew bridge for about two years, Hoppe and Bagnall (2008) estimated K_p to be 1.2, which is much lower than the VDOT (2010) recommended value of $K_p = 4$. After all, the benefits of inclusion of an EPS layer are obvious and have a great potential to minimize the forces developed in the transverse restraint systems of skew bridges.

Three dimensional models were analyzed under thermal expansion loads to calculate transverse forces on the wingwall. Transverse restraint at the bearings over the abutment was released to calculate the resultant force on the wingwall. EPS with K_p of 0.08 was used as the backfill. The resultant wingwall force variation with skew is presented in Figure 5-30. The calculated force on the wingwall is smaller than the values presented in literature for different backfill material. For this reason, using an EPS layer in between the backwall and backfill material and providing adequate tolerances at the bearings over the abutment is recommended to release girder end forces that are developed under uniform thermal loads. It is also recommended to use geotextile filter fabric in between EPS and backfill for protection. Due to lack of data on passive pressure coefficient of EPS, it is recommended to use the values suggested in VDOT (2010), i.e., $K_p = 4$, for design. Further, due to lack of guidelines, the equation given in VDOT (2010) section 20-06-6 can be used to calculate EPS

layer thickness (i.e., Eq. 2-2 in Chapter 2 section 2.4.4). Transverse force on the wingwall should be calculated following the procedure described in VDOT (2010).

Wingwalls are not effective under thermal contraction. Hence, it is recommended that wingwalls are used in conjunction with a concrete key to assure stability of the bridge with the increased alignment pin slot tolerances to accommodate thermal movement.

Further, minimizing friction at the approach-base and approach-sleeper slab has a great influence on link slab stresses. This issue is highlighted in section 5.4.5.4. This is extremely important in the case of thermal contraction which can develop significantly larger stresses than the concrete modulus of rupture. Hence, providing a 0.025 in. thick polyethylene sheet underneath the entire surface of the approach is recommended. Application examples of such practices can be found from Minnesota and Pennsylvania DOT jurisdictions.

Considering the use of EPS, reducing friction at interfaces, and providing adequate tolerances for girder end movement, bearing details, wingwall and concrete key configurations, and abutment configurations were developed. Proposed detail in standard MDOT Bridge Design Guide format is presented in Appendix H.

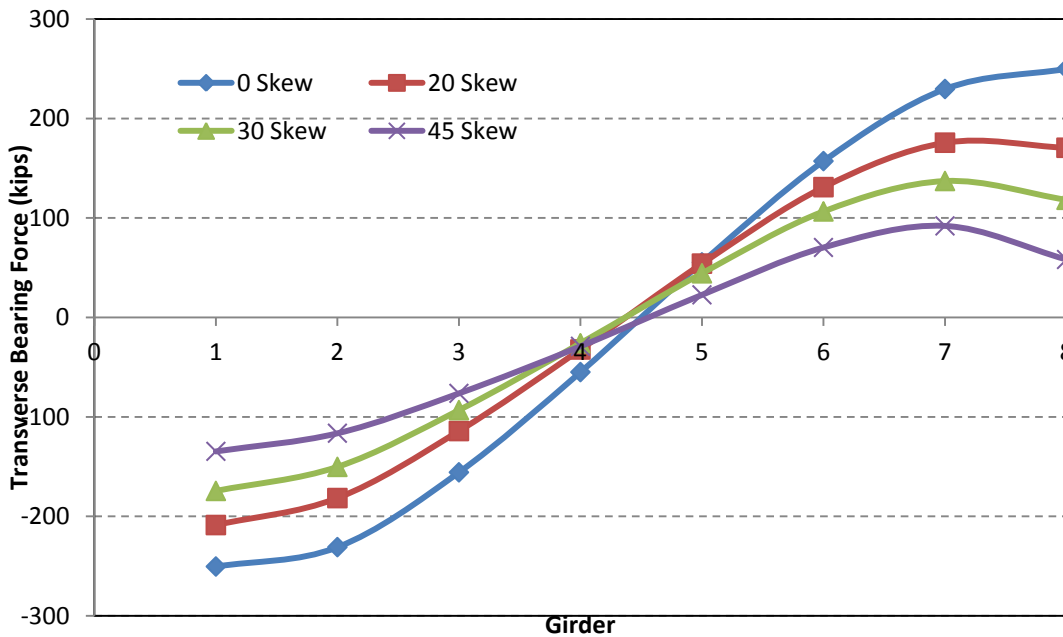


Figure 5-28. Transverse bearing force over abutment under thermal contraction strength load combination

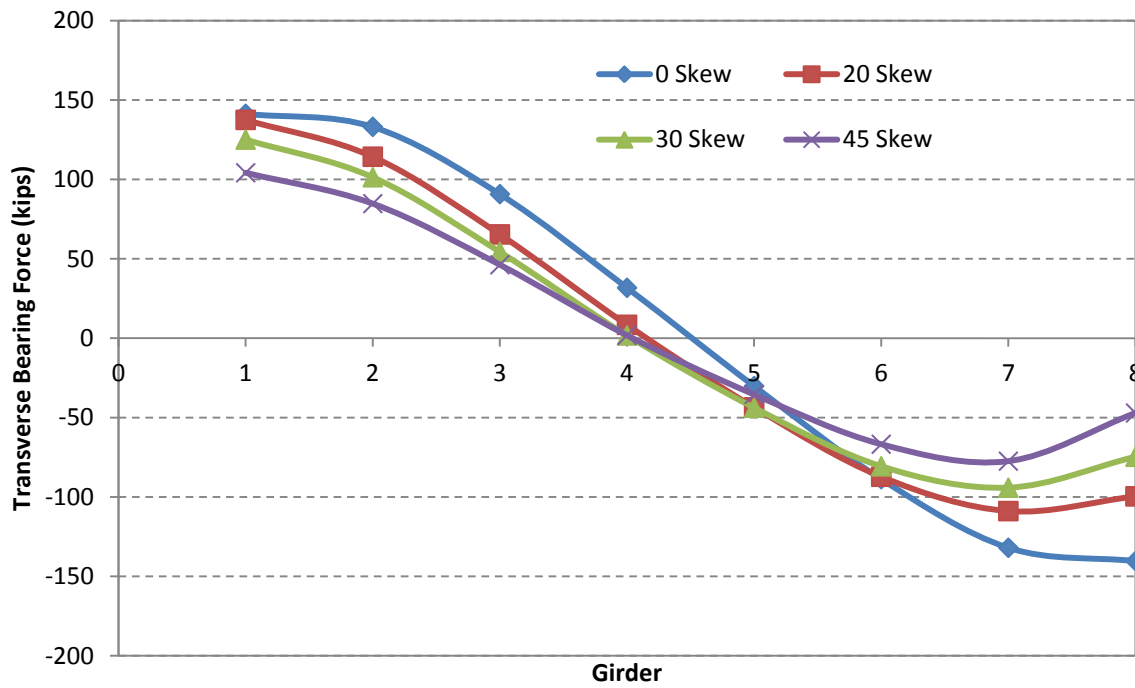


Figure 5-29. Transverse bearing force over abutment under thermal expansion strength load combination

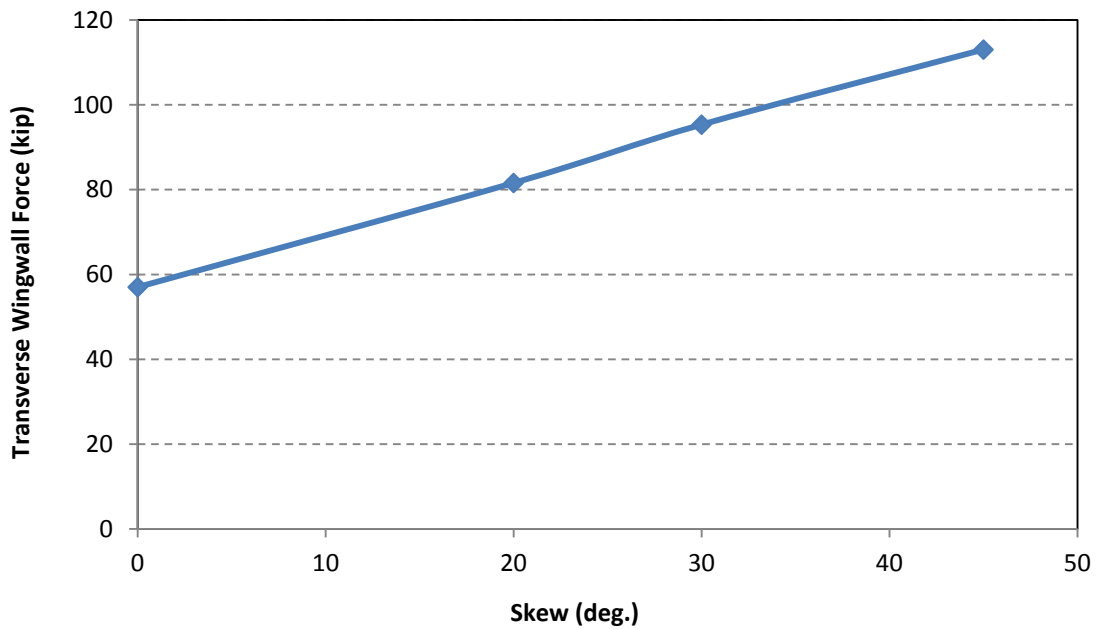


Figure 5-30. Wingwall force due to thermal expansion without transverse restraint over the abutment under strength load combination

5.5 ANALYSIS AND DESIGN PROCEDURES AND DETAILS FOR ABUTMENTS AND BEARINGS

Detailed analysis of two skew abutment configurations namely deck sliding over backwall and semi-integral systems was performed for a range of skew angles from 0^0 to 45^0 and loads and configurations specified in AASHTO (2010) and the Michigan Bridge Design Manual (MDOT 2005). The deck sliding over backwall and semi-integral abutment details presented in Aktan et al. (2008) were used to develop FE models and later modified to accommodate various bearing configurations and wingwalls. The following is a summary of conclusions that are derived from the analysis results and information presented in related literature and design specifications /guidelines.

1. A bridge span with deck sliding over backwall or semi-integral abutments can be analyzed as simply supported spans to calculate girder end rotations and translation (expansion/contraction) demands.
2. Skew bridges expand and contract along the diagonal between acute corners. The movement results in transverse forces at the bearings and other restraint systems. The restraint force magnitudes become considerably larger if adequate tolerances are not provided to accommodate the movements due to thermal loads. The situation requires special consideration when link slabs are implemented over the piers, which in turn increase the effective length of thermal expansion and contraction. Further, the direction of bridge movement under expansion and contraction loads needs to be restricted to the bridge axis. In plane twisting results in large stresses along the edge of link slab (see Chapter 4). Link slab is also flexible under torsion compared to the deck-girder integrated system. Hence, controlling bridge alignment is critical when link slabs are implemented.
3. It is recommended that deck sliding over backwall abutments, is restrain the transverse movement of the center girder end (for odd number of girders) or two centermost girder ends (for even number of girders) using concrete keys with rub plates (shown on Figure 5-8.). Also, larger tolerance is required for the slot in the sole plate and bearings in order to accommodate the transverse movement of unrestrained

- girder ends. Proposed detail in standard MDOT Bridge Design Guide format is presented in Appendix F. The required formulations and variables for movement calculations are presented with the drawings. The rub plate design procedure is based on the VDOT Bridge Design Manual section 20.04 (2010) with modifications and presented in Appendix G.
4. Transverse movement of bearings over the semi-integral abutment is facilitated by increasing the tolerance of the slot at the bearing plate. Transverse restraint for expansion thermal load is provided by a wingwall at the acute corner. Alignment of semi-integral abutment bridge deck with backwall offset from the abutment is managed under contraction thermal loads by placing a concrete key at the center girder. Calculation of the transverse force on the wingwall is adopted from the procedure described in VDOT (2010). Proposed detail in standard MDOT Bridge Design Guide format is presented in Appendix H.
 5. It is recommended that an EPS layer is placed behind the backwall of semi-integral bridges. This will minimize the passive pressure and results in lower transverse forces at the wingwall. Although the passive pressure coefficient of EPS is in reality much lower than four (4), a coefficient of four (4) is recommended for conservative design until additional supporting data is developed (VDOT (2010)). Further, the equation given in VDOT (2010) section 20-06-6 can be used to calculate EPS layer thickness (i.e., Eq. 2-2 in Chapter 2 section 2.4.4).
 6. It is recommended that the maximum bearing tolerance in transverse direction is limited to 0.25 in. Further investigations can be carried out analyzing the impact of the increased fit tolerances of the girder position dowels on the bridge components.
 7. Following link slabs are implemented, controlling friction at the approach slab interfaces is very critical. Increased friction hinders bridge movement restricting expansion bearing movement over the abutment. This results in stresses greater than the concrete modulus of rupture under negative thermal loads. Hence, it is vital to reduce friction at all the contract surfaces at the abutment and approach to facilitate

movement of the bridge under expansion and contraction thermal loads. To reduce friction a 0.025 in. thick polyethylene sheet can be placed during construction over the fill supporting the approach slab.

8. Bridge expansion length, excluding the approach slab, was calculated for width and skew angle ranges of single span steel and prestressed concrete bridges under the MDOT jurisdiction. Strip seal joint width of 3 in. available for thermal movement in the traffic direction and an expansion and contraction thermal load of 115 °F (Figure 5-20 and Figure 5-21) were assumed. Under such limits, expansion length of concrete bridge superstructure without skew should be limited to 300 ft. When steel girder bridges without skew are considered, length should be limited to 275 ft. For skew bridges, length limits are described in the charts shown in Figure 5-20 and Figure 5-21.

Intentionally left blank

6 SUMMARY, CONCLUSIONS, DESIGN RECOMMENDATIONS, AND IMPLEMENTATION PLAN

6.1 SUMMARY AND CONCLUSIONS

Four tasks were performed in this project. The first task was to review and synthesize information related to skew/jointless bridge behavior, modeling and analysis of skew bridge structural system/components, design and detailing of jointless abutments, and performance of jointless bridges. In this task specific design configurations with records of better performance were identified. High skew link slab analysis and design guidelines could not be found in the literature review. Hence, a detailed analysis of a high skew link slab bridge system was performed; design procedures and details were developed. Literature review was very useful in identifying abutment configurations and design details with better performance records. The most functional detail in these configurations were the use of EPS to reduce passive earth pressure and the use of rub plates to guide the bridge expansion and contraction under thermal loads. The Virginia DOT bridge design manual provided calculation details of EPS layer thickness and rub plate design. The manual also provided the passive pressure coefficient of EPS and a detailed procedure for calculating design forces on wingwall.

Task two was field monitoring of a high skew bridge under truck loads and thermal loads. This task was for identifying and documenting the performance of sliding bearings and the behavior of a skew bridge under various loads types. In-depth understanding of skew bridge behavior was essential for the defining the analyses framework carried out in task three and four.

Task three was detailed analysis of skew link slabs and calculation of the associated moment and force envelopes at the link slab section directly over the pier centerline. The analysis was performed for a specific bridge span length, width, and girder type, and at various angles of skew from 0° to 45° . The finite element (FE) models, for these configurations up to 45° skew, were developed and analyzed under loads and load combinations described in AASHTO (2010). Further, the influence of different bearing configurations on the link slab moment and force resultants are also investigated. Finally, the design recommendations were developed for the utilization of link slabs in high skew bridges. The design recommendations

were developed by integrating findings from the literature review, with the FE analysis results, and AASHTO (2010) requirements on strength and service load combinations. A detailed example of skew link slab design procedure is presented in Appendix C.

Task four was the detailed analysis of two skew abutment configurations namely deck sliding over backwall and semi-integral systems. The analysis models were developed for a range of skew angles from 0^0 to 45^0 and analyzed under loads and configurations specified in AASHTO (2010) and the Michigan Bridge Design Manual (MDOT 2005). Deck sliding over backwall and semi-integral abutment details presented in Aktan et al. (2008) was the basis of the FE models. These models were modified to incorporate selected bearing configurations and wingwalls. Based on findings from the FE analysis combined with findings from the literature, design recommendations for bearings, abutments, and restraint systems were developed.

6.2 RECOMMENDATIONS

From the literature review on field assessment of skew bridge behavior under static truck loads and thermal expansion, and simulations by numerous FE models, three design recommendations were developed. One recommendation is for the high skew link slab design, and the other two address the transverse restraint systems, bearing details, and the abutment configuration of deck sliding over backwall and semi-integral abutments in link slab bridges.

6.2.1 Link Slab Design

Current link slab design procedures do not incorporate skew effects. A design procedure was developed following a detailed analysis of skew link slabs and the moment and force envelopes for various boundary and load configurations. Two major findings are (1) moment developed in a link slab under temperature gradient loads remains constant irrespective of span and (2) moment developed in a link slab under live load decreases with increased span. Analysis results verified that the minimum reinforcement amount required in AASHTO LRFD Section 5.7.3.3.2 is adequate for the majority of skew link slabs with HRRR or RRHR support configuration. However, additional reinforcement at the bottom layer is needed to resist large tensile stresses that develop near the boundaries of the debonded region. A

detailed design example is presented in Appendix C. Proposed link-slab detail in standard MDOT Bridge Design Guide format is presented in Appendix E. Three saw cuts are recommended: one at each end of the link slab and one directly over the pier centerline.

6.2.2 Deck Sliding over Backwall

Two changes are proposed to the current MDOT independent backwall detail. The first one is to incorporate 0.025 in. thick polyethylene sheet underneath the approach slab. The second one is a transverse restraint system designed with concrete keys and rub plates. The restraint system is essential to manage the bridge alignment under thermal effects. In conjunction with these change recommendations, design procedures are presented. Proposed detail in standard MDOT Bridge Design Guide format is presented in Appendix F. All the required formulations and variables are presented with the drawings. The rub plate design procedure was adopted from VDOT Bridge Design Manual section 20.04 (2010) with some modifications and presented in Appendix G.

Bridge expansion length, which is the distance along the longitudinal axis measured from abutment to the nearest fixed bearing, is a function of bridge length, width, and skew. Expansion joint effective movement rating and allowable movement at bearings are the limiting factors of bridge expansion length when link slabs are implemented. Based on maximum strip seal joint width of 3 in and expansion and contraction thermal load of 115 °F, the following maximum expansion length are recommended:

Straight concrete bridge ≤ 300 ft.

45° skew concrete bridge of 100 ft wide ≤ 200 ft.

Straight steel bridge ≤ 275 ft.

45° skew steel bridge of 100 ft wide ≤ 175 ft.

6.2.3 Semi-Integral Abutment

Changes are also proposed to semi-integral abutment details. These changes are necessary for managing bridge alignment. Details include the use of wingwalls and girder end restrains such as concrete keys with rub plates. Further, EPS layer is included behind the backwall to reduce passive pressure acting on the backwall. The EPS layer will help with reducing transverse forces on wingwalls and girder end restrains. It is also recommended that a 0.025

in. polyethylene sheet is provided underneath the approach to reduce frictional forces. Reducing frictional forces is necessary for preventing link slab cracking. Transverse force calculation on the wingwall is based on the procedure described in VDOT (2010). Proposed detail in standard MDOT Bridge Design Guide format is presented in Appendix H. The bridge expansion length limitations presented in section 6.2.2 are also valid when link slabs are implemented in semi-integral bridges.

6.3 IMPLEMENTATION PLAN

The focus of this work has been the investigation of the behavior and load demands on high skew link slab and jointless abutment configurations and to develop design modifications to the current link slab, bearing, wingwall, and other girder end restraint configurations. The abutment configurations were limited to those commonly used in Michigan, namely deck sliding over backwall and semi-integral abutments. Also, national and international best practices on controlling abutment distress in skew bridges were reviewed, and promising configurations and details were recommended.

Below, the required future work is outlined. Implementation of the following is required before incorporating the recommendations in MDOT specifications, manuals and guides.

- The proposed link-slab details and support configurations should be incorporated as a pilot implementation project. The implementation project needs to be monitored to document the behavior and performance in order to evaluate and fine-tune the proposed analysis and design procedures.
- An increase to bearing tolerances is recommended for the slot dimensions of the alignment pins. This recommendation is for reducing forces developed at the abutments under thermal expansion and contraction loads. A maximum tolerance limit of 0.25 in. was recommended after reviewing typical bearing details and specification requirements. Additional recommendations were also provided for reducing friction forces on the backwall and approach slab. Again, a pilot implementation project with monitoring that incorporate the recommended details for the abutment region is the next step.

7 REFERENCES

AASHTO (2010). *AASHTO LRFD Bridge Design Specifications*, Fifth Edition, Washington, DC, 20001.

AASHTO (2008). *AASHTO LRFD Bridge Construction Specifications*, Second Edition with 2008 Interims, Washington, DC, 20001.

Aktan, H.M., Attanayake, U., and Ulku, A. E. (2008) *Combining Link-Slab, Deck Sliding over Back-Wall and Revising Bearings*, MDOT RC-1514, Report to the Michigan Department of Transportation, Detroit, MI 48226.

Aktan, H., Koyuncu, Y., Rutyna, J., Ahlborn, T.M., & Kasper, J.M. (2002). *Causes and cures for prestressed concrete I-beam deterioration*, Research report RC-1412, Michigan Department of Transportation, Lansing, Michigan.

Badie, S. S., Tadros, M. K., and Pedersen, K. E. (2001). "Re-examination of I-Girder/Pier Connection Jointless Bridges." *PCI Journal*, Vol. 46, No. 2, pp. 62-74.

Burke, M. P., Jr., (1999). "Cracking of Concrete Decks and Other Problems with Integral-Type Bridges." *Transportation Research Record 1688*, Paper No. 99-0104, Transportation Research Board, Washington, D.C.

Burke, M. P., Jr. (1994a). "Semi Integral Bridges: Movements and forces." *Transportation Research Record 1460*, Transportation Research Board, Washington, D.C.

Burke, M.P., Jr. (1994b). "Semi-Integral Bridges: A Concept Whose Time Has Come?" *Continuous and Integral Bridges*, EAFN Spon, pp. 213-224.

Caner, A. and Zia, P. (1998). "Behavior and Design of Link Slab for Jointless Bridge Decks." *PCI Journal*, May-June 1998, pp. 68-80.

Chandra, V., et al. (1995). *Draft Report on Precast Prestressed Concrete Integral Bridges, State-of-the-Art*. Precast/Prestressed Concrete Institute, 113 pp.

Elragi, A.F. (2011). <http://www.softoria.com/institute/geofoam/material.html#36> (Last accessed May 26, 2011).

FHWA (2011). Rapid embankment construction: Expanded polystyrene (EPS) geofoam. <http://www.fhwa.dot.gov/bridge/abc/eps.cfm> (Last accessed May 27, 2011).

Frydenlund, T. E. and Aabøe, R. (2001). “Long term performance and durability of EPS as a lightweight filling material, EPS Geofoam.” *3rd International Conference*, Salt Lake City.

Gilani, A., and Jansson, D. (2004). *Link Slabs for Simply Supported Bridges: Incorporating Engineered Cementitious Composites*. Draft Report No. MDOT SPR-54181, Michigan Department of Transportation, Lansing, Michigan.

Hambly, E.C. (1991). *Bridge Deck Behavior*, Second Edition, Van Nostrand Reinhold, 115 5th Avenue, New York NY 10003.

Hoppe, E. J. (2005). *Field Study of Integral Backwall with Elastic Inclusion*. Research report VTRC 05-R28, Virginia Department of Transportation, Richmond, VA.

Hoppe, E. J. and Bagnall, T. M. (2008). *Performance of a Skewed Semi-Integral Bridge: Volume I: Field Monitoring*. Research report VTRC 08-R20, Virginia Department of Transportation, Richmond, VA.

Husain, I. and Bagnariol, D. (1999). *Semi-Integral Abutment Bridges*, Report BO-99-03, Ministry of Transportation, Ontario, Canada.

Lutenegger, A. J. and Ciufetti, M. (2009). *Full-Scale Pilot Study to Reduce Lateral Stresses in Retaining Structures Using GeoFoam*, Vermont Agency of Transportation, Materials and Research Section, Montpelier, VT.

Maruri, R., and Petro, S. (2005). “Integral Abutment and Jointless Bridges (IAJB) 2004 Service Summary.” *Proceedings of the IAJB 2005*, March 16-18 2005, Baltimore, Maryland.

MDOT (2006). *Bridge Design Guide*. Michigan Department of Transportation, Lansing, MI.

MDOT (2005). *Bridge Design Manual*. Michigan Department of Transportation, Lansing, MI.

MnDOT (2011). MnDOT Standard Plans, Minnesota Department of Transportation, MN.

Moorty, S., and Roeder, C. (1992). "Temperature-Dependent Bridge Movements." *Journal of Structural Engineering*, Vol. 118, No.4, pp. 1090-1105.

Menassa, C., Mabsout, M., Tarhini, K. and Frederick, G. (2007). "Influence of Skew Angle on Reinforced Concrete Slab Bridges." *Journal of Bridge Engineering*, Vol. 12, No. 2, pp. 205-214.

Nakai, H. and Yoo, C.H. (1988). *Analysis and design of curved steel bridges*, McGraw-Hill, New York, pp. 575.

Najm, H., Patel, R. and Nassif, H. (2007). "Evaluation of Laminated Circular Elastomeric Bearings." *Journal of Bridge Engineering*, Vol. 12, No. 1, pp. 89-97.

NCDOT (2007). <http://www.ncdot.org/doh/PRECONSTRUCT/highway/structur/springfield/2007/site2/default.html> (Accessed: March 2009).

Nicholson, B.A.; Barr, J.M.; Cooke, R.S.; Hickman, R.P.; Jones, C.J.F.P.; and Taylor, H.P.J., (1997). *Integral Bridges: Report of a Study Tour to North America*. Concrete Bridge Development Group, U.K., 93 pp.

Oesterle, R.G., Tabatabai, H., Lawson, T.J., Refai, T.M., Voltz, J.S., and Scanlon, A. (1999). *Jointless and Integral Abutment Bridges*. Summary Report, Final Report to Federal Highway Administration, Washington D.C.

Parke, G. A. R. and Hewson, N. R. (2008). *ICE Manual of Bridge Engineering, 2nd edition*, Thomas Telford, London.

Purvis, R. (2003). *Bridge Deck Joint Performance*. NCHRP Synthesis 319, Transportation Research Board, Washington, D.C.

Roeder, C. W. and Stanton, J. F. (1996). *Steel Bridge Bearing Selection and Design Guide, Highway Structures Design Handbook*, Vol. II, Chapter. 4, American Institute of Steel Construction, Inc., National Steel Bridge Alliance, Chicago, IL.

Romkema, M., Attanayake, U., and Aktan, H. (2010). *Incorporating link slabs in high skew bridges during repair activities - design recommendations*, Technical Report: CCE-10-01, Department of Civil and Construction Engineering, Western Michigan University, Kalamazoo, Michigan.

Sanford, T. C., and Elgaaly, M. (1993). "Skew Effects on Backfill Pressures at Frame Bridge Abutments." *Transportation Research Record*, 1415, Transportation Research Board, Washington, D.C., 1–10.

Stark, T. D., Arellano, D., Horvath, J. S. and Leshchinsky, D. (2004). *Geofoam Applications in the Design and Construction of Highway Embankments*, NCHRP Web Document 65 (Project 24-11), National Cooperative Highway Research Program, Transportation Research Board, Washington, DC 20008.

Steinberg, E. and Sargand, S. (2010). *Forces on Wingwalls from Thermal Expansion of Skewed Semi-Integral Bridges*, FHWA/OH-2010/16, Ohio Department of Transportation, Columbus, Ohio.

Steinberg, E., Sargand, H., and Bettinger, C. (2004). "Forces in Wingwalls of Skewed Semi-Integral Bridges." *Journal of Bridge Engineering*, Vol. 9, No. 6, pp.563-571.

Tabatabai, H., Oesterle, R.G., and Lawson, T.J. (2005). *Jointless Bridges, Experimental Research and Field Studies*. Volume I, Final Report to FHWA, August 2005.

Tindal, T.T. and Yoo, C.H., (2003). "Thermal Effects on Skewed Steel Highway Bridges and Bearing Orientation." *Journal of Bridge Engineering*, Vol. 8, No. 2, pp.57-65.

Ulku, E., Attanayake, U., and Aktan, H. M. (2009). "Jointless Bridge Deck with Link Slabs: Design for Durability," *Transportation Research Record: Journal of the Transportation*

Research Board, No. 2131, Transportation Research Board of the National Academies, Washington, D.C., pp. 68–78.

Van Lund, J., and Brecto, B. (1999). “Jointless Bridges and Bridge Deck Joints in Washington State.” *Transportation Research Record, 1688*, Transportation Research Board, Washington, D.C., 116–123.

VDOT (2010). *Structure and Bridge Manuals*, Virginia Department of Transportation, Richmond, VA.

Weakley, K. (2005). “VDOT Integral Bridge Design Guidelines.” *Proceedings of the IAJB 2005*, March 16-18 2005, Baltimore, Maryland.

Yazdani, N., and Green, T., (2000). *Effects of Boundary Conditions on Bridge Performance*. WPI# 0510843, March 2000, Tallahassee, FL.